**ISTANBUL TECHNICAL UNIVERSITY ★ EURASIA INSTITUTE OF EARTH SCIENCES**

# ACTIVE TECTONICS AND PALEOSEISMOLOGY OF THE GANOS FAULT SEGMENT AND SEISMIC CHARACTERISTICS OF THE 9 AUGUST 1912 MÜREFTE EARTHQUAKE OF THE NORTH ANATOLIAN FAULT (WESTERN TURKEY)

**PhD. Thesis by**
**Murat Ersen AKSOY**

**Department : Solid Earth Sciences**

**Programme : Earth System Sciences**

**OCTOBER 2009**

**ISTANBUL TECHNICAL UNIVERSITY ★ EURASIA INSTITUTE OF EARTH SCIENCES**

# ACTIVE TECTONICS AND PALEOSEISMOLOGY OF THE GANOS FAULT SEGMENT AND SEISMIC CHARACTERISTICS OF THE 9 AUGUST 1912 MUREFTE EARTHQUAKE OF THE NORTH ANATOLIAN FAULT (WESTERN TURKEY)

**PhD Thesis by**
**Murat Ersen AKSOY**
**(602022012)**

**Date of submission : 09 October 2009**
**Date of defence examination: 30 October 2009**

**Supervisor (Chairman) : Asst. Prof. Ziyadin ÇAKIR (ITU)**
**Members of the Examining Committee : Prof. Dr. Mustapha MEGHRAOUI (IPGS)**
**Prof. Dr. Aral OKAY (ITU)**
**Prof. Dr. Okan TUYSUZ (ITU)**
**Asst. Prof. Semih ERGINTAV (TUBITAK)**

**OCTOBER 2009**

**İSTANBUL TEKNİK ÜNİVERSİTESİ ★ AVRASYA YER BİLİMLERİ ENSTİTÜSÜ**

# KUZEY ANADOLU FAYI GANOS FAY SEGMENTİNİN AKTİF TEKTONİĞİ VE PALEOSİSMOLOJİSİ VE 9 AĞUSTOS 1912 MÜREFTE DEPREMİNİN SİSMİK KARAKTERİSTİKLERİ (BATI TÜRKİYE)

**DOKTORA TEZİ**

**Murat Ersen AKSOY**
**(602022012)**

**Tezin Enstitüye Verildiği Tarih : 09 Ekim 2009**
**Tezin Savunulduğu Tarih : 30 Ekim 2009**

**Tez Danışmanı : Yrd. Doç. Dr. Ziyadin ÇAKIR(İTÜ)**
**Diğer Jüri Üyeleri : Prof. Dr. Mustapha MEGHROUI (İPGS)**
**Prof. Dr. Aral OKAY (İTÜ)**
**Prof. Dr. Okan TÜYSÜZ (İTÜ)**
**Doç. Dr. Semih ERGİNTAV (TÜBİTAK)**

**EKİM 2009**

In memory of his 200th birthday…

*…the earth, the very emblem of solidity, has moved beneath our feet like a thin crust over a fluid; one second of time has created in the mind a strange idea of insecurity, which hours of reflection could not have produced.*

Charles Darwin

1845

## FOREWORD

Before all, I feel the need to acknowledge, it is thanks to the late Aykut Barka that I have been able to enter into the distinguished community of earthquake geologists. The collaborative and optimistic attitude in his profession has always been my inspiration that allowed me accomplishing this PhD study. Therefore I owe my deep gratitude to his memory.

My most sincere thanks go to my advisors Mustapha Meghraoui and Ziyadin Çakır, who provided me unique scientific support with endless patients. It is thanks to their efforts and their precision in scientific research that I was able to complete this work.

I should not forget to mention the help and guidance of my initial supervisor Serdar Akyüz during my field studies and would like to thank him and my friends Matthieu Ferry, Taylan Sancar, Gürsel Sunal, Ayşe Kaplan, Aynur Dikbaş, Çağlar Yalçıner, Volkan Karabacak and Murat Topkan for their helping hand in the field. I also owe thanks to Ramiz Ilter who fished out a poorly known historical document from the dusty shelves of the National Library in Ankara.

During this study I had well support and fruitful discussions with many of my colleagues. Therefore I am very grateful to Cenk Yaltırak for sharing his wide knowledge on the geology of the Ganos region; Martin Valleé, Antoine Schlupp, Onur Tan, Michel Cara, Cengiz Tapırdamaz, Michel Bouchon, Semih Ergintav, Yaser Mahmoud and Louis Rivera guiding me in the collection, correction and modelling process of the historical seismograms, Tom Rockwell and Koji Okumura sharing their unique experience in paleoseismology, Cengiz Zabcı for our exciting discussion on earthquake geology, Dilek Şatır for practical solutions in GIS and drainage analysis and Ahmet Akoğlu for sharing his experience in computer science and GMT.

Special thanks go to Gülsen Uçarkuş, my fellow in this French-Turkish co-supervisor program. Her precious friendship and support since we ever met will never be forgotton. I owe special thanks to my dear friend and colleague Tayfun Kındap for his financial support and motivation during my study. I am indebted very special thanks to Kezban Saki-Yaltırak. She was always an important backer during my entire stage of the PhD, providing great motivation and wisdom. Her help is invaluable and will be always remembered.

Special thanks go to the Belabbes family who always welcomed me during my stays in Strasbourg. I bothered Samir and Mounia very often by asking awful translations to French and they never refused; merci beaucoup!

I can not ignore the great last minute help of Barış Yerli for finalizing my map; teşekkürler dostum!

A great thank you goes to Mustafa, Dilek and other members of the Tuzluca family who provided me great logistic support during my field works in Şarköy. I thank to all villagers of Yörgüç, Yeniköy, and Sofuköy who were always interested in my work in the trenches and showed me great hospitality.

The French Embassy in Ankara supported me during my whole stays in France. Together with the CROUS-Strasbourg they provided my great facilities to complete my study successfully. I would like to thank especially to Hamide İbikcan and Virginie Tigoulet for they kind help.

Last but not least, I am grateful to all members of my family; my father Erden, my mother Birsen and my brothers Serhat and Tunç, who patiently tolerated all my good and bad times while preparing this thesis.

September 2009-09-02 Murat Ersen AKSOY

**TABLE OF CONTENTS**

**Page**

## ABBREVIATIONS

**DEM** : Digital Elevation Model
**DSF** : Death Sea Fault
**E** : East
**EAF** : East Anatolian Fault
**EGF** : Empirical Green Function
**Fig.** : Figure
**GPS** : Global Positioning System
**IASPEI** : International Association of Seismology and Physics of the Earth's Interior
**KOERI** : Kandilli Observatory and Earthquake Research Institute
**LT** : Local Time
**N** : North
**NAF** : North Anatolian Fault
**NAFZ** : North Anatolian Fault Zone
**NE** : Northeast
**NNAF** : Northern North Anatolian Fault
**NNW** : North-Northwest
**NW** : Northwest
**p.** : Page
**RSTF** : Relative Source Time Function
**S** : South
**SE** : Southeast
**SRTM** : Shuttle Radar Topography Mission
**SW** : Southwest
**TUBITAK** : The Scientific and Technological Research Council of Turkey
**W** : West
**WWSSN** : World Wide Standardized Seismograph Network

## LIST OF TABLES

**Page**

## LIST OF FIGURES

**Page**

## LIST OF SYMBOLS

**M** : Magnitude
$\boldsymbol{M_0}$ : Seismic Moment
$\mathbf{m_b}$ : Body wave magnitude
$\mathbf{M_D}$ : Duration magnitude
$\mathbf{M_s}$ : Surface wave magnitude
$\boldsymbol{M_w}$ : Moment magnitude
$\boldsymbol{S}$ : Area of the rupture fault plane
$\boldsymbol{U}$ : Average slip along the ruptured fault plane
**μ** : Shear modulus

**ACTIVE TECTONICS AND PALEOSEISMOLOGY OF THE GANOS FAULT SEGMENT AND SEISMIC CHARACTERISTICS OF THE 9 AUGUST 1912 MÜREFTE EARTHQUAKE OF THE NORTH ANATOLIAN FAULT (WESTERN TURKEY)**

## SUMMARY

The North Anatolian Fault generated 9 large earthquakes (M>7) in Turkey during the last 100 years. We investigate the Ganos fault, the westernmost segment of the North Anatolian Fault that was responsible for the 9 August 1912 Mürefte earthquake (M 7.3). The Ganos fault is exposed onland for 45 km while the rest is covered up by the Aegean and Marmara seas, to the west and east respectively. The Ganos fault forms the western section of a large step-over area that corresponds to the Marmara pull-apart and experienced the 1999 Kocaeli earthquake on its east. The two ends of the 1912 and 1999 earthquake ruptures define the seismic gap in the Sea of Marmara.

Geomorphic analysis along the 45-km-long onland section of the Ganos fault allowed documenting typical structures of strike-slip faulting; i.e. step-overs, pull-aparts, bends, pressure ridges, sag-ponds, offset ridges, shutter ridges and stream displacement. The onland section of the Ganos fault is expressed as ~N68°E striking linear geometry, segmented by two extensional step-overs at Gölcük and Kavak. The combined analysis of offshore and onland fault morphology suggests a minimum of 4 sub-segments limited by geometrical complexities which are from east to west, the Central Marmara basin, Ganos bend, Gölcük step-over, Kavak step-over and Saros Trough. The Saros Trough and the Central Marmara basin are the largest structural complexities along the Ganos fault and may serve as barriers to earthquake rupture propagation.

Cumulative displacements determined at 69 localities and tectonic reconstructions provide insights on the long-term and short-term deformation characteristic of the Ganos fault segment. Measurements of displaced streams, ridges and partly ancient roads yield right lateral offsets ranging from 8 to 575 m. Furthermore, we suggest larger offsets from 200 to 9000 m based on reconstructions of the present-day drainage system. A classification of the stream offsets shows 8 distinct classes of cumulative slip. We used sea level fluctuation curves of the Black Sea in order to constrain the timing of high precipitations periods which can trigger channel incisions. Consecutive 5 cumulative slip groups (from 70 to 300 m) show well correlations with subsequent sea level rise periods at 4 ka, 10.2 ka, 12.5 ka, 14.5 ka and 17.5 ka. Slip rate estimations yield a constant slip rate of 17.9 mm/yr for the last 20.000 years and a variable slip rate of 17.7 mm/yr, 17.7 mm/yr, 17.9 mm/yr and 18.9 mm/yr for the last 10.2 ka, 12.5 ka, 14.5 ka and 17.5 ka, respectively.

Paleoseismology at three sites (Güzelköy, Yeniköy and Yörgüç) showed evidence of 8 faulting events, 5 of which post-date 1043 – 835 BC and 1500 – 830 BC at Güzelköy site and Yeniköy site, respectively. A better timing was constrained for the last three events at Güzelköy which are most probably the earthquakes in (1) 1344 or 1354 (2) 1659 or 1766b and (3) 1912. We suggest two earthquake recurrence

scenarios for the last historical earthquakes attributed to the Ganos fault. Scenario 1 yields an average recurrence interval of 285 ± 36 years and encompasses the 1912, 1659, 1354/1344, 824, 484 events, whereas Scenario 2 gives an average recurrence interval of 285 ± 93 years and includes the 1912, 1766, 1354/1344, 824, 484 events. Considering that earthquakes occur periodic the suitable seismic history corresponds to Scenario 1. However scenario 2 is also valid if a non-periodic earthquake occurrence is accepted. The combination of geomorphic analysis and trenching results provides slip rates for the North Anatolian Fault at the Ganos region. At Güzelköy two paleo-channels offset for 16 m and 21 m yield 22.3 ± 0.5 mm/yr for the last ~700 years and 26.9 mm/yr for the last 781 years, respectively. At Yeniköy dating from the lowermost units of the 46 ± 1 m offset stream provided a maximum 17 mm/yr slip rate for the last 2840 years.

The 9 August 1912 Mürefte earthquake ($M_s$=7.3) struck along the Ganos fault causing severe destruction ($I_o$ = X) between Tekirdağ and Çanakkale. A second large shock occurred on 13 September 1912 ($M_s$ = 6.8) with an epicentral region to the west of the first main shock, giving rise to $I_o$ = VII damage west of Gaziköy and along the Gallipoli peninsula. Surface breaks have been recorded along the entire 45-km-long onland section. We determined a maximum slip of 5.5 m that was previously suggested as 3 m (Ambraseys & Finkel et al, 1987). We extend the slip measurements of Altunel et al., (2004) from 31 localities to 45 with a better distribution along the fault. The offset distribution indicates that a certain length of the rupture is offshore, i.e., in the Saros bay and Sea of Marmara.

73 historical seismograms have been collected for the 9 August, 10 August and 13 September 1912 shocks. Comparable pairs have been digitized using TESEO software. The modelling and deconvolution of seismic waveforms allowed retrieving a relative source time function using the 13 September and 9 August shocks and provided a source duration of 40 seconds for the 9 August earthquake. Considering a unilateral rupture propagation of 3 km/s, this duration implies rupture length of 120 km, consistent with the earthquake size ($M_w$ 7.4). P-wave polarities at 5 stations and field based N68°E fault strike allow us to construct the focal mechanism solution for the 9 August shock.

The size of the 13 September shock requires 30 ± 10 km of surface faulting and constrains the western limit for the 120 ± 20 km long 9 August rupture. Taking into account the two events, an epicentre location in the Saros bay for the 13 September shock, the 150 ± 20 km long total rupture length would extend from Saros Trough towards east and reach the Central Marmara Basin, consistent with major geometric complexities along this section of the North Anatolian Fault. Therefore, the eastern termination of the 9 August 1912 rupture and the western termination of the 1999 earthquake rupture imply a minimum 100-km-long seismic gap in the Sea of Marmara. This fault length suggests an earthquake size M>7 that should be taken into account in any seismic hazard assessment for the Istanbul region.

The results of this study will be published in four articles which are in preparation.

1-Aksoy, M.E., Meghraoui, M., Vallee, M., Çakır, Z, 2009, Rupture Characteristics of the 1912 Mürefte (Ganos) Earthquake Segment of the North Anatolian Fault (Western Turkey); submitted to Geology.
2-Meghraoui, M., Aksoy, M.E., Akyüz, S., Ferry M., Dikbaş, A., Altunel E., Paleoseismology of the North Anatolian Fault at Güzelköy (Ganos segment, Turkey): Size and recurrence time of earthquake ruptures in the West Marmara Sea.

3-Aksoy, M.E., Meghraoui, M., Ferry M., Dikbaş, A., Akyüz, S., Ucarkus, G, Çakır, Z, Altın U., Sancar, T., Saki-Yaltırak, K., 2009, Paleoseismic history of the 1912 Mürefte earthquake segment of the North Anatolian Fault (Western Turkey); (in preparation for TJES)

4-Aksoy, M.E., Meghraoui, M., Çakır, Z, Ferry M., Uçarkuş, G, 2009, A 20 kyr slip rate history deduced from stream offset along the Ganos fault segment of the North Anatolian Fault (Western Turkey); (in preparation for EPSL).

## KUZEY ANADOLU FAYI GANOS SEGMENTİNİN AKTİF TEKTONİĞİ VE PALEOSİSMOLOJİSİ VE 9 AĞUSTOS 1912 MÜREFTE DEPREMİNİN SİSMİK KARAKTERİSTİKLERİ (BATI TÜRKİYE)

## ÖZET


Son 100 yılda, Kuzey Anadolu Fayı üzerinde 9 adet büyük deprem (M>7) meydana gelmiştir. Bu çalışmada en son 9 Ağustos 1912'de kırılan ve Kuzey Anadolu Fayı'nın en batı parçasını oluşturan Ganos fayı çalışılmıştır. Ganos Fayı'nın karada görülen kısmı 45 km uzunluğundadır, geri kalanı Ege ve Marmara denizleri tarafından örtülmüştür. Bu fay büyük bir açılmalı sıçramanın batı kolunu oluşturmaktadır. Marmara çek-ayır havzasını oluşturan bu sıçramanın doğu kesimi ise 1999 Kocaeli depremi sırasında kırılmıştır. 1912 ve 1999'da kırılan parçaların karşılıklı iki ucu Marmara denizindeki sismik boşluğu oluşturmaktadır.

Ganos fayının karada görünen 45 km'lik kesiminde yapılan jeomorfik incelemeler neticesinde, doğrultu atımlı faylara has birçok morfolojik yapı tespit edilmiştir; ör. fay sıçramaları, çek-ayır havzalar, fay büklümleri, basınç sırtları, sırt ve dere ötelenmeleri, sürgü sırtları ve çöküntü gölleri. Fayın karada görülen parçası yaklaşık K68°D doğrultulu bir geometriye sahip ve Gölcük ve Kavak gerilmeli sıçramalarla bölünmüştür. Fayın kara ve deniz içindeki morfolojisi incelendiğinde fayın en az 4 parçadan oluştuğu ve bu parçaların doğudan batıya, Orta Marmara Havzası, Ganos büklümü, Gölcük sıçraması, Kavak sıçraması ve Saroz çukuru sınırlandığı gözlenmiştir. Saroz çukuru ve Orta Marmara Havzası Ganos fayı üzerinde yer alan en büyük geometrik engellerdir ve bir deprem kırığının ilerlemesini durdurma potansiyelini taşımaktadır.

69 adet birikimli ötelenme ve tektonik geri kurulumlar Ganos fayının kısa ve uzun dönem deformasyon niteliği hakkında bilgi sunmaktadır. Dere, sırt ve kısmen antik yollar üzerinden alınan atım ölçümleri 8 ila 575 m arasında değişmektedir. Bununla birlikte güncel drenaj sistemi üzerinden gerçekleştirilen geri kurulumlarla 200 m'den 9000 m'ye kadar ötelenmeler önerilmiştir. Dere ötelenmelerinin sınıflandırması sonucunda 8 adet birikimli atım grubu tespit edilmiştir. Karadeniz deniz seviyesi salınım eğrilerinden faydalanarak yeni dere yatakları oluşturabilecek yoğun yağış dönemleri belirlenmiştir. Ardışık 5 birikimli atım grubu (70 ila 300 m arası) birbirini izleyen deniz seviyesi yükselim dönemleriyle deneştirilmiştir. 4 bin, 10.2 bin, 12.5 bin, 14.5 bin ve 17.5 bin yıl öncesi zaman dilimlerine denk gelen bu atımlar sırasıyla 17.7 mm/yıl, 17.7 mm/yıl, 17.9 mm/yıl, ve 18.9 mm/yıl değişken fay hızı vermiştir. Fay hızı sabit kabul edildiği takdirde bu değerler 17.9 mm/yıl'lık bir hıza karşılık gelmektedir.

3 ayrı yerde (Güzelköy, Yörgüç, Yeniköy) gerçekleştirilen paleosismoloji çalışmalarında 8 adet faylanma olayı belirlenmiştir. Bu olaylardan son 5 tanesi Güzelköy'deki sahada M.Ö. 1043 – 835, Yeniköy'deki sahada da M.Ö. 1500 – 830 yıllarında meydana gelmiştir. Güzelköy hendek sahasındaki son 3 faylanma olayı iyi bir şekilde yaşlandırılabilmiştir ve bu olayların (1) 1344 veya 1354, (2) 1659 veya 1766 ve (3) 1912 depremlerine karşılık geldiği düşünülmektedir. Ganos fayı üzerinde

olduğu düşünülen son 6 tarihsel deprem için 2 farklı deprem tekrarlanma senaryosu önermekteyiz. Birinci senaryo da 1912, 1659, 1354/1344, 824 ve 484 depremlerinin Ganos üzerinde gerçekleştiği kabul edilmiş ve 285 ± 36 yıllık bir tekrarlanma aralığı hesaplanmıştır. İkinci senaryo 1912, 1766 1344/1354, 824 ve 484 depremlerini kapsamakta ve 285 ± 93 yıllık bir tekrarlanma aralığı vermektedir. Ganos fayının düzenli aralıklarla deprem ürettiği kabul edilecek olursa uygun deprem tarihçesi birinci senaryodaki gibidir. Ancak depremlerin düzensiz olarak meydana gelmesi halinde ikinci senaryodaki deprem tarihçesi kabul edilebilir hale gelmektedir. Hendek çalışmalarına paralel olarak gerçekleştirilen jeomorfik incelemeler Kuzey Anadolu Fay'ının bu kesimi için fay hızı hesaplamayı mümkün kılmıştır. Güzelköy'de yaşlandırılan 16 m ve 21 m'lik dere atımları sırasıyla son 700 yıl için 22.3 mm/yıl ve son 781 yıl için 26.9 mm/yıl'lık fay hızı vermiştir. Yeniköy'de ise 46 ± 1 m ötelenmiş bulunan bir dere yatağının en alt çökellerinden elde edilen yaşlarla son 2840 yıl için 17 mm/yıl'lık bir fay hızı elde edilmiştir.

9 Ağustos 1912 Mürefte depremi ($M_s$=7.3) Ganos fayı üzerinde meydana gelmiştir ve Tekirdağ'dan Çanakkale'ye kadar uzanan bir bölgede ciddi hasara neden olmuştur ($I_o$=X). 13 Eylül 1912'de merkezi ilk sarsıntıya göre daha batıda yer alan ikinci büyük bir deprem ($M_s$=6.8) meydana gelmiştir. Bu deprem Gaziköy'den Gelibolu'ya kadar uzanan bir alanda $I_o$=VII şiddetinde hasar meydana getirmiştir. Karada görülen 45-km'lik kesim boyunca yüzey kırıkları gözlenmiştir. Daha önceleri 3 m olarak önerilen (Ambraseys & Finkel, 1987) azami atımın 5.5 m olduğunu tespit edilmiştir. Altunel vd. (2004) tarafından ölçülen 31 adet atım gözlemi sayısı 45'e yükseltilmiştir. Atım dağılımı meydana gelen yüzey kırığının önemli bir bölümünün Saroz körfezi ve Marmara denizine doğru devam ettiğini göstermektedir.

Bu çalışmada, 9 Ağustos, 10 Ağustos ve 13 Eylül 1912 depremlerine ait 73 adet tarihi deprem kaydı toplanmıştır. Karşılaştırılabilir kayıt çiftleri TESEO programı aracılığıyla sayısallaştırılmıştır. Elde edilen deprem sinyallerinin modellenmesi ve ters çözümlenmesi sonucunda 9 Ağustos ve 13 Eylül depremleri için göreceli kaynak zaman denklemi elde edilmiş ve 9 Ağustos depreminin kaynak süresinin 40 saniye olduğu tespit edilmiştir. 3 km/sn'lik, tek yönlü doğrusal bir kırık ilerlemesi kabul edildiğinde bu süre 120 ± 20 km'lik bir fay uzunluğunda karşılık gelmektedir ki bu değer depremin büyüklüğüyle ($M_w$=7.4) uyumludur. 5 istasyona ait P-dalgası ilk varış analizi ve saha çalışmalarından elde edilen K68°D'luk ortalama doğrultu kullanılarak 9 Ağustos 1912 depremi için ilk olarak bir odak mekanizması çözümü önerilmiştir.

13 Eylül 1912 depreminin büyüklüğü 30 ± 10 km'lik bir kırığı gerekli kılmaktadır. Ayrıca, bu deprem 9 Ağustos yüzey kırığı için bir batı sınır teşkil etmektedir. Her iki depremi ve ikinci şok için önerilen merkez üstünü dikkate aldığımızda, toplamda 150 ± 20 km olan kırık uzunluğu batıdan Saroz çukurundan başlayarak Orta Marmara Havzasına kadar uzanmaktadır. Bu iki havza aynı zamanda fay üzerindeki en büyük geometrik engellere karşılık gelir. Bu durumda, Marmara denizi içindeki 9 Ağustos 1912 depreminin doğu ucuyla 1999 depreminin batı ucu arasında en az 100 km'lik bir sismik boşluk olduğunu söylemek mümkündür. Bu boyuttaki bir sismik boşluk en az 7 büyüklüğünde bir deprem üretme potansiyeline sahiptir. İstanbul için yapılan deprem risk analizlerinde bu asgari değer dikkate alınmalıdır.

Bu tez çalışmasından dört adet makale hazırlık aşamasındadır:

1-Aksoy, M.E., Meghraoui, M., Valleé, M., Çakır, Z, 2009, Rupture Characteristics of the 1912 Mürefte (Ganos) Earthquake Segment of the North Anatolian Fault

(Western Turkey) Geology'e gönderilmiştir. 2-Meghraoui, M., Aksoy, M.E., Akyüz, S., Ferry M., Dikbaş, A., Altunel E., Paleoseismology of the North Anatolian Fault at Güzelköy (Ganos segment, Turkey): Size and recurrence time of earthquake ruptures in the West Marmara Sea (hazırlık aşamasında). 3-Aksoy, M.E., Meghraoui, M., Ferry M., Dikbaş, A., Akyüz, S., Uçarkuş, G, Çakır, Z, Altın U., Sancar, T., Saki-Yaltırak, K., 2009, Paleoseismic history of the 1912 Mürefte earthquake segment of the North Anatolian Fault (Western Turkey) (TJES için hazırlık aşamasında). 4-Aksoy, M.E., Meghraoui, M., Çakır, Z, Ferry M., Uçarkuş, G, 2009, A 20 kyr slip rate history deduced from stream offset along the Ganos fault segment of the North Anatolian Fault (Western Turkey) (EPSL için hazırlık aşamasında).

## 1. INTRODUCTION

Large continental faults generate large earthquakes that produce significant surface ruptures and coseismic displacement. The North Anatolian Fault is one of the most remarkable strike slip fault systems in the world which generated 8 large earthquakes (M > 7) in the last 70 years. The seismic sequence from 1939 to 1999 ruptured nearly 1100 km of the fault system and showed a westward migration pattern from Erzincan towards the Sea of Marmara. Each earthquake was associated with large surface ruptures and co-seismic displacement exposing evidently the segmentation and slip characteristic of the fault system. This recent seismic activity revealed invaluable information about large continental strike-slip fault system and turned the North Anatolian Fault to an open-air laboratory for active tectonic studies. Detailed field investigations incorporating quantitative geomorphology, earthquake geology and paleoseismology along the exposed fault segments can provide access to seismic parameters and the size of the earthquakes. Furthermore, an integration of seismology to field based results can widen our understanding of fault behaviour and earthquake occurrence. These methods have been widely applied along major fault systems within different tectonic domains (McCalpin, 1996; Keller & Pinter, 1996; Yeats et al., 1997).

The North Anatolian Fault is one of best rupture zones to study earthquake geology and paleoseismology because the rupture morphology and co-seismic slip of the 1939-1999 seismic sequence is still accessible. In addition, the historical seismicity is well documented within the long archaeological history of Anatolia (Ambraseys, 1970, Ambraseys & Jackson, 1998) and allows constraining the timing of faulting events identified in paleoseismic trenches. Trenching studies have been conducted to constrain the timing of past events and estimate recurrence intervals for several segments of the North Anatolian (Rockwell et al., 2001 & 2009; Hartleb et al., 2003; Puchi, 2006; Pantosti et al., 2008; Palyvos et al., 2007). Additionally, the rupture segments of the seismic sequence have been documented through several field investigations (Ketin, 1969; Ambraseys & Zatopek, 1969; Barka, 1996; Kondo et al., 2005)

Quantitative geomorphology analysis revealed systematic offset along the entire section of the North Anatolian Fault. Together with Quaternary dating methods slip rates ranging from 15 to 21 mm/yr have been constrained for some sections of the North Anatolian Fault (Puchi et al., 2008, Kozaci et al., 2007 & 2009, Hubert-Ferrari et al., 2002).

Continuous geodetic measurements through GPS networks along the North Anatolian Fault quantified the westwards movement of the Anatolian block and yield velocities from 17 to 26 mm/yr (Kahle et al., 1998; Straub et al., 1997; McClusky et al., 2000; Reilinger et al., 1997 & 2006).

Following the 1999 earthquakes, studies on the active tectonics of the North Anatolian Fault increased drastically. A large number of studies presented the 17 August Izmit and the 12 November Düzce earthquake source characteristics and related ruptures (Bouchon et al., 2000 & 2002; Barka et al., 2002; Akyüz et al., 2002, Lettis et al., 2002, Langridge et al., 2002, Hartleb et al., 2002, Pınar et al., 2001; Tibi et al., 2001; Aydın et al., 2002; Ergintav et al., 2002; Gülen et al., 2002; Sekiguchi et al., 2002; Rockwell et al., 2002). The Sea of Marmara has been intensively investigated during several cruises and a wealth of multi-beam bathymetry data and seismic reflection data have been collected in these cruises (Armijo et al., 2002 & 2005; Le Pichon et al., 2001 & 2003; Imren et al., 2001; Gazioğlu et al., 2002). The offshore extension of the North Anatolian Fault in the Sea of Marmara is know well documented and exhibits complex fault geometry associated with several segments and branches. Studies on the offshore extension of the 1999 earthquake in the Sea of Marmara allowed locating the western termination of the related rupture (Uçarkuş et al., 2006 & 2008)

A large earthquake postdating the seismic sequence occurred on 9 August 1912 (M 7.3) and ruptured the westernmost 45-km-long onland section of the North Anatolian Fault (Ambraseys & Finkel, 1987; Altunel et al., 2004; Altınok et al., 2003). Historical documents on the 1912 event report significant surface ruptures along the entire onland section (Macovei, 1912, Sadi, 1912, Mihailovic, 1927, 1933). However many parameters such as the rupture length, total slip, fault geometry and source characteristics remain poorly known. The 1912 and the 1999 earthquake ruptures limit a seismic gap, which is expected to produce a large earthquake near the metropolis Istanbul and surrounding area (Hubert-Ferrari et al., 2000). Hence, the

seismic parameters of the 1912 Mürefte earthquake are essential to evaluate the hazard in the Marmara region. During this study we used quantitative geomorphology, earthquake geology, paleoseismology and seismology in order to constrain the characteristics of the 1912 event and the related fault section; the Ganos fault.

The Ganos fault segment experienced several destructive earthquakes during its history. Successive earthquakes left behind significant traces in morphology and geology. These traces indicate the long term and short term deformation of the Ganos fault. This study aimed to investigate the structural and tectonomorphic characteristics of the Ganos fault and documented the co-seismic deformation related to the 9 August 1912 Mürefte earthquake; as well as its source characteristics. The entire onland fault zone has been mapped at a 1/25.000 scale using field observation and remote sensing software and data. Step-overs, pull-aparts, bends, and pressure ridges, which are typical structures of right lateral strike slip faulting have been documented all along the fault. We measured co-seismic and cumulative displacement at several localities. In addition we used paleoseismic trenching to constrain the timing of past faulting events and correlated events with historical seismic catalogues. Finally we collected historical seismograms of the 1912 earthquakes in order to apply modelling and deconvolution of seismic waveforms and retrieve earthquake rupture properties, focal mechanism and related seismic moment for the 9 August 1912 shock, which are parameters either incomplete or inconsistent among prior studies.

This thesis consists of eight (8) chapters:

Chapter 1 explains the objective of the study and gives reasons why the Ganos fault and the 1912 earthquake has been chosen as the research area and event. Some basic information of the region, such as the general geological setting and the geographical properties are shortly given within this part. The final part of the chapter summarizes the structure of the manuscript.

Chapter 2 focuses on the methods applied during this study. The theoretical aspects of active tectonic studies and principles of seismotectonics, tectonic geomorphology and earthquake geology are given with example studies. Paleoseismology, as a tool to investigate past earthquakes is briefly explained within this chapter. The use of

historical seismograms to constrain source characteristics of past earthquakes is given with proper examples.

Chapter 3 describes the tectonic setting and seismotectonic properties of the study area. The setting of the study area in relation to the North Anatolian Fault is clearly expressed in this part. An analysis of the historical seismicity provides an insight to the locations and affects of the major earthquakes of the Marmara region. The present day seismicity is given in this chapter to show the spatial distribution of the active deformation. Prior studies concerning GPS, paleoseismology and geology of the Ganos fault segment are summarized as well in this section.

Chapter 4 gives information about the tectonic geomorphology of the onland section of the Ganos fault. Descriptions of morpho-tectonic structures from large scale to small scale are given within this section. Studies concerning the long- and short-term deformation characteristics of the site are explained in detail. Mapping, drainage analysis, cumulative offset measurements, tectonic reconstructions, fault structures and segmentation characteristics are explained in this chapter. Determined cumulative offset have been dated using climatic fluctuations and yield a slip rate for the last 20 ka for the westernmost part of the North Anatolian Fault.

Chapter 5 presents our findings about the 9 August 1912 Mürefte earthquake. The collected historical documents are briefly described. The seismic activity and related damage distribution is briefly given. Details of the earthquake rupture, its geometry and related co-seismic slip are summarized within this chapter. The segmentation characteristics, potential fault barriers along strike and estimations for possible rupture length are discussed as well in this part.

Chapter 6 summarizes the paleoseismic investigation along the Ganos fault segment. Three sites, Güzelköy, Yeniköy, and Yörgüç have been excavated to determine the historical earthquakes of the Ganos fault. The stratigraphy and earthquakes determined in the trenches are given in detail. Measurements of offsets by micro-topographic surveys are included in this chapter. A comparison of trenching results and the seismic history of the region underlines the possible recurrence intervals of the Ganos fault.

Chapter 7 explains the historical seismogram study. The purpose of such an analysis, the procedure of seismogram collection, digitization and necessary corrections on the

signals are explained in this part. The results of the signal processing are given at the end of the chapter.

Chapter 8 summarizes all results obtained for the Ganos fault section and the 1912 earthquake. The new inputs of the study with regard to active tectonic studies along the North Anatolian Fault are emphasized. The proposed dimensions for the 1912 event are considered in relation to the earthquake hazard in the Marmara region. Problems encountered during the study and possible solutions are discussed for better perspectives for future investigations.

The present thesis was carried out in the frame of the co-supervisor program between Istanbul Technical University – Eurasia Institute of Earth Sciences (ITU) and University of Strasbourg - Institute de Physique du Globe Strasbourg (UMR 7516) with the support of the French Embassy in Ankara and the CROUS in France. In addition the study was founded by the European Union project "Large Earthquake Faulting and Implications for the Seismic Hazard Assessment in Europe" - RELIEF (Contract EVG1-2002-00069) and the ITU Scientific Research Program.

# 2. METHODOLOGY

The North Anatolian Fault is a major seismic source generating large disruptive earthquakes in Turkey. Identifying the characteristics of such a seismic source is a critical task in defining the earthquake risk in Turkey. A seismic source is usually defined in terms of displacement, rupture length, deformation mechanism (strike-slip, normal, reverse, or a combination of these), geometry and kinematics of associated fault segments, and slip rate (Meghraoui, 2001). The large earthquakes in Turkey are related particularly to strike-slip faults. Therefore, understanding features of strike-slip faulting and how they produce earthquakes is important.

## 2.1. The Physics of Earthquakes

### 2.1.1. The rupture process

The elastic-rebound theory is the first satisfactory explanation build by Reid (1910) on the occurrence of earthquakes. The idea is simply based on that earthquakes are a sudden release of elastic strain energy in the rocks on either side of the fault which is stored during a interseismic period. The energy is stored while plates (blocks) move relative to each other but are actually locked by roughness and asperities along a fault (Fig 2.1). The continuous far field plate motions cause the rocks in the region of the locked fault to accumulate elastic deformation and induce a sigmoidal bend perpendicular to the fault (Fig 2.1-Time 2). When the accumulated strain exceeds the strength of the rocks an earthquake occurs and near-field coseismic deformation catches up the far-field interseismic deformation within a few seconds (Fig 2.1-Time 3). The stored energy is released during the rupture as heat, rock damage and elastic waves. The Reid model supposes that plate movement in other words deformation is constant from event to event and suggests that earthquakes occur periodically with similar magnitude.

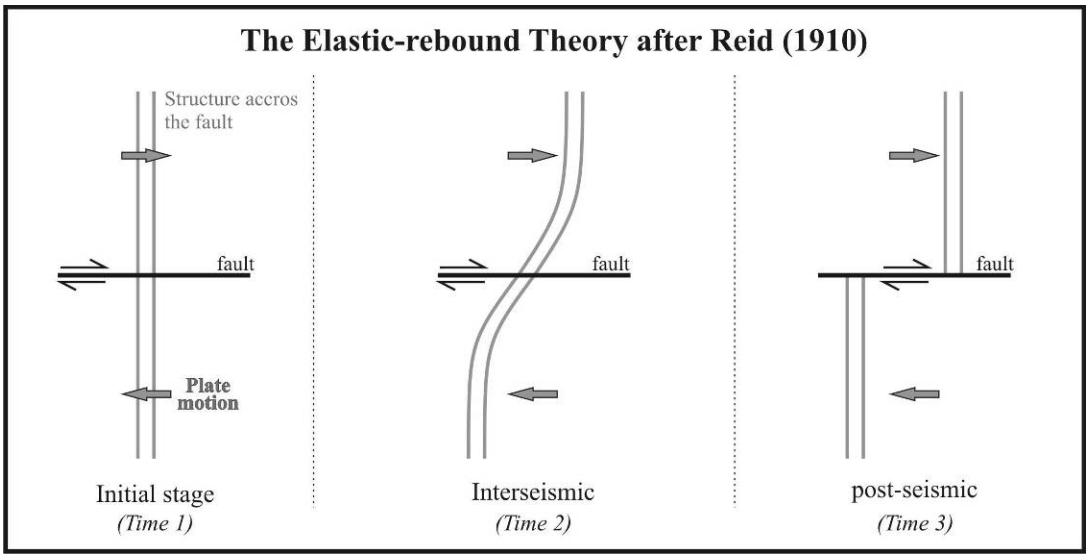


**Figure 2.1 :** The elastic-rebound theory explains how the elastic strain energy is accumulated in rocks on the two sides of a fault (Reid, 1910; see text for detail).

### 2.1.2. Earthquake occurrence

The Reid's model puts forward a perfectly periodic model whereby the stress drop and magnitude of each event are the same, and the stress build-up in time is constant. Two other models suggested by Shimazaki & Nakata (1980), predict an earthquake based on the stress threshold at which failure either occurs or stops. In the time-predictable model the stress threshold at which failure occurs is constant and a prediction is possible when the slip of the previous event is known. Assuming a constant slip rate and using the co-seismic slip of the previous earthquake the timing of when the stress threshold will be achieved can be calculated, but not its slip or magnitude. In the slip-predictable model the stress threshold which failure stops is known and constant, but the stress level where earthquakes occur is variable. Therefore the time of the earthquake can not be calculated, but its slip (using the elapsed time since the previous earthquake and a constant slip rate). The most important difference between Reid's and Shimazaki & Nakata's models lies on the characteristics of each event within a sequence of earthquakes. The Reid model suggest that earthquake along a fault segment occur perfectly periodic with similar slip and magnitude, whereas the Shimazaki & Nakata's models consider that earthquake occur non-periodic and can be at different size (and different co-seismic slip) along the same fault segment.

### 2.1.3. The characteristic earthquake concept

Models considering the slip variation along the fault length were discussed by Schwartz and Coppersmith (1984). They suggested three possible models for co-seismic slip along a fault segment. The first model, called Variable Slip model considers variable earthquake segments length and slip (Fig 2.2a). Earthquakes may occur at different magnitudes, but the cumulative slip deficit is always completed by subsequent events. The second model is the Uniform Slip Model, where large earthquakes are uniform in size, co-seismic slip and rupture length and the cumulative slip is levelled by moderate earthquakes ($5.5 < M < 6.5$; Fig. 2.2b). The third model is the Characteristic Slip Model in which earthquake size is constant producing a uniform slip pattern along definite rupture length. It should be noted that the characteristic earthquake model impose a variable cumulative slip rate along the fault (Fig. 2.2c). Therefore it is suggested that ruptures on adjacent fault segment may overlap (dashed lines in Fig. 2.2c) to fill the slip deficit. Another model, the Patch Model was introduced by Sieh (1996) whereby large earthquake are also of characteristic type, but differently the variable total displacement is levelled by moderate earthquakes producing local fault segments (or patches) with limited co-seismic slip (Fig. 2.2d)

The significance of the models b, c and d is that they allow predicting the approximate time and size of future earthquakes under constant slip rates, if detailed data of the previous large event is available. Therefore any significant earthquake should be studied in great detail in terms of earthquake geology and seismology. Such a dataset would also test suggested models and will improve our understanding of fault behaviour and earthquake occurrence.

### 2.1.4. The size of an earthquake; Seismic Moment and Magnitude

The seismic moment is a physical measure to quantify the size of an earthquake. It is defined by the equation

$M_0 = \mu S U \; dyne\; cm$ (Aki 1966) **(2.1)**

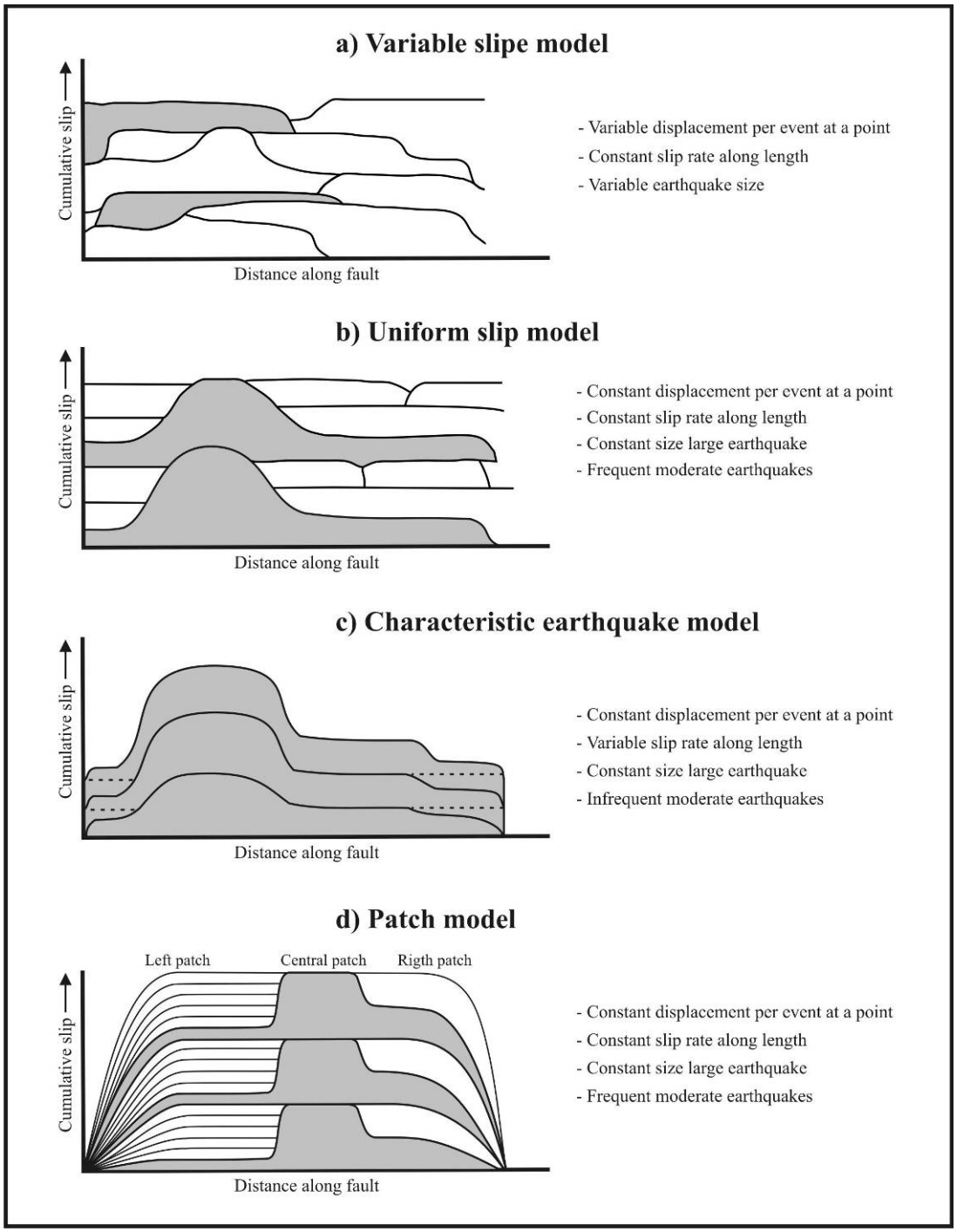


**Figure 2.2 :** Suggested models considering the variation of slip along a certain fault segment. Models a to c are from Schwartz & Coppersmith (1984), while model d is taken from Sieh (1996).

where μ is the shear modulus of the rocks involved in the earthquake (a constant ~ 3 x $10^{11}$ dyne/$cm^2$), *S* is the area of the rupture along the geologic fault, and *U* is the average displacement of the ruptured area *S*. The seismic moment is calculated from seismograms using long-period seismic waves. However, comprehensive field data may also allow constraining the moment using rupture length, the depth of

aftershocks (which define the depth of the seismogenic zone) and the average displacement observed on the surface. The critical part in this estimation is to consider that surface slip distribution is not equal to the distribution in the depth, but connected.

As mentioned before, earthquakes are a sudden release of stored strain energy in the rocks. The measure of the released energy is defined as the moment magnitude, symbolize as $M_w$ meaning "mechanical work accomplished". The moment magnitude is dimensionless and defined as

$$M_w = \frac{2}{3} \log Mo - 10.73 \text{ (Kanamori, 1977)} \quad \textbf{(2.2)}$$

where $M_0$ is the seismic moment. The moment magnitude is the most accurate measure of energy release and is therefore worldwide used to define the size of an earthquake. The Richter (or Local) magnitude, the body wave magnitude ($m_b$), the surface magnitude ($M_s$) and duration magnitude ($M_D$) are also other measures of earthquake magnitude. However these magnitudes are based on one aspect of the related seismogram and do not capture the overall size of the source.

## 2.2. Faulting Behaviour, Fault Geometry and Segmentation

The concept of faulting behaviour involves the fact that the coseismic displacement along a fault evolves with time both locally and regionally, which concerns both temporal and spatial aspects. The characteristic earthquake model assumes the rupture geometry to be fixed in order to produce equivalent earthquakes through time. In deed, earthquake segments are limited by boundaries that correspond to major geometric complexities along the strike of a fault (Schwartz & Sibson, 1989, Barka, 1996). These obstacles arrest the rupture propagation and limit the size of an earthquake along a certain section of an active fault (Aki, 1989; Schwartz & Simpson, 1989; Zhang et al., 1999 Wesnousky, 2006). Thus it can be assumed that a fault behaves characteristically for some period in which its general geometry is preserved. As a result, the detailed study of fault geometry and structure of active fault will allow determining its segments capable of producing large earthquakes. The dimension of the segments will also provide a measure to estimate the size of the expected earthquake.

### 2.2.1. Fault geometry and segmentation

The geometry of an active faults trace at the surface is an expression of the fault's nature at depth. Hence, it indicates changes in geology or structure along the fault zone. Such asperities break up the fault plane into sub-planes (segments). These sub-planes or sections of a fault are called segments. However, the term segment is used at a variety of scales. A segment can define the total length of a historical rupture along a large fault zone, nevertheless a sections of a surface rupture with individual characteristics. Alternatively were no historical earthquake rupture is evident, segments can be defined based on static geologic or structural criteria McCalpin, (1996). To avoid any ambiguity it is essential to follow a consistent terminology. Therefore we follow the terminology suggested by McCalpin (1996) for fault segments (Table 2.1). In addition, we use the term sub-segment to define sections along an earthquake segment (rupture), which shows distinct differences in geometry, slip and orientation.

**Table 2.1 :** Types of Fault segments and the characteristics used to define them (McCalpin, 1996)

| Type of segment | Characteristics used to define the segment | Likelihood of being an earthquake segment |
|---|---|---|
| 1. Earthquake | Historic rupture limits | By definition 100% |
| 2. Behavioural | 1) Prehistoric rupture limits defined by multiple, well-dated paleoearthquakes. | High |
| | 2) Segment bounded by changes in slip rates, recurrence intervals, elapsed times, sense of displacement, creeping versus locked behaviour, fault complexity. | Mod (26%) |
| 3. Structural | Segment bounded by fault branches, or intersections with other faults, folds, or cross-structures. | Mod.-High (31%) |
| 4. Geologic | 1) Bounded by Quaternary basins or volcanic fields. | Variable (39%) |
| | 2) Restricted to a single basement or rheologic terrain. | |
| | 3) Bounded by geophysical anomalies. | |
| | 4) Geomorphic indicators such as range-front morphology, crest elevation. | |
| 5. Geometric | Segments defined by changes in fault orientation, step-overs, separations, or gaps in faulting. | Low-Mod. (18%) |

The segmentation of faults, particularly strike-slip faults occur through discontinuities called step-overs and bends along strike. A step-over consists of two fault planes (segments) which are not directly connected to each other. On the other

hand, a fault bending is a continuous fault plane with significant change in orientation; in other words strike. Along a right lateral strike slip fault left stepping bends of step-overs form restraining structures, whereas right stepping geometries produce releasing structures. The releasing or restraining nature of these changes forms several structures and morphologies at various scales; i.e. pull-apart basins, releasing basins, sagponds, relay ramps, mountains, pressure ridges and mole tracks. Some large scale tectonic structures related to releasing and restraining geometries are illustrated in Figure 2.3 (Cummingham & Mann, 2007).

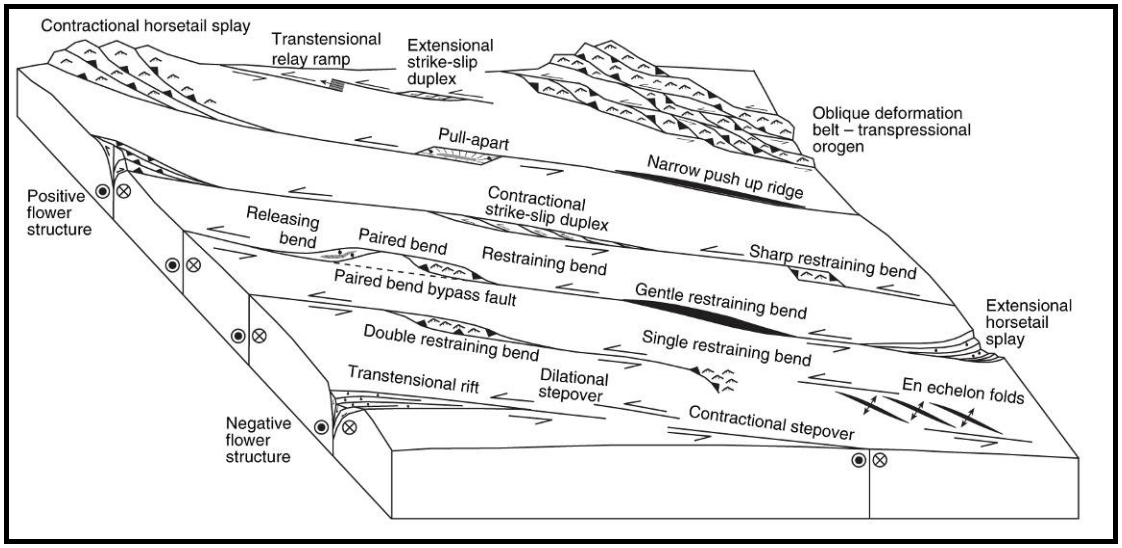


**Figure 2.3 :** Tectonics feature along strike slip restraining and releasing bend and step-overs (Cummingham & Mann, 2007).

# 3. SEISMOTECTONIC BACKGROUND OF THE MARMARA REGION

The Ganos fault is a segment of the North Anatolian Fault (NAF) and is located between the Marmara Sea and the Aegean Sea. Only about a 45-km-long section of the Ganos fault is onland, the rest being offshore in the Marmara Sea and Aegean Sea. The segment is situated next to a transition zone between pure right-lateral tectonics and Aegean N-S extensional tectonics. The structural and tectonic characteristics of this segment play a significant role to evaluate the existence of an interaction between the two tectonic regimes in that region. The GF ruptured in 1912 causing considerable damage and surface faulting. This section determines an important earthquake segment of the 1500-km-long transform fault of Anatolia. Hence, the attitude of this segment signifies the seismic hazard in the Ganos-Tekirdağ region.

This chapter addresses the geologic evolution, present day tectonics and seismicity of the main land where the NAF and Ganos fault are located (from regional scale to local scale, respectively). The seismic and geologic characteristics of the major earthquakes along the NAF will be discussed for comparison in the Ganos region. Finally, an introduction to the regional geology, morphology, paleoseismology and seismology of the Marmara region and particularly the Ganos site will be provided.

## 3.1. Tectonic Setting

The Ganos fault is the westernmost section of the North Anatolian Fault Zone (NAFZ), one of the most active and large strike-slip fault systems in the world. The 1500-km-long, arcuate fault system forms a major continental plate boundary between the Anatolian plate and the Eurasian plate and takes up the relative motion among the two plates (Fig. 3.1). The NAF extends from the Karlıova triple junction in East Anatolia to the Aegean Sea in the West and its right lateral movement occurs predominantly through a fault zone of few hundred meters to 120 km width. Several large earthquakes have been recorded since historic time causing severe damage to the urban areas along this fault.

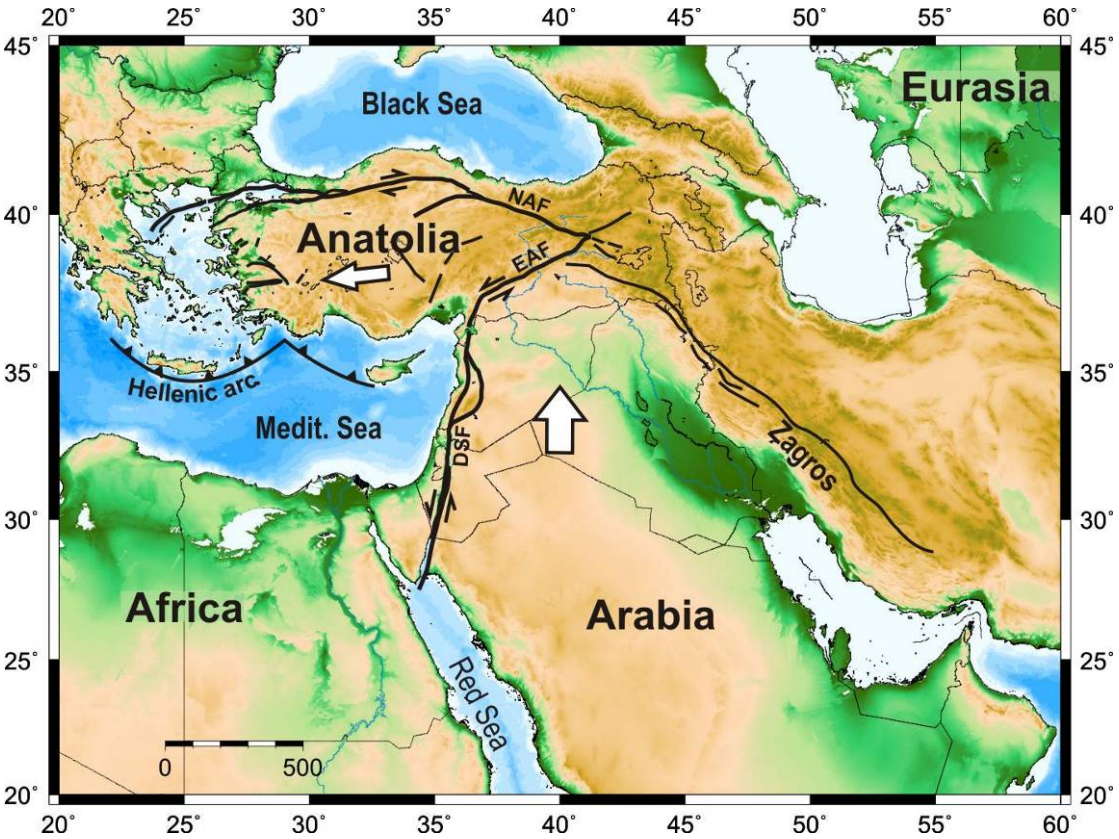


**Figure 3.1 :** Tectonic setting of Eastern Mediterranean and Middle East where the Arabian, African, Eurasian and Anatolian plates meet. The northward movement of the Arabian plate along the Dead Sea Fault (DSF) causes the Anatolian plate to escape westwards via the right-lateral North Anatolian Fault (NAF) and the left-lateral East Anatolian Fault (EAF).

### 3.1.1. Tectonic evolution of Anatolia

The NAF forms the northern boundary of the Anatolian block, which exposes a composite geology and signifies a complex geologic history. The Anatolian plate experienced a series of continental collisions starting in the Late Palaeozoic. Two oceans, the Palaeo-Tethys and Neo-Tethys, were demised between the two large continents of Gondwana to the south and Laurasia to the north (Fig. 3.2; Şengör and Yılmaz, 1981; Okay and Tüysüz, 1999). A N-S convergence caused the closure of the Palaeo-Tethys and amalgamated the surrounding continental fractures to a main land. Together with relics of oceans, different continental fragments joined together to form the primordial Anatolian block. Nevertheless, until the end of Oligocene the Neo-Tethyan Ocean existed partly as a narrow strait between the Arabian platform and southeast Anatolia (Okay, 2008). The Neo-Tethys entirely disappeared in Miocene, when the Arabian and the Anatolian plates finally collided along the

Assyrian-Zagros suture (Fig. 3.2). The closure initiated a new tectonic regime in the eastern Mediterranean, particularly for Anatolia. The continent-continent orogeny caused crustal thickening and uplift in eastern Anatolia. By early Pliocene the contractional tectonic regime evolved into the westward extrusion of the Anatolian block. The westward movement was and is still accompanied by two intracontinental transform faults; the right-lateral NAF and the left lateral EAF (Fig. 3.1; Hempton, 1987; Şengör and Kidd, 1979; Şengör et al., 1985; Yılmaz, 1993; Barka, 1992; Bozkurt 2001).

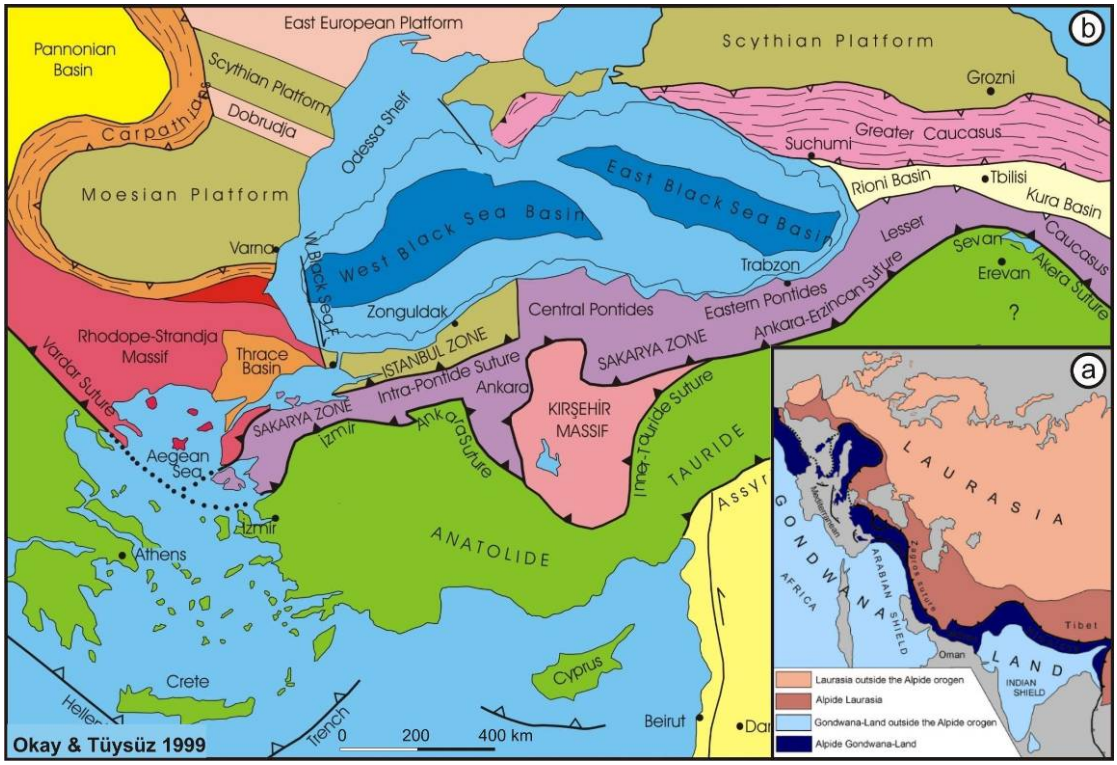


**Figure 3.2 :** Paleotectonic maps of Turkey and surrounding regions (Okay, 2008). a) The location of the Anatolian plate with regard to the large contintents Laurasia and Gondwana. The location of the Anatolian plate is in the central part of the Alpide-Gondwana Land (dark blue) south of the Black Sea. b) The Anatolian plate consists of several continental fragments (e.g. Pontides, Istanbul Zone, Kırşehir Massif, Anatolide-Tauride block) surrounded by continuous suture zones (e.g. Intra-Pontid suture, Izmir-Ankara-Erzincan suture).

The complex tectonic background of Turkey is exposed inland as suture zones (representing the abducted oceanic lithospheres) and several continental fragments between these sutures. Six main tectonic units and suture zones constitute the fundamental geology of the Anatolian plate; the Pontides, the Anatolides-Taurides, the Arabian Platform and the Bitlis-Zagros suture, Izmir-Ankara-Erzincan suture and

the Intra-Pontid suture (Fig. 3.2; Ketin, 1966). In the Marmara region the Intra-Pontid suture constitutes the boundary between two continental domains; the northern Istanbul Zone (Western Pontides) and the southern Sakarya Zones. Towards east, the Izmir-Ankara-Erzincan suture forms the boundary between the Sakarya zone and the Anatolide-Tauride domains (Şengör and Yılmaz, 1981, Okay and Tüysüz 1999, Okay 2008). This geologic background affects the setting of the two major fault systems in Anatolia; the North Anatolian Fault System and the East Anatolian Fault System.

## 3.2. The North Anatolian Fault Zone

The NAFZ starts at the Karlıova triple junction in the east, and runs roughly NW direction to Vezirköprü, where it makes a bend and continuous WSW until Bolu. West of Bolu, the NAF splays into two major strands: 1) The northern strand strikes through the major basins in Marmara Sea, runs westwards crossing the Ganos Mountain and diminishes west in the Aegean Sea. This section is the most active strand and experienced three earthquakes M>7 in the 20th century (including the 1912 Mürefte shock). 2) The southern strand runs WSW direction west of Bolu, crosses the south of the Iznik bay and the Marmara Sea, makes another left bend near Erdek and runs in SW direction into the Aegean Sea. The southern branch lacks evidence of a significant earthquake history. The only well known event is the 18 March 1953 Yenice-Gönen earthquake ($M_w$ 7.2) causing surface faulting of about 70 km along this branch (Pınar, 1953; Kürçer et al., 2008).

The location of the NAF is close to the boundary of the aforementioned Pontides and Anatolides. However, the largest section of the NAFZ does not follow the sutures zone. It is rather semi parallel to the Ankara-Erzincan suture and Intra-Pontid sutures and cuts the sutures twice; at Erzincan and Suşehri (Şengör, 1979; Barka, 1992).

### 3.2.1. The Onset and Offset of the North Anatolian Fault

The onset and total offset of the NAF is controversial because the total amount of slip along the fault and the ages of the related structures are not well constrained. The reason for the uncertainty comes from the geologic configuration described above, which comprises the Pontides and the Anatolide-Tauride blocks and is quite complex. Therefore, correlations of older geologic units can easily mislead and

demand comprehensive mapping. Nevertheless, many studies yield comparable results on the onset and the total offset of the NAF.

The discrepancy concerning the age of NAF is fairly low compared to the total displacement. The onset of the fault is mostly in agreement, which is sometime between the late Miocene and the early Pliocene, following the collision between the Arabian and Anatolian plates. Ketin (1948), providing one of the first comprehensive studies of the NAFZ, wrote that the NAF disrupted orogenic structures of Turkey, and concluded that the fault must have begun in the Neogene (15-20 Ma ago; Ketin, 1957). In a later study he pointed that, the basins fills along the fault are no older than Middle Miocene, indicating the NAF did not create a distinct morphology prior to this time (Ketin, 1976). Erinç (1973) suggested that the original drainage network around the fault zone was formed by Late Miocene and shows a distinct influence of fault activity. Therefore, he concluded that the network necessarily predates the formation of the NAF. Seymen (1975) showed that the NAF displaces the Ankara-Erzincan suture and consequently it has to post-date the suture of Burdigalian age. Koçyiğit (1989) studied the Suşehri basin and pointed out that the Pliocene basin fills rest unconformably on Burdigalian age deposits and concluded that this would imply that the basin was formed during a new tectonic regime, post dating Burdigalian (Late Miocene). Şengör (1979) stated that the Arabian-Eurasian collision started in Late Miocene, right after the closure of the Bitlis Ocean. Considering the well fit with the models of McKenzie (1972) and Dewey & Şengör (1979) he deduced and that the NAF initiated right after the collision (Late-Middle Miocene). Hempton (1987) suggested a broader time frame, sometime between Early Miocene and Early Pliocene, for the commencement of the fault zone.

Other studies proposed a younger age for the NAF where they considered that a wide shear zone evolved first in Late Miocene (Barka and Hancock 1984, Barka 1985, Barka and Gülen 1988, 1989) and developed afterwards into a main fault plane in the early Pliocene (Barka 1992). Barka & Hancock (1984) suggest 25 km right lateral displacement since Tortonien based on a sedimentary facies boundary in the Havza-Ladik Basin. Studying the Tosya and Kargı basins, Andrieux et al. (1995) concluded that the deformation along this section of the NAF was widely distributed during the Upper Neogene-Pleistocene and that a more localized fault zone was developed only after Late Neogene.

Fault propagation theories were also proposed for the evolution of the NAF. Gautier (1999) suggested that the fault zone developed first in the east 16 Ma ago, propagated westwards and reached the Marmara after 3 Ma. According to Şengör et al (2005) the NAF formed in Serravallian (13-11 Ma ago) in the east, propagated westward and reached the Marmara no earlier than 200 ka ago. This inference is based on the observation that on the east basin fills are as old as late Miocene, whereas in the Sea of Marmara, basins are younger than Pleistocene. However, the Pleistocene age for the 2 to 3-km-thick Marmara basin fills (Carton et al 2007) is extrapolated from sedimentation rates obtained from one 40-m-long shallow drilling, which yield a rate of 40 ka (1 m/ka).

Slip measurements along the NAF yield a wide range of results, such as 7.5 km to 300 to 400 km (Hece and Akay, 2001). The largest total slip proposed is about 350 to 400 km, which is actually based on an erroneous correlation of volcanic units of different age and origin (Cretaceous-Eocene and Mio-Pliocene volcanics; Pavoni, 1962). The first well defined total displacement was measured by Seymen (1975), where he proposed ~85 km right-lateral displacement along the Ankara-Erzincan suture near Erzincan. This is the same result measured by Bergougnan (1975) along the suture. Barka et al (2000) calculate a comparable offset of ~80 km based on the total lengths of the Taşova–Erbaa and Niksar basins along the North Anatolian fault. Lower values of slip were measured by Barka & Hancock (1984). They measured 25 ± 5 km of right-lateral displacement on the Miocene sediments in the Havza-Ladik basin. A re-evaluation of the displacement of some geologic and geomorphic markers yield comparable results on three structures (Hubert-Ferrari, 2002); 1) large river valleys (80 ±15 km), 2) the Pontide suture 85 ± 25.3) Tosya-Vezirköprü basin (80 ± 15 km). Şengör et al. (2005) outlined a number of offsets, which he considered to be the most reliable measurements and draw attention to the decrease in total slip towards west. The estimations ranged from 4 km to 75 km (Armijo et al. 2002; Barka & Gülen, 1989; Gaudemer et al., 1989; Herece & Akay, 2003; Hubert-Ferrari et al 2002; LePichon et al, 2003; Şengör et al., 2005). Barka (1992) observed the same characteristic and wrote that offsets decrease from east to west, from 40 ± 5 km to 25 ± 5 km respectively and increase again in the Marmara region. However, these observations are contradictory with the 70-km-long dextral offset proposed by Armijo et al, (1999) for the westernmost section of the NAF. Armijo et al. (1999)

indicated the presence of two truncated anticlines (Ganos Mountain and Gelibolu peninsula) apart for ~70 km and covered unconformably by flat lying deposits of 5 Ma age in the south. Accordingly he inferred that these units post-date the deformation, hence the offset. However the age and structural constrains of this observation are disputed by Yaltırak et al. (2000).

As summarized above, the age and total offset of the NAF are still not well constrained and require further investigation. However, it can be deduced that the maximum slip along the NAF is about 80 km and is probably decreasing towards west. In addition the initiation of a main fault zone started most probably at Late Pliocene following the Arabian-Eurasian collision.

### 3.2.2. Present Day Kinematics of the NAF

The NAF is the largest and most active strike slip fault in the eastern Mediterranean region. The right lateral motion of the fault is actually interrelated with the present-day tectonics of a large region, encompassing the Eurasia, Africa, Arabia, Anatolia and Aegean region (Fig. 3.1). The African and Arabian plates move northwards in a complex tectonic system accompanied with the Red Sea Oceanic Rift System and cause a continent-continent collision between the Arabian and Anatolian plates along the Bitlis-Zagros Mountain Chains (Şengör, 1979). This tectonic setting forms three major fault systems in eastern Mediterranean. The Dead Sea Fault (DSF), EAF and NAF. Together with the EAF, the NAF forms the plate boundaries of the Anatolian block. The two fault systems accomplish the lateral escape of the block to the west (Ketin 1948). In addition, the subduction of the eastern Mediterranean oceanic lithosphere along the Hellenic trench results in widespread extension the Aegean and western Turkey (McKenzie, 1970, 1972).

GPS measurements in the eastern Mediterranean region indicates an anticlockwise rotation of large region comprising the Aegean, Arabian and the Anatolian plates about an Euler Pole near to the Nile Delta (McClusky et al., 2000). The rotation of the Anatolian block occurs along a small circle of that pole, which conforms the NAF (Fig. 3.3, Le Pichon et al, 1995; McClusky et al., 2000, Reilinger et al, 2006). The mean motion along the NAF is measured as ~ 24 mm/yr (Straub et al 1997; Reilinger et al, 1997; McClusky, 2000). However the slip rates show an increase

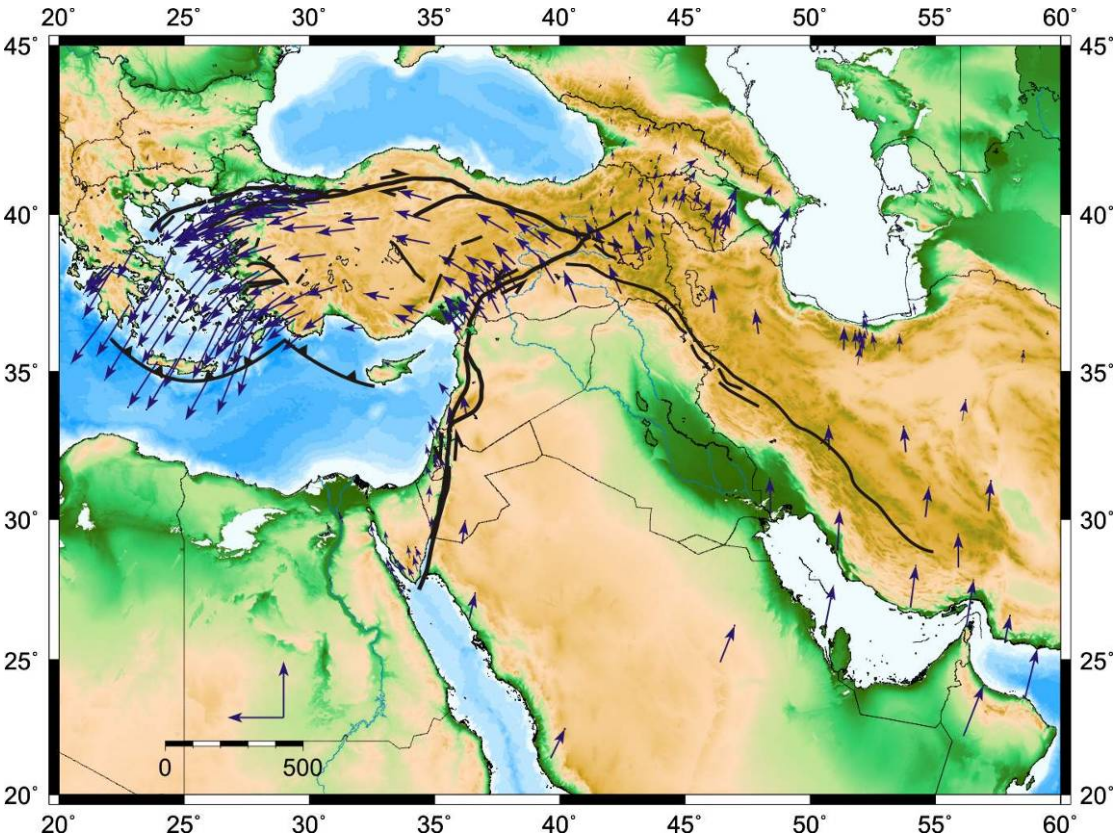


**Figure 3.3 :** The GPS velocity field relative to Eurasian reference frame in the eastern Mediterranean region shows an anticlockwise rotation of a large region, compromising the Arabian, Zagros, Anatolian and Aegean regions (GPS data from Reilinger et al., 2006). GPS velocities along the NAF present also an increase from east to west.

from east to the west, from 20.6 ± 0.8 mm/yr to 24.6 ± 1.0 mm/yr (Reilinger et al, 2006). The increase is thought to be due to the slab suction along the Hellenic subduction zone in the Aegean Sea (Reilinger et al, 2006).

The westwards movement of the Anatolian block is accomplished by successive earthquakes along the North Anatolian Transform Fault. The long history of the region documents a good seismic history since the antiquity with more than 50 disastrous earthquakes. Since 1912 the NAF alone produced 9 destructive earthquakes M>7, which occurred in a time interval between 3 months to 32 years (Fig. 3.4). The earthquake sequence since 1939 shows a significant westward migration along the fault (Toksöz et al., 1979; Barka, 1996; Barka et al., 2002). The 17 August 1999 Kocaeli ($M_w$ 7.4) and the 12 November 1999 Düzce ($M_w$ 7.2) earthquake are the most recent two shocks along the western section of the NAF (east of Marmara Sea). The historical seismicity of the Marmara Sea region is summarized in Appendix A.1.

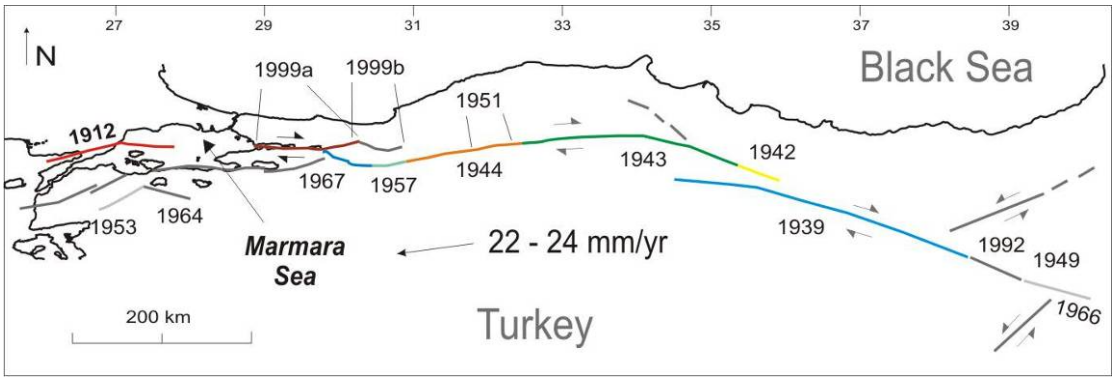


**Figure 3.4:** The seismic sequence between 1939 and 1999, ruptured ~63% of the North Anatolian Fault.

The 1939-1999 earthquake sequence ruptured in total about 1100 km long portion of the 1500-km-long NAF. If we include the 9 August 1912 earthquake ($M_s$ 7.3) rupture (Ambraseys, 2002), the length of the broken section reaches over 1200 km. This means that almost 80% of the NAF has been reactivated during earthquakes in a very short time, i.e., in about one century. Such behaviour has not been documented on any other strike-slip fault elsewhere in the world. Hence, studies on fault interactions, rupture geometry, segmentation, geometrical complexities and related earthquake activity of these events provide unique and invaluable information to estimate rupture nucleation and termination points along major strike-slip fault of the world.

### 3.2.3. The Earthquake Fault Segments of North Anatolian Fault

Below is a summary of the rupture characteristics of the 1939-1999 earthquakes that provides crucial hints in understanding the rupture characteristics of the NAF and evaluating the 9 August 1912 earthquake.

**The 26 December 1939 Erzincan earthquake ($M_s$ 7.8)** is the first and the largest event in the sequence, and gave rise to the longest surface rupture (i.e., ~360 km) ever recorded along the NAF (Fig. 3.5). Surface faulting produced right lateral offsets as much as 7.5 m. The epicentre was located west of the Erzincan Basin at a restraining bend of 10-20° (Dewey, 1976). The rupture initiated there and propagated bilaterally about 330 km to the west and 30 km to the east. The surface rupture was mostly confined to narrow valleys along continuous linear segments. Barka (1996) divided the 1939 rupture into 5 sub-segments with lengths from 50 to 100 km. The linear geometry is interrupted by 10° to 20° bends and the 2 to 4 km wide basins; Suşehri and Gölova basins respectively along the Kelkit Valley. The eastern

termination is at the 15-km-wide Erzincan pull-apart basin. To the west, the rupture runs along southern margin of the Niksar pull-apart basin and, instead of following the plate boundary northwest, it veers the west propagating in to the Anatolian block (Barka & Kandinsky-Cade, 1988; Barka, 1996, Yoshioka, 1996).

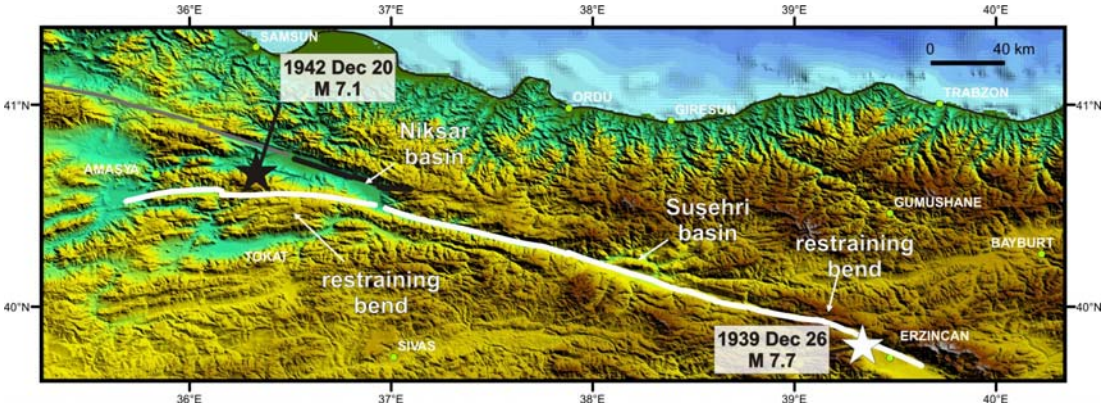


**Figure 3.5 :** The 1939 Erzincan earthquake produced nearly 360 km of surface rupture limited by the Erzincan basin on the east and by a restraining bend on the west. The 1942 earthquake ruptured along the northern limit of the Erbaa-Niksar basin.

**The 20 December 1942 Erbaa-Niksar earthquake ($M_s$ 7.1)** took place west of the 1939 event and caused a 50-km-long surface rupture, significantly shorter than the 1939 rupture (Fig. 3.5). The rupture took place along the northern boundary fault of the Niksar-Erbaa basin regarded as a lazy "Z" type pull-apart basin (Barka & Kandinsky-Cade, 1988; Barka et al., 2000; Mann, 2007). The maximum lateral displacement is measured to be 1.7 m. The extension of the surface rupture is not well constrained however it is known that it ruptured the northern margin of the Niksar-Erbaa basins consisting of 3 sub-parallel strands (Barka, 1996). The fault forms an 11° restraining bend on the east which may correspond to the eastern tip. The western tip disappears westwards within the 7-km-wide Erbaa basin. The earthquake is located north of the western bend of the 1939 rupture. The bend caused some stress localization along this section (Stein et al., 1997) that was subsequently released during this event.

**The 26 November 1943 Tosya earthquake ($M_s$ 7.6)** broke a 260 km long section of the NAF, with an epicentre near Bayramören-Kurşunlu (Fig. 3.6). The maximum right-lateral slip measured is about 4.5 m. The rupture initiated on the west and ruptured towards east. The morphology along this earthquake segment is similar to that along the 1939 segment. The fault lies in a narrow fault zone with continuous

linear segments running trough a narrow valley. Having ~1.5-km-wide releasing steps, the Kargı and Ladik basins are the two largest basins along the rupture zone. In addition, the whole rupture forms a large smooth bend by changing its strike from NW to WSW towards the west. The eastern and western tips of the rupture are located within the Erbaa Basin and the Bayramören-Kurşunlu releasing step-overs (2-km-wide), respectively. These observations show that the 1943 segment contains more structural complexities along strike compared to the 1939 segment.

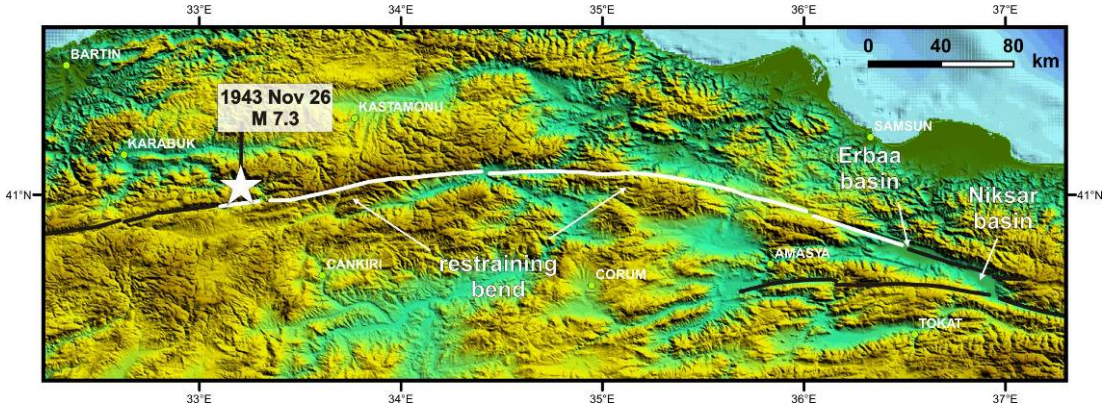


**Figure 3.6 :** The 1943 Tosya earthquake produced ~260 km surface rupture and 4.5 m right lateral slip. The rupture was limited by the Erbaa pull-apart basin on the east and by a minor step over on the west.

**The 1 February 1944 Bolu-Gerede earthquake ($M_s$ 7.3)** has an epicentre close to the 1944 shock at the eastern end of the rupture (Fig. 3.7). The total rupture length is given as 180 km ($M_s$ 7.3) with a maximum displacement of 3.5 m (Ketin, 1969; Kondo et al., 2005). The fault trace is well expressed in morphology with a narrow valley slightly wider than that observed east of the NAF. The fault is associated with basins 1 to 5 km-wide located at releasing step-overs or bends. The eastern tip of the surface breaks are located in the 2-km-wide Bayramören-Kurşunlu releasing step-over, while the western tip is at Abant Lake, where the fault forms 11° restraining bend (Barka & Kandinsky-Cade, 1988).

**The 26 May 1957 Abant earthquake ($M_s$ 7.0)** broke a 50-km-long section of the southern margin of the Almacık block (Fig. 3.7). The epicentre is given on the western end of the rupture (Dewey, 1976). The observed maximum right-lateral slip is 1.65 m. The fault consists of a continuous narrow zone. The rupture is limited on its east with the 11° bend at Abant Lake. The western termination is determined by a 1.5-km-long step-over. The westernmost 10 km of the rupture overlaps with the 1967 rupture.

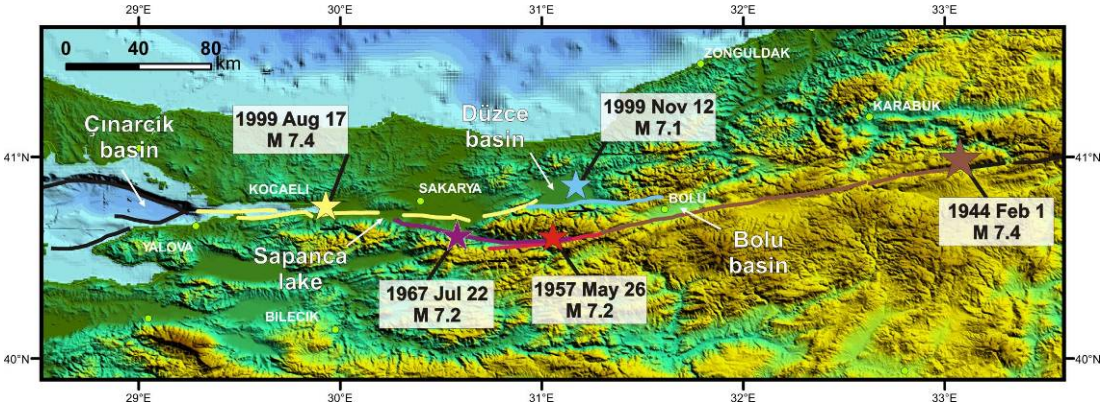


**Figure 3.7 :** Towards west the geometry of the North Anatolian Fault becomes more complex consisting of several shorter segments. Five earthquakes occurred from 1944 to 1999 exposed the dimension of these segments.

**The 22 July 1967 Mudurnu Valley earthquake ($M_s$ 7.1)** has an 80 km of surface rupture, with a maximum slip of 2.6 m (Fig. 3.7). The epicentre is located on the central part of the rupture, southeast of Akyazı. While to the east, the rupture is determined by the step-over with the 1957 rupture, to the west, the rupture diminishes within the Adapazarı basin. The fault forms a ~45° angle with August 1999 surface rupture.

**The 17 August 1999 Izmit earthquake ($M_w$ 7.4)** caused about 150-km-long surface faulting onshore and offshore (Fig. 3.7; Çakır et al., 2003; Wright et al., 2001). The epicentre was located near Gölcük, on the central part of the earthquake segment (Özalaybey et al., 2002). The maximum offset of 5.5 m was measured west of the epicentre Near the Lake of Sapanca. The rupture consists of 5 sub-segments, each 20-30 km in length (Akyüz et al., 2002; Barka et al., 2002). The sub-segments are divided by significant step-overs or bends (e.g., Sapanca Lake). Rupture termination of the 1999 earthquake coincides well with major geometrical complexities. After an abrupt change (~20°) in strike, the rupture trends NE-SW to the east of Akyazı and terminates at the entrance of the Düzce basin where the fault yet to be broken by the Düzce earthquake trends EW. Similarly, to the west, the rupture terminates at the entrance of the Çınarcık basin where the main fault makes a sharp turn towards the north following the northern boundary of the basin and forming a 40 km-wide releasing step-over in the Marmara Sea (Armijo et al., 2002, Uçarkuş et al., 2006).

**The 12 November 1999 Düzce earthquake ($M_w$ 7.1)** occurred to the west and about 3 month after the 17 August event (Fig. 3.7). The epicentre location is 5 km north of the surface rupture; ~5 km southeast from the town Düzce (Utkucu, 2003). The event

caused 60-km-long surface faulting, with a maximum displacement of 5 m (Akyüz et al., 2002; Konca et al., 2009) along the northern boundary of the Almacık block. The rupture overlapped 9 km with the August surface rupture near the Eften Lake. The eastern end terminates in the Bolu Mountains. The rupture was associated with minor complexities (e.g., two restraining step-over areas of 200 m and 500 m wide (Akyüz et al., 2002, Pucci, 2006).

**Characteristics of the Earthquakes along the North Anatolian Fault**

The earthquakes described above broke a total of 1100 km of the NAF. Each event was associated with significant surface breaks showing remarkable complexities which determine the segment boundaries and termination points of the earthquake fault segments. Almost all of the rupture termination points coincide with geometric complexities. A comparison of geometrical characteristics of these surface rupture show that geometrical complexity increases towards west (Fig. 3.5, Fig. 3.6, Fig. 3.7, Table 3.1). The 1939, 1943 and 1944 ruptures have continuous long segments (> 150 km) located in a very narrow fault zone. Basin along the fault zone are usually elongated, sub-parallel to the fault. The size of the fault jogs is usually less 3 km, except for fault termination points (Table 3.1). East of Bolu, the earthquake segments (1957 to 1999) have rupture lengths ranging from 40 to 150 km with discontinuous patches of 20-30 km long. In this region, the NAF strikes through or adjacent to large basin such as Düzce basin, Adapazarı basin and Izmit bay.

In summary, the geometry of the NAF is simpler at its east, and more complex to the west. The number, size and complexity of discontinuities increase in relation to the simplicity of the fault (the simpler the less complex). It seems that the geometrical simplicity allows larger earthquake ruptures, such as observed in 1939 and 1944 (360 and 260 km, respectively). However ruptures in the west are usually less than 150 km long.

**Table 3.1 :** Characteristics of the earthquake segments along the NAF. Rls - releasing step-over, Rts - restraining step-over, Rlb - releasing basin, Rtb – restraining basin. Values taken from Barka, 1996; [1]Barka et al., 2002; [2]Konca et al., 2009, [3]Akyüz et al., 2002.

| EQ | Ms | RL | Max Ū (H) | Max Ū (V) | Western Termination | Eastern Termination |
|---|---|---|---|---|---|---|
| **1939 Dec. 26** | 7.8 | 360 | 7.5 | 3.5 | Amasya Rstb - 24° | Erzincan B. Rls - 4-5 km |
| **1942 Dec. 20** | 7.1 | 40 | 1.7 | 0.66 | Erbaa Basin 7-km-wide | Rtb 11° |
| **1943 Nov. 26** | 7.6 | 280 | 4.5 | 1.0 | Bayramören Rls – 1.5-2 km | Erbaa Basin 7-km-wide |
| **1944 Feb. 1** | 7.3 | 180 | 3.5 | 1.0 | Abant Lake 11° Rstb | Bayramören Rls – 1.5-2 km |
| **1957 May 26** | 7.0 | 40 | 1.7 | 0.55 | Rls | ? |
| **1967 Jul. 22** | 7.1 | 80 | 2.6 | 0.9 | Sapanca Lake Fault junction | Rls |
| **1999 Aug. 17** | 7.4 | 150[1] | 5.2[1] | 2.3[1] | Çınarcık B. Halfgraben | Eften Lake Rls |
| **1999 Nov. 12** | 7.1 | 65[2] | 5.0[3] | 3.5[3] | Eften Lake Rls | Rtb |

### 3.3. The Sea of Marmara Region

The Ganos region is located on the west of the Marmara region. A thorough comprehension of the regional tectonic/geologic evolution is essential in order to better understand the characteristics of the Ganos fault. The knowledge of the Marmara region will serve as a base for our study here and thus, a summary of the characteristics of the region will be given.

#### 3.3.1. Geology of the Marmara region

The Marmara region has a complex geology consisting of several paleotectonic units. The units are separated by major structural elements such as suture zones or transform faults, and each of the units record a different geological history. They are overlain by Cenozoic deposits. To simplify the description, the geology may be divided into two sections; the lower basement units and the upper assemblage. The lower units consist of paleotectonic entities which represent the Tethyan closure. From north to south they are: the Strandja massif, the Istanbul Zone, the Intra-Pontid suture and the Sakarya zone. These entities consist of metamorphic to non-metamorphic Palaeozoic rocks at the base and Mesozoic rocks on the top. The upper

assemblage is formed by Cenozoic rocks deposited after the closure of the Tethyan Ocean and is composed mainly of marine to terrestrial sedimentary and volcanic rocks. In addition, the Sea of Marmara coasts, particularly those located south of the NAF embody an abundance of uplifted Late Pleistocene marine terraces (Sakınç & Bargu, 1989; Yaltırak et al., 2002).

### 3.3.2. Paleogeographic evolution of the Marmara Region

As described in the Anatolia's paleo-tectonic evolution, following the closure of the Intra-Pontid suture, the intracontinental convergence continued during the Miocene and caused both uplift and erosion in the region. Fluvio-lacustrine conditions were dominant following this time in the Biga Peninsula and Thrace Basin (Görür et al., 1997). The Marmara region experience two stages of extension since the middle Eocene. The first stage corresponds to the opening of the Thrace basin; the second stage is related to the NAF.

### 3.3.3. Regional Morphology

The terrain around the Sea of Marmara displays a clear difference in elevation comparing the regions in the north and south (Fig. 3.8). The south and southeast parts show high topography with elevations from 700 to 1600 m in the Armutlu-Almacık highland and the Biga regions. Whereas, in the north at Thrace and the Kocaeli peneplain, the overall topography is fairly low, flat, particularly smoothed and the highest mountain reach only 950 m (Ganos Mtn.). On both terrains the highest regions are localized adjacent to the NAF (e.g. Ganos Mtn., Armutlu Peninsula). The drainage system shows similar disparity; while the northern systems are mainly characterized by typical dentritic drainage system with only short small streams discharging into the Sea of Marmara, in the south at least three large river systems outflow into the Sea of Marmara (e.g. Gönen and Kocasu rivers).

### 3.3.4. The Sea of Marmara basin floor

Following the 1999 earthquakes, the seismic gap in the Sea of Marmara experienced additional stress and the possibility of a large earthquake in the vicinity became dramatically larger. However, the poorly known bathymetry obstructed determination of the length and structure of the submarine fault segments. Hence, a large number of researches have been conducted recently in the Sea of Marmara. The

Sea of Marmara has been intensively investigated during several cruises and a wealth of multi-beam bathymetry data and seismic reflection data have been collected in these cruises. The Sea of Marmara turned from a poorly known sea into one of the World's best-studied seas. Below is an introduction to the main characteristics of the Sea of Marmara and submarine fault geometry of the NAF.

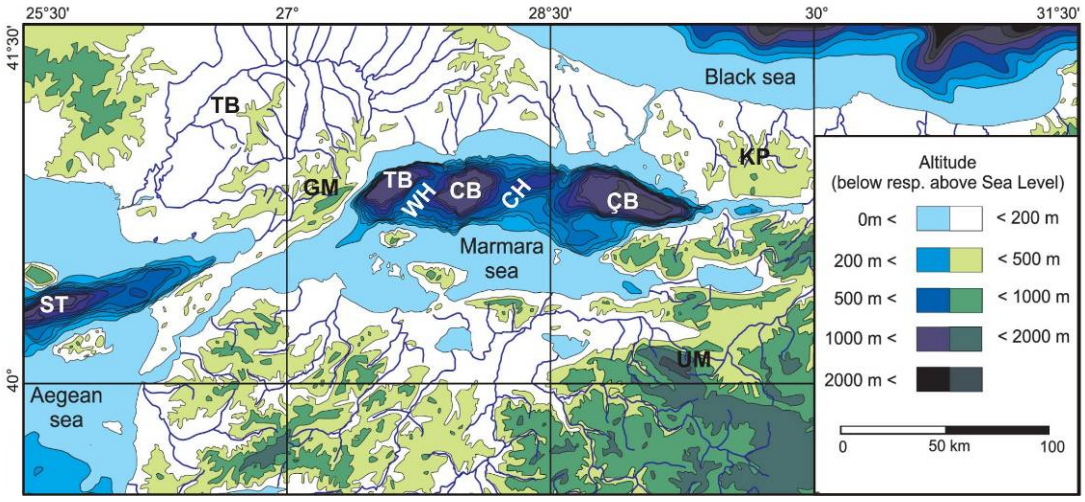


**Figure 3.8 :** Main morphologic structures in the Marmara region. TB: Thrace Basin, KP: Kocaeli Peneplain, UM: Uludağ Mountain, GM: Ganos Mountain, ÇB: Çınarcık Basin, CB: Central Basin, TB: Tekirdağ Basin: CH: Central High, WH: Western High, ST: Saros Trough (modified from Schindler et al., 2007).

The acquirement of high-resolution bathymetric data by several cruise campaigns exposed tremendously the detailed morphology within the Sea of Marmara (Fig. 3.9; Armijo et al., 1999, 2002, and 2005).

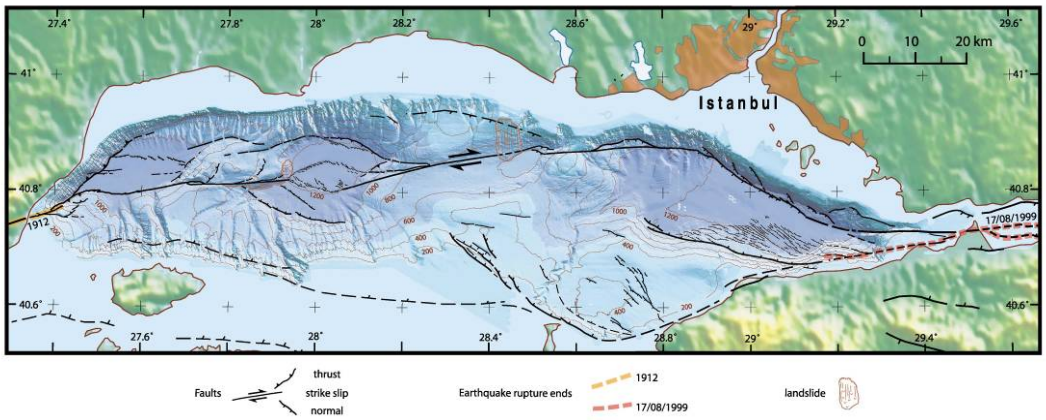


**Figure 3.9 :** The Sea of Marmara pull-apart basin along the North Anatolian Fault (Armijo et al., 2005)

The Sea of Marmara is the largest basin along the NAF, composed of several sub-basins, slopes, ridges and shelves. Canyons and submarine landslides accompany to these morphological elements. The shelves are significantly more developed at the southern shores and show a noteworthy break at 100 m depth. The northern part has also a slope-break at the same depth however slopes are fairly steeper all along the coast and are associated with several landslides. The steepest slopes are located offshore of Tekirdağ and Istanbul regions (15° to 30°). The most prominent elements in the Sea of Marmara are the three large basins which reach a depth of 1200 m; from east to west, the Çınarcık basin (-1270 m), Central basin (-1250 m) and the Tekirdağ basin (-1120 m). The basins are isolated by two ridges which rise about 700 m from the mean basin floor. The highest point of the Central High is at -330 m depth, while on the Western High it is at -550 m.

The morphology is an arrangement of a major transtensional system along the NAF. Mainly three different views are put forward to describe the active faulting system in the Marmara region. One class of interpretations ascribes the extensional pattern in the region to the prevalent extension in the Aegean rather than a localized pull-apart stretching (Parke et al., 2002). Regional scale GPS results do not support that the substantial Aegean extension is significant in the finite deformation of the Marmara region (Flerit et al., 2003). Another view argues that the pull-apart structures in the Marmara basins formed prior to the NAF as a part of an extensional regime and the present basins are now cut by a single throughgoing strike-slip fault; the NAF (Le Pichon et al., 2001), Imren et al., 2001). However, this model ignores the highly segmented structure of the NAF within the Sea of Marmara. A pull-apart model was first proposed by Barka and Kadinsky-Cade, (1988) despite the meagrely known bathymetry of the Sea of Marmara. Armijo et al., (2002; 2005) illustrated the complex fault system in the Sea of Marmara and corroborated the model of a dominant pull-apart system in the Sea of Marmara. The following paragraphs give a comprehensive outline on the morphology, structure and geology of the above mentioned complexities because their overall characteristics determine their significance in fault segmentation.

The largest basin in the Sea of Marmara is the Çınarcık basin, with a maximum depth of -1270 m and located 10 km east of Istanbul. Its wedge shaped geometry strikes NW-SE direction and is characterized with a linear steep slope on its northern

margin. The basin floor is flat and slightly inclines to the east (Okay et al., 2000). The northern escarpment is interpreted as representing the principle displacement zone of a dominant right-lateral fault by Le Pichon et al., (2001). The purely dextral motion is considered to occur along the young scarps at the foot of the northern escarpment. However, the entire 1000-m-high steepness of the northern slope and the scarps at the foot indicates a significant component of vertical displacement. Hence this fault is thought by Armijo et al. (2002) to be a composite normal and strike-slip fault, which is concomitant to strike-slip faults in a step-over geometry.

The Central basin is about 1250 m deep and bounded by the Central and Western High. The large basin is marked by linear boundary strike-slip faults. A smaller basin with distinct rhombohedral shape is nested within the basin. The basin floor is flat and inclines gently to the NNW. The long axis of the inner basin trends almost E-W. The margins of the nested basin are associated with left stepping, en-echelon small fault segments. Le Pichon et al., (2001) illustrate the en-echelon array in the inner basin as antithetic faults. However Armijo et al., (2002) considers them as normal faults in correspondence to the NE-SW extension direction. The SW boundary is formed by a 50-km-high cumulative scarp representing recent successive earthquake faulting. In the seismic profiles, the subsidence of the basin appears to be faster than the sedimentation rate (Armijo et al., 2005). The Central basin when its size is taken into account is a critical obstacle along the NAF in the Sea of Marmara in terms of rupture segmentation.

The 1120-m-deep Tekirdağ Basin is located to the west of the Sea of Marmara. It has a SW-NE stretched rhombohedral shape and is bounded by two ridges on its east and west; the Western High (-550 m) and Ganos Mtn. (924 m), respectively. The basin floor lies at about -1150 m depth and is nearly structureless (Okay et al., 1999). The Basin is connected to the Ganos Mountain (945 m) on its NW with a ~1000 m high steep slope below the sea level. The southern margin is limited by fresh fault scarps, which signifies the principle displacement zone of the NAF (Okay et al., 1999). To the west, this escarpment veers to the SW and forms a restraining band before connecting to the inland fault section. The Tekirdağ basin and the bend are critical complexities of the Ganos fault.

### 3.3.5. Neo-tectonic setting of the Marmara region

Early studies in the Marmara region consider the Sea of Marmara as a large graben system (Pfannenstiel 1944, Crampin & Evans, 1986). The poor resolution of available bathymetry was hampering proper observations. The models put forward were highly linked to the onland fault structures around the sea. Consequently, the extensional pattern in the region was related to the distinct Aegean extensional tectonics rather than the NAF (Allen, 1969, Ambraseys 1970). It was first Barka & Kadinsky-Cade, (1988) and Barka, (1992) who pointed out that the NAF consisted of three continuous strands and interpreted the Marmara basin as a pull-apart structure along the northern strand. They suggested that several large extensional step-overs are forming the tree basins in the Sea of Marmara; Çınarcık, Central and Tekirdağ basins.

Onshore, the NAF splays into two strands west of Bolu. Additionally, the southern strand splits farther west again into two branches, near Iznik Lake. The northernmost branch strikes through the Adapazarı basin and the Sapanca Lake. It continuous towards the Gulf of Izmit in an EW direction and crosses three large basins in the Sea of Marmara before appearing again onshore. This fault section is seismically the most active one among the three branches. Most of the motion of the Anatolian plate occurs along this part of the NAF (Flerit et al., 2003). The middle branch is sub-parallel to the northern strand and runs along the southern coast of the Iznik bay and Sea of Marmara. At Çınarcık it veers to the SW and continuous to the Aegean Sea. The southernmost branch strikes WSW crossing the Bursa and Edremit regions before entering the Aegean Sea.

The northern strand, which is the main concern in this work experienced significant earthquakes in the 20th century; the 9 August 1912 Mürefte earthquake ($M_w$7.4), the 17 August 1999 Izmit earthquake ($M_w$7.4) and the 12 November 1999 Düzce earthquake ($M_w$7.1) (Ambraseys & Finkel, 1987; Barka et al., 2002; Akyüz et al., 2002). The Izmit and Mürefte earthquakes caused considerable amount of stress accumulation on the submarine faults in the Sea of Marmara and determine the limits of the Marmara seismic gap. Although located offshore, the consequences of an earthquake in this region embraces a highly populated, industrial region.

### 3.3.6. Seismicity

#### 3.3.6.1. Historical Seismicity

The history of the Marmara region is rich in earthquakes, which many of them caused considerable damage to the cities in the region. Destructive shocks occurred often within a few years of intervals. The complex geometry of the NAF in the Marmara region reflects as a dense, as much as puzzling earthquake history.

The existence of numerous historical documents provides useful information about the seismic activity since the 5th century B.C. There are two main historical earthquake catalogues where information of earthquakes for the Marmara region is available. The historical earthquakes described in appendix A1 are mainly based on these two catalogues. The earthquakes up to the 15th century are primarily based on Guidoboni et al., (1994) and Guidoboni et al., (2005). The events after the 15th century derive from Ambraseys and Finkel, (1995). Additional information, when available, was obtained from Ambraseys & Finkel, (1991), Ambraseys, (2002a, 2002b, 2006) or other sources.

For each event, the following information has been provided, when possible: The date and its precision, number of accounts, damage distribution, loss of live and the seismotectonic significance of the available information. I aimed to determine the ruptured segments of NAF for the related earthquakes in relation to the damage distribution and note this in the interpretation sections. The difficulty in such an analysis is strongly depending on available information, which was very limited for events prior to the 10th century.

It should be considered that the information; provided by the historical accounts, is mostly local and its presence depends on the distribution of the settlements at the time of the earthquake. There are cases where a large event is recorded very poorly due to the lack of habitants in the region. On the other hand, a relatively smaller shock can be overestimated because of the abundance of records. The social level and culture of the societies play also an important role in the abundance of records. In cultures, where writing is not promoted it can lead to absence of any record. Through history, Istanbul has almost always been the capital city of the region. Consequently all earthquakes in Marmara; regardless of their distance to the city, contain records originating from Istanbul, which easily can cause to misleading, if no

other source is available. Hence, while evaluating historical earthquakes, the abundance and quality of the records should be considered in relation to the demographic and cultural state of the region.

#### 3.3.6.2. Historical earthquakes

Historical catalogues note more than 150 earthquakes, for the Marmara region, since the 5th century B.C. A selection and detailed description of these earthquakes is available in Appendix A1. The selection is based on which segments of the NAF might have been ruptured during the event. Only earthquakes which link to either to the Ganos fault, or to its neighbouring segments have been taken into consideration. Here we summarize our analysis of the above mentioned catalogues and provide a list of all selected events and their regional effects (Table 3.2).

The table grid correspond regions along the NAF in the Marmara region. The shaded boxes define the level of damage and/or quality of information for the related event. If damage is reported in the catalogues for a certain site, the corresponding region (grid) is highlighted with corresponding colour. The damage distribution of the 1912 earthquake is the best defined among other events, thus it can serve as a key to evaluate the significance of the damage information of older events.

The damage of the 1912a event is localized in Tekirdağ grids which comprise a region roughly from Tekirdağ to Gölcük on the west. A comparable localized damage is available for the 1766b, 1659, 1354, 1344, and 1063 historical earthquakes. As can be noticed in the table 3.2, some ambiguity is present for prior events. For the 477/484 and the 447 events damage is reported in Istanbul and in Saros and Gelibolu, whereas in between at the Tekirdağ no damage is mentioned. Several explanations may be valid for such cases. The earthquake might have caused damage in Tekirdağ, but it was not recorded or the record is lost. The reliability of the original accounts might be also questioned. The source or the date of the event may be wrong, too. The location of the 447 event is refined in recent studies and considered to have occurred near the Izmit region (Sapanca Lake; Ambraseys, 2006). While for the 477/484 some accounts report two large shocks (Guidoboni, 194). If the 477/484 earthquake consisted of two shocks then we may consider that one of these events occurred nearby the Ganos fault. Considering the uncertainty of available accounts and that some of the records might be missing we can even

speculate that it occurred on the Ganos fault. Another event, although poorly defined is the 824 earthquake. A castle in Tekirdağ is reported to have been damaged by an earthquake in this year. Therefore we also attribute this event to the Ganos fault. As a result, we consider that the 1912a, 1912b, 1766b, 1659, 1354, 1344 and 1063 might have occurred on the Ganos fault. In addition we conclude that among events prior to the 10$^{th}$ century the 824 and 477/484 are most likely earthquakes to have occurred on the Ganos fault.

### 3.3.6.3. Present day Seismicity

The Marmara region is one of the most seismically active regions in Turkey. Only in the last century, the region was affected by 9 earthquakes M > 6.8, causing severe damage in their epicentral areas. In the Marmara region, instrumental seismic observations date back to 1912, but limited with only two stations in Istanbul. The first standard seismograph was established in 1962, after the World Wide Standardized Seismographs Network (WWSSN) program. Seismic data collection in Turkey has been mainly managed by the Kandilli Observatory and Earthquake Research Institute (KOERI)[1]. The coverage and standard of the seismic network improved post 1980's, but the breakthrough occurred following the 1999 devastating earthquakes of Kocaeli (Izmit) and Düzce. The seismicity presented here relies primarily on a catalogue of 8456 events, downloaded from the KOERI – National Earthquake Observation Centre's online homogenized database. The catalogue covers a time frame from 1900 to 2009 (Fig. 3.10, 3.11, 3.12, 3.13). I classified the catalogue into time frames based on the standards of the network (e.g. prior/post to WWSSN and 1999 EQ's). The horizontal and vertical uncertainties may vary among the time frames and better hypocenter estimations are expected in more recent events. The W-E cross sections of hypocenters are filtered and correspond only to events located within the deformation zone of the northern strand of NAF. It is worth to note that we recognize two fixed hypocenter depths at 10 and 5 km within the catalogue.

[1] Today in Turkey, earthquake monitoring is performed manly by three centres, KOERI, TUBITAK - Marmara Research Centre (MAM) and the General Directorate of Disaster Affairs.

**Table 3.2 :** The distribution from west to east of earthquakes occurred in the Marmara region. The shaded boxes show the affected regions by each event. Indications of colours are given in the legend.

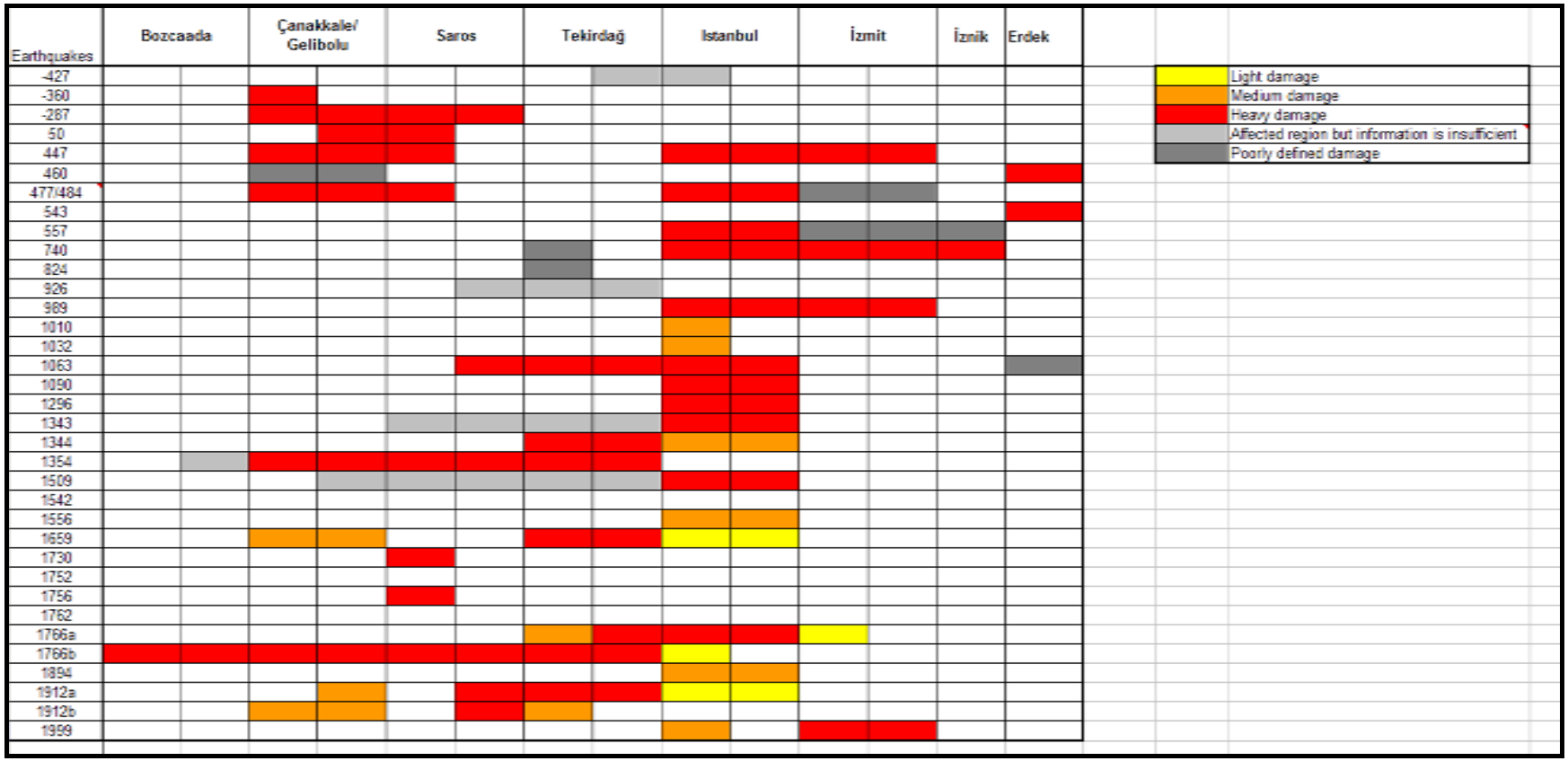

The figures 3.10, 3.11, 3.12, 3.13 illustrate the seismicity of the Marmara region for four time intervals:

1) 1900 to 1964 (prior to WWSSN)

2) 1964 to 1999 (WWSSN until 1999 events)

3) 1999 - 2003 (The 1999 earthquake sequence)

4) 2003 - 2008. (post 1999 earthquake sequence)

Between 1900 and 1964 there are only 114 events, however 4 significantly large earthquakes occur in this time frame (Fig. 3.10). The 9 August 1912 $M_w$ 7.4 and 13 September 1912 $M_w$ 6.8 earthquakes occurred west to the Sea of Marmara and are the main interest of this study. The two events are associated with some large aftershocks at the epicentral area. A similarly large event occurred at the Tekirdağ basin; however it is apart from the 1912 sequence (M5.6 - 16.06.1942). The other two main shocks are the 18 March 1953 Yenice-Gönen $M_s$ 7.2 and the 26 May 1957 Bolu-Abant $M_s$ 7.1 earthquakes, which occurred southwest and east respectively, to the Sea of Marmara. The E-W cross section illustrates are fixed between 10 to 20 km, therefore we think hypocenter estimations are not reliable for this period.

The number of earthquakes between 1964 and 1999 increases drastically to 2125 events and show a nearly full coverage of the Marmara region (Fig. 3.11). The epicentres demonstrate notably a better distribution in relation to fault strands. North of the Sea of Marmara, earthquakes are clustered linearly along the northern strand of NAF. Two dense clouds of earthquakes can be identified on the east and on the west along the NAF main branch. The earthquake swarm on the east is the aftershock activity of the 22 July 1967 Adapazarı earthquake $M_s$ 7.2. Considerable large events are located here at a depth of 20 to 30 km, which is significantly deeper than the 1999 earthquakes; particularly than the Düzce event which occurred only a few ten kilometres north. These estimations might be wrong, because the network and instrumental standards of that time was primitive. Other two large shocks are the 6 October Manyas earthquake ($M_s$ 7.0) located at 40.30°N/28.23°E and the 27 March 1975 Saros earthquake ($M_s$ 6.7). The latter occurred within the Saros bay and has an almost pure strike-slip mechanism (Fig. 3.14). The region illustrates high earthquake activity and events are concentrated within the Saros Trough. A similar but less dense activity is present in the western Marmara basins (Tekirdağ and Central

basins). The swarm shows a clear linearity located at the southern margin of the basins. The swarm augments towards the west, where the NAF forms a 17° bend. These two earthquake clouds in the Saros and in the Sea of Marmara limit a distinct aseismic zone along the northern branch of NAF. Similar but shorter sections can be observed on the Central High, Gulf of Izmit and Düzce basin. Hypocentres are mostly located within the upper 15 km of the crust. However their reliability is unclear since some events are clearly fixed to 10 km depth.

Earthquakes of the period from 1999 to 2002 are separately plotted to cover only the seismicity of the 17 August 1999 Kocaeli (Izmit) earthquake ($M_w$ 7.4) and the 12 November 1999 Düzce earthquake ($M_w$ 7.2) (Fig. 3.12). During this 2.5 year period most of the earthquakes were monitored reasonably in the related epicentral region (1255 shocks in total). The dense seismic activity extends on the west until the eastern margin of the Çınarcık basin. The E-W cross section points out a gap of seismicity between the latitude 29.5°. Initially, the rupture of the 17 August shock was considered to terminate east of Hersek at this locality (Barka et al., 2002). However interferometry data analysis illustrated that east of Hersek, the coseismic slip started to decrease from 4.5 to 2 m and tapered towards west of Hersek (Çakır et al., 2003). The termination point of the rupture corresponds to the eastern entrance of the Çınarcık basin, where the simple linear fault transforms into more complex geometry (Çakır et al., 2003; Bouchon et al, 2003; Uçarkuş et al., 2006 & 2008). Hence the high seismicity in that location corresponds to post-seismic deformation and the gap does not determine the termination of the 17 August 1999 earthquake rupture. Additional observation towards west is a high activity at the Ganos bend and the southern limits of the Tekirdağ and Central basins. The Central High shows poor seismic activity with small magnitude shocks. Further west, the Ganos inland section is again aseismic. Some activity is again present within the Saros Trough.

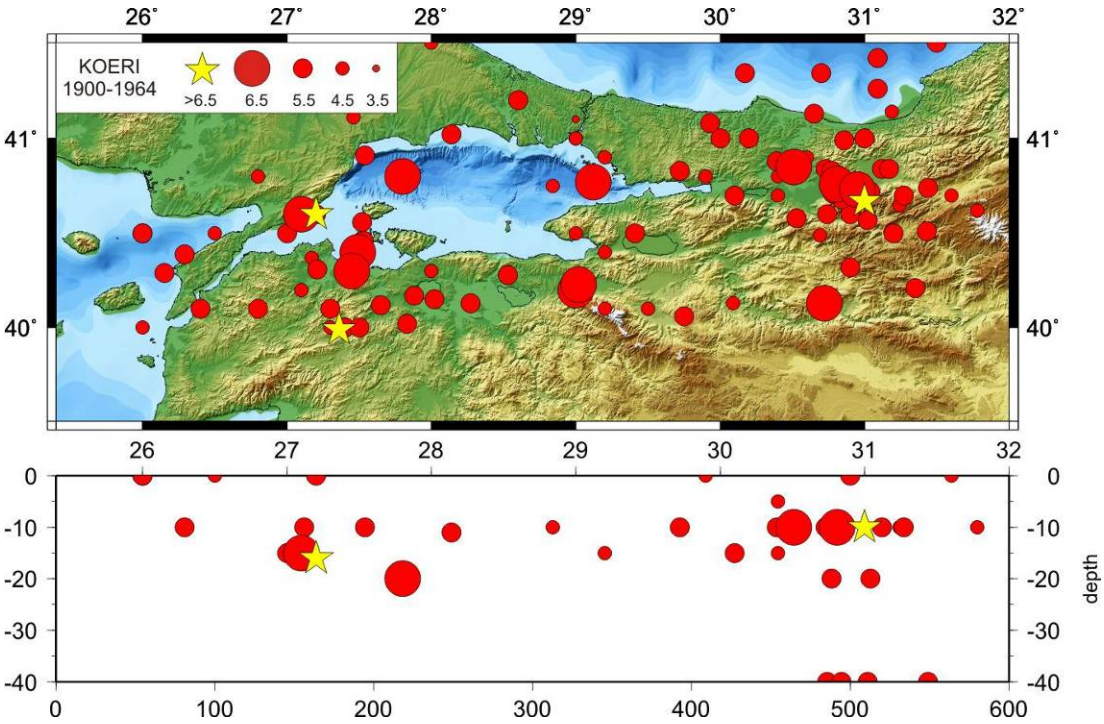


**Figure 3.10 :** From 1900 to 1964, 114 earthquakes were recorded at seismological stations. 4 large events occurred during this time period. Western upper star corresponds to epicentre of 1912 Mürefte earthquake (M 7.3), western lower star is the 1953 Yenice-Gönen earthquake (M 7.2). The star on the east corresponds to the 1957 Bolu earthquake (M 7.2).

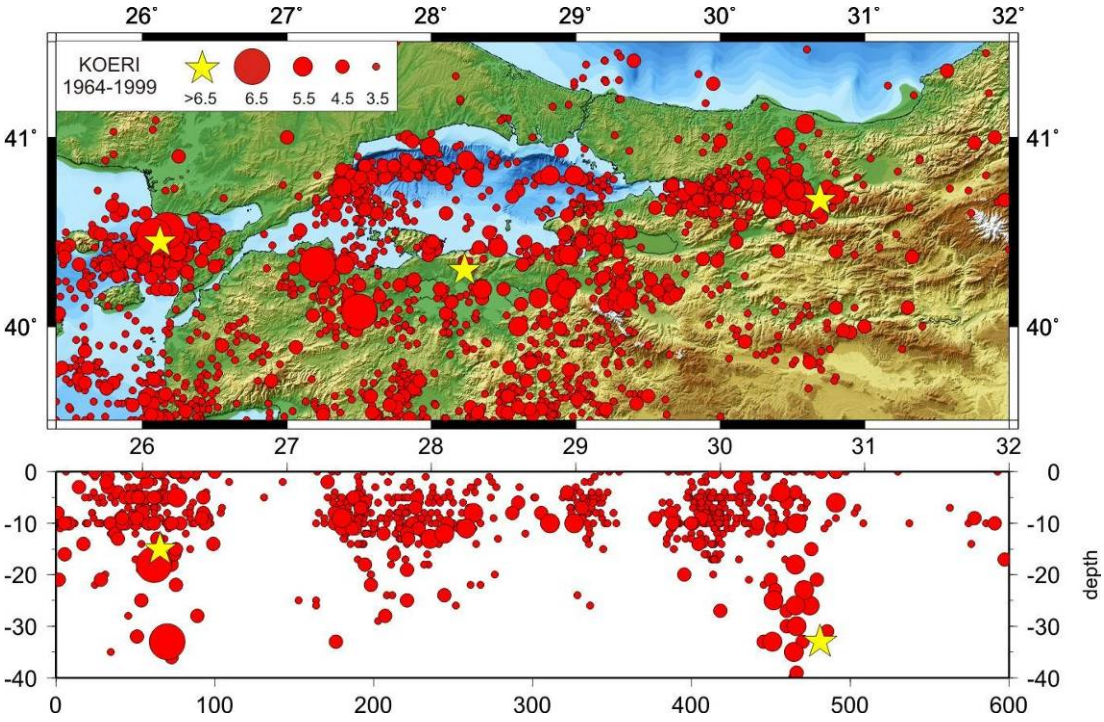


**Figure 3.11 :** The number of registered earthquakes increased after the establishment of the WWSSN. Three large events (M > 6.7) were recorded during this period (Karabulut et al., 2006; see text for detail).

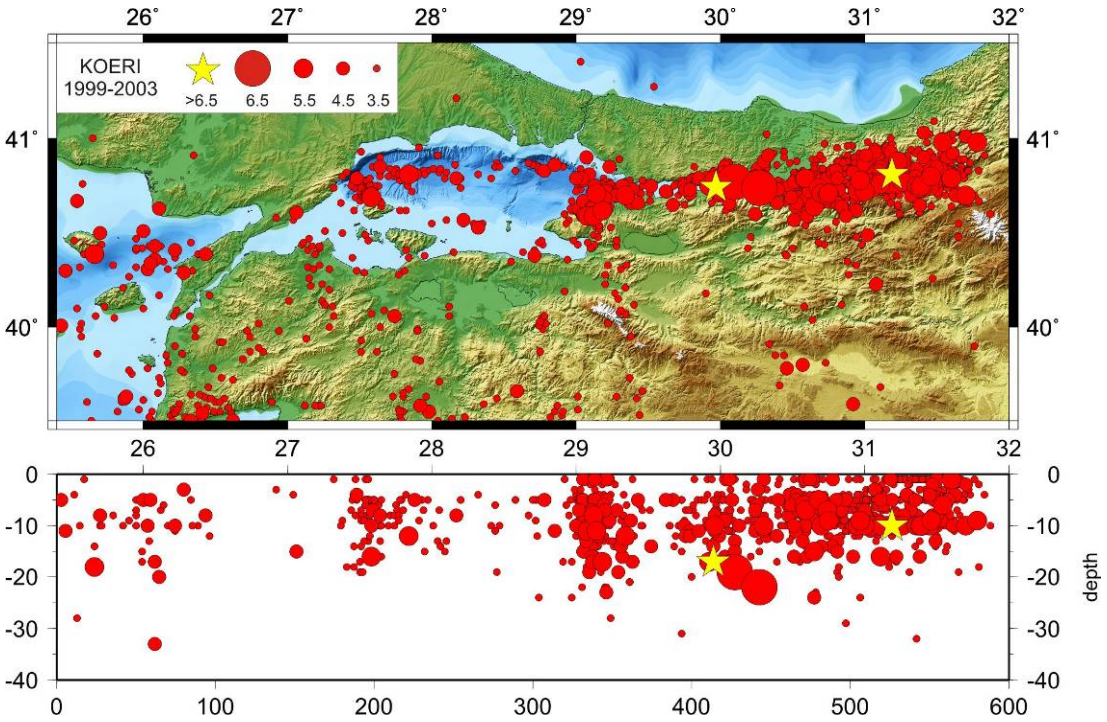


**Figure 3.12** : After 1999, a large seismic activity was recorded on the eastern part of the Marmara region due to the 1999 earthquakes and aftershocks (Karabulut et al., 2006).

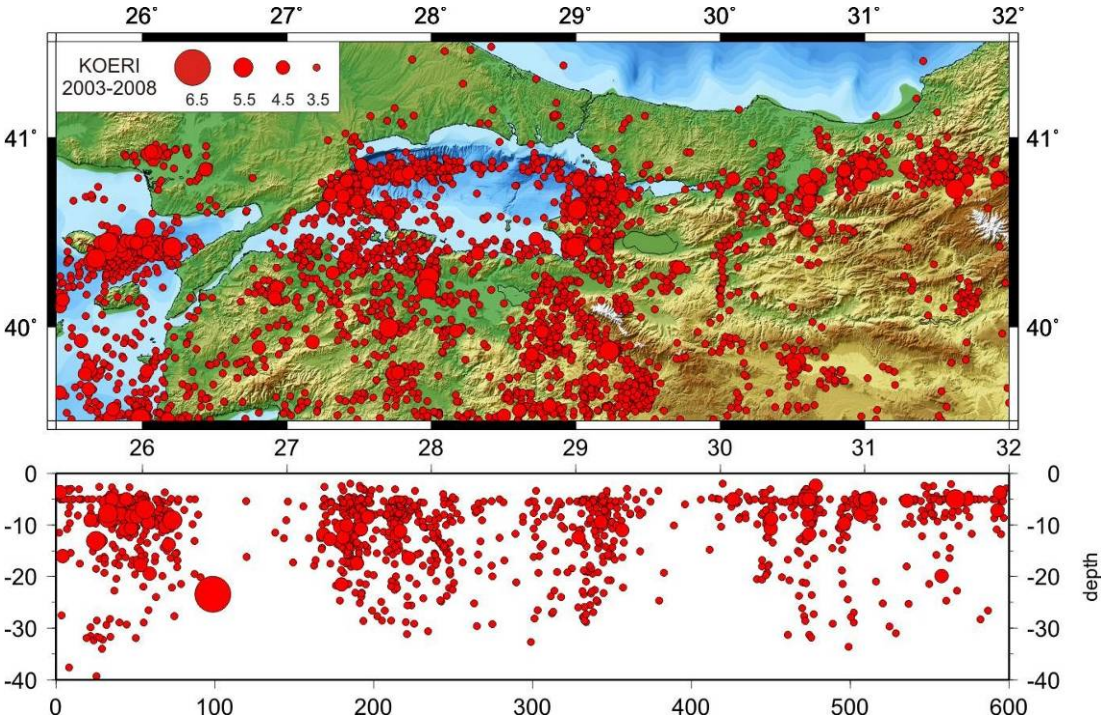


**Figure 3.13** : Recent improvements on the seismic network showed the presence of a high earthquake activity towards west with a distinct aseismic zone between the Sea of Marmara and Saros bay, which may be related to the 1912 earthquake segment (Karabulut et al., 2006).

To illustrate the seismicity post to the 1999 sequence I selected a time interval beginning from 2003 until present (March 2009) comprising 3541 events (Fig. 3.13). This time interval shows no significant large earthquake. However, it is noticeable that the number of earthquakes increases from east to west. The region, where the 1999 earthquakes occurred, show significantly lower seismicity than the 1999-2002 time frame. The epicentres here, are linearly clustered along the northern branch of NAF. They follow the northern margin of the Çınarcık basin and the southern margins of the Central and Tekirdağ basins with relatively larger shocks compared to the south of Marmara region. The high activity at east of the Çınarcık basin is still present. However the Gulf of Izmit and partly the Sapanca region show poor activity. Further east, the two tips of the Düzce earthquake rupture show also high seismicity, but the ruptured section is aseismic. At Saros we recognize small to moderate size events, which epicentres are aligned within the Saros Trough. The seismicity clusters along the northern basin margin. Most of the moderate size earthquakes are also located at this margin, while the smaller size shocks diffuse to the south, see also Karabulut et al., (2006). This is related to an asymmetric basin structure, as observed in the Marmara basins (Karabulut et al., 2006). An E-W cross section demonstrates that hypocenters are deeper on the west than on the east. The aseismic zones of the Ganos and the Gulf of Izmit are distinct. The area which corresponds to the Central High (Lat: 28°/29°) has also a significantly poor activity. The seismicity at Tekirdağ and Saros is distributed to a similar depth of 15 to 18 km. Karabulut et al, (2006), shows that earthquake activity is concentrated to the upper 20 km in the Saros bay and that all shocks occur along a very narrow vertical zone indicating a pure vertical fault plane.

Focal mechanism solutions of some earthquakes of the region are illustrated in Figure 3.14 and listed in Table 3.3. The majority of the solutions, particularly the ones on the NNAF yield pure right lateral strike slip faulting, especially large shocks. A few normal faulting mechanisms are located at Gölcük and at the Çınarcık basin. These observations are in accordance with regional morphology and tectonics. Normal co-seismic slip was observed during the 17 August rupture in the Gölcük area, where steep slope limit the southern margin of the gulf. The Çınarcık basin is also limited on its north with a nearly 1000 m high steep slope, which indicates a substantial amount of normal faulting mechanism. The NNAF forms a restraining

bend west of the Çınarcık before it strikes through the Central High. Here, some focal mechanisms have a dominant compression component. At the Tekirdağ basin some shocks give normal faulting solution with minor strike-slip component. This might be related to minor normal faults sections within the pull-apart system. A remarkable feature is the solutions in the Saros Trough which illustrate pure strike-slip faulting (see also Karabulut et al., 2006). This can be interpreted that the influence of the Aegean back-ark, N-S extension is not observed in this region and that the NNAF is the superior cause of deformation in this region.

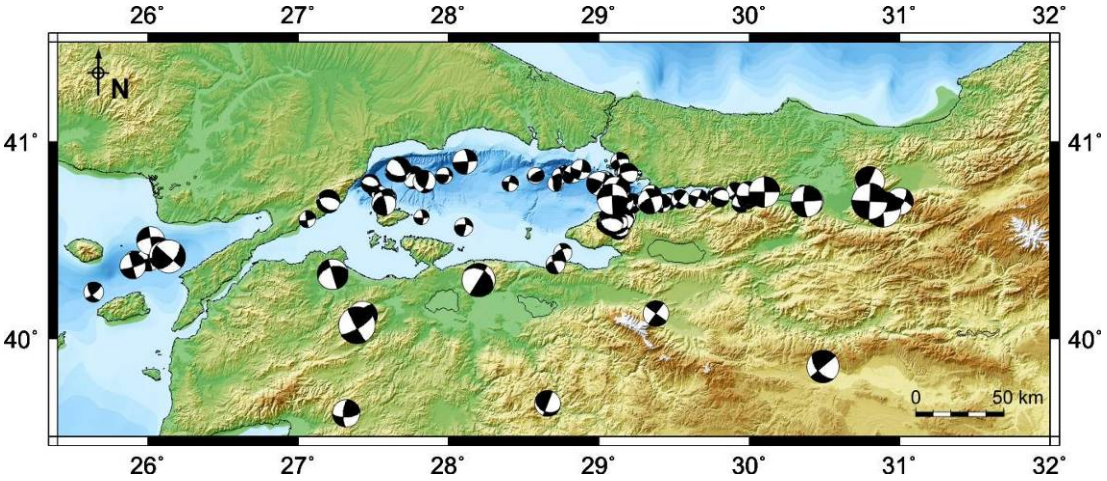


**Figure 3.14:** Focal mechanism solution for the Sea of Marmara region assembled from various (see Table 3.3 for details). The solutions show a dominant strike-slip character along the NNAF, including the Saros bay area. Some thrust faulting is located at the bend of Ganos.

The above described seismicity allows defining the most active areas, consequently the most dynamic fault strands and their characteristic. We observe that the majority of the earthquakes, especially large ones occur on the NNAF with mainly strike-slip mechanism. Earthquakes to the south of the Sea of Marmara are smaller and diffused.

Offshore some clustering may be recognized at the south-eastern boundary fault of the Çınarcık basin and the Iznik gulf. Although apart from the study area, we note a sharply linear seismicity west-southwest of the Uludağ Mt. (Bursa) trending NW-SE direction. Time frames post 1964 allowed to localize aseismic zones along the NNAF. The seismicity along the 1999 ruptures has significantly reduced in the following years. While aftershocks of the first two years were distributed in the upper ~15 km of the crust, hypocentres post 2003 are concentrated in the upper 10 km (excluding the fixed hypocentres at 5 km depth). The ruptured segments of the

1999a and 1999b events are clearly zones of poor seismicity. On the other hand, the seismicity is still continuous at the rupture termination points; however with decreasing character after 10 years (Fig. 3.12, 3.13). A similar pattern is observed along the 1912 earthquake segment, where a nearly 70 km long aseismic zone is limited by two dense earthquake swarms (Saros and West Marmara). Other studies related this distribution to the extend of the 9 August 1912 earthquake rupture (Karabulut et al., 2006). However interpreting this activity as post-seismic deformation is arising a question: How long do aftershocks at termination points continue? The Mürefte earthquake struck 97 years ago. One would expect that the post-seismic deformation would have reached equilibrium during that time interval.

Consequently, we should not see dense seismicity at the two tips of the rupture. This is the case for the eastern large earthquakes along the NAF. We do not observe significant seismicity at the rupture termination points for the 1939 to 1967 sequence; but for the 1999 events since 10 years. We consider that this kind of seismicity is related to the complex structure of the NAF in the Sea of Marmara and Saros bay.

### 3.3.7. GPS studies and crustal deformation

As illustrated from the seismicity most of the earthquakes, hence the deformation occurs along the northern branch of the NAF. Geodetic measurements in the Sea of Marmara region yield the same result, showing that the northern branch accommodates 3-4 times more motion than the southern branch. GPS data give 20 to 25 mm/yr slip rate along the northern branch relative to Eurasia (Meade et al., 2000, Straub et al., 1997; Mc McClusky, et al., 2000, Reilinger et al., 2006). Meade (2002) derived 24 ± 2 mm/yr right lateral motion on the northern branch, where they assumed the Marmara region to be of two main branches with nearly linear geometry . Using a similar fault pattern Reilinger et al., 2006 obtained higher slip rates of 27 ± 0.5 mm/yr.

**Table 3.3 :** List of earthquake parameters for event given in Figure 3.14.

| Date | Lat | Lon | M | Strike | Dip | Rake | Source |
|---|---|---|---|---|---|---|---|
| 18.03.1953 | 40.07 | 27.39 | 7.4 | 59 | 76 | 174.00 | Gurbuz et al 2000 |
| 06.10.1964 | 40.30 | 28.20 | 6.7 | 302 | 36 | -90.00 | Gurbuz et al 2000 |
| 23.08.1965 | 40.50 | 26.02 | 5.6 | 261 | 70 | -132.00 | Gurbuz et al 2000 |
| 03.03.1969 | 40.12 | 27.43 | 5.8 | 107 | 50 | 147.00 | Gurbuz et al 2000 |
| 27.03.1975 | 40.42 | 26.14 | 6.6 | 41 | 60 | -128.00 | Gurbuz et al 2000 |
| 05.07.1983 | 40.33 | 27.23 | 6.1 | 218 | 32 | 71.00 | Gurbuz et al 2000 |
| 05.07.1983 | 40.33 | 27.23 | 6.1 | 254 | 49 | -173.00 | Gurbuz et al 2000 |
| 24.04.1988 | 40.90 | 28.11 | 5.0 | 356 | 71 | -11.00 | Gurbuz et al 2000 |
| 08.02.1995 | 40.82 | 27.77 | 4.5 | 33 | 42 | -137.00 | Pinar et al 2003 |
| 13.04.1995 | 40.86 | 27.67 | 5.0 | 92 | 46 | -137.00 | Pinar et al 2003 |
| 18.04.1995 | 40.80 | 27.84 | 4.5 | 20 | 70 | 133.00 | Pinar et al 2003 |
| 14.04.1996 | 40.70 | 27.20 | 4.6 | 274 | 61 | -112.00 | Pinar et al 2003 |
| 29.05.1999 | 40.79 | 28.71 | 3.1 | 341 | 22 | 72.00 | Pinar et al 2003 |
| 17.08.1999 | 40.38 | 28.71 | 3.8 | 255 | 59 | -169.00 | Pinar et al 2003 |
| 17.08.1999 | 40.44 | 28.76 | 3.7 | 248 | 60 | 177.00 | Pinar et al 2003 |
| 21.08.1999 | 40.83 | 28.81 | 3.2 | 5 | 72 | -40.00 | Pinar et al 2003 |
| 21.08.1999 | 40.84 | 28.77 | 3.1 | 293 | 58 | -143.00 | Pinar et al 2003 |
| 23.08.1999 | 40.57 | 28.10 | 3.7 | 270 | 67 | 162.00 | Pinar et al 2003 |
| 03.09.1999 | 40.83 | 28.74 | 3.2 | 353 | 70 | 19.00 | Pinar et al 2003 |
| 20.09.1999 | 40.71 | 27.59 | 3.6 | 238 | 42 | 166.00 | Pinar et al 2003 |
| 20.09.1999 | 40.70 | 27.57 | 3.3 | 246 | 51 | 156.00 | Pinar et al 2003 |
| 20.09.1999 | 40.70 | 27.59 | 3.2 | 211 | 50 | 138.00 | Pinar et al 2003 |
| 20.09.1999 | 40.72 | 27.60 | 3.2 | 209 | 77 | 160.00 | Pinar et al 2003 |
| 20.09.1999 | 40.69 | 27.57 | 4.0 | 245 | 40 | 166.00 | Pinar et al 2003 |
| 21.09.1999 | 40.71 | 27.56 | 3.4 | 224 | 75 | 168.00 | Pinar et al 2003 |
| 21.09.1999 | 40.70 | 27.57 | 3.4 | 208 | 34 | -42.00 | Pinar et al 2003 |
| 21.09.1999 | 40.72 | 27.59 | 3.3 | 273 | 46 | -168.00 | Pinar et al 2003 |
| 22.09.1999 | 40.62 | 27.82 | 3.0 | 89 | 79 | -163.00 | Pinar et al 2003 |
| 24.09.1999 | 40.74 | 27.54 | 3.1 | 195 | 39 | 135.00 | Pinar et al 2003 |
| 02.10.1999 | 40.76 | 27.51 | 3.0 | 272 | 75 | 170.00 | Pinar et al 2003 |
| 06.10.1999 | 40.72 | 27.60 | 3.2 | 208 | 46 | 139.00 | Pinar et al 2003 |
| 07.10.1999 | 40.71 | 27.59 | 3.0 | 214 | 74 | 142.00 | Pinar et al 2003 |
| 16.11.1999 | 40.61 | 27.06 | 3.4 | 79 | 79 | 172.00 | Pinar et al 2003 |
| 17.11.1999 | 40.83 | 27.97 | 3.4 | 276 | 82 | 132.00 | Pinar et al 2003 |
| 03.12.1999 | 40.71 | 27.58 | 3.8 | 237 | 22 | -139.00 | Pinar et al 2003 |
| 20.12.1999 | 40.79 | 27.48 | 3.6 | 99 | 65 | -96.00 | Pinar et al 2003 |
| 29.12.1999 | 40.83 | 28.58 | 3.4 | 98 | 27 | 132.00 | Pinar et al 2003 |
| 07.01.2000 | 40.79 | 28.41 | 3.2 | 283 | 77 | -165.00 | Pinar et al 2003 |
| 14.03.2001 | 40.85 | 27.64 | 3.7 | 75 | 79 | 147.00 | Pinar et al 2003 |
| 24.03.2001 | 40.86 | 28.88 | 4.0 | 105 | 78 | -170.00 | Ozalaybey. 2002 |
| 24.03.2001 | 40.84 | 28.83 | 3.7 | 106 | 87 | -160.00 | Pinar et al 2003 |
| 10.06.2003 | 40.24 | 25.64 | 4.0 | 51 | 81 | 152.00 | Karabulut 2006. |
| 05.07.2003 | 40.43 | 26.08 | 4.3 | 78 | 73 | 171.00 | Karabulut 2006. |
| 06.07.2003 | 40.43 | 26.10 | 5.7 | 257 | 89 | 179.00 | Karabulut 2006. |
| 06.07.2003 | 40.44 | 26.11 | 5.3 | 253 | 89 | 175.00 | Karabulut 2006. |
| 06.07.2003 | 40.41 | 26.01 | 4.7 | 252 | 85 | 178.00 | Karabulut 2006. |
| 06.07.2003 | 40.41 | 26.00 | 4.2 | 89 | 53 | 173.00 | Karabulut 2006. |
| 09.07.2003 | 40.39 | 25.91 | 4.7 | 71 | 78 | 178.00 | Karabulut 2006. |
| 09.07.2003 | 40.39 | 25.90 | 4.1 | 75 | 87 | 174.00 | Karabulut 2006. |
| 09.07.2003 | 40.39 | 25.91 | 3.8 | 74 | 89 | 173.00 | Karabulut 2006. |
| 13.07.2003 | 40.39 | 25.92 | 4.0 | 69 | 83 | 165.00 | Karabulut 2006. |
| 18.07.2003 | 40.39 | 25.96 | 3.8 | 244 | 87 | 176.00 | Karabulut 2006. |
| 15.07.2004 | 40.37 | 25.90 | 5.1 | 74 | 82 | 178.00 | Karabulut 2006. |

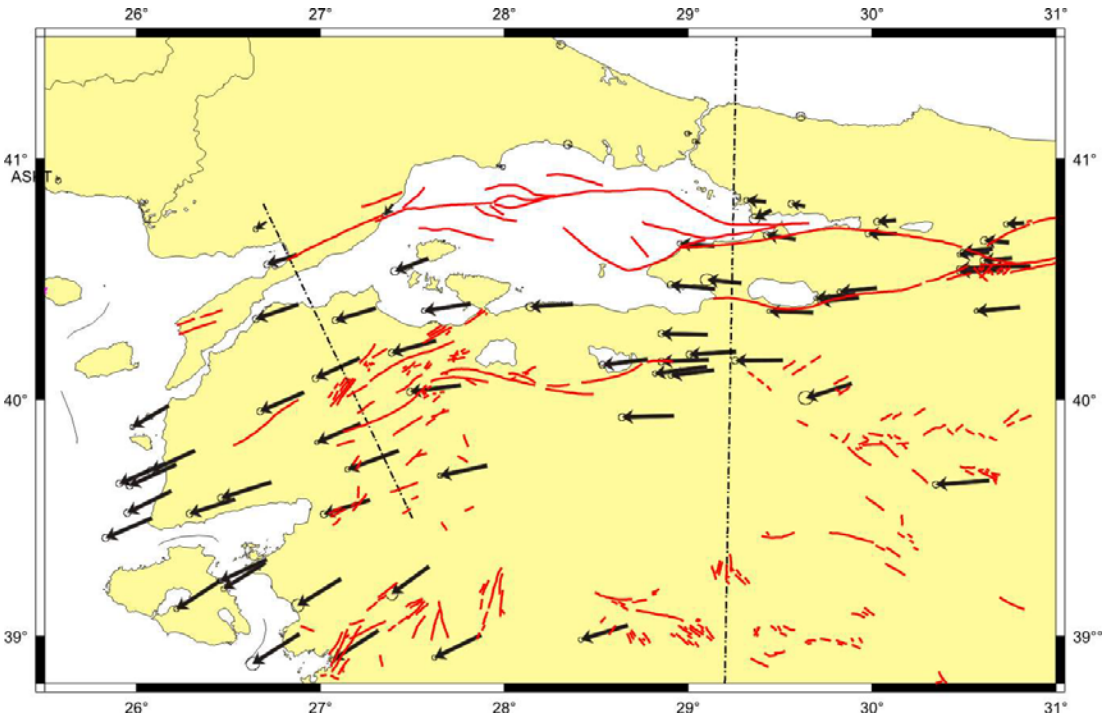


**Figure 3.15 :** GPS velocities for the Marmara region (Reilinger et al., 2006)

Locking depth estimations derived from GPS data is a well know method. The locking depth determines the width of the fault and plays an important role to calculate the possible moment release in a future earthquake in the region. There have been several studies where locking depths were estimated for the Sea of Marmara region; however with widely different results. Meade et al., (2002) calculated a regional locking depth of 17 km for the Marmara region. However, for the northern section of NAF they used a single through going fault model with an average slip of 24 mm/yr and concluded that a local locking depth of 6-7 km gives the best fit to the GPS velocities.

An even lower value is used in the models of Flerit et al., 2003, where they test a pull-apart geometry for the northern branch. Their model yields the best fit in velocity for a locking depth of 5 km. Le Pichon et al., 2003 derived locking depths ranging from 10-14 km for several GPS profiles across the northern branch. Using a 10- year period of GPS observation in the Izmit area (before the 1999 earthquakes), Reilinger et al., (2006) obtained a locking depth of 20-21 km for this region.

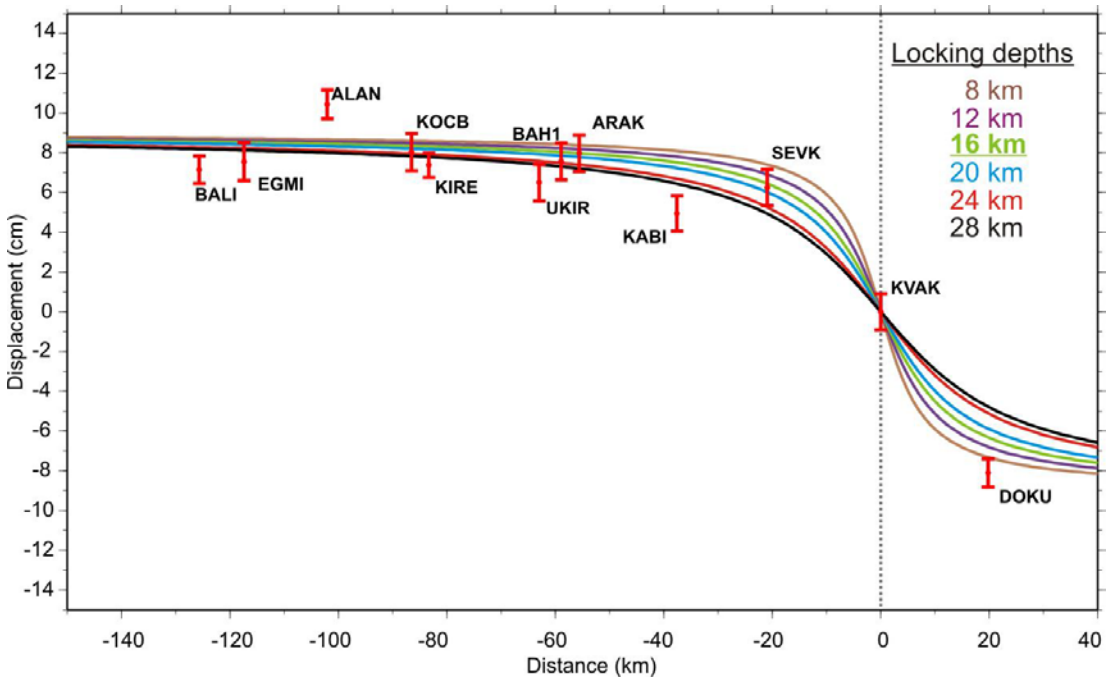


**Figure 3.16 :** GPS profile across the western part of the Ganos fault. Locking depth estimation shows the best fit for a locking depth at 16 km.

Variations at such scale have great influences on seismic hazard assessments. The moment release during an earthquake is connected to several parameters including the locking depth. Hence, the rupture length may double for shallow depth or the moment magnitude may decrease significantly taking into account the segmented fault structure in the Sea of Marmara. The problem lies in the offshore location of the northern fault branch of NAF. The sea hinders measurements close to the fault. Therefore GPS stations lack of an appropriate distribution across the fault. Inferences on locking depth are then fairly varying. Our locking depth estimations yield 16 km depth (Fig. 3.16). A proper estimation on locking depth should taken into account the seismicity and related thickness of the seismogenic zone. For the Sea of Marmara region an average fault width (in other words locking depth) of 16 km is reasonable and comparable with the Izmit region and the 1999 earthquakes seismicity.

# 4. ACTIVE TECTONICS, GEOMORPHOLOGY AND SLIP RATE ON THE WESTERNMOST SEGMENT OF THE NORTH ANATOLIAN FAULT ZONE

## 4.1. Introduction

One of the main targets in this work is to investigate the long-term and short-term fault behaviour and the segmentation characteristics of the Ganos section of the North Anatolian Fault. We studied the geomorphology and fault related deformations with the hope of estimating long-term and short-term slip-rates and use this information to understand the manner of earthquake occurrence along this part of the North Anatolian Fault. In addition, we examined its structural and geometrical fault complexities to evaluate the segmentation character, which would help estimating possible rupture length for individual earthquakes in the region.

The study relies on two approaches of observation; remote sensing and field investigations. The former was accomplished using 1:25,000 scale topographic maps, SPOT5 images at 5 m resolution, Landsat TM images at 30 m resolution, 1:12.000 and 1.35.000 scale aerial photographs, paraglide-aerial (ultra-light aircraft) photography and partly Google Earth images (0.5 m resolution). The analyses were performed by the software ENVI, ERMapper and ArcGIS. In addition we used Digital Elevation Model (DEM) and SRTM data. 10-m-equidistance, digital contour lines of 1:25.000 scale topography maps were interpolated to obtain a 20-m-resolution DEM. Consequently the DEM was used to produce standard morphometric derivatives such as hillshade-, slope-, aspect-, density-plot- and sun-angle-maps for topographic analyses. Following the remote mapping of geomorphic and tectonic structures, intensive field investigations were carried out to establish a detailed geomorphology and fault map at 1:25.000 scale. At certain sites, we performed micro-topographic surveys to obtain a detailed morphology.

This chapter firstly presents the geologic and geomorphic setting of the study area. Subsequently, we focus on the fault zone and define tectono-morphic features at several scales. After a description of the main fault zone characteristics, short-term offsets and long-term offsets are examined and compared to analyse the fault

behaviour. Finally we study the cumulative slip distribution, compare groups of offsets with climatic fluctuations and provide a slip-rate for the westernmost segment of the North Anatolian Fault.

## 4.2. Geology of the Ganos Region

The Ganos Mt. is the most prominent and isolated topographic high of the eastern Thrace. The Ganos region is characterized by well exposed Tertiary to Quaternary sedimentary deposits of the southern part of the Thrace basin. The hydrocarbon-bearing sedimentary fill is mostly composed of Middle Eocene to Miocene aged units. The formations are truncated by the Ganos fault, which is thought to be a right lateral strike-slip fault pre-dating the North Anatolian Fault (Yaltırak, 1996; Zattin et al., 2005; Kaymakcı 2007, Tüysüz et al., 1998). The region consists of two different basements on each side of the fault. Both sections are well exposed in the region, particularly along the Ganos fault. The two stratigraphic sequences are described here as the Northern section and the Southern section (Fig. 4.1).

**Northern section**

The north of the Ganos fault is composed by a sedimentary pile of Lower Eocene to Lower Oligocene deposits, unconformably lying on top of a fluvial sequence (Middle Eocene). The fluvial base is not exposed in the study area. The sequence starts with the Lower to Middle Eocene Gaziköy formation. This unit consist of a siltstone – shale intercalation (Sümengen, 1987; Turgut et al., 1983) and is well exposed at the village Gaziköy. The Gaziköy formation is overlain by the Upper Eocene Keşan formation made of sandstone with sparse intercalations of shale (Sümengen, 1987). It covers most of the northern area and to some extent the south of the study area (Plate 1). Shale deposits with some marl sequences are overlain on top of the Keşan formation. This unit is named the Mezardere formation and is of Upper Eocene to Lower Oligocene age (Ünal, 1967; Gerhard, 1987). These three formations represent the northern section of the Ganos fault including the Ganos Mt. They signify a regressive sedimentary assemblage from a submarine outer fan environment to prodelta fan facies.

The Gaziköy and Keşan, formations are well exposed on slopes north of the Ganos fault. They are well consolidated and built a distinct uniform morphology, where high steep slopes are deeply incised by mainly 2 km-long, N-S flowing stream

segments. Quaternary deposition occurs where slopes are lower than 10°. We observe slope debris at the lower parts of the hills between Gaziköy and Mursallı. They are composed of poorly sorted and rounded coarse material within a loose sand matrix. On the section between Gaziköy and Yörgüç alluvial fans are formed on sites where large stream beds reach a surface lower than 10° dip. Yörgüç, Gölcük, and Yeniköy are fault related basins and serve as deposition centres of Quaternary sediments. The largest basin in the study area is the Evreşe plain.

**Southern section**

The southern section has a relatively more composite geology than the North. Upper Cretaceous to Upper Pleistocene units comprises the southern highs of the Ganos area. The Çetmi formation, Maastrichtian of age is an ophiolitic melange representing the basement of the southern sequence (Okay et al., 1991, Şentürk and Okay 1984). The base is visible south of Gölcük and South of Yeniköy along the ridge of the Helva Hill. The Çetmi formation is unconformably overlain by the Upper Eocene limestone named as the Soğucak formation (Holmes, 1966; Sümengen & Terlemez 1991). The limestone is mainly exposed on the highest parts of the Doluca Hill. The Ceylan formation overlays conformably the Çetmi formation; it consists of sandstone – shale intercalation, Middle-Upper Eocene of age (Ünal, 1967). The Ceylan formation is a deltaic deposit overlain unconformably by a Miocene sequence (Yaltırak, 1995). The lowest part the Miocene sequence is represented by the Gazhanedere formation, which is mainly exposed on the lower slopes of the Kirazlı stream and west of Şarköy. The Gazhanedere formation represents a transgressive deposition from fluvial to lacustrine and partly shore deposits (Yaltırak, 1995). The age of the unit is constrained to Lower to Middle Miocene (Gutzwiller, 1923, Izdar, 1959). Gazhanedere continues transitionally to the Kirazlı formation, which is Upper Miocene of age and widely distributed on the southern part of the study area (Saltık, 1974; Yaltırak, 1995). The unit consists mainly of fine sandstone representing a beach environment with some sequences of conglomerates. The Gazhanedere and Kirazlı formations consist of unconsolidated clastics, which are very sensitive to erosion. At localities where groundwater is substantial landslides are common in these units. The Kirazlı formation is overlain by the Alçıtepe formation, which is an oolitic limestone, exposed at a few localities next to Hoşköy. The formation represents brackish conditions. The age of the unit is

contradiction; the unit is considered to be conformable with the Kirazlı Formation is of Upper Miocene age (Yaltırak, 1995, 1996, Yaltırak et al., 2000). However other studies suggest that the Alçıtepe formation is above an unconformable contact and is of Pliocene age (Armijo et al., 1999; Melinte et al., 2009)

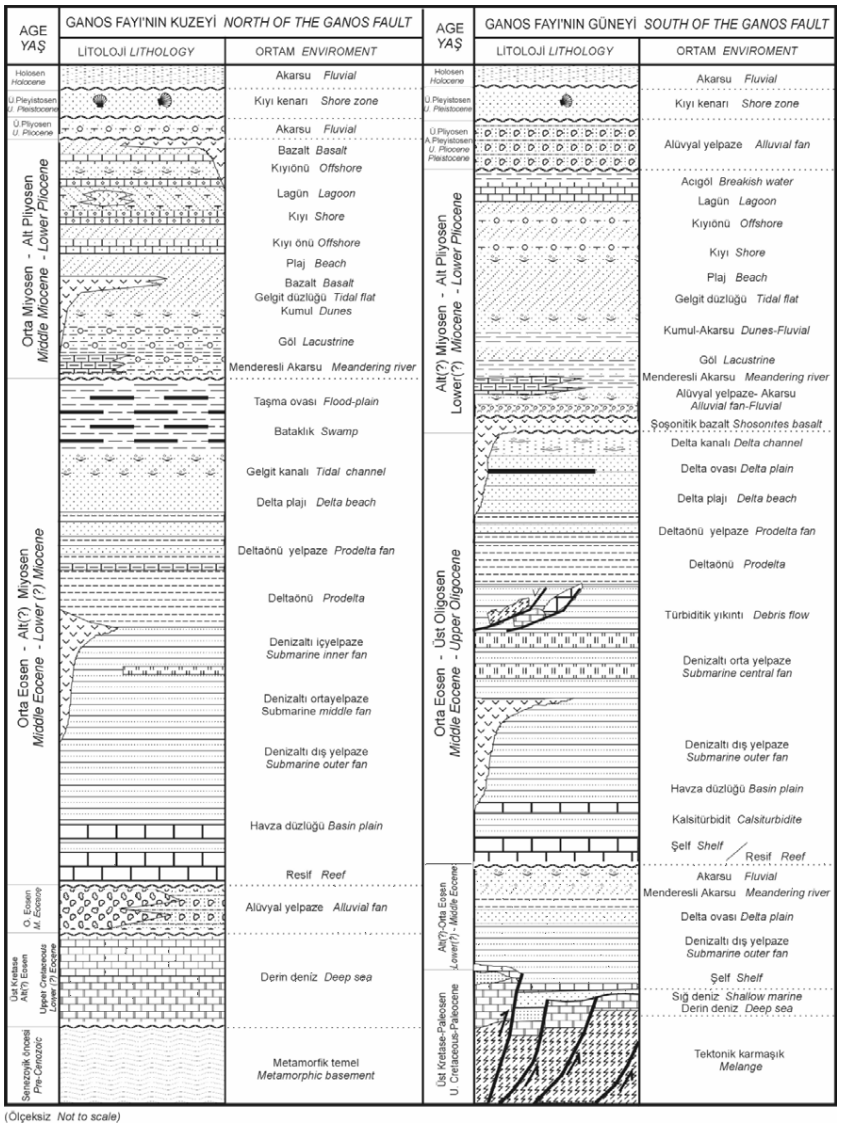


**Figure 4.1 :** The stratigraphy of the northern and southern part of the Ganos fault (from Yaltırak, 1996).

At Gaziköy, Pleistocene coastal deposits (Marmara Formation) on top of the Gaziköy Hill characterize a series of transgressive and regressive events. The Marmara formation is composed here, of a 36-m-thick sedimentary package made of aragonite-cemented coarse gravels with abundant shells, tilted 17° to the southwest and resting with an angular unconformity over Middle-Upper Miocene sandstones. The base of the succession lies at 21.5 m and 14.0 m elevations in the north and

south, respectively and confirms the active post-depositional tectonic movements near the Ganos Fault (Yaltırak et al., 2002).

Quaternary deposits along the fault show different geology at the east and west. On the east, at Gaziköy alluvial fans form 10 to 15 m thick deposits constituted of coarse gravels with sand matrix. Gravels are poorly sorted and rounded and show imbrications south-southeast. Between Gaziköy and Mursallı the Quaternary is mainly represented by debris deriving from the steep slopes of the Ganos Mtn. that is made of Eocene turbitides. Poorly sorted and rounded coarse gravel with coarse sand matrix form colluvial packages up to 10 m thickness along the southern limp of Ganos Mtn. (Plate 1). West of Mursallı, the fault forms small step-over basins field with reworked sediments from the Miocene sandstones (Kirazlı formation). The medium consolidated sandstone are easily eroded and deposit as fine grained material (sand to clay) along the depressions and streams beds between Mursallı and Yörgüç. At Gölcük, a step-over basin is filled with coarse to fine sediments deriving from several sources; ophiolites, turbidites, and fine grained beach rocks. The basin is filled with coarse alluvial units on its north, while finer sediments deposit along the linear depression on the south (Plate 1). The Quaternary deposits on the western part of the Ganos fault are sediments of the Evreşe basin. The basin is filled with alluvial and fluvial deposits mainly of the Kavak River. However, at outcrops next to some hills in the basin, marine sediments and shells are observed.

### 4.3. Morphologic Framework of the Ganos Region

The most prominent geomorphic structures in the Ganos area are the two topographic highs (white areas in Fig. 4.2) separated by a distinct linear narrow valley (Fig. 4.2, 4.3). In The northern high area, the Ganos Mt forms a 35-km-long elliptical-shape smooth high topography with an average 7-8 km width. The broad morphology of the mountain suggests that uplift occurred within a uniformly distributed deformation. The southern limb of the ridge is truncated by the Ganos fault, which is the origin of the linear narrow valley. The ridge axis of the Ganos Mt. is sub-parallel (~N65°E) to the Ganos Fault (N70°E).

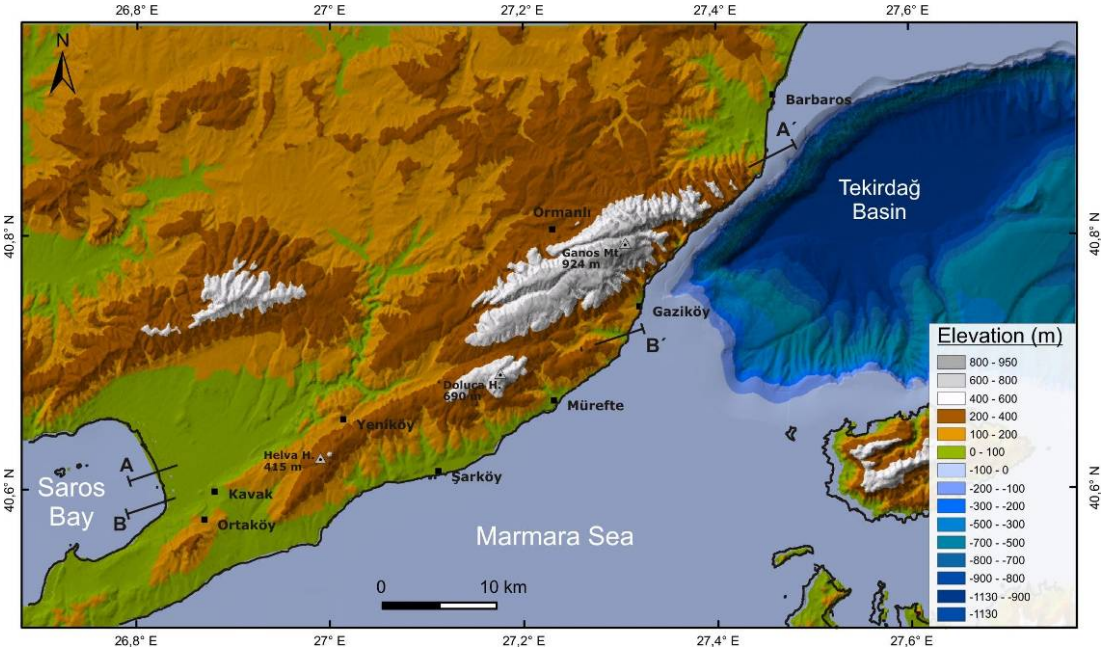


**Figure 4.2 :** Classified elevation map of the Ganos region. The linear valley marks the N70°E trending Ganos fault, which is expressed in between two topographic highs; Ganos Mt. and Doluca H. The uniform structure of the Ganos Mt. and the drastic decrease in elevation from 924 to -1125 m on its eastern part is distinct (see text for detail).

The highest point of the Ganos Mt. (924 m) is located at the eastern part, nonetheless a few kilometre farther east the elevation decreases drastically about 2000 m. Steep slopes of 40-50° on the east plunge into the Marmara Sea where a depth of -1125 m is reached; at the Tekirdağ Basin (Fig. 4.2). The top of the Ganos Mt. is flat and the surface is slightly tilted to the SW. This plateau is a relic surface now uplifted to > 600 m. The western termination of the Ganos Mt is smoother, where it dies out in the ~100 m high Evreşe plain (Fig. 4.2). The topography south of the fault is significantly lower and more composite (Fig. 4.2). Three linear ridges are identical, which highest points are the Doluca Hill (689 m) on the east, Helva Hill (446 m) in the centre and Tahta Hill (280 m) on the west. The ridge axis of these three highs are oblique (N40-50°E) to the Ganos Fault. The northern limbs of the eastern two hills are truncated by the Ganos fault, too. Armijo et al., (1999) notes the difference in morphology among the three folds. The highest anticline is to the northeast (669 m), is very well preserved; has a nearly intact domal shape. The middle anticline is less elevated (444 m) and clearly more eroded.

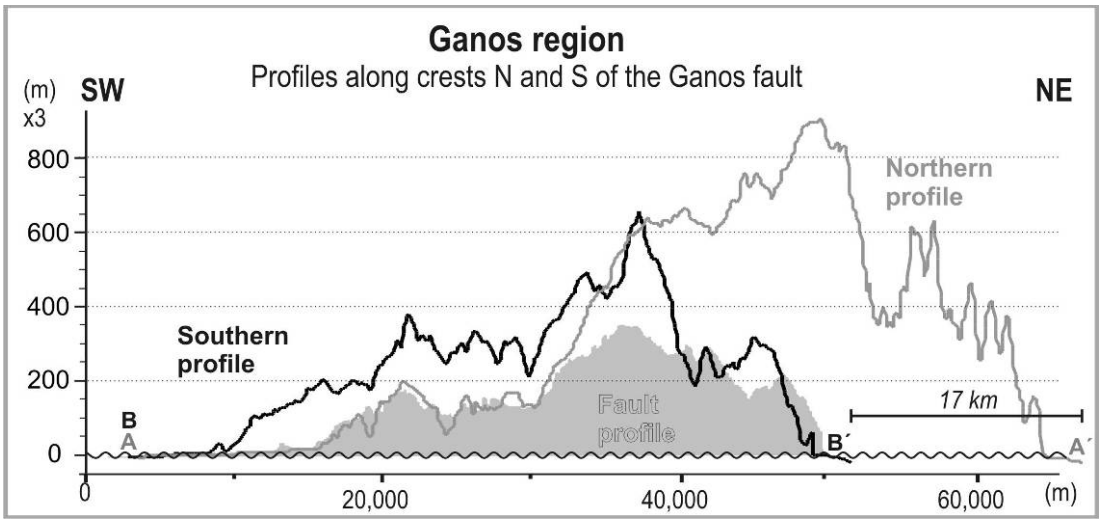


**Figure 4.3 :** Topographic profiles taken sub-parallel to the Ganos fault on each side and along the fault itself. Grey line illustrates the topography of the northern highest points, whereas the black line corresponds to the southern highs. The filled area shows the elevation of the Ganos fault. The depression formed by the fault is significant. The elevation on each side of the fault shows similar fluctuations. Comparable elevation changes are about 15-17 km apart on the NE, while they are parallel located on the SW. See Fig 4.2 for location of profiles.

The third anticline to the southwest, where the envelope of Miocene strata is the most eroded and almost entirely blanketed by younger alluvium and colluvium, is the lowest (280 m). Based on these observation Armijo et al., (1999) propose that the less eroded anticline (Helva Hill) is the youngest and currently the most active. For that reason south of the Ganos fault, folding activity decays south-westward along the trace of the North Anatolian Fault. As a result the oldest anticline located 70 km southwest on the Gelibolu peninsula represents the total offset of the North Anatolian Fault since the last 5 Ma (Armijo et al., 1999). The suggested age for the North Anatolian Fault in this region is disputed by Yaltırak et al., (2000). The 5 Ma age is constrained by an angular conformity between the Alçıtepe and Kirazlı formations that dates back to the Messinian crisis. However, Yaltırak et al., point out that the related units are conformably overlain and the correct age of the NAF is 3.7-3.4 Ma. The debate still continues since recent investigation of calcareous nannoplankton content of the related showed that the Alçıtepe formation is a Pliocene unit postdating the Messinian crisis and that the Kirazlı formation is a Late Miocene unit predating the crisis (Melinte-Dobrinescu et al., 2009).

The southern land is formed of several smaller hills intersected by deep and wide incisions, which suggests that the southern landscape experienced more erosion than

the north of the Ganos fault. The advanced erosion may be a result of two reasons: 1) a longer period of erosion or 2) due to the difference in lithology. Both interpretations may be valid. Zattin et al, (2005) applied apatite fission track analyses on sandstone samples on both sides of the Ganos fault and concluded that exhumation took place ~10 Ma earlier (Late Oligocene) on the southern part; hence erosion started at an earlier stage. Additionally, it also implies that a pre-existing structural discontinuity was present between the highs in Late Oligocene (Zattin et al; 2005; Yaltırak; 1996; Yaltırak & Alpar, 2002). As mentioned in the previous section the geology on two sides is also different. Lower Eocene to Lower Oligocene turbitides on the North are more resistive to erosion, while the Miocene fluvial and coastal deposits on the south are unconsolidated and erode easily. Hills in this region are associated with several landslides (Plate 1). For instance, the valley slopes of the Hoşköy river are regions were intense land sliding occurs. The south-eastern slopes of the Palamut H., Armutluk H., Bayrak H., and Panayır H. are also other areas were land-slides can be observed. Documents of the 1912 earthquake report land-slides triggered by tremor in these regions (Mihailovic, 1927).

The topography on both sides of the fault is highest on the east and decreases significantly down to sea level on their west with an important dissimilarity. The change in elevation is not proportional on the two sides. The decrease on the north is more drastic than on the south. In addition, the highest point along the fault and on the south is reached west of Yörgüç; after this locality the elevation is continuously higher on the south. The difference in elevation between the North and South is ~200 m. The Ganos fault shows also dissimilarity east and west of Yörgüç. On the east it runs along the southern limb of the Ganos Mt with an average trend of N70°E, while west of Yörgüç it strikes along the northern limb of Doluca Hill trending N67°E. The change occurs where the fault reaches its maximum elevation. The 3° anticlockwise rotation necessarily yields further compression in the region. Offshore and onland studies suggest that the Ganos fault dips to the north (85° - 50°) between the Tekirdağ basin and Mursallı (Yaltırak, 1996; Yaltırak & Alpar, 2002; Okay et al., 2004). West of this area, alterations of structure, geometry and dip may be associated. The morphology suggests that west of Yörgüç the compressional deformation is not anymore localized on the south. This is also consistent with geodetic observations where the GPS vectors strike parallel to the fault (see p. 44).

## 4.4. Morpho-tectonic Expression of the Ganos Fault Zone (onland)

The North Anatolian Fault is apparent as a linear narrow valley, trending approximately N70°E in the Ganos region. This valley is in general less than 1.5 km wide between the two topographic highs. Most of the deformation of the North Anatolian Fault is localized in this narrow zone. The dominant strike slip motion is well expressed by abundant morphologic structures along the entire onland section, (e.g. pressure ridges, shutter ridges, stream offsets, step-overs with right or left stepping jogs, releasing and restraining bends, back-tilted slopes and sagponds). Rectilinear valleys and pressure ridges reach a length up to 4 km with cumulative displacements of streams that vary from 10 to 1000 meters. The following paragraphs describe from east to west the main tectono-morphic features of the onland section of the Ganos fault.

The eastern most section of the Ganos fault is at Gaziköy, located close to the restraining Ganos bend (~17°) and uplift is evident in the region (Yaltırak et al., 2002). The Gaziköy village rests on a topographic high, south of the Ganos fault (Figure 4.4, Figure 4.5). This small hill (~58 m) consists of Upper Pleistocene coastal marine deposits tilted ~17° the southwest (Yaltırak et al, 2002).

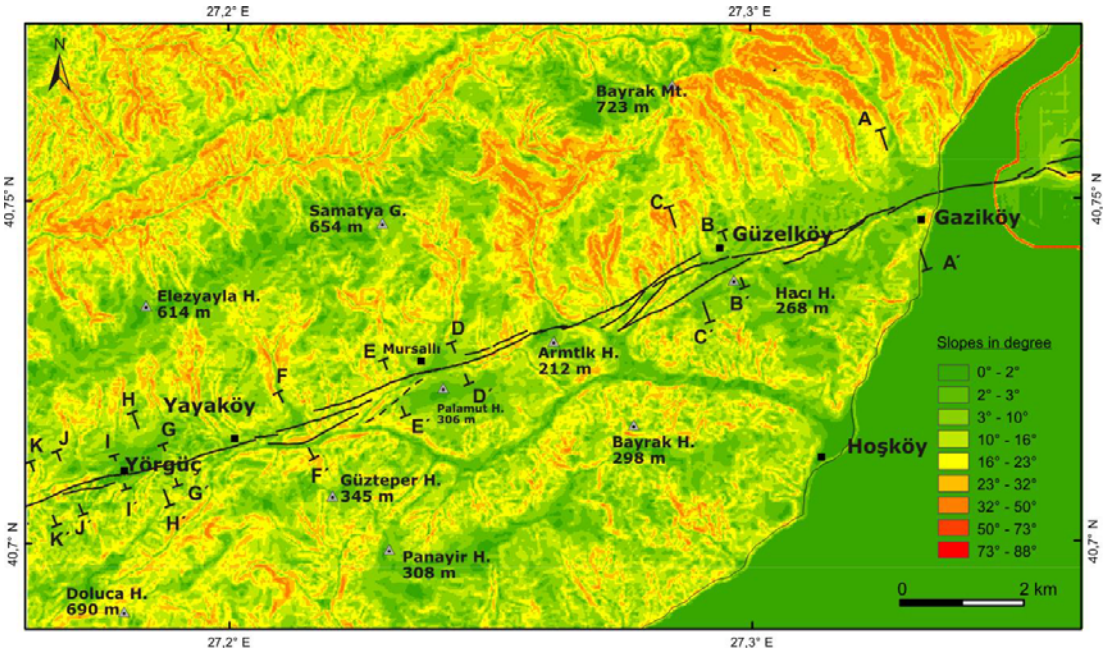


**Figure 4.4 :** Slope map of the eastern Ganos region. Slopes north of the Ganos fault are steeper, particularly to the east. The top of the Ganos Mt. is flat and slightly tilted to SW. Letters (A – A') and related lines indicate locations of topographic profiles in Fig 4.5

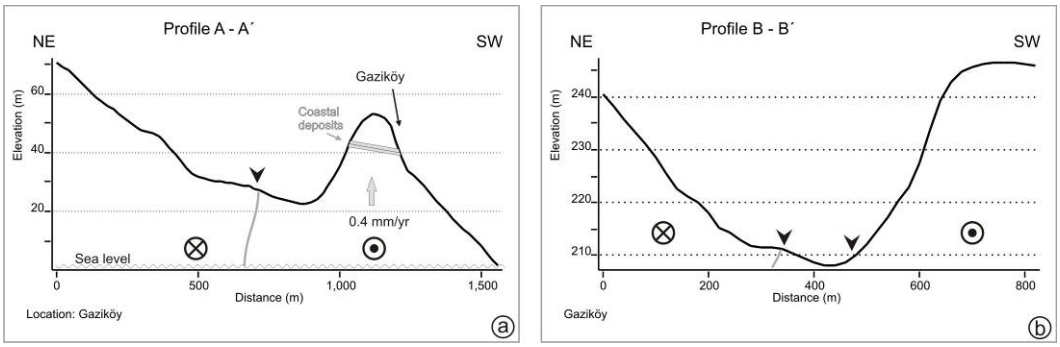


**Figure 4.5 :** Topographic profiles perpendicular to the Ganos fault. See Fig 3 for the location of profiles. Black arrow heads show the location of the Ganos fault. a) A profile near the Gaziköy coast. The uplift on the southern part is identical. b) A profile near Güzelköy. Two branches form scarps on the two sides of the depression. Most of the motion occurs on the northern branch; therefore its scarp is more identical. See Fig 4.4 for location of profiles.

The present day location of these deposits (at 40 m) and U/Th dating of marine shells suggest sustained uplift since 225 ka and an uplift-rate of 0.4 mm/yr for the Gaziköy region. The Ganos fault is located north of the hill. Here, SE trending linear channels and ridges are truncated by the Ganos Fault (Fig. 4.5). 1 to 5 m right-lateral offsets related to the 1912 earthquake were documented at this part of the fault (Yaltırak, 1996). The southern ends of the ridges are right laterally displaced by successive strike-slip faulting and act therefore as shutter ridges. Other drainages are merged into a tectonic linear depression between Gaziköy and Güzelköy (Fig. 4.6). Streams join along this depression and flow towards the coasts of Gaziköy or Hoşköy. At Güzelköy, south of the village the fault forms minor releasing step-overs. This geometry creates a saddle-like linear depression. Towards west of the village, cumulatively displaced structures are abundant and their slip ranges from a few to several hundred meters. Along the whole section between Güzelköy and Yayaköy, the Ganos fault is associated with southward branching (Fig. 4.4, 4.7). The branches are mainly 1-2 km long and show minor deflections on streams. Most of the slip occurs significantly along the northern main portion. This is evident by steep scarps forming a single deep narrow valley and cumulative displacements (Fig. 4.6, 4.7). The southern branches express minor slip and fault morphology.

The main fault branch shapes the southern slopes of the Ganos Mt. by creating steep slope breaks and successive stream offsets until Mursallı. Fault splays are noticeable until Yayaköy. West of this village, branching is no more significant. The fault is

localized in a relatively narrow zone. Tectonic movement, associated with rapid erosion of poorly consolidated Miocene sedimentary deposits creates a deep and narrow valley east of Yörgüç. The valley is bounded with steep walls, particularly the northern wall. Scarps of 1 to tens of meters signify the Ganos fault on the northern valley side (Fig. 4.7, 4.8). The fault geometry is composed of several right-steps which control the formation of the linear depression.

At the western end of the valley the fault climbs up to the plain land of Yörgüç. Here, the fault is apparent by sagponds and saddles. At a larger scale, the Yörgüç area is a Quaternary basin consisting mainly of reworked Miocene sandstones. The basin is formed by a 200-m-wide releasing bend. The Ganos fault reaches its maximum elevation west of Yörgüç and looses continuously elevation farther west.

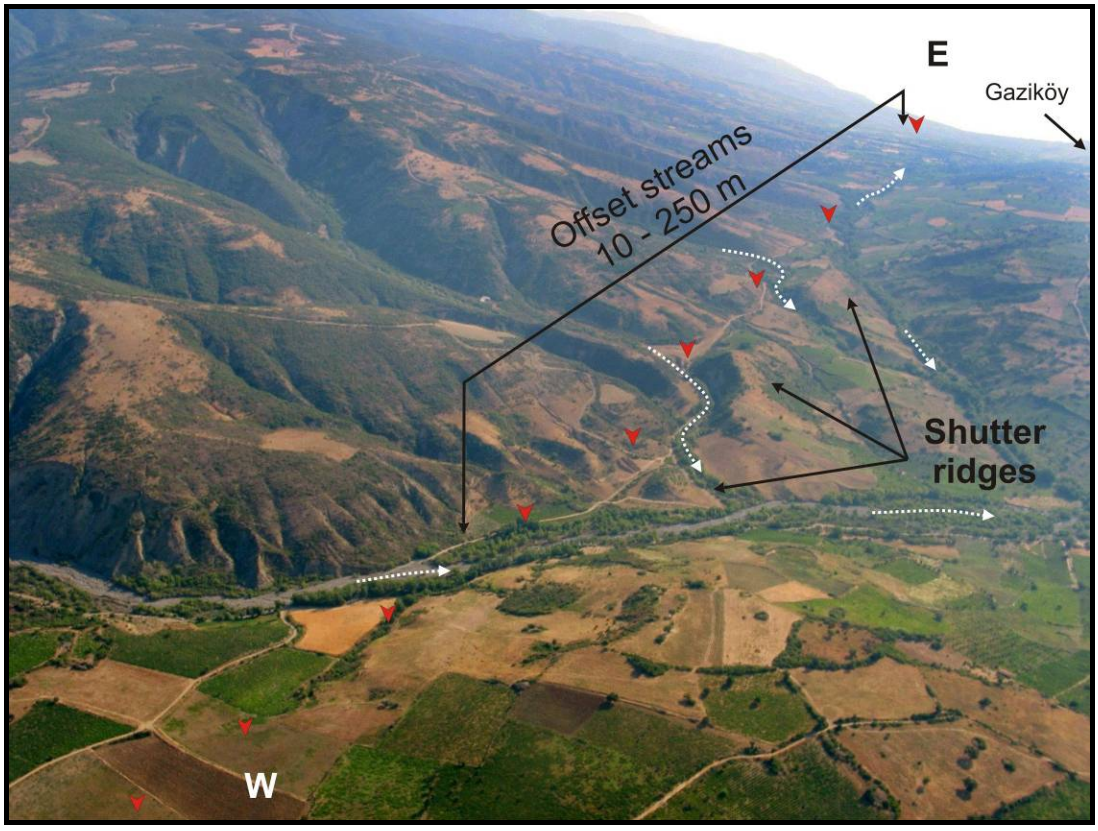


**Figure 4.6 :** Oblique aerial photo of the Mursallı – Gaziköy region shows the linear fault morphology (red arrows) that truncates several streams and ridges and forms shutter ridges and offsets. White arrows show streams. A trenching study conducted at this locality exposed evidence of recent faulting.(Aerial photo from S. Pucci).

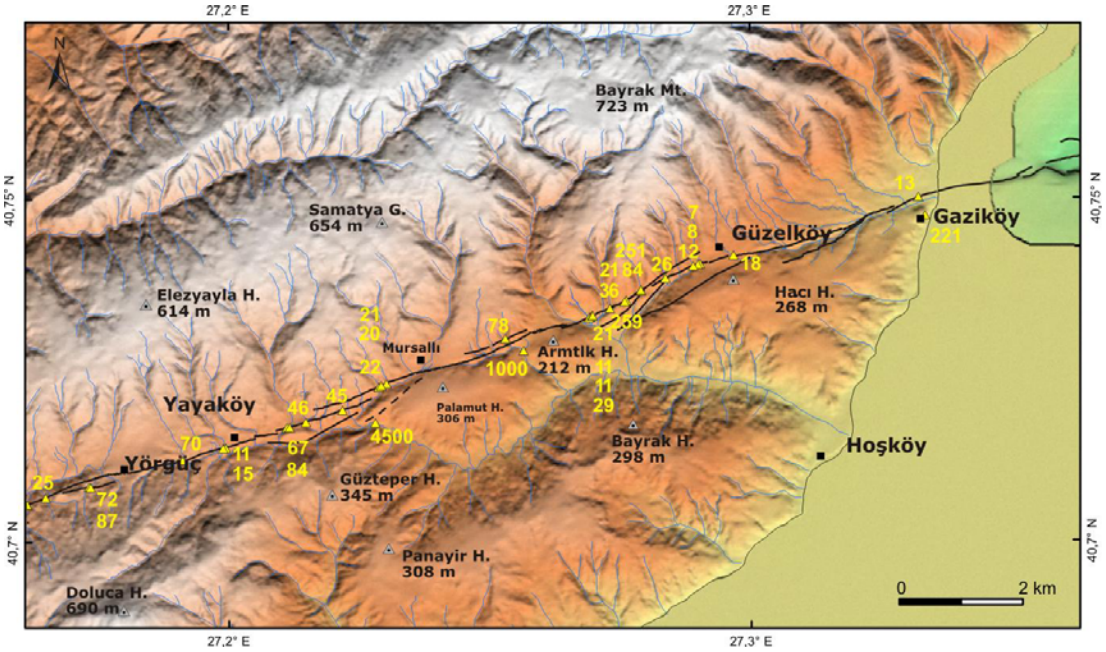


**Figure 4.7 :** Shaded relief map of the eastern part of the Ganos fault. Blue lines indicate streams, yellow numbers are cumulative offsets in meters. The fault is characterized here with short southward branches. Between Gaziköy and Yörgüç the North Anatolian Fault strikes along the southern slope of the Ganos Mt (Northern High).

West of the village the fault enters again an NE-SW trending linear valley. This valley is wider than the eastern one but here the width is established with significant erosion of the Gölcük River's drainage system. The bedrock on the north and south of the fault are deeply incised by SW and NW flowing short streams, respectively. The fault runs along the northern wall, where 10 - 30° slopes are interrupted by flat surfaces (Fig. 4.9, 4.10). This surfaces lie on the southern slope of the Doluca H. valley (Fig. 4.10). They are distinct and from east to west at an elevation of 40 to 20 m respectively (relative to the valley floor). They consist of basement rocks and bear no fluvial deposits, hence are not terrace risers.

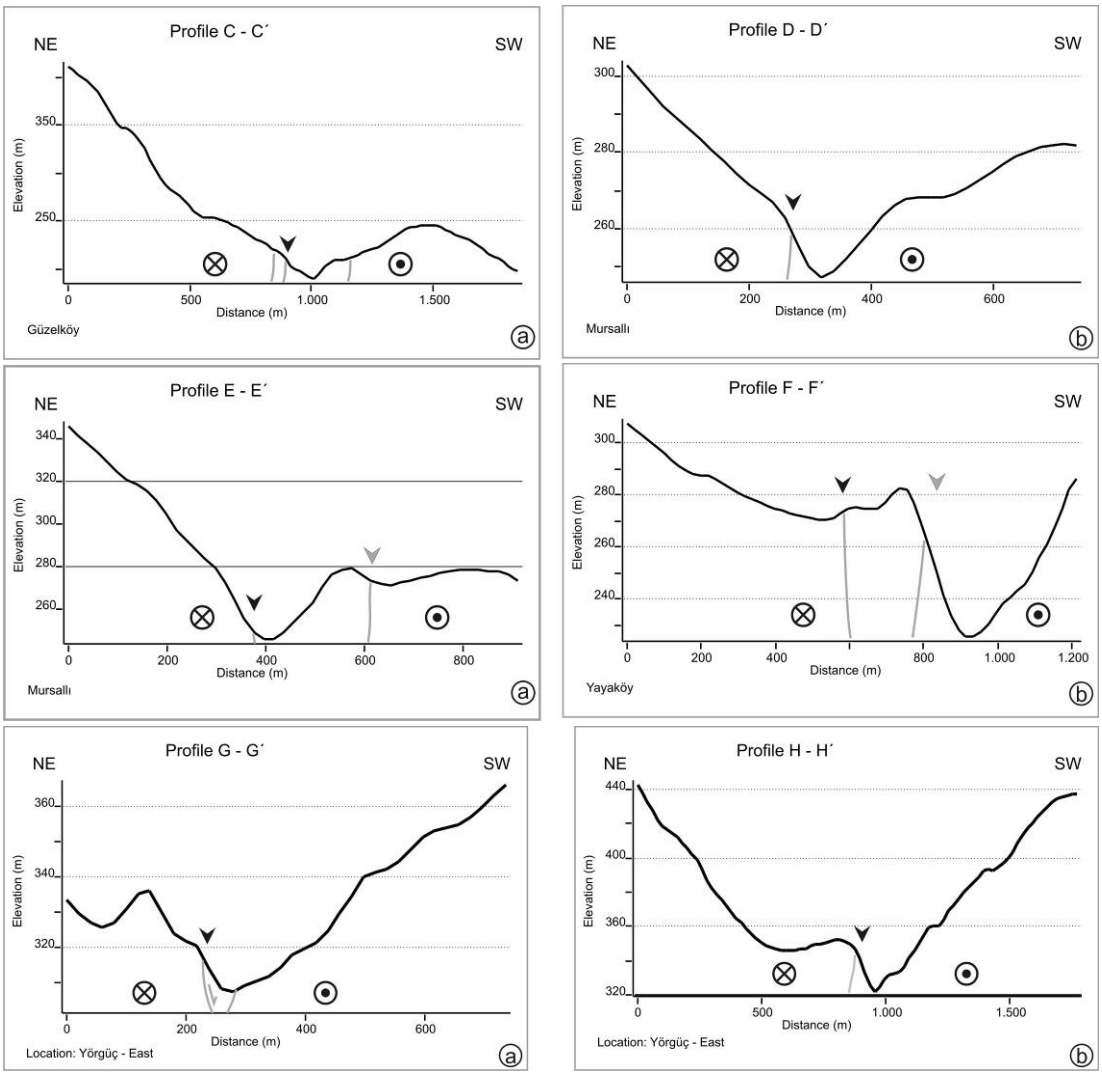


**Figure 4.8 :** Topographic profiles from Güzelköy, Mursallı, Yayaköy and Yörgüç regions; taken orthogonal to the fault direction. On both profiles the valley formed by the North Anatolian Fault is clearly visible. The northern slopes show scarps representing recent earthquake faulting, while southern slopes are relatively smoother. Black arrows indicate the main active branch, grey arrows point secondary branches (Scales are various among profiles; see axes for reference).

Consequently, we consider that they are formed by back-tilting along a strike-slip fault, which encompasses a significant amount of vertical component on the northern block. For instance, near Gölcük we observe alluvial fans at a height of 20 - 30 m to the basin bottom; they are developed on these surfaces and signify the uplift in the region (Fig. 4.11b). These surfaces experience less erosion and bear good indicators of recent earthquake faulting. For example, ~100 m on the east of the alluvial fans the Ganos fault forms two sagponds on such a tilted surface (Fig. 4.11c). The first pond is ~10-m-wide, ~30-m-long and shows subsidence of about 1.5 m, while the second is smaller in size (~3x6 m with ~30 cm subsidence). Both sagponds show a

linear northern margin, while their southern limit is convex. The surface where the sagpond are located is dipping southward, due to back-tilting. This type of sagpond is abundant at various scales along the Ganos fault. A similar large sagpond is visible at Kavak, which is described in the following lines.

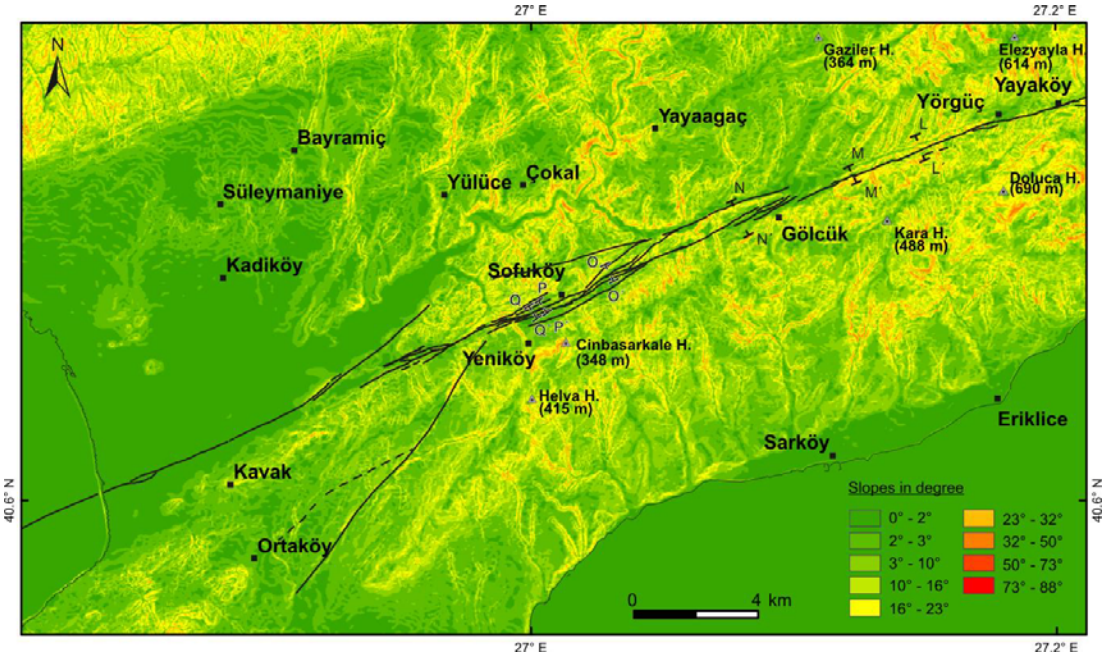


**Figure 4.9 :** Slope map of the western part of the Ganos fault. The Evreşe plain is prominent with low slope values. The near field of the Ganos fault is comprised by steep areas. Another distinct feature along the fault is the Gölcük basin, where the fault is associated with right steps.

The drainage in this area shows a specific character. Southern streams flow almost perpendicular to the fault and exhibit cumulative displacement. The northern streams however are all NE-SW oriented. The streams on both sides join in the valley to a single main river, which flows westward to Gölcük. Bedding on the north is sub-parallel to the Ganos fault and layers dip north with high angles (Fig. 4.12). The distinct NE orientation of the streams may be either related to the local geology or due to continuous rotation within the strike-slip system.

Between Yörgüç and Gölcük the geology shows also a fault contact relation among the north and south. The north of the valley consists of Eocene turbitides, while the south is made of Palaeocene metamorphic and Miocene sedimentary units, limited by a fault contact (Plate 1).

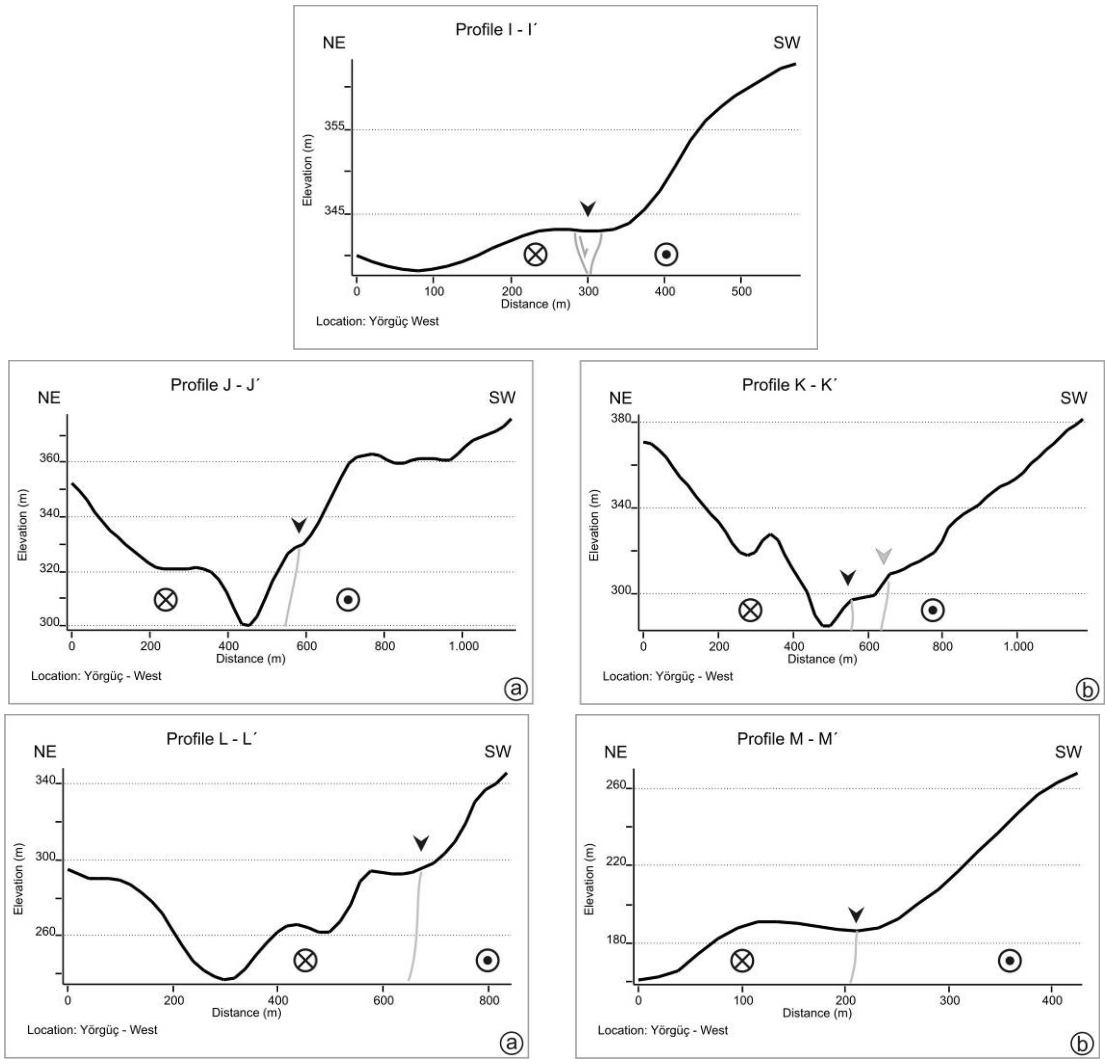


**Figure 4.10 :** Topographic profiles west of Yörgüç. Here the fault strikes along the southern margin of the valley. The elevation of the fault decreases westwards and back-tilted slopes become distinguishable. Profiles are at various scales; see axes for reference. Location of the profiles is given in figure 4.9.

From Yayaköy to Gölcük the Ganos Fault runs as a single linear fault section. We observe no branching along this section like on the east. All short-term displacements are on the southern streams and ridges limited in a zone of < 30 m. This shows that slip of the Ganos fault is localized here on a very narrow zone and all offsets illustrate the concentrated displacement of the NAF.

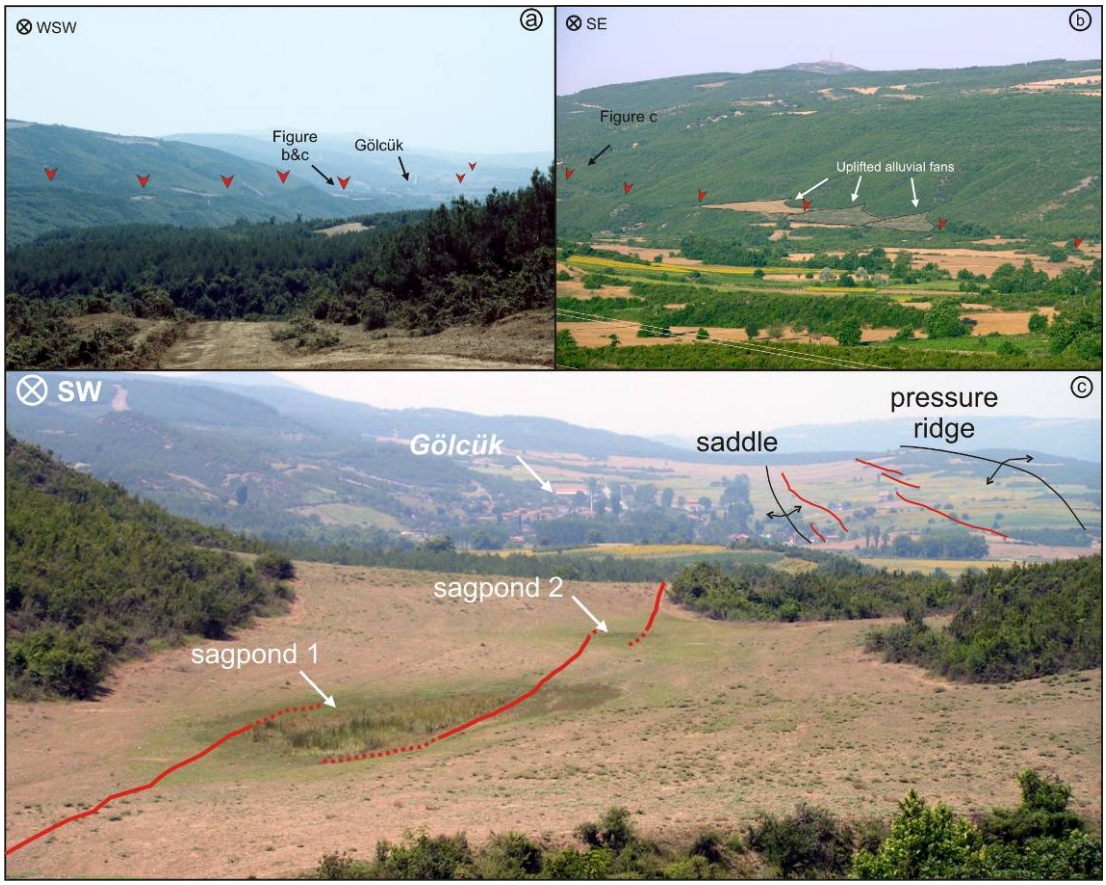


**Figure 4.11 :** Figure a, b, and c illustrate the prominent morphology of the Ganos fault east of Gölcük. The fault forms back-tilted surfaces on the northern limb of the Doluca Hill (a, b). Alluvial fans at 20-30 m above alluvial plane signify uplift in the region. c) East of these fans the fault forms two sagponds; sagpond 1 is about 10 x 30 m in dimension and a subsidence of ~1,5 m, whereas sagpond 2 is about 3 x 6 m and shows subsidence of ~30 cm. The sagponds have a straight northern boundary; however their southern limit is convex. Note that the surface is tilted against the main slope direction. West of Gölcük the fault strikes along the southern margin of a pressure ridge and smoothes the slope with several releasing step-overs. Description of en-echelon strike-slip faulting was reported here, after the 9 August 1912 earthquake (Mihailovic, 1927).

At Gölcük the topography is fairly low (100 - 200 m). Hills are highly eroded and the land is flat, but slightly tilted (1 - 5°) to the NW (Fig. 4.9). At Gölcük two relatively large streams (the Gölcük river and the Koca river) join and flow towards east. Both rivers deposit significant amount of sediment in this area; however the shape of the basin is nearly rhombus, which points to a tectonic origin (Plate 1). In deed, at Gölcük the Ganos fault makes a 300-m-wide releasing step-over, hence pull-apart tectonics is dominant in the basin formation. Just west of Gölcük the fault forms a 6-km-long linear ridge, bounded by strike-slip faults on its two sides. The eastern tip of

the ridge is exposed at a road cut (Fig. 4.13). The units in the exposure are highly sheared and faulted. We determined several faults striking to the top of the hill and capped by the soil part. The outcrop represents a part of~12 m of the ridge; however the maximum width of the ridge reaches 600 m and is asymmetric in NS direction. The southern slopes of the ridge are < 10°, whereas the northern slopes range from 10° - 30° (Fig. 4.9). In addition, the elevation south of the ridge is ~50 m higher than on the north (Fig. 3.15a). The significant difference in elevation indicates that the linear ridge is not formed dominantly as a push-up structure. The formation is associated with continuous back-tilting and right-lateral slip. The western ridge is oriented ~18° oblique to the strike of the Ganos fault (N65°E). It is also bounded by strike-slip faults on its two sides. Sagponds on top of the ridge suggest a complex uplift such as observed on positive flower structure. The orientation of the fault results in compression and the ridge is pushed-up in form of positive flower structure. Sagponds form between two lifted blocks.

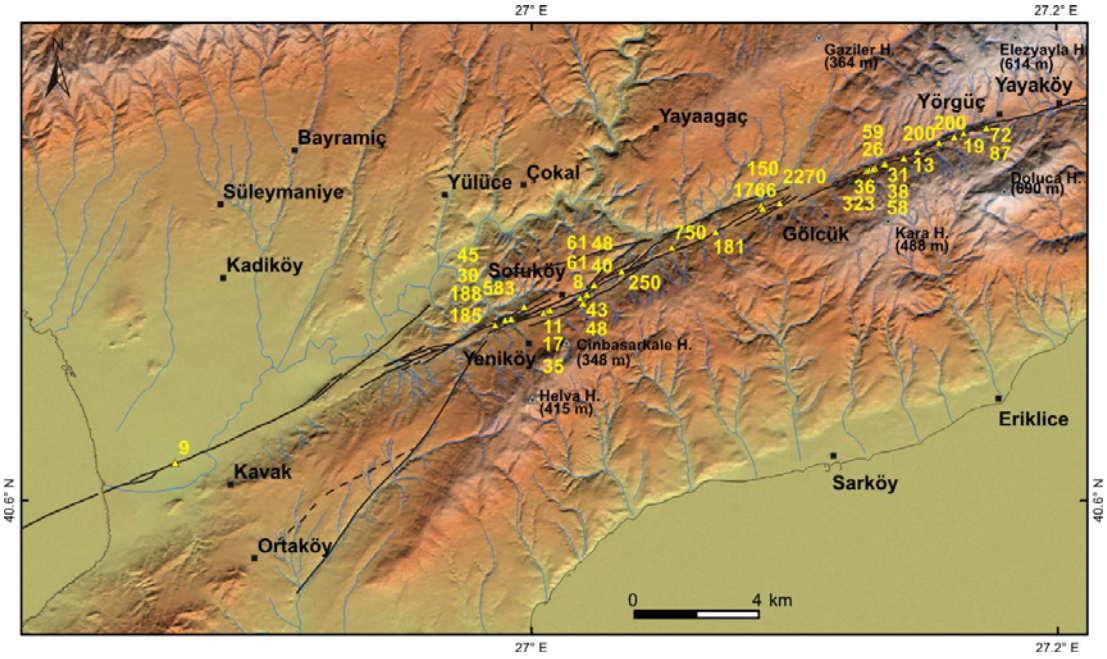


**Figure 4.12 :** Shaded relief map of the western part of the Ganos fault. Blue lines indicate streams, yellow numbers are cumulative offsets in meters. The fault is characterized with continuous linear strands between Yörgüç and Gölcük. Further west the structure becomes more complex. The fault runs mainly along the northern slope of the southern high land. A very linear narrow fault section is visible North of Kavak where the fault runs into the Evreşe plain and from there to the Saros bay.

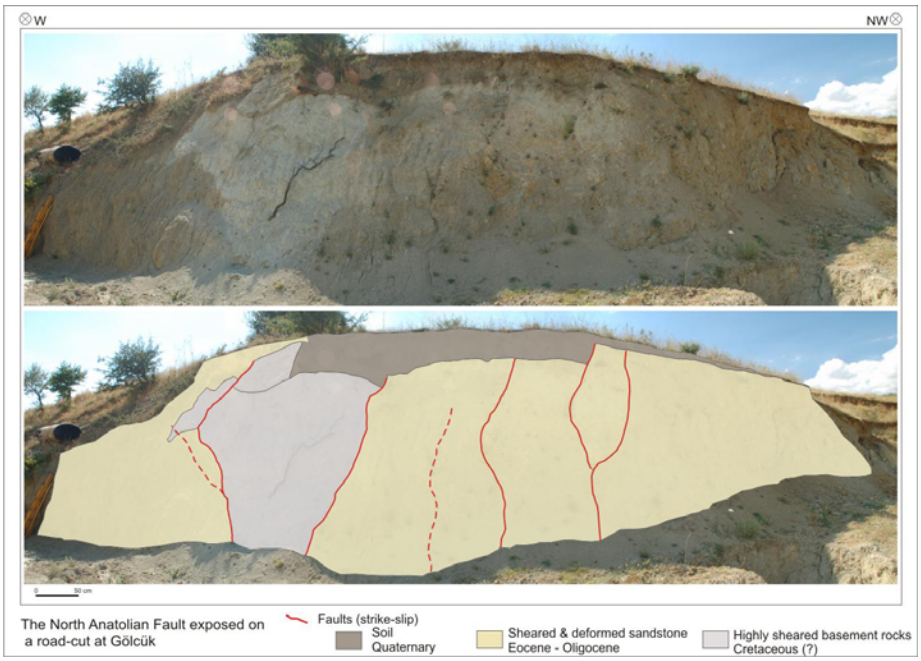


**Figure 4.13 :** Road-cut south of Gölcük exposing the eastern tip of the linear ridge west. Intense faulting is exposed in the outcrop indicating that the ridge is of tectonic origin

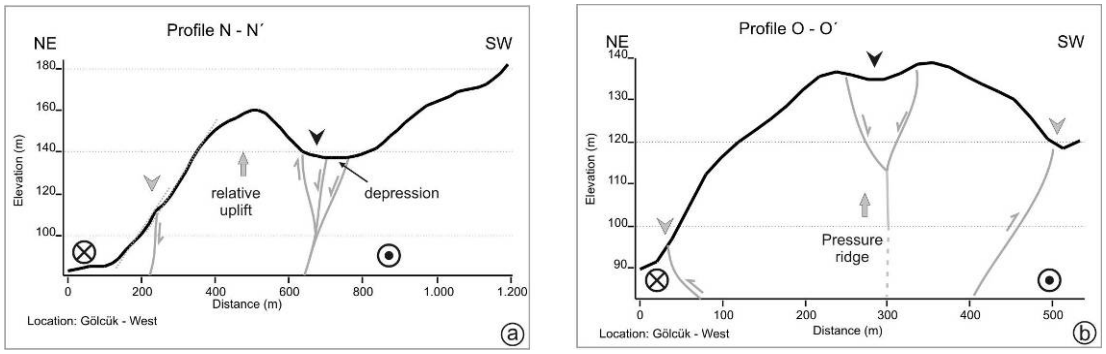


**Figure 4.14 :** Topographic profiles from west of Gölcük. a) Correspond to the linear ridge located just west of Gölcük. The ridge is formed by continues strike-slip faulting and back-tilting associated with uplift. b) is a ridge oriented oblique to the Ganos fault. It is bounded by strike-slip fault and is formed as pressure-ridge.


**Figure 4.15 :** A linear pressure-ridge west of Gölcük oriented 18° oblique to the Ganos fault. It is bounded by strike-slip faults and rises as a push-up structure.

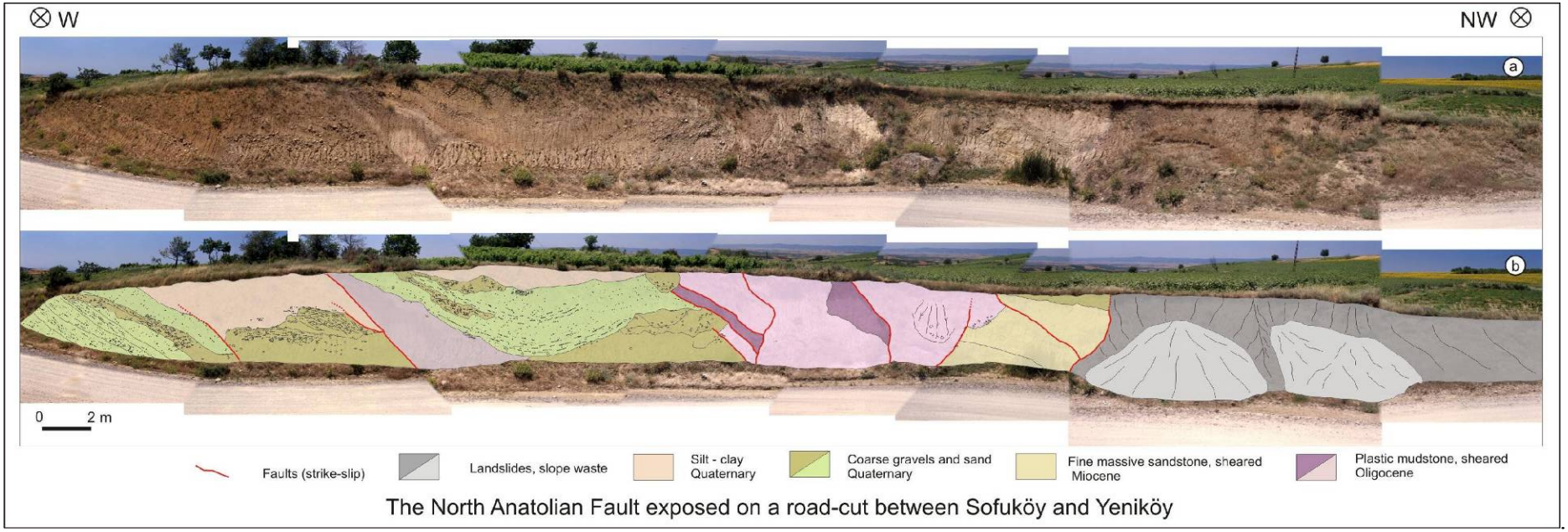


**Figure 4.16 :** An outcrop of the North Anatolian Fault zone on the road between Sofuköy and Yeniköy. b) The detailed mapping of the out-crop shows that Oligocene to Quaternary deposit are limited by fault contacts

The area between Gölcük and Yeniköy is associated with several parallel fault segments. At a large scale the Ganos fault forms here a ~350 m-wide restraining bend (Plate 1). This structure is coupled with minor releasing and restraining step-overs. We observe sagponds and linear depressions on the top of the ridges (Fig. 4.14b).

At Sofuköy the fault zone is again exposed on a 60 m long road-cut. Figure 4.16 illustrates the mapped section of the out-crop. Four main units have been identified; Gazhanedere Fm. Kirazlı Fm. Fluvial deposits and lacustrine deposits. They are limited by faults. The sense of motion could not be clearly identified, no vertical component was evident. We consider that the main sense of slip is right lateral strike-slip faulting. Right lateral displacement is evident in the region, where we observe several prominent right-lateral co-seismic offsets of field limits; a hundred meter east of the road-cut. West of the road-cut a depression is significant. The northern margin of the pond is limited by a ~70 cm high scarp. This structure is formed as a tectonic depression. To the west the northern branch, the fault runs along a 2-3 m high scarp. An abandoned valley is right-laterally offset a few tens of meters. Further west, the fault is evident by further offsets, with shutter ridges which are cumulatively displaced. West of Yeniköy the fault runs through a fairly low and smooth land. The landscape is highly eroded. Agricultural facilities are dominant and the fault runs through fields. Tectonic movement is evident by distinct slope breaks on the slopes of linear ridges. The fault strikes as a nearly single linear strand forms linear depressions on the slope breaks (Fig. 4.17). This pattern is continuous until the Kavak Lake.


**Figure 4.17 :** West of Yeniköy the fault runs through a fairly low and smooth land. The fault can be observed along linear ridges, where slopes are apparently interrupted by back-tilted surfaces.

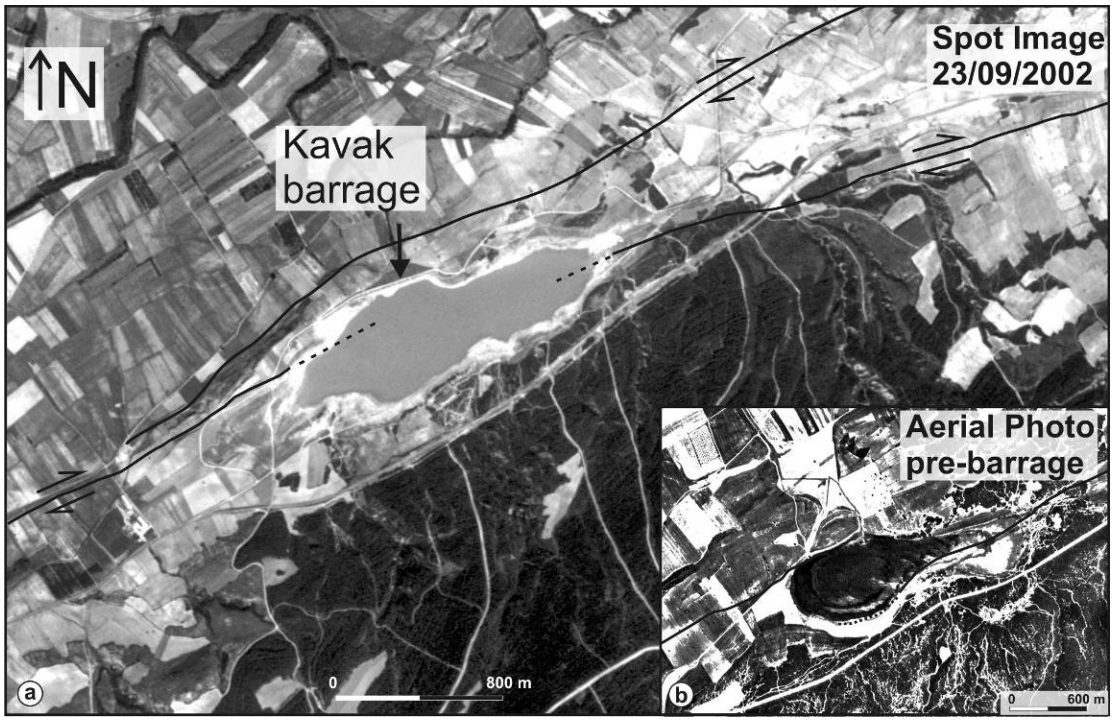


**Figure 4.18 :** A lake east of Kavak located on the Ganos fault. The spot image shows the modified shores of the lake. A barrage is located on its northern part, built in 1989. The barrage is filled into a valley from which the fluvial water input was discharged. b) the aerial photo shows the site prior to the construction of the dam. A depression of tectonic origin is apparent. See text for detail.

Kavak Lake is an elongated dam lake built on the Ganos fault in 1989 (Fig. 4.18). The size and morphology suggested a tectonic origin. However, landscape modifications in the surrounding of the lake are hindering proper interpretation. Aerial photos prior to its construction provide an insight into this problem (Fig. 4.18b). The apparent original morphology designates a typical sagpond structure. The pear like shape, and two convexities on the south points to an origin of probably two sagponds of which the western one was larger. Progressive faulting and subsidence may have joined the adjacently situated two ponds to a single pond (comparable with ponds in figure 4.11c). The pond rests ~20 m above the floor of the Evreşe plain. This surface is a part of the hill slope on the south, which is also back-tilted. Therefore, the geometry and location of the ponds are identical to the sagponds illustrated in Fig. 4.11, 4.17. The barrage was built by filling a valley north of the lake. This valley was formed by streams which flew into the depression. At stages of high water level the discharge occurred through this valley. It is important to note that the depression is of tectonic origin and served as a collector for the streams on the south. Such configuration of streams and sagponds lying on a slope break are

visible along the Ganos fault. However, they represent a younger stage; while the Kavak lake is a mature sagpond.

West of the Kavak Lake the fault enters a flat plain, the Evreşe plain. Evidence of the location of the fault is poor. The linear drainage parallel to the strike of the Ganos fault rests most probably in the tectonic depression. Clear evidence is available on the coast of Kavak where a large sagpond; 300 m x1400 m in dimension is visible (Fig. 4.19). The shape of the sagpond is elongated. However the northern boundary is clearly sharper and linear, while the south shows a smooth convex shape. Although this pond is one of the largest along the Ganos fault, it shows minor subsidence; less than 70 cm. A few hundred meters east of the pond paleoseismic studies exposed evidence of successive earthquake faulting (Rockwell et al.; 2001, 2009)

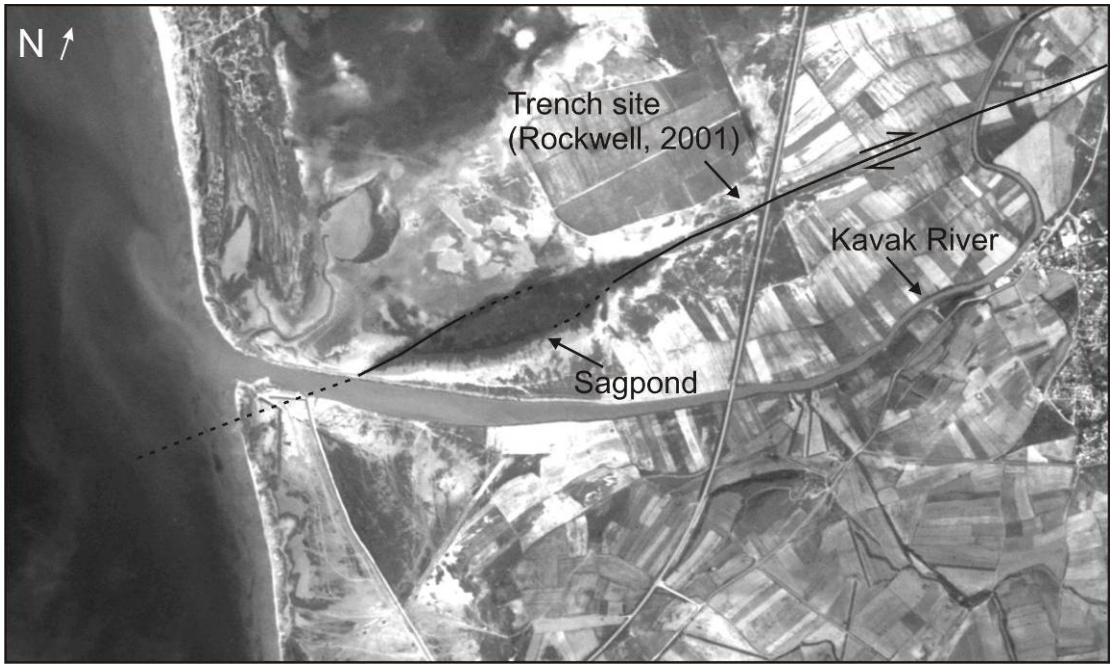


**Figure 4.19 :** The sagpond represents the westernmost fault morphology of North Anatolian Fault . The site is located closely to the paleoseismic trench site of Rockwell et al (2001, 2009) where historical earthquakes are identified in the Holocene stratigraphy and a co-seismic slip is measured for the last two events.

The pond is the westernmost onland morphologic feature and an evidence of the NAF. West of this point the fault runs into the Aegean Sea through the Saros bay. Recent offshore studies provide detailed bathymetric data and exposed the offshore continuation of the NAF in the Saros bay (Ustaömer et al. 2008)

### 4.4.1. Offset measurements along the Ganos fault

Cumulative offset are prominent markers of the short- and long-term deformation of a fault system. We investigated the 45-km-long onland section of the Ganos fault in order to establish the long term behaviour of the NAF on its western most part. The observed offsets are mainly on streams; in addition significant displacement was recorded on ridges, paleo-channels and man made structures (e.g. roads). Measurements were carried out using various remote sensing methods. Digital Elevation Model (DEM) data was used as a base to determine significant slips. The DEM's were processed in multiple ways to enhance structures along the strike; e.g. hill-shading, sun angle maps, slope maps, density plots and 3D visualization. Aside we used SPOT 5 images (5 m resolution), regular aerial photos, paraglide aerial photos and partly Google Earth images to document offsets. Remote observations were afterwards verified by field investigations. At some sites we used total station or DGPS system to obtain more precise measurements.

The analysis of the entire onland fault section allowed to document 69 right-lateral cumulative displacements. Most of our measurements resulted in slip values less than 100 m; nonetheless even if sparse higher measurements were present. Table 4.1 lists the long- and short-term slip distribution of the Ganos fault. The detailed locations of offsets are given in Fig. 4.7, 4.12; indicated with yellow numbers. The offsets values range from tens to thousands of meters and signify the slip of different time intervals. Therefore, we classify these values into two main groups; long-term offsets and short-term offset.

#### 4.4.1.1. Long-term-offsets

Large scale offset bear the slip record of a fairly long time interval depending on the slip-rate of the fault system. We investigated the large slips along the Ganos fault to establish the long-term behaviour of the westernmost segment of NAF. We determined 31 right-lateral offsets larger than 50 m, along the whole onland fault section (Table 4.1). The following paragraph describes some of the prominent displacements starting from the east towards west.

The steep slopes between Güzelköy and Mursallı form streams and ridges trending almost orthogonal to the fault. The NAF truncates and displaces these structures at various scales. Displacements larger than 50 m are displayed in figure 4.20, where

two offset streams and shutter-ridges are significant. We measured 8 offsets (> 50 m) in this region. The most distinct features in the area are the Palamut Hill (306 m) and the Armutlu Hill (212 m). Both hills are intersected by large deep incisions on their SW and NE sides. The size of their channels is not comparable with the incisions and size of their present day drainage catchment. The incisions must be a remnant of other drainage basins which are now disconnected by successive right-lateral motion. We made correlations between channels to estimate the amount of slip in the drainage system. Individual measurement of comparable size of channels yield right-lateral offsets of ~250 m, ~1000 m, and ~4500 m. Reconstructions at these rates of slip showed good matching with other catchment systems (Fig. 4.12).

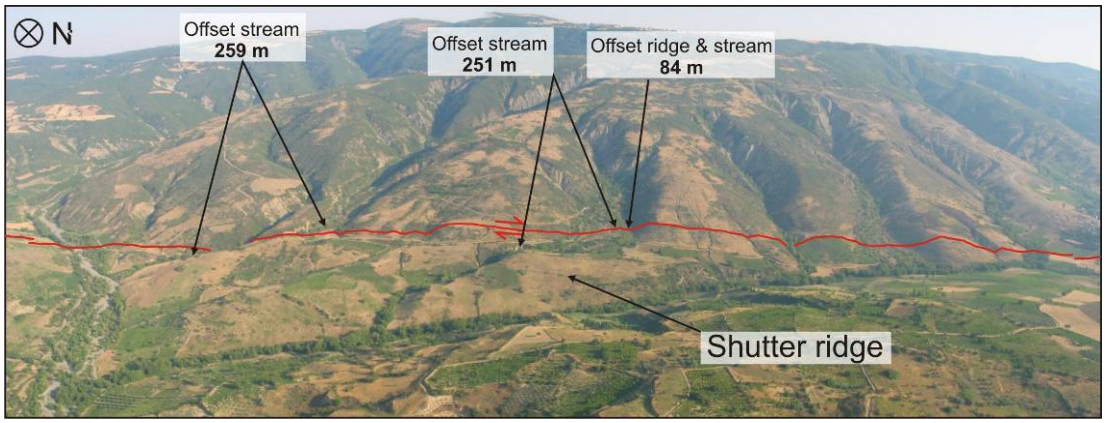


**Figure 4.20 :** The fault section between Güzelköy and Mursallı. Streams on the steep slopes of the Ganos Mt. form deep incisions orthogonal to the fault strike. This orientation allows a good correlation of displaced structures on each side of the fault. At some localities streams are highly deflected because shutter-ridges blocked their initial flow direction. For exact locations of the offsets see the map on Figure 4.12 and 4.21

**Table 4.1 :** List of measured cumulative offsets See Appendix A2 for locations.

| Id | Offset | Error | Location | Structure | Dist. Along fault (km) |
|---|---|---|---|---|---|
| 1 | 7.0 | 0.3 | Güzelköy | Tree limit | 0.30 |
| 2 | 8.0 | - | Güzelköy | Stream | 0.42 |
| 3 | 8.0 | 2.0 | Sofuköy Lok 495 | Stream | 3.44 |
| 4 | 9.0 | 1.0 | Kavak | Paleo-channel | 42.74 |
| 5 | 10.6 | 0.5 | Sofuköy | Stream | 4.00 |
| 6 | 11.0 | 0.5 | Güzelköy | Paleo-channel | 4.03 |
| 7 | 11.0 | 0.3 | Güzelköy | Stream | 4.11 |
| 8 | 11.0 | 1.0 | Yayaköy | Stream | 4.60 |
| 9 | 12.1 | 0.3 | Güzelköy | Stream | 5.04 |
| 10 | 12.6 | 0.2 | Güzelköy | Ridge | 5.05 |
| 11 | 12.7 | 0.5 | Gaziköy | Road | 5.32 |
| 12 | 12.9 | 2.0 | Yörgüç | Stream | 5.35 |
| 13 | 15.0 | 0.5 | Yayaköy | Road | 5.61 |
| 14 | 17.1 | 0.5 | Sofuköy | Stream | 5.91 |
| 15 | 18.0 | 0.5 | Güzelköy | Stream | 5.92 |
| 16 | 19.0 | 2.0 | Yörgüç | stream | 5.96 |
| 17 | 20.0 | - | Mursalli | Stream | 5.98 |
| 18 | 21.0 | 0.5 | Güzelköy | Paleo-channel | 7.16 |
| 19 | 21.0 | 1.0 | Mursalli | Ridge | 7.16 |
| 20 | 22.0 | 1.0 | Mursalli | Stream | 7.37 |
| 21 | 25.0 | 2.0 | Yörgüç | stream | 9.43 |
| 22 | 25.5 | 2.0 | Yörgüç west | Stream | 9.52 |
| 23 | 26.0 | 2.0 | Güzelköy west | Stream | 9.56 |
| 24 | 29.0 | 0.5 | Güzelköy | Stream | 9.82 |
| 25 | 30.0 | 1.0 | Yeniköy | Stream | 10.24 |
| 26 | 31.0 | 2.0 | Yörgüç | Stream | 10.86 |
| 27 | 35.0 | 0.5 | Sofuköy | Stream | 11.14 |
| 28 | 36.0 | 1.0 | Güzelköy | Stream | 11.18 |
| 29 | 36.0 | 3.0 | Gölcük east | Ridge | 12.23 |
| 30 | 38.0 | 4.0 | Gölcük east | Ridge | 12.27 |
| 31 | 40.0 | 5.0 | Sofuköy east | Stream | 12.95 |
| 32 | 43.0 | 2.0 | Yeniköy | ridge | 14.50 |
| 33 | 45.0 | 5.0 | Mursalli west | Ridge | 14.52 |
| 34 | 45.0 | 1.0 | Yeniköy | Ridge | 15.25 |
| 35 | 46.0 | 5.0 | Yayaköy east | Stream | 15.58 |
| 36 | 47.0 | 2.0 | Yeniköy | stream | 16.12 |
| 37 | 48.0 | 5.0 | Sofuköy east | Ridge | 16.86 |
| 38 | 58.0 | 2.0 | Yörgüç | Stream | 17.34 |
| 39 | 59.0 | 5.0 | Gölcük east | Stream | 17.95 |
| 40 | 61.0 | 5.0 | Sofuköy east | stream | 17.96 |
| 41 | 61.0 | 5.0 | Sofuköy east | Ridge | 18.02 |
| 42 | 67.0 | 5.0 | Yayaköy east | Stream | 18.32 |
| 43 | 70.0 | 10.0 | Yayaköy | Stream | 18.37 |
| 44 | 72.0 | 5.0 | Yörgüç | stream | 18.52 |
| 45 | 78.0 | 10.0 | Mursalli east | Stream | 18.61 |
| 46 | 84.0 | 10.0 | Güzelköy east | Stream | 21.5 |
| 47 | 84.0 | 5.0 | Yayaköy east | Stream | 21.59 |
| 48 | 87.0 | 5.0 | Yörgüç | Ridge | 22.16 |
| 49 | 150.0 | 5.0 | Gölcük | Ridge | 22.17 |
| 50 | 181.0 | 10.0 | Gölcük | Stream | 23.85 |
| 51 | 185.0 | 10.0 | Yeniköy west | Stream | 25.34 |
| 521 | 188.0 | 10.0 | Yeniköy West | Stream | 27.11 |
| 53 | 200.0 | 10.0 | Yörgüç west | Stream | 28.07 |
| 54 | 200.0 | 20.0 | Yörgüç west | stream | 28.10 |
| 55 | 221.0 | - | Gaziköy | Terrace | 28.42 |
| 56 | 250.0 | 15.0 | Alibey west | Stream | 28.47 |
| 57 | 251.0 | 10.0 | Güzelköy west | Stream | 28.62 |
| 58 | 259.0 | 15.0 | Güzelköy west | Stream | 28.65 |
| 59 | 323.0 | 10.0 | Gölcük east | Stream | 28.67 |
| 60 | 575.0 | 15.0 | Yeniköy West | Stream | 29.70 |
| 61 | 575.0 | 15.0 | Yeniköy West | Ridge | 29.77 |
| 62 | 583.0 | 10.0 | Yeniköy west | stream | 29.93 |
| 63 | 725.0 | 15.0 | Güzelköy west | Stream | 30.46 |
| 64 | 750.0 | - | Gölcük west | Stream | 30.96 |
| 65 | 1570.0 | 20.0 | Güzelköy west | Stream | 31.00 |
| 66 | 1766.0 | 10.0 | Gölcük | Stream | 31.18 |
| 67 | 2270.0 | 50.0 | Gölcük | Stream | 31.18 |
| 68 | 4500.0 | 50.0 | Güzelköy west | Stream | 31.18 |
| 69 | 9000.0 | 100.0 | Gölcük | Stream | 31.53 |

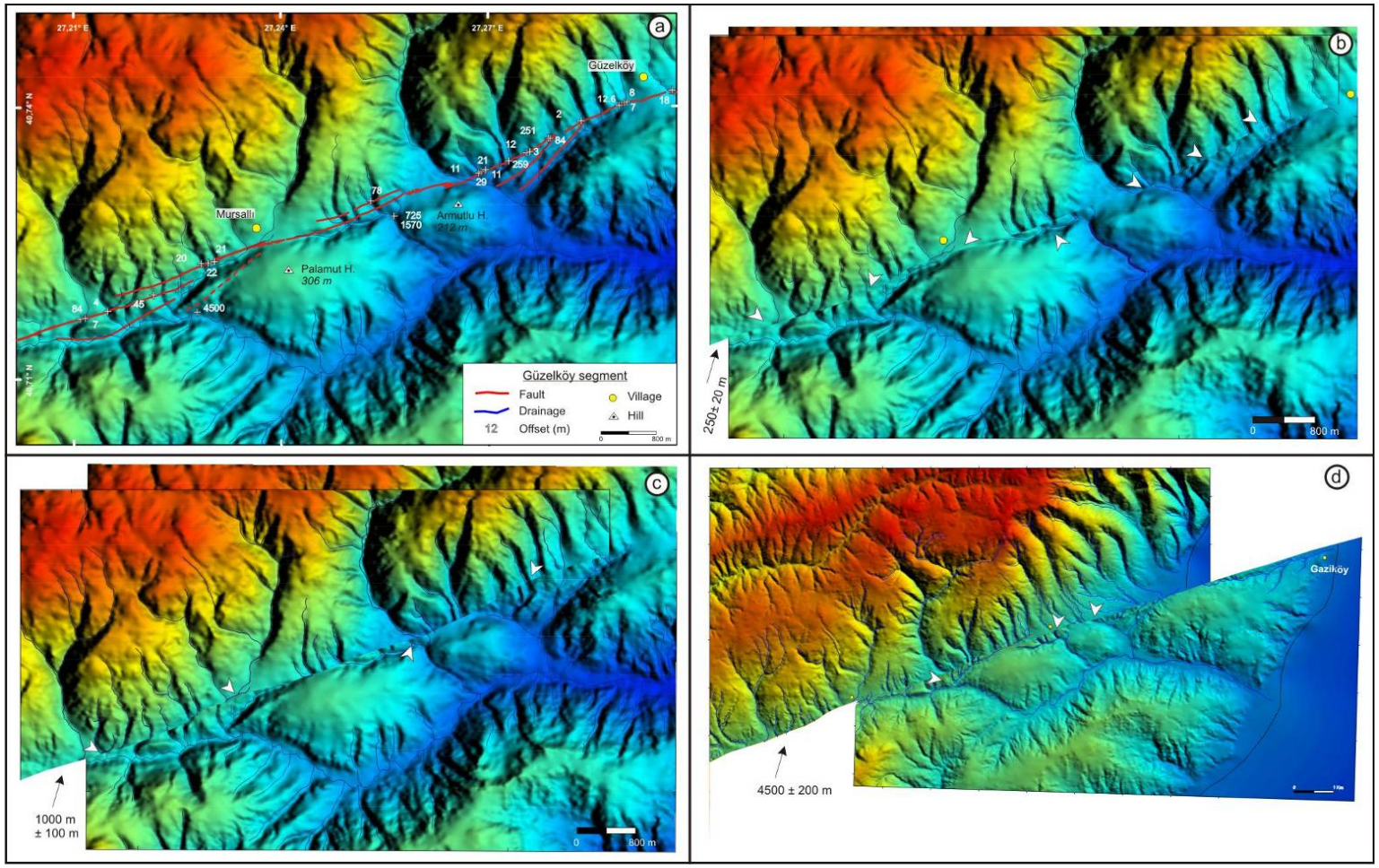


**Figure 4.21 :** a) DEM map showing morphology, streams, fault orientation and offsets of the area between Güzelköy and Mursallı. The largest offset are about 250, 750, 1000 and 4500 m b) Show the reconstruction of 250 m of right-lateral slip. 7 catchments on the north of the fault show a well match with channels on the south. The larger channels indicate that they relatively existed for a longer period than the small ones, hence experienced more slip. A reconstruction of 1000 m (c) and 4500 m (d) shows also a well fit among catchments on the north and southern stream beds.

The section between Mursallı and Gölcük is comprised with 15 localities of significant right-lateral slip (> 50 m). The offsets range from 50 to 2000 m. Most of the displacements are stream deflections; however ridges provided also well markers for slip measurement. Figure 4.22 illustrates a site west of Yörgüç where a stream and related channel walls are apparently displaced. The slip of the stream bed was constrained from Spot5 images and 1/25.000 scaled topographic maps and yield an offset of 72 ± 5 m. Additional measurement were performed using slope map and 3D visualization. The slope of eastern wall is less than 20° and although its right-lateral offset is noticeable, clear markers to quantify the offset is not present (Fig. 4.22). The western wall on the other hand is steeper (~ 30°) and significantly larger. A slope map makes the structure and offset apparent (Fig. 4.22b). Measurements yield a slip of 87 ± 5 m of the slope which is not far from the stream offset. The eastern valley wall is more resistive to atmospheric conditions rather the stream bed and gives better markers to measure the displacement; therefore we consider the cumulative slip at this site is closer to the higher value and can be considered as ~80 ± 5 m.

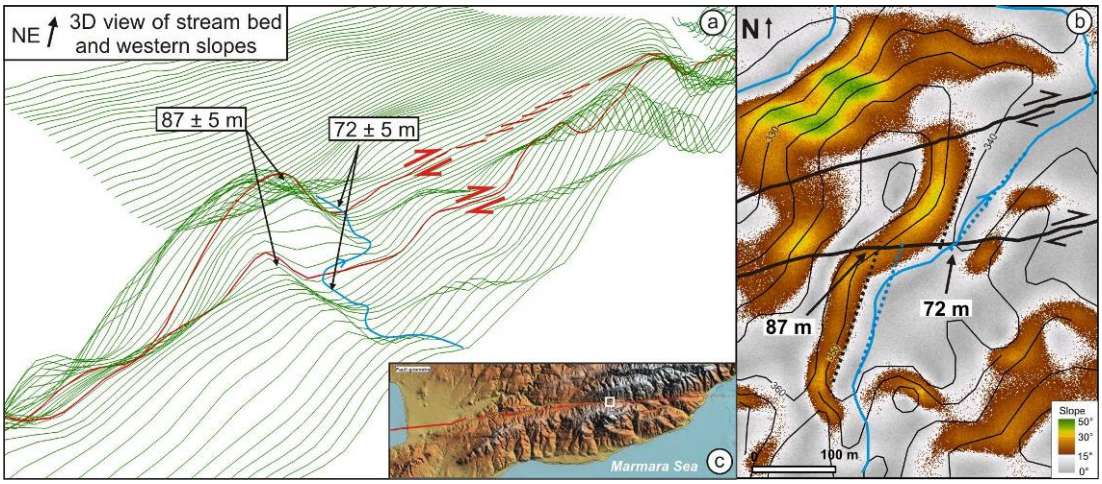


**Figure 4.22 :** Exhibits the right-lateral offset on a stream and related ridges west of Yörgüç. The stream yield a offset of 72 m a) Illustrates a wireframe 3D view of the site were the deflections of the channel walls becomes clearly visible. b) Show the slope map of the site. The offset of 87 m of the western wall is obvious.

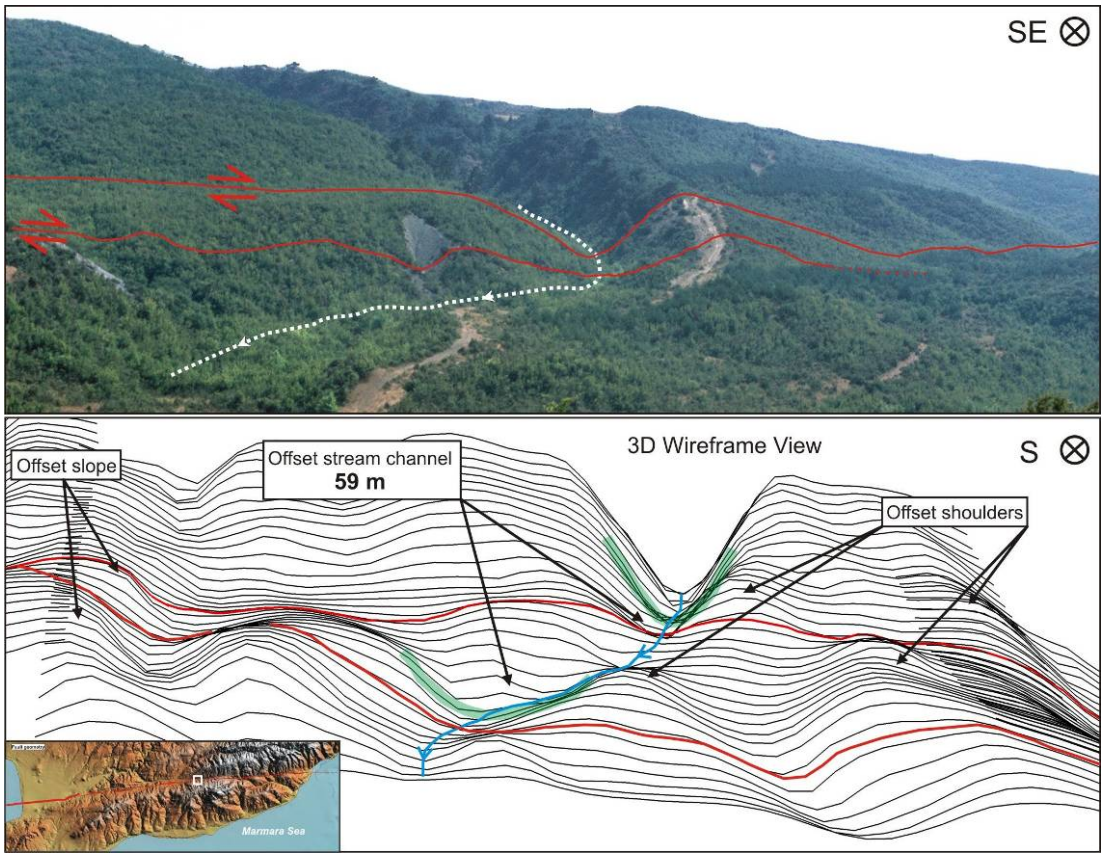


**Figure 4.23 :** The site is located between Yörgüç and Gölcük. The V shaped valley south of the fault is apparent. Towards the north the stream is deflected to NE and flows oblique to the fault. However the 3D view (b) exposes the northern continuation of the valley. We measure 59 m of right-lateral offset between the two valley sections. Other displaced ridges are evident on the image, which are less than 50 m. They will be described in the short-term offset section.

Another prominent displacement is available 4 km west of Yörgüç, where a large stream valley is significantly displaced by the fault (Fig. 4.23). North of the fault the stream flows orthogonal to the fault, however on the south it forms a lower angle with the fault strike, which obstructs measuring the displacement. We use GIS tools to obtain a better view of the site. The 3D wireframe image illustrates clearly the southern continuation of the valley (Fig. 4.23b). In addition, other offsets of stream beds and ridges are apparent. For instance, on the westernmost part we notice an abandoned stream bed, which shoulders are comparably displaced. On the easternmost part another small channel offset is apparent. The adjacent ridges are similarly displaced by the southern fault-branch. The image noticeably illustrates that the fault is constituted by branches, which is also confident with field observation. This offset represents cumulative offsets of single branches however they do not

signify the total cumulative offset in the region. Between Gölcük and Kavak we determined 11 cumulative offsets larger than 50 m. These measurements range from 50 – 2000 m. Stream offsets are dominant along this section of the valleys, which are mostly orthogonal to the fault and provide good markers for measurement. A distinct valley offset is observed 2 km southwest of Gölcük. The SPOT5 image shows the location of the fault in respect to the Valley (Fig. 4.24a). Recent faulting is evident as linear depressions; marshy fields next to Gölcük. A 20-40 m deep incision on a fairly plain surface is significantly deflected by the fault (Fig. 4.24b). We used DEM data, aerial photos and 3D imaging to demonstrate and measure the displacement, which yield a total right-lateral slip of 181 ± 10 m.

We compare the southern part of this valley with other incision on the 2-km-long linear ridge (Fig. 4.25). These incisions are apparently disconnected from their initial catchments. There is no comparable stream on the south of the fault which could drive such an amount of erosion. The only comparable drainage is the southern part of the ~181 m offset stream. We speculate that these incisions might be related to this stream and are currently offset by the NAF by 1690 ± 50 m and 2080 ± 50 m.

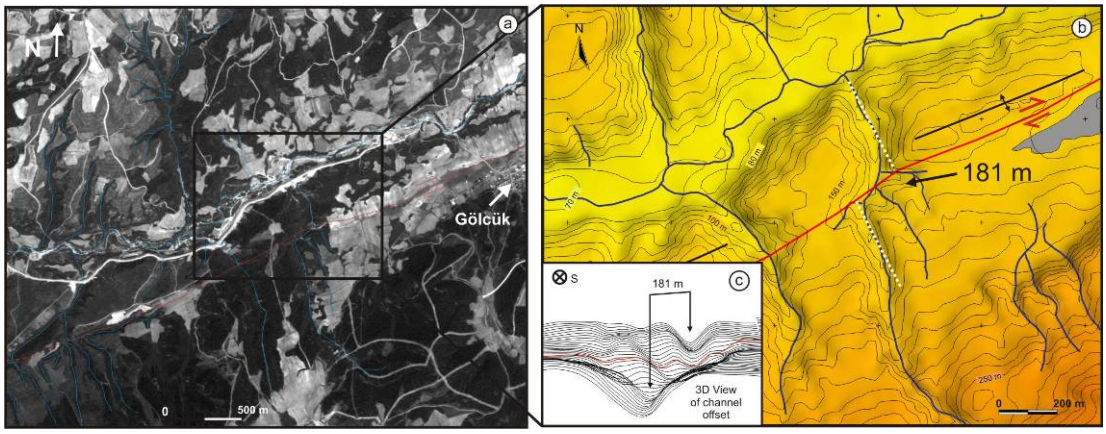


**Figure 4.24 :** a) This is a SPOT5 image of the site. Recent faulting is expressed as linear ponds northwest of Gölcük. Northward flowing streams are truncated and displaced by the fault. b) Illustrates a ~181 ± 10 m right-lateral offset of a well incised linear valley. The offset is also shown in the 3D image (Fig. c).

Another good example of offset is visible North of Yeniköy. The location of the fault is well constrained by prominent fault morphology and several displacements from 5 m to a few hundred meters. A linear stream segment, located west of Yeniköy is flowing across to the Ganos fault and incises the land considerably forming a V shaped valley (Fig. 4.26). A similar incision is located to the northeast.

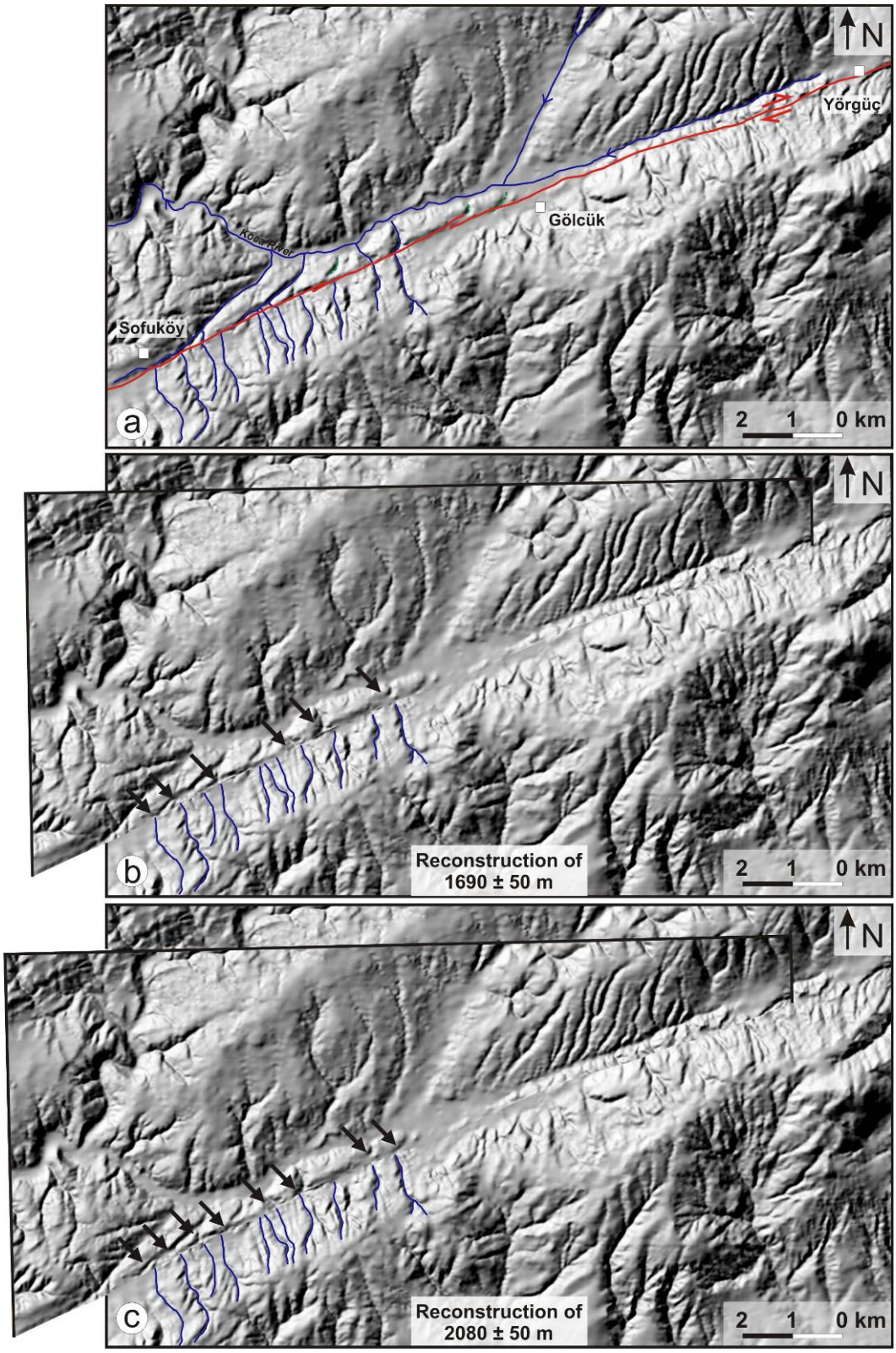


**Figure 4.25 :** Streams located south of the fault show systematic offset. The linear ridge between Gölcük and Sofuköy is cut by several incisions. Two incisions are not connected to any stream and may be abandoned stream channels. The reconstruction of 1690 ± 50 m shows the 6 matches of southern streams with incisions on the north of the fault. If the reconstruction is applied for 2080 ± 50 m the match increases to 8.

This well incised, V shaped valley is lacking of an analogous drainage catchment like the prior stream. Therefore we consider that this valley was initially connected to the south-western valley and was truncated and successively displaced by the fault. DEM data and reconstructions allowed determining a cumulative offset of 575 m ± 15 m.

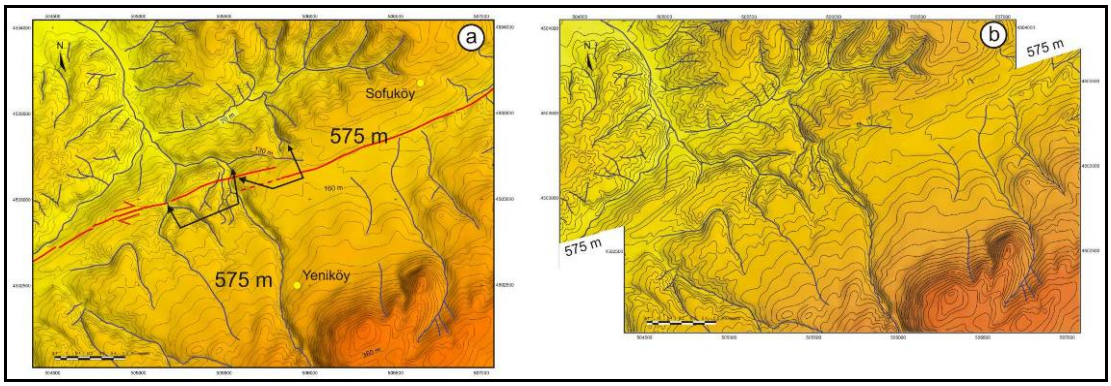


**Figure 4.26 :** The linear stream west of Yeniköy flows across the Ganos fault. The stream forms relatively deep V shaped valley almost along its entire length. A similar incision exists northeast of this stream. However the is incision lacks of a comparable stream source. We consider that the north-eastern valley was once connected to the south-western stream and was offset by the NAF. b) A reconstruction of 575 m demonstrates an earlier stage of the drainage system. Two streams show well correlation with other drainage catchments and the reconstructed morphology.

**Two large scale valleys and their offset possibility**

The 45-km-long onland fault section is in general composed of 2 to 3-km-long streams. However a considerably large valley is located on the top of the Ganos Mt (Fig. 4.27). The valley is oriented parallel to the fault, veers southwards near Gölcük and terminates abruptly in the Gölcük basin. The related stream flows from Gölcük for 5 km, along the fault and turns northwards to join the Koca River (Fig. 4.26). The morphology west of Gölcük however is not comparable with the eastern part of the valley. Ridges are significantly smaller and the size of the valley is not analogous to the North. The size of the northern valley indicates necessarily a continuation on the southern part of the basin. We investigate the south of the fault and notice another large valley, located south of Kavak. This stream flows southwards into the Marmara Sea and has a length of ~7 km. The valley floor on the lowest parts is ~500 m wide indicating significant erosion and deposition. The drainage basin is fairly small to support such erosion. All tributaries are shorter than 3 km, except one which is ~9-

km-long and has a very linear channel striking SW. This abnormal tributary is bounded on its east with a very linear SW-NE trending ridge. The western boundary ridge is highly eroded but has a similar orientation.

We propose that the two valleys north and south of the fault are identical and they were once connected. They formed a drainage flowing into the Marmara. Such a relation implies a cumulative offset of 9 ± 1 km. A reconstruction of related offset is shown in Figure 4.26. The significance of the large slip is that it implies an older age for the western part of the NAF than suggested by Şengör et al, (2005) and Le Pichon et al., (2001). A 200 ka age is proposed for the NAF in the Marmara region using a constant slip-rate of 19 mm/yr and a right-lateral offset of 4 ± 1 km on the eastern margin of Central Basin, which they assume to represent the total offset of NAF in the Sea of Marmara. A substantiation of a 9 ± 1 km offset along the Ganos fault would imply necessarily an older age for the North Anatolian Fault such as suggested by Armijo et al (1999).

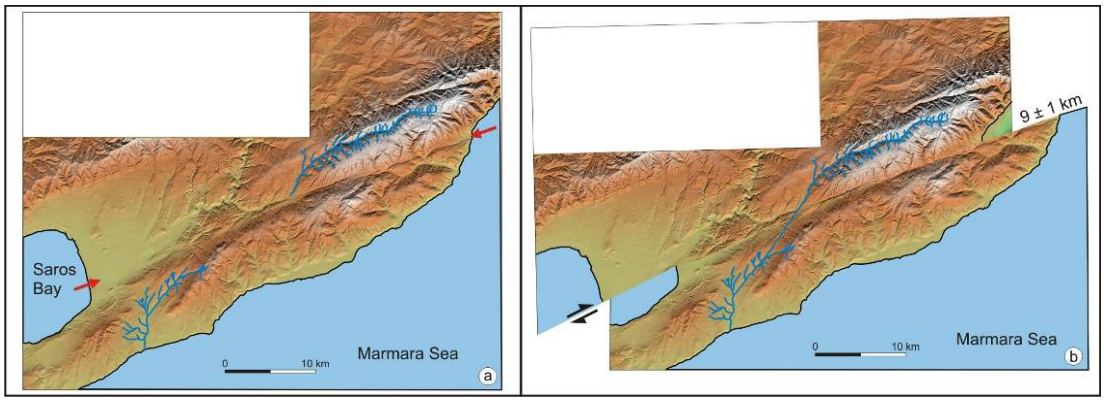


**Figure 4.27 :** North of the Ganos fault we observed a large and deep incised valley which terminates abruptly at Gölcük. The morphology shows necessarily a continuation of the valley. The nearest valley on the south of the Ganos fault is on the southwest of Gölcük. The morphology indicates the possibility of a 9 km offset along the Ganos fault.

#### 4.4.1.2. Short-term offsets

Beside large offsets, we determined 37 right-lateral displacements shorter than 50 m. These offset are measured almost along the entire fault. We were limited only between Gölcük and Sofuköy to determine short-term offset because of dense vegetation and hilly topography. Most of the short-term cumulative displacements are streams, ridges and road offsets. Below are some examples of such offsets.

Field investigation between Gaziköy and Yörgüç yield 22 offsets. The eastern most are determined at Gaziköy. Altunel et al., (2004) measured 22 ± 1 m cumulative offset on the coast of Gaziköy. Altınok et al., (2003) suggest a 3.5 m co-seismic offset for the same site (Fig. 4.28). The coast line here is significantly deflected but evidence of fault morphology is poorly available at Gaziköy. The smooth topography is covered by large alluvial fans and cultivation modified the landscape. The related deflection of the coast line coincides with an outflow of a 20-m-wide stream bed. Successive sediment accumulation on the coast may increase the deflection and may cause to over estimations of right-lateral offset. The offshore sediment accumulation is also visible in the Landsat image. Discharged sediments are transported southward after reaching the Marmara Sea. A lob like feature is visible just southwest of the 22 m deflection. This structure indicates a shallower shelf rather than the north. However, successive right-lateral faulting would yield opposite offshore topography (where the north of the fault would be shallower rather than the south). Detailed field investigations at the site yield more evidence that the main branch of the Ganos fault is probably located near to the northern slope of the Gaziköy hill. Here, the hill slope consists of highly southward tilted coarse conglomerates, while on the north comparable sediments are nearly flat. This indicates likely a fault contact. In addition, the offshore sediments show a linearity trending southward along the coast. The linearity corresponds possibly to the former shoreline. The paleo-shoreline is deflected on the south for 30 m, which can be related to faulting. On the other hand we observe co-seismic and cumulative displacements on two roads along the general strike of the fault. Therefore we conclude that the main branch of the Ganos fault is located closer to the village than suggested by Altınok et al., (2003) and Altunel et al., (2004). However it is possible that the fault might be constituted of several branches at Gaziköy; such as illustrated by Mihailovic (1927) (see p. 114, Fig. 5.6). Our constrained fault orientation is also consistent with the offshore bathymetry data where a small pull-apart basin is determined 2 km offshore of Gaziköy (Seeber et al., 2004; McHugh, 2006).

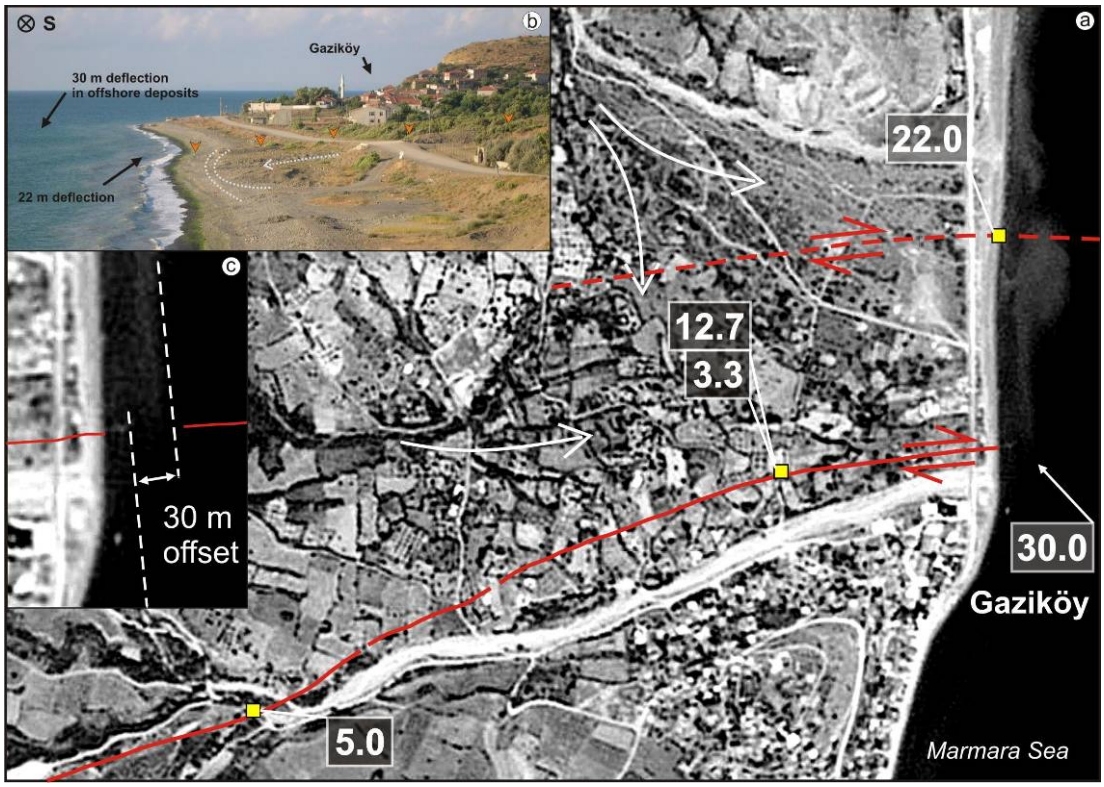


**Figure 4.28 :** The Ganos fault enters the Sea of Marmara at Gaziköy (a). A 22-m-long prominent deflection along the coastline is suggested as a cumulative offset of the Ganos fault (Altunel et al., 2004). The offset is located south of a 20-m-wide channel discharge (b). The SPOT5 image (a) shows the offshore sediment accumulation that may contribute to an eastward progression of the shoreline and result as an overestimated offset measurement. We determined co-seismic and cumulative displacement on roads. In addition, we noticed a linear paleo-shore line east of Gaziköy that is deflected ~30 ±1 m. Combined with the onland geology and offshore fault geometry we suggest a location farther south and consider that the 22 m deflection may be associated with a secondary fault branch. Surface breaks were widely spread at this site during the 1912 earthquake as documented by Mihailovic (1927), (see also Fig. 5.6).

Other cumulative displacements were determined west of Güzelköy. A number of shutter ridges and stream offset are present along the fault section between Güzelköy and Gaziköy (Fig. 4.7, 4.20). At a site 2.5 km west of Güzelköy we determined a prominent offset of a ridge and a stream (Fig. 4.29). The site was also chosen for paleoseismic trenching. Therefore we conducted a detailed topographic survey to document the cumulative offsets of the structure. A survey of nearly 9000 levelled points cumulative yield 11 ± 0.5 m and 29 ± 0.5 m right-lateral slip of a stream and a shutter ridge, respectively.

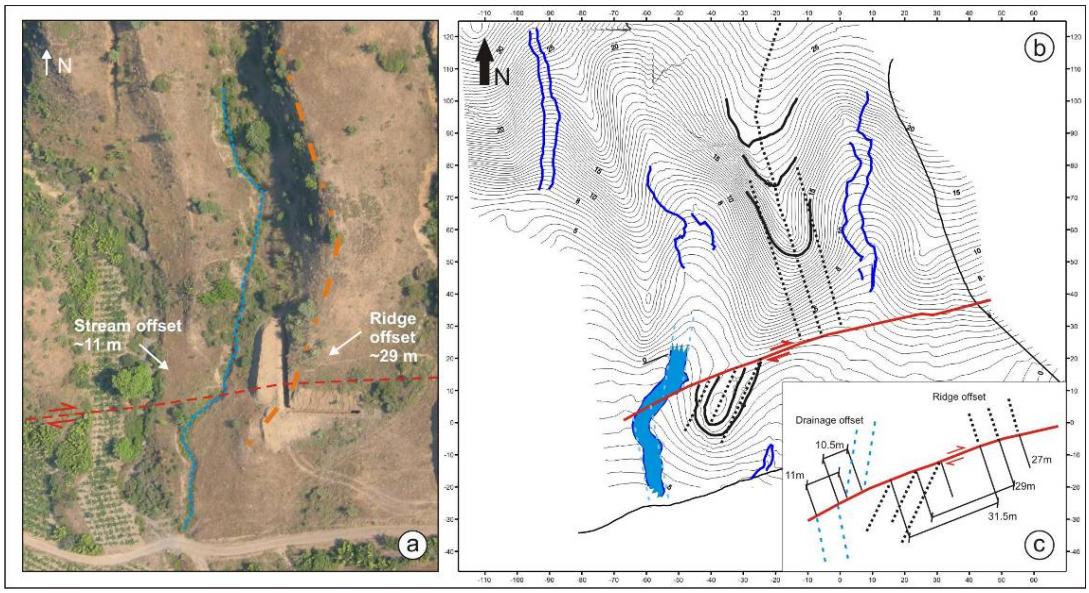


**Figure 4.29 :** a) The right-lateral offsets are distinct in the aerial photograph (Photo by Pucci). Figure b) illustrates the contour map obtained by 9000 levelled points at the site. We measure 11 ± 0.5 m and 29 ± 0.5 m lateral offset on the stream and shutter ridge, respectively (Fig. c).

A second topographic survey has been performed at Mursallı. We determined significant displacements on streams and ridges west of the village (Fig. 4.30). A topographic survey yield an offset 21 m and 22 m of two streams and 20 m of a shutter ridge. Other offset measurements have been performed near Yayaköy and a cumulative displacement of 15 m has been identified on an ancient road south of Yayaköy. The offset for the 1912 has been estimated as 5 m. The remaining 10 m displacement is due to two previous events.

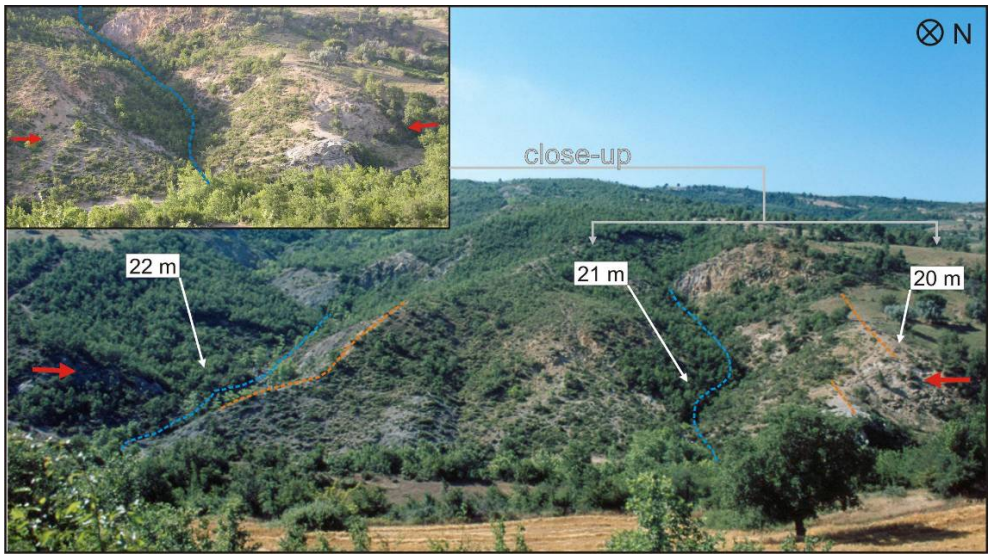


**Figure 4.30 :** Shutter ridges and displaced streams at Mursallı measured with total station yield ~21 m right-lateral displacement.


**Figure 4.31 :** Shutter ridges and a displaced stream west of Yeniköy. We conducted paleoseismic investigations along this site and documented co-seismic faulting. Detailed DGPS measurements yield a total slip of 30 m along the shutter

We determined 14 short-term cumulative offsets on the segment between Yörgüç and Kavak. A site near Yeniköy shows a stream offset and a shutter ridge (Fig. 4.31). We conducted topographic survey using DGPS system and collected ~2000 topographic points to establish the total offset of the related structures. Measurements yield a right-lateral offset of 96 ± 1 m and 46 ± 1 m, on the shutter ridge and the stream, respectively. In the Evreşe plain only few evidence are available to locate the fault. Near the Saros bay, Rockwell et al. (2001) opened several trenches and determined a channel offset. Measurements yield 9 m of right-lateral displacement.

### 4.4.2. Slip history of the Ganos fault using offset classification and correlation with climatic fluctuations

#### 4.4.2.1. Cumulative slip distribution and classification

A detailed study on the morphology of the Ganos fault yield 37 short-term and 32 long-term lateral displacements. These offsets are measured from streams, ridges, man-made structures, shore-lines and paleo-channels. All measurements correspond to nearly pure right-lateral slip. Vertical displacements were documented particularly for the 1912 earthquake displacements. However, observations yield uplift for both blocks. For example, Altınok et al., (2003) reports 1.5 m uplift on the northern block west of Güzelköy. However they also measure 0.5 m uplift for the southern block

near Gaziköy. Similar observations are available in contemporary accounts (Mihailovic, 1927, Macovei, 1912). We consider that these measurements do not signify the real uplift and are related mostly to a topographic effect due to lateral movement. Uplift is evident in the region by the marine terraces at Gaziköy, and by the prominent morphology of the Ganos Mt. and the Doluca Hill. However individual offset measurements mostly express pure right-lateral slip along this section of the NAF. The compressional deformation caused by the Ganos bend is probably diffused to a large area and is therefore not significant along the main fault branch.

Figure 4.32 illustrated the long-term and short-term cumulative displacements along the onland section. Most of our measurements cluster between 100 m and 10 m. Determined offsets are in general well distributed along the fault. Minor displacements lack only in the area between Gölcük and Sofuköy (20 - 27 km). The hilly and forestry landscape limited our observations in this region. The western most section (> 30 km) corresponds to the Evreşe plain, where fault morphology is mostly eroded or modified by cultivation. No offset are preserved in this area.

Some statistical analysis on the lateral offset measurements showed 3 main groups among offsets with distinct gaps in between. Most of the offsets (68%) are smaller than ~87 m. We have no measurements between 87 to 150 m. A second group is apparent between 150 – 750 m; 16 sites represent 24% of the total measurements. Another gap exists between 750 m and 1570 m. The remaining offsets (7%) are larger than 1570 m. We also determined two fairly large offset of 4500 m and 9000 m on large valley systems. From the largest to the smallest offsets, they indicate a continuous right-lateral deformation of westernmost part of the NAF.

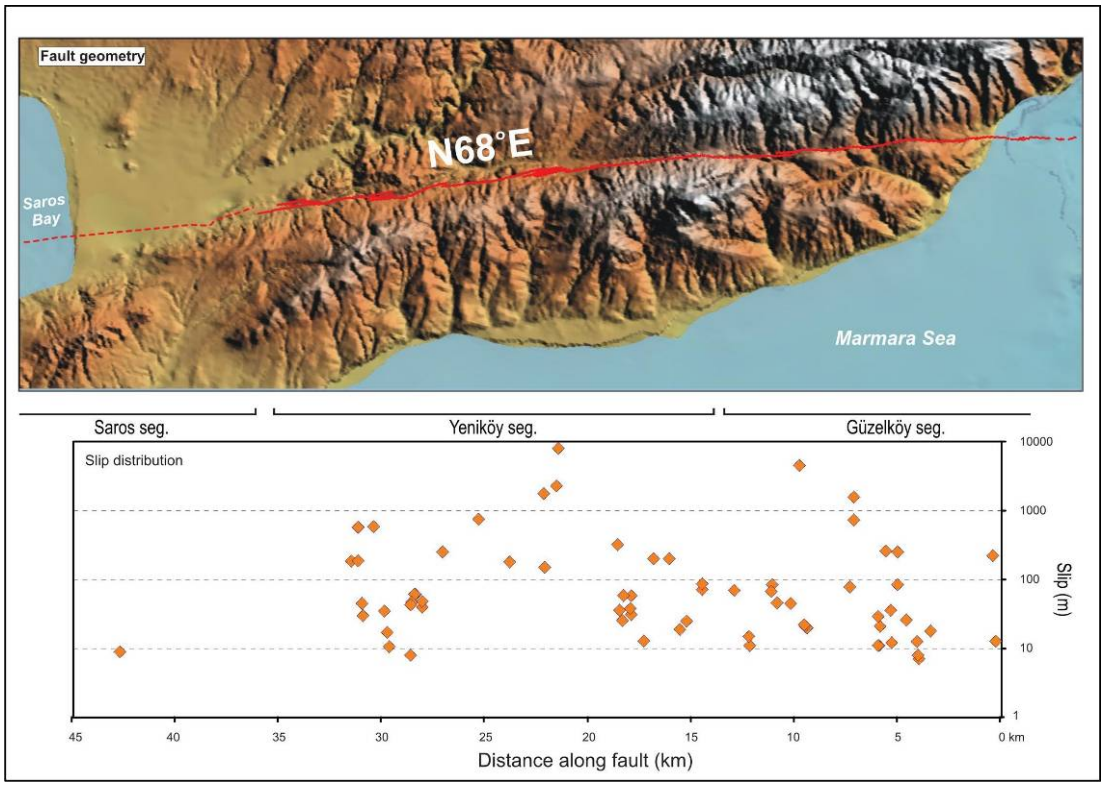


**Figure 4.32 :** Slip distribution and fault geometry along the Ganos fault. 67 cumulative offsets illustrate the short-term and long term slip along the westernmost section of the NAF. Measured structures are streams, ridges, paleo-channels and man-made structures.

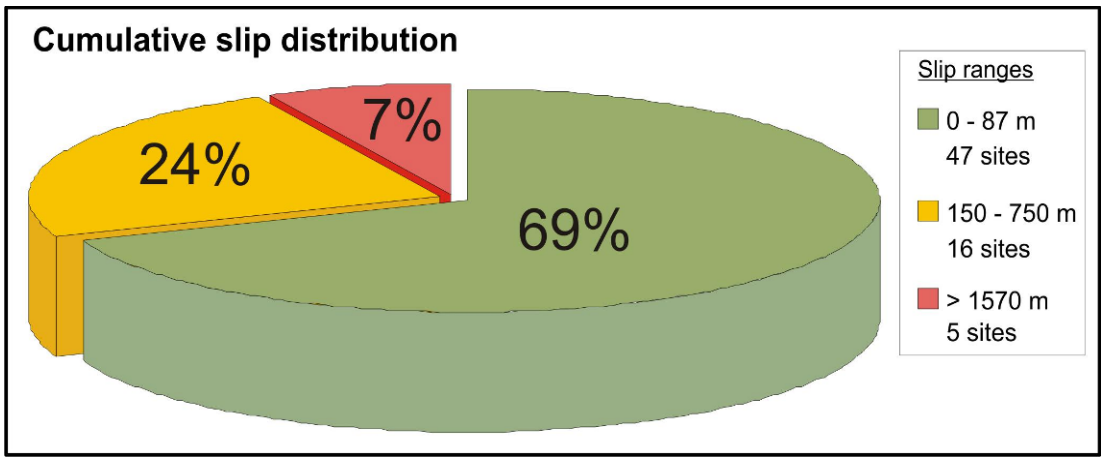


**Figure 4.33 :** A pie chart illustrating the presence of classes within the offset measurements. Our measurements show 3 main groups in which the smallest offsets corresponds to 69% of all measurements

Most of the measurement, 69% correspond to stream channel offsets. Stream offsets are important because in the Ganos region stream channels are dominantly formed by periods of high rainfall, when surface water incises the steep slopes North and South of the Ganos fault. Hence streams are indicator of climatic events. Streams flowing

across a fault are like counters that record the co-seismic slips. Each new channel would start recording cumulatively the displacement. On the other hand, during arid periods new streams would not be formed and slip would be recorded cumulatively on existing channels. This process would lead to gaps within the slip record. A detailed analysis of stream offset may allow differentiating periods of high rainfall and aridity.

We measured 48 stream offsets along the Ganos fault. Figure 4.33 shows the slip measurements as column graphics. Right-lateral displacements, particularly between 8 to 750 m show 7 distinct gaps and 8 groups of offset (Fig. 4.33). As mentioned above the gaps and groups signify periods of dryness and high rainfall, respectively.

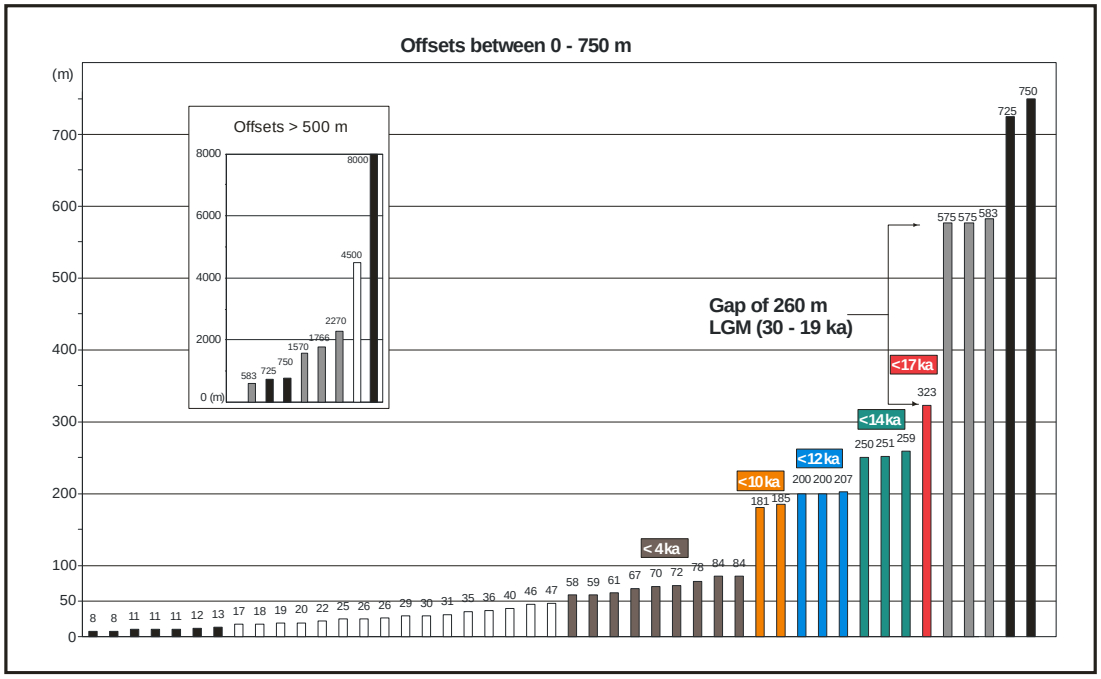


**Figure 4.34 :** 48 right-lateral stream offset are presented as a column graphic. The graphic allows identifying 8 groups of offsets limited by distinct gaps of slip measurement. Groups are displayed as different shades of grey. The gaps signify periods where new stream incisions do not occur due to dry climatic conditions. We correlate these periods with climatic fluctuations. Numbers in coloured boxes correspond to time intervals of high rainfall determined from the sea-level changes of the Black Sea (see Fig 4.36). The 260 m gap represents the Last Glacial Maximum when cold and arid conditions were dominant in the Marmara region.

#### 4.4.2.2. The link between sea (lake) level changes, climatic fluctuations and. offset groups

The idea is based on the simple observation that streams form only during periods of high water discharge, here rainfall. Accordingly, a period of high rainfall in a certain region will form new incision (streams). Each new stream running across a fault is a new counter ready to record co-seismic slip. During intervals of arid climate, new counters are not formed and slip is cumulatively recorded on existing stream segments. The duration of arid condition determines the length of the gap. The groups of slip represent a series of periods of counter occurrence and absence, in other words rainfall and aridity. Other markers representing climatic fluctuation, such as sea-level curves, can therefore be correlated with offset.

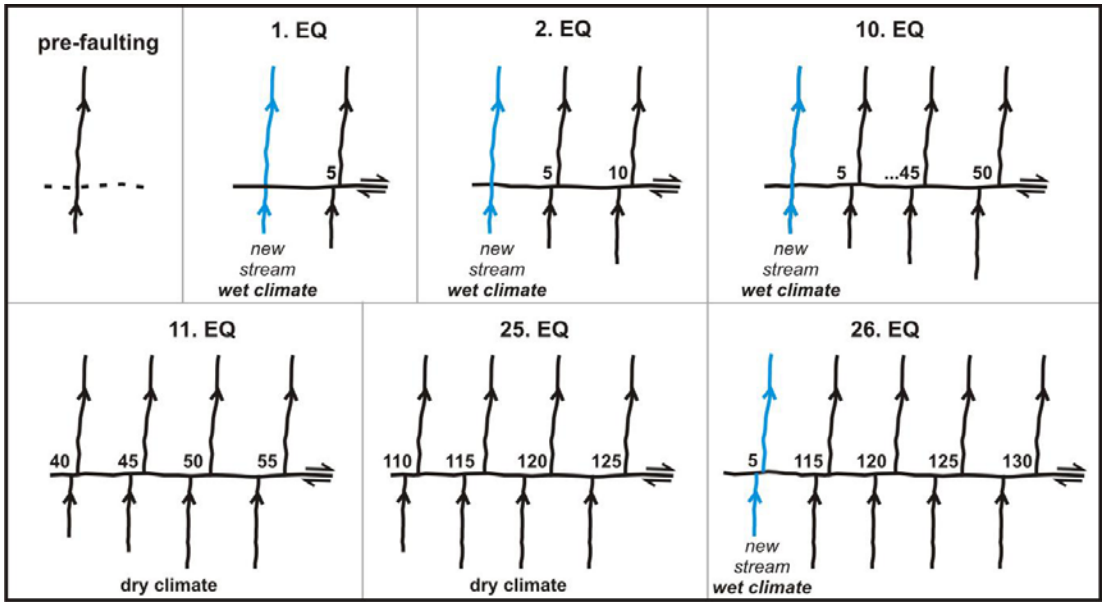


**Figure 4.35 :** Drainage development model for wet and arid climatic conditions. During a high precipitation period (1. to 10. earthquakes-EQ) new incisions form continuously and start recording displacement. When arid conditions are dominant new incisions are not created and existing channels continue recording slip (11. to 25.EQ). As soon as the climate turns again to wet conditions (high precipitation) new channels start forming and recording offsets. The arid period appears as a gap in a group of offsets.

Such a study is performed along the left lateral Dead Sea fault. Ferry et al., (2007) shows how climatic changes in the Jordan Valley affect offset accumulation on streams along the Dead Sea Fault. They measure a number of gully offset along the Dead Sea fault and classify them into 6 groups. The gullies form during periods of high rainfall in the Jordan Valley. These periods reflect as sea level rise in the Dead

Sea (Lake Lisan). Sea level fluctuations are dominantly controlled by precipitation at Lake Lisan, which allows a unique correlation with stream formation and sea level changes. Lake Lisan level fluctuations are well constrained covering a period of nearly 50 ka. This permits a correlation with offsets for a long time interval. Ferry et al., (2007) determined a well correlation with Lake Lisan sea level increases and the determined classes of offsets and calculated a slip-rate of the Dead Sea Fault for the last ~50 ka.

The Ganos region is surrounded by open seas; Aegean Sea, Sea of Marmara and Black Sea. However, Lake Lisan was a closed system in which sea-level fluctuations were controlled dominantly by high rainfall or arid periods. In such a setting, lake-level rise necessarily implies stages of high precipitation; subsequently period of new stream formations. Paleo-climatic studies documented that the Black Sea and the Sea of Marmara were once isolated from the Mediterranean Sea and were lacustrine waters (Aksu et al, 2002, Çağatay et al. 2000; Bahr et al., 2005, 2006). At low stages of the global sea level, access of Mediterranean water was blocked to enter the Sea of Marmara by the -70 m sill depth in the Strait of Dardanelles and by the -40 m sill depth of the Strait of Bosphorus to the Black Sea (Aksu et al., 2002). The Quaternary water-mass exchanges of the Sea of Marmara and the Black Sea have been extensively studied and their sea-level fluctuation is well documented. In general it is agreed that the Marmara Lake existed between 75ka and 12 ka and the Black Sea until 8.4 ka until marine waters breached the Strait of Dardanelles and the Strait of Bosphorus, respectively (Çağatay et al; 2009; Smith et al., 1995; Aksu et al., 1999; 2002b; Çağatay et al., 2003; Hiscott et al., 2007; Eriş et al., 2007 & 2008; McHugh et al., 2008, Ryan et al., 2003, & 2007; Major et al., 2006; Bahr et al., 2005, & 2006).

Climatically the western Black Sea is situated in the transition between the humid climatic regime of the mid-latitudes in SE Europe, a more continental climate in the northern part of the Black Sea and the eastern Danube lowlands and third, the Mediterranean climate region in the south towards the Sea of Marmara (Bahr et al., 2006, Mudie et al., 2002). Cyclones carrying precipitation to this region follow mainly 3 paths (Fig. 4.36); Path 1) which originates from north of Turkey over the south-western parts of Russia and passes from the Black Sea region, Path 2) which originates from the Balkans and affects Marmara and the Black Sea region, and also partly affects inner parts of Anatolia, Path 3) which is generated in the Genoa Gulf

and divides in two routes, Path 3a) which moves to the northeast direction and affects the northern Aegean region, all the Marmara region and western and middle Black Sea region, Path 3b) which moves towards the east and affects western Turkey and passes over middle Anatolia (Karaca et al., 2000). The Quaternary fresh water input into the Black sea has two sources; precipitation and riverine input. The latter occurs dominantly through large drainage systems of Europe and Russia (e.g. Danube River, Dnieper River, Kızılırmak River). Two reasons increase the water discharge of these rivers, higher precipitation and increase in melt-water during warmer periods (this is particularly the case for the northern rivers of the Black Sea). Following the Last Glacial Maximum considerable amount melt-water contributed into the fluvial systems of Eastern Europe and increased precipitation rates in the vicinities (Issar, 2003; Huhmann, et al., 2004). This shows that both reasons for sea-level rises favour precipitation in their vicinity. Therefore we can consider that periods of sea-level rising of the Black Sea corresponds to periods of high precipitation.

A very detailed curve showing the sea-level changes for the last 20.000 years of the Black Sea is illustrated in Figure 4.37 (Dolukhanov & Arslanov 2009; Izmailov, 2005). The data is based on recently summarized palaeo-oceanological, geological, seismic and radiometric evidence (Yanko-Hombach et al., 2007). The curve shows periods of major rise and falls after the Last Glacial Maximum (30 ka – 19 ka BP). Four main periods of sea-level rises at 17.5 ka, 14.5 ka, 12.5 ka and 10.2 ka are distinct in the graphic. All indicate significant increase of fresh-water input mainly by precipitation (as described afore). However post 9 ka the rise is associated with marine water input from the Marmara Sea over the Bosphorus sill, which continuous until ~5.5 ka. Post 5.5 ka the sea level seems to reach an equilibrium (Fig. 4.37). Therefore, we may speculate the existence of another period of high precipitation between 4.1 to 3.9 ka.

The last Glacial Maximum was a period of dry climate in the eastern Mediterranean and lasted for ~11 ka (Aksu et al., 2002; Peyron et al., 1998; Ramrath et al., 1999). Considering that stream formations were absent or reduced during that interval, one would expect a large gap within the offset records. Although with little evidence, such a gap is present between two groups of measurements; offsets around 580 m and 323 m (Fig. 4.34). We postulate that this gap correspond to the period of the Last

Glacial Maximum and correlate the younger offset groups to the periods of 4 main sea-level rises and the period between 4.1 – 3.9 ka, mentioned above (Fig. 4.37).

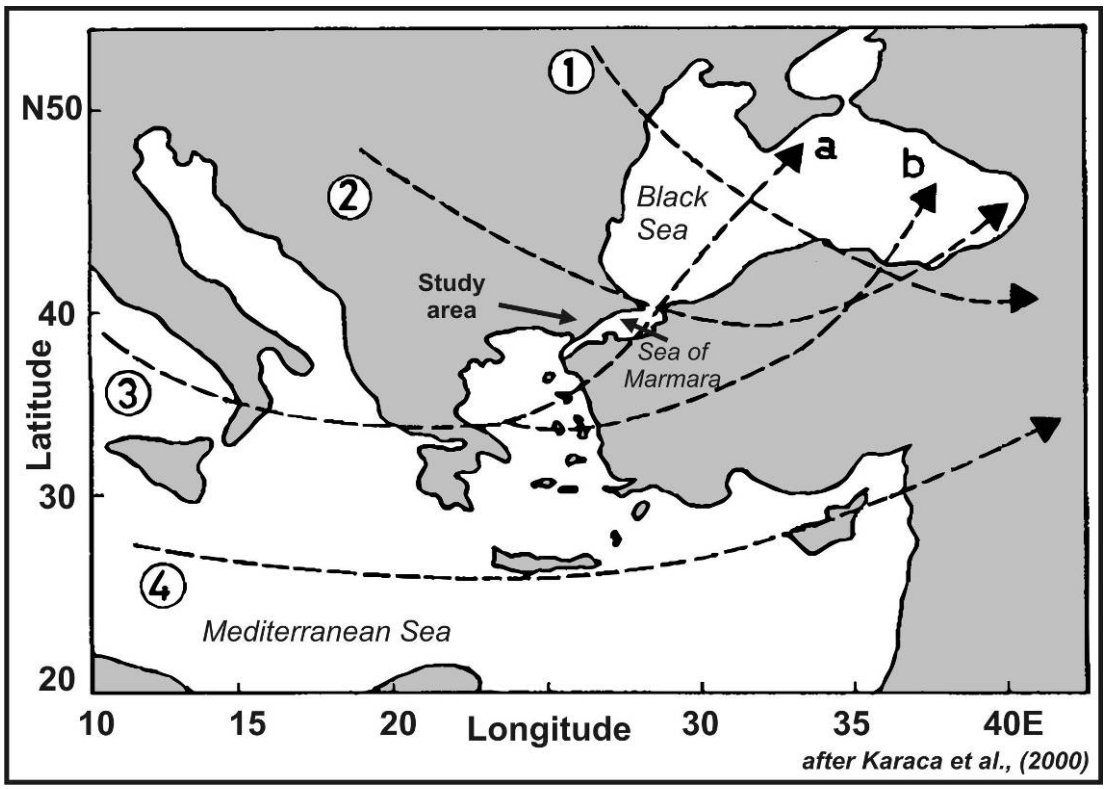


**Figure 4.36 :** The paths of atmospheric cyclones over Turkey. Path 1, 2 and 3 are the main cyclones responsible of rainfall in the catchments of the Black sea. Path 2 and 3a have major influence in rainfall over the Marmara region (Karaca et al, 2000).

#### 4.4.2.3. Slip rate estimations

We use the average displacement of the each group and the average age of the related time period and calculate collective slip rate and individual slip rates for the western most part of the NAF. The calculations for each offset group yields 17.5 mm/yr, 18.3 mm/yr, 17 mm/yr, 18.4 mm/yr and 20.5 mm/yr slip rate for the last 4 ka, 10.2 ka, 12.5 ka, 14.5 ka and 17.5 ka, respectively. This implies a constant slip rate of 17.9 mm/yr for the last 20.000 years and a variable slip rate of 17.7 mm/yr, 17.7 mm/yr, 17.9 mm/yr and 18.9 mm/yr for the last 10.2 ka, 12.5 ka, 14.5 ka and 17.5 ka respectively (Fig. 4.38).

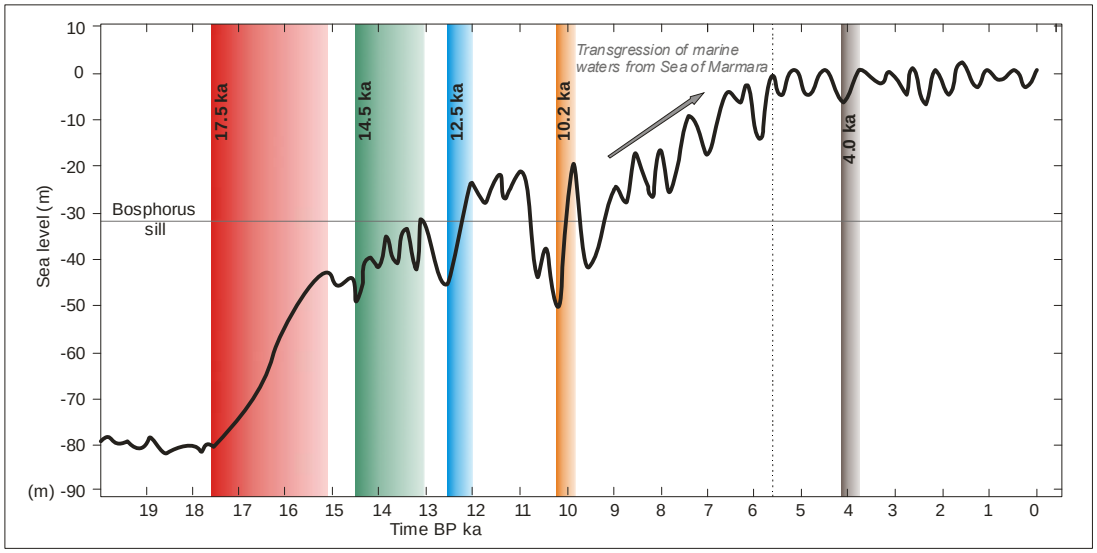


**Figure 4.37 :** Sea-level fluctuations of the Black Sea for the last 20.000 years. We determine 4 major periods of like rise at 17.5 ka, 14.5 ka, 12.5 ka and 10.2 ka. These periods are considered to represent stages of high rainfall. Post 9 ka marine waters of the Sea of Marmara start flowing into the Black Sea and sea level changes occur within a more complex system. However, we may consider another rainfall period at 4 ka, after the sea level reaches an equilibrium (dashed line; Izmailov, 2005; Dolukhanov, 2009).

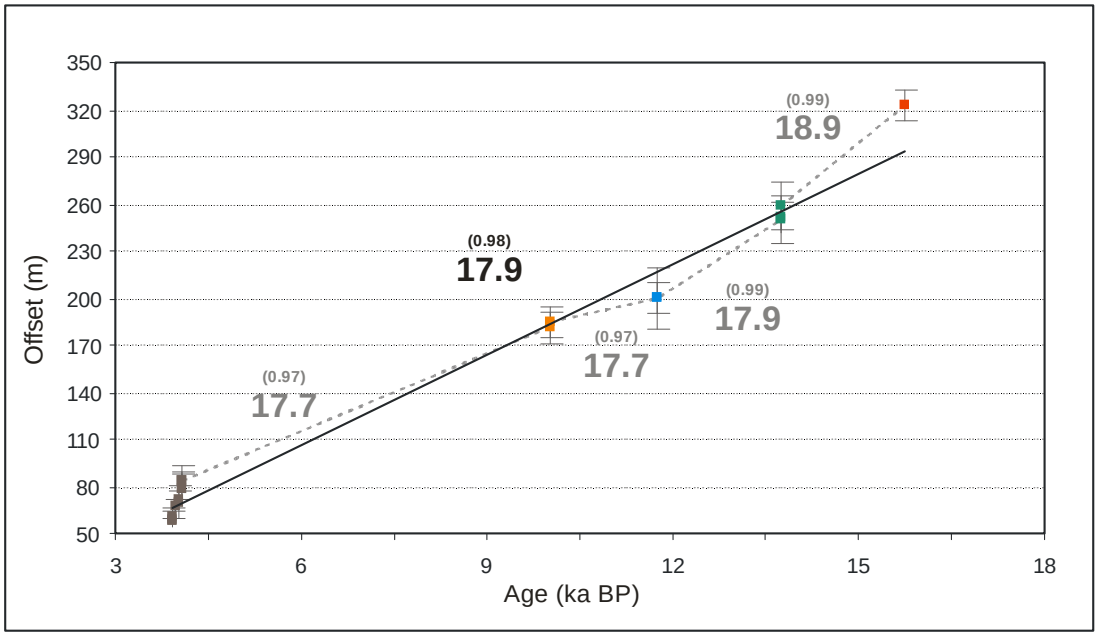


**Figure 4.38 :** Plot of cumulative slip of groups of stream offset versus their age inferred from climatic events. A standard model of constant slip-rate (black line and numbers) we calculate a mean value of 17.9 mm/yr for the last 20 ka. A variable slip-rate model revealed very comparable results (grey dashed lines and numbers), where values fluctuate between 17.7 to 18.9 mm/yr.

### 4.5. Morpho-tectonic Results along the Ganos Segment

1 - Major morphological structures comprising the Ganos region are from east to west, the offshore Tekirdağ Basin (-1125 m), the Ganos High (924 m), the Doluca Hill (689 m), the Evreşe plain (0-100 m) and the Saros bay (-50 to -600 m). The morphology suggests a change from compressional structures on the east to extensional structures towards the west.

2 - The geology along the Ganos fault is different on its two sides; north and south. The north is composed by a sedimentary pile of Lower Eocene to Lower Oligocene age deposits, unconformably lain on top of a fluvial sequence (Middle Eocene). The southern section has a relatively more composite geology composed of Upper Cretaceous to Upper Pleistocene units. Quaternary deposits lie unconformably on top of these sequences. They develop as slope debris, alluvial fans, fluvial deposits and basin fills, mostly in control of the Ganos fault. Apatite fission-track analysis showed that the exhumation of the southern Ganos region was about ~10 Ma earlier (Late Oligocene) than the northern region (Zattin et al., 2005). Therefore an earlier right-lateral strike-slip fault was present in the region prior to the NAF (Zattin et al; 2005; Yaltırak; 1996; Yaltırak and Alpar, 2002).

3 - We documented the detailed geometry of the 45-km-long onland section of the Ganos fault at a 25.000 scale. Right-lateral strike slip faulting was dominantly observed along the onland section. Prominent strike-slip morphology was evident by lateral stream and ridge offset, shutter ridges, linear depressions (saddle), sagpond and pressure ridges. The morphology provides us valuable information about the fault characteristics. Several lateral offsets documented the dominant right-lateral fault movement. On the other hand, the Ganos Mountain and the uplifted coastal terraces at Gaziköy indicate the existence of a compressional component on the eastern section of the right-lateral Ganos fault. The central segment of the Ganos fault is forming more linear structures like linear valleys or elongated ridges. The 2-4 km long pressure ridges indicate a more pure strike slip faulting. The western part of the fault represents different morphology than the east. The large Evreşe plain, Kavak Lake pull-apart and the Saros bay indicate transtension on the western segment of the Ganos fault.

4 – 69 cumulative offset measurements exposed the long-term and short-term fault behaviour of the western most section of the North Anatolian Fault. We analyzed stream offset and determined 8 classes off comparable slip limited by distinct gaps of slip record. A correlation of stream displacements and climatic fluctuations allowed calculating slip rates for 5 of the classes. The calculations yield a constant slip rate of 17.9 mm/yr for the last 20.000 years and a variable slip rate of 17.7 mm/yr, 17.7 mm/yr, 17.9 mm/yr and 18.9 mm/yr for the last 10.2 ka, 12.5 ka, 14.5 ka and 17.5 ka respectively. The variable rates are very comparable with the mean slip rate. Slip rate estimations for offset smaller than 60 m is limited by the resolution of the sea level curve of the Black Sea. A more detailed curve would allow a better constrain for climatic events post 4 ka and their related influence on the geomorphology

5 – We suggest a large valley offset of 9 km using morphologic and partly geologic evidence along the Ganos fault. This offset may have major implications on the age of the western part of the NAF .Şengör et al, (2005) and Le Pichon et al., (2001) suggest an age of 200 ka for the NAF in the Marmara region. They extrapolate the age using a constant slip-rate of 19 mm/yr and a right-lateral offset of 4 ± 1 km on the eastern margin of Central Basin, which they assume to represent the total offset of NAF in the Sea of Marmara. A substantiation of an 9 ± 1 km offset along the Ganos fault would suggest necessarily an older age for the NAF. Armijo et al (199) suggested a total slip of 80 km for this section of the large strike slip fault.

6 – The analysis of structural complexities yield that the onland section of the Ganos fault is composed of 3 sub-segments. From east to west, the Güzelköy segment, Yeniköy segment, and Saros segment.

# 5. THE 9 AUGUST 1912 MÜREFTE EARTHQUAKE (Mw 7.4); EVIDENCE OF SURFACE FAULTING AND CO-SEISMIC SLIP FROM HISTORICAL DOCUMENTS AND FIELD OBSERVATIONS

The 9 August 1912 Mürefte earthquake is the most recent large earthquake occurred on the westernmost section of the NAF. The large moment magnitude of $M_w$ 7.4 indicates a surface rupture length of minimum 100 km comparable to the 17 August 1999 Izmit earthquake ($M_w$ 7.4) that took place on the eastern side of the Sea of Marmara. The length of the Mürefte earthquake rupture plays a significant role in evaluating the seismic hazard in the Marmara region. We know that the surface rupture broke the 45-km-long onland section of the Ganos fault (Ambraseys & Finkel, 1987). Therefore, we applied a detailed investigation on the onland section, to document the surface rupture characteristics and related co-seismic slip distribution. The field data were collected during several field campaigns, starting from 2004, 92 years after the event. We traced the onland section of the rupture to prepare a fault map at a scale of 1/25.0000 and document the related co-seismic slip. The rupture morphology was partly preserved in the region, despite the high agricultural activities. Localities with minor landscape alteration allowed mapping out the 1912 surface rupture. At other sites where the surface breaks are not evident, we used the main fault morphology and the preserved 1912 co-seismic displacements to locate the rupture. The rupture is mainly expressed by scarps, sagponds, and co-seismic offsets on various structures (e.g. streams, field limits and roads). The main course of the rupture follows the fault line described previously in Chapter 4. Therefore, we only describe sites where clear evidence is present for the 9 August 1912 earthquake surface breaks.

The following section presents some introductory information about the 9 August 1912 Mürefte earthquake and related studies and a summary of the damage distribution and co-seismic ground deformations apart from faulting. Consequently, we document the surface rupture and co-seismic offsets. Finally, we evaluate our observations and propose a fault segmentation pattern, focal mechanism and a possible rupture length for the 1912 earthquake sequence.

**The 9 August 1912 Mürefte earthquake ($M_w$ 7.4)**

The 9 August 1912 Mürefte earthquake ($M_w$ 7.4) occurred with an epicentre near the Mürefte village according to Ambraseys and Finkel (1987). The earthquake was accompanied with major surface faulting and co-seismic slip all along the onland section. In addition, some considerable amount of land-sliding occurred off the fault. The earthquake attracted interest of several scientists of that time and field investigations were carried out within a few days and weeks after the shock. The tremor was considered to be similar in size to the 28 December 1908 Messina- Italy earthquake (M 7.5) (Mihailovic 1918, 1923, 1927). Three key contemporaneous reports (i.e. Macovei, 1913; Mihailovic 1927; Sadi, 1912) provide ample descriptions of surface faulting and right-lateral offsets, landslides and detailed accounts of damage distribution. It is important to note that coeval documents describe any co-seismic surface deformation as "cracks" and surface ruptures were not distinguished from other phenomena like landslides, spreading or other surface deformation types. Nevertheless the descriptions and given locations permit identifying the origin and the type of the structures. They are mainly localized in four regions; Mursallı, Ormanlı, Kirazlı and Saros. Additional information is available for Gaziköy, Güzelköy, and Gölcük areas. Surface faulting is evident at Gaziköy, Güzelköy, Mursallı, Gölcük and Saros, other localities experiencing land slides or lateral spreading. Photographs are available for some part of the fault and express typical strike-slip surface faulting morphology. We will refer to these documents and describe the surface rupture with more detail in the following section. Aside of historical documents, we made interviews with local people, who had either own memories or information from their elders about the surface rupture.

## 5.1. Historical and Recent Studies on the 9 August 1912 Mürefte Earthquake

There are a number of dissertations about the 9 August 1912 Mürefte earthquake. Some of them rely on field observation collected right after the event. The seismograms, building damage and partly the surface breaks were studied within a few months by scientist of that time (Agamennone 1912; Macovei, 1912; 1913; Mihailovic 1918, 1923, 1927; Sadi, 1912; Hecker, 1920; Sidgreaves, 1912, Walker, 1912, see Table 5.1). The number of contemporary studies may seem rich, but they lack of well descriptions on the seismic characteristics and particularly the related

surface faulting. We present here the previous studies on 1912 earthquake in two categories; 1) Contemporary studies, and 2) Recent studies. The following paragraphs contain brief descriptions of the related publications. Further details are available in the related text, with the corresponding citations.

### 5.1.1. Contemporary Studies

We aimed to collect the originals or digital copies of any coeval document related to the 1912 earthquake event. Our searches yield thirteen articles, some of which were poorly known or unpublished –unknown articles (Table 5.1). We provide here a short description of the articles we managed to collect.

**Table 5.1 :** The list shows collected publications of contemporary authors of the event. Language abbreviations: eng: English, fra: French, deu: German, ota: Ottoman, ron: Romanian, tur: Turkish, srp: Serbian.

| | Author | Title | Year | Document type | Lang. |
|---|---|---|---|---|---|
| **1** | Macovei Gheorghe | Sur La Tremblement De Terre De La Mer De Marmara Le 9 Aout 1912 | 1912 | Article | fra |
| **2** | Doc. Yüzbaşı Sadi | Marmara Havzasının 26-27 Temmuz Hareket-i Arzı 15 Eylül 1328 | 1912 | Article | ota, tur |
| **3** | Sidgreaves, W. | The earthquake in Turkey on August 1912 | 1912 | Article | eng |
| **4** | Walker, W. George | Turkish Earthquake of September 13 | 1912 | Article | eng |
| **5** | Macovei Gheorghe | Aspura Cutremurului de Pamant dela Mare de Marmara dela 9 August 1912 | 1913 | Article | ron |
| **6** | Allen C.G. | Agamennone, G. - 1912, Il disastroso terremoto nel bacino occi-dentale del Mar di Marmara | 1913 | Review | eng |
| **7** | Bigourdan M. | Note de Michailovic Jelenko - Resultats des études sur le tremblement de terre d'aout et de septembre 1912 sur la mer de Marmara - 1918 | 1918 | Review | fra |
| **8** | Hecker, Oskar | Mitteilungen über Erdbeben im Jahre 1912 | 1920 | Report | deu |
| **9** | Michailovic Jelenko | Mehanizam Trusvih pokreta ha Mramornom Moru | 1923 | Booklet | srp, fra |
| **10** | Gutzwiller Otto | Beitraege zur Geologie der Umgebung von Merfete am Marmara-Meere | 1923 | Article | deu |
| **11** | Michailovic Jelenko | Trusne katastrofe na Mramornome moru | 1927 | Report | srp,fra |
| **12** | Michailovic Jelenko | La séismicite de la Thrace, de mer de Marmara et de l'Asie Mineur | 1933 | Article | fra |
| **13** | Mâmâcânyam, Edvâd | Mürefte civarı büyük zelzele ve yangını garib destanı | 19?? | Epic | ota |

**Macovei, (1912) - Bull. Sect. Sci. Acad. Rumanie**

This is a 10 page report in French, published in the Bulletin of the Rumanian Science Academy. It presents preliminary field observations of the earthquake. The author was in Istanbul when the event occurred and went immediately after to the epicentre region. The earthquake is briefly described including timing, duration, damage, casualties and partly faulting. A Rossi-Forel isoseismal map provides the damage distribution. The earthquake is evaluated in the context of the tectonic and geologic setting of the area, which is given in detail. The North Anatolian Fault is mentioned as a E-W trending tectonic boundary starting from the Gulf of Izmit, crossing the Marmara little south of Tekirdağ, passing the Gulf of Saros between the Gökçeada (Imbros) and Semadirek (Samothrace) islands.

**Sadi (1912) - Report**

This is a 39 page article written in Ottoman Turkish and includes photographs and two maps. Sadi, who was a surgeon of the Ottoman army, prepared a report after he visited the earthquake area. A summary on the geology and tectonic setting of the region is given, but on a very basic level to enable the reader understanding the earthquake phenomena. As a physician his observations are concentrated on the damage and the living conditions of the sufferers. However, geologic and seismologic characteristics of the event are not neglected. Several information on the pre- and aftershocks and the duration of the main shock are available in the text. Descriptions on the surface deformation are given based on secondary sources. Beside, we read a short evaluation on the tsunami effect of the tremor. This work is one of the unique studies which contain a fault map; although very large scaled. A sociologic and economic review of the Ganos region helps us also to understand the percentage of loss, especially for Şarköy, Mürefte and Gelibolu.

**Sidgreaves (1912) - Nature**

This a one paragraph text published in Nature and presents preliminary results of a Milne seismogram reading from the Stonyhurst College Observatory (England). They give the timing of the 9 August 1912 earthquake as 01:45 (LT) and interpret the epicentre as west of the Sea of Marmara.

**Walker (1912) - Nature**

This is also a one paragraph text published in Nature and presents results of seismogram readings from the Eskdalemuir Observatory (England) and the Pulkovo Astronomical Observatory (Russia) for the 13 September 1912 earthquake. They calculate the earthquake epicentre as 40.7° N / 26.5°.

**Macovei, (1913) – Publ. Fond. Vasile Adamachi Acad. Românâ**

This is a more detailed work of the author than the 1912 publication. It is a 13 page report supported with 10 photographs, one figure and an isoseismic map; written in Romanian for the Rumanian Science Academy. Macovei was in Istanbul when the earthquake occurred and experienced the shock heavily. His notes are based on a one-week field investigation in the region after the event. The document provides information on aftershocks and the damage in the earthquake vicinity mostly obtained by field observations between Gelibolu and Tekirdağ. We obtain also evidence of the co-seismic surface deformation along the fault and the regions around. The report ends with a geologic and tectonic review and interpretation of the Marmara region.

**Allen C.G ( 1913; review of Agamemon 1912) – BSSA**

G. Agamennone published a paper about the 9 August 1912 earthquake in Italian in the journal "Rivista di Astronomiae Scienze affini". We were able to access a review of the paper by Allen C. published in the Bulletin of the Seismological Society of America. Allen notes that Agamennone's work is based on articles from the newspapers "La Reforma" and "La Tribuna". Severe damage is described at Dardanelles (Gelibolu) using eye-witnesses. Ground deformation is also given along a part of the city. Agamennone (1912) summarizes the damage distribution and gives an earthquake intensity for the region.

**Bigourdan (1918; review of Mihailovic 19??) – Acad. Scien. France**

This is a review prepared by Mr. Bigourdan about one of the publications by Mihailovic (reference not known). The review is two pages in French. It describes preliminary results of a 5-week field work in the earthquake vicinity. Mihailovic published the detailed results in 1927. This review bears the summary of the earthquake activity before and after the main shock. The epicentre area of the 9 Aug earthquake is given as the Ganos region, however with notes that the movement

caused autonomous shocks in the Manyas region and in the Dardanelles. Surface faulting, landslides and damage in the Ganos region are also briefly described. The conclusion part presents an appraisal of the tectonics of the region.

**Hecker (1920) – Seism. Bull. Jena**

Another report in German was prepared and published by the Head Office of Seismological Research in Germany. It is a section of a monthly publication, which was revised by A. Sieberg. The report gives information on the damage distribution and loss of live. An isoseismal map prepared by A. Sieberg, is inserted. The detailed list of earthquakes for the whole year of 1912 provides information on the for- and after-shock activity of the region. We read some evidence on the tsunami caused by the main shock

**Mihailovic, (1923) – Srb. Kralj. Akad.**

This is a 48 page booklet describing the geology, seismicity and tectonics of the Marmara region with an analysis of the 1912 earthquake. The text is written in Serbian with an 11 page insert of a summary in French and published in the Serbian Royal Academy. It bears 3 maps, 2 figures and one seismogram. The geology section is a general evaluation of tectonic components in the region, noting that the region consists of two main blocks; Anatolia and Thrace. In the seismology section the 1912 earthquake sequence is described with its pre and aftershocks. A comparison of the characteristics of the 1894 and the 1912 earthquakes are also presented in the study, with isoseismic maps for both events. Six large aftershocks are given with location and time. An image of the seismogram recorded at St. Beniot Licee in Istanbul is given and analyzed in this work. The co-seismic surface deformation such as ruptures, landslides and cracks are described with approximate locations. The last section is an appraisal of the active tectonic forces in the region, where the Marmara region is divided into several zones, which are considered to represent different seismic characteristics.

**Gutzwiller (1921, 1923) – PhD Thesis (Univ. Basel)**

This is a dissertation written in German, by a Swiss geologist who visited the site in 1914 (May – June) and studied the oil reserve potential around Mürefte. The geology of the region is given in detail and the tectonics is also discussed. The report contains 6 figures and a map. The map is noteworthy because the fault has been drawn with a

distinct detail and geometry, which is unusual for a regular geology map of that time. The detail derives most probably because the author traced the 1912 surface rupture, which was likely still visible after two years. In contrast, the 1912 earthquake is mentioned only in one sentence noting its significant damage in the region. Nevertheless, the possibility that this map is the only rupture map available for this earthquake makes this report remarkable (The dissertation was reprinted in 1923, hence different reference are present in the literature).

**Mihailovic, (1927) – Srb. Kralj. Akad.**

This is a 300 page report giving the most detailed information among the other contemporary documents. It is based on Mihailovic's personal field observations from 15 August to 26 September 1912. During his field study, he was forced to turn back owing to the breakout of the Balkan Wars (8 Oct. 1912 - 29 Sept. 1913). The report is written in Serbian, with a 24 page French summary and consists of 78 photographs 46 figures, 6 diagrams and one map. The damage and its characteristics are given in detail, supported with photographs and drawings for several buildings. Personal observations on damage extend to a wide area; from Rodosto (Tekirdağ) to Dardanelles (Çanakkale). The co-seismic surface deformation is also documented by numerous descriptions, photographs and drawings. Evidence of ruptures, land slides and other phenomena's are given for several locations like Mursallı, Yörgüç, Gölcük, Kirazlı, Ormanlı and other location away from the fault; Dardanelles, Appollonia, Heraklica. We obtain also some information on tsunami effects within the Marmara Sea. He remarks the historical and instrumental seismicity of the region; presents an extensive list of fore- and after-shocks with intensity for several locations. A list of 68 stations where the earthquake and related aftershocks were recorded is placed in the report, including arrival time of different phases of waves. The last section of the reports is a general tectonic evaluation of the region. The drawback of this study is that it does not include any detailed map of the fault.

**Mamaçyan (19??) – Sukâyân Publ. Istanbul**

This is an epic about the earthquake disaster written in Ottoman-Turkish. The text is one page and is most probably published in the same year of the event. We were not able to translate the text for now.

**Newspapers**

We collected articles from newspapers and journals of that time, where short descriptions of the earthquake and its affects were available. We managed to access articles from the newspaper Freiburger Nachrichten (Germany), La Liberte, Le Croix, Le Temps and Le Figaro (France), as well an article with photographs in the journal La Illustration (France) (See Appendix A3).

### 5.1.2. Recent studies:

There have been recent attempts to investigate the 9 August 1912 earthquake. Here we provide a summary of these studies and note their significance.

**Table 5.2 :** List of recent studies on the 9 August 1912 earthquake.

| | Author | Title | Year | Document type | Lang. |
|---|---|---|---|---|---|
| **1** | Tabban A. and Ateş A. | 9 August 1912 Şarköy-Mürefte Earthquake studies – Preliminary report | 1976 | Report | tur |
| **2** | Ambraseys, N.N., and Finkel, C.F. | The Saros-Marmara earthquake of 9 August 1912 | 1987 | Article | eng |
| **3** | Öztin, F., | 9 Ağustos 1912 Şarköy-Mürefte depremi | 1987 | Article | tur |
| **4** | Altunel et al., | Slip distribution along the 1912 Mürefte-Şarköy earthquake, the North Anatolian Fault, Western Marmara, | 2000 | Article | eng |
| **5** | Rockwell et al | Paleoseismology of the Gaziköy-Saros segment of the North Anatolia fault, north-western Turkey | 2001 | Article | eng |
| **6** | Altınok et al, | Şarköy - Mürefte 1912 Earthquake's Tsunami, extension of the associated faulting in the Marmara Sea, Turkey | 2003 | Article | eng |
| **7** | Altınok et al, | Tsunami of Şarköy-Mürefte 1912 earthquake: Western Marmara, Turkey | 2003 | Article | deu |
| **8** | Altunel et al., | Characteristics of the 1912 co-seismic rupture along the North Anatolian Fault Zone | 2004 | Article | srp,fra |
| **9** | Rockwell et al., | Paleoseismology of the North Anatolian Fault near the Marmara Sea: Implications for Fault Segmentation and Seismic Hazard | 2009 | Article | eng |

**Tabban and Ateş (1976)** is the earliest recent work on the 1912 earthquake. They visited the epicentre area and investigated traces of the surface rupture. Their study aimed to collected preliminary data to launch an extensive project on the event. Therefore, the detail of the introductory report is minor. Valuable information is eye-

witness interviews with locals, where some description of faulting is available at Güzelköy and Kavak.

**Öztin (1987):** This study is only a translation of Sadi (1912) from Ottoman Turkish to Modern Turkish.

Ambraseys and Finkel (1987) is one of the most comprehensive recent studies, in which descriptions of surface faulting and co-seismic slip is available. In addition, the damage distribution is investigated in detail and summarized in an intensity map. Milne seismogram readings were used to calculate an empirical magnitude of Ms 7.4.

**Rockwell et al., (2001, 2009)** provide evidence of surface faulting and a co-seismic slip of 4.5 m at Kavak from trench results.

**Altınok et al., (2003)** measured right lateral co-seismic offsets at three localities ranging from 3.5 to 4.5 m between Gaziköy and Gölcük. They calculate a moment magnitude of 7.3 for the 9 August shock derived from 4.5 m average slip, 15 km of rupture width and 56 km of rupture length. Hence, they propose a rupture extending from the Kavak region to the bend offshore of Gaziköy; 56 km in total. Aside, using multibeam bathymetry and seismic profiles they determine a landslide and note the potential of tsunamis. Based on the GPS shear velocity of 17 mm/yr for the region, they consider that the 1766 can not be the penultimate event and suggest the 1659 earthquake must have ruptured this segment.

**Altunel et al. (2004)** measured right lateral displacement on 24 new sites and compiled a slip distribution with 31 measurements. The co-seismic offsets range from 1.4 to 5.5 with cumulative slips reaching up to 35 m. The co-seismic slip distribution shows clustering near villages nested along the fault but lacks especially towards west. They determined three sub-segments along the 1912 Mürefte earthquake rupture and consider a total rupture length of 100-150 km; 50 km inland, 30 km in Marmara, 20 km in Saros.

**Mc Hugh et al., (2006)** used 1-2 m drillings from the offshore Ganos (Gaziköy) basin and analyzed their homogenite content. Interpretation combined with multibeam bathymetry and seismic profiles yield that the 1912 Mürefte earthquake caused deposition of a ~3 m thick homogenite sequence within the basin floor of the Gaziköy basin. The homogenites overlay disrupted reflectors; hence they interpreted

this as the related earthquake rupture. In addition, cores from Tekirdağ and Central basins showed some sharp discontinuity of short lived radioisotopes and sedimentation of ~30 cm which they attribute to the 1912 event.

They determine also some historical events of the region, such as 740, 1063 and 1343. They observe the 1063 in two cores only from the Tekirdağ Basin and the 740 and 1343 events in two and one cores respectively in the Central Basin. In the Ganos basin they determine a mass-wasting event prior to the 1912 earthquake and relate it to an older rupture. The cores on the west of the Sea of Marmara shows also homogenites related to earthquakes in the Saros (e.g. 1859, 1965). McHugh states that homogenites of events located far from cores show distinguishable stratigraphic characteristics from homogenites located next to ruptures.

**Ustaömer et al., (2008)** collected multibeam bathymetric data and high resolution seismic data from the Saros bay and exposed the poorly known morphology of the Saros bay. They show fresh fault scarps located on the Saros shelf and along the inner parts of the Saros Trough. They divided these scarps into 3 main fault segments and associated the eastern most segments to surface breaks of the 1912 Mürefte earthquake. However they also note that, some sediment covers this scarp at some localities along the segment, where they also observe landslides. These are either depositions post-dating the Mürefte earthquake or the scarps belong to an older event. The length of this segment is about 40 km. It appears as a vertical fault in seismic sections however shows northwards dipping at a high angle in the morphology, along the eastern slopes of the basin. They interpret this as a result of a slight reverse component.

**Armijo et al., (2005)** used multibeam bathymetric data, high resolution seismic data and ROV (Remotely Operated underwater Vehicle) to document the structure and morphology of the Marmara basins.

They define a large component of normal slip along the southern margin of the Tekirdağ basin, connected with the adjacent strike-slip fault system to the east and west. They use topographic profiles across the fault to determine vertical component of slip. A vertical slip of 1-1.5 m is documented on the eastern part of the Tekirdağ basin. The total offset of 2-3 m of this scarp is interpreted as a cumulative displacement of two events. At the same site a scarp shows slickensides with a rake

of 15° in accordance to the right-lateral motion. A total of 4-6 m oblique slip is determined from this free face. The geometry at the Ganos bend is also well illustrated showing a combination of strike-slip and thrust scarps. The fault scarps are in a right-stepping en-echelon array. Micro-bathymetry profiles show a steep escarpment up to 10-m-high that incorporates the 1912 event.

The narrow linear fault section along the Central High also exposes typical structures of strike-slip faulting (e.g. sagponds and pressure ridges). Armijo et al. (2005) measures a 6 ± 1 m right-lateral offset on a sea-bottom landform and relates it to the most recent one or two events. Additionally they determine a set of scarps with < 0.5 m height that are also attributed to the 1912 earthquake.

The high resolution bathymetry of the Central Basin documents an array of small-scale, steep scarps which lacerate the larger cumulative scarps. Profiles from these scarps yield vertical displacements of 0.5 to 2 m for each scarp and give an incremental throw of 2-4 m which can be ascribed to one or two events. This set of scarps is continuous all along the south-western basin boundary and probably indicate rupturing during the 1912 Mürefte event. They conclude that the 1912 earthquake rupture terminated within the Central Basin.

### 5.2. Seismic Activity Before and After the Mürefte Earthquake and Their Possible Locations

The Mürefte earthquake occurred at a time when only primitive instrumental seismograms were present at several seismological and meteorological stations around the world. In the year of 1912, seismic activities were recorded at 198 stations located all around the world; in Africa, Asia, Australia, Europe and America (IASPEI). The 9 August 1912 earthquake was recorded at more than 56 seismic stations (Appendix 2). The seismic activity was studied by seismologist of that time (Mihailovic, 1923, 1927, Sidgreaves, 1912, Walker, 1912, Hecker, 1920). Between July and October 314 small sized earthquakes took place in the Ganos region, foreshocks being recorded by instruments starting 15 days before the main shock (Fig 5.1; Mihailovic 1923, 1927). 28 shocks were registered on 9 August, and 24 the day after. Three major shocks are reported to have occurred on 9 August, 10 August and 13 September. However, historical catalogues document additional events (Table 5.2, Tan et al., 2008). Aftershocks continued to occur at least for three months. The

given fore- and aftershock distribution is limited to four months (15 July to 18 October) and is likely that aftershocks continued for some more time. Here, we are limited to the comprehensiveness of contemporary documents, particularly the report of Mihailovic, (1927).

A comparison of historical catalogues and contemporary documents for the seismic activity showed some slight difference among the events (Tan et al., 2008; Mihailovic, 1918, 1927, Macovei, 1913). Two tables present the events registered in catalogues and in coeval studies (Table 5.2 and 5.3). Catalogues report 6 large events; on the other hand historical documents described 7 destructive shocks (see Table 5.3; Mihailovic, 1927, 1923).

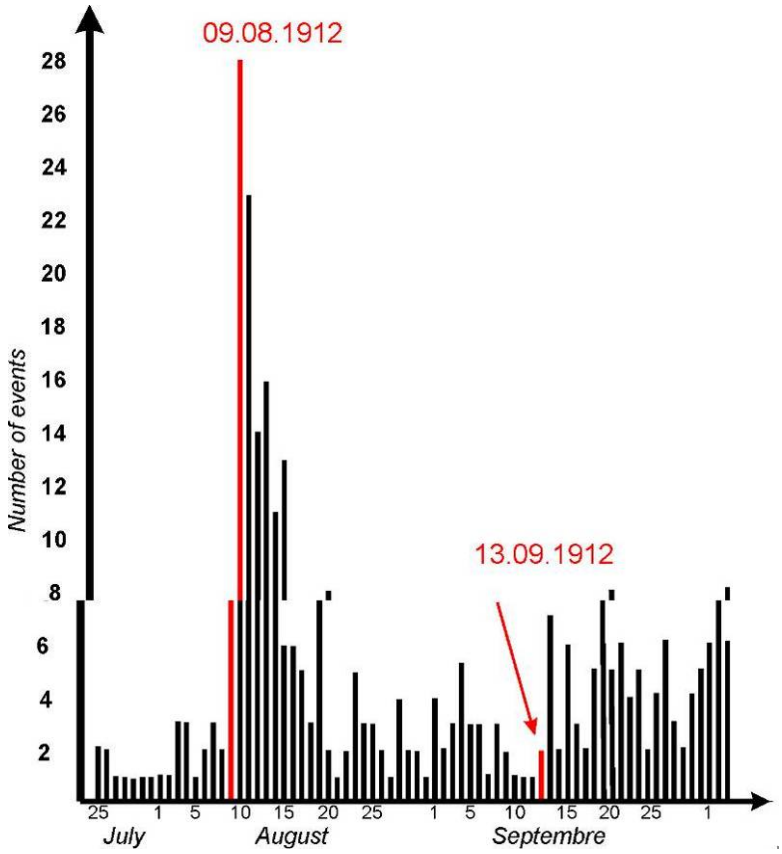


**Figure 5.1 :** Plot of earthquakes per day during the 1912 earthquake sequence (Mihailovic, 1927). A total of 314 earthquakes occurred between July and October, which the largest stroke on 9 August (M 7.4), 10 August (5.7, 6.2) and 13 September (M 6.8). Mihailovic (1927) reports 28 shocks on 9 August and 24 on 10 August.

**Table 5.3 :** Mainshocks (bold) and major aftershocks of the earthquake sequence (Tan et al., 2008). See Figure 5.2 for epicentre locations.

| | Date | Time | Lat | Lon | Magn. | Reference |
|---|---|---|---|---|---|---|
| **1)** | **1912.08.09** | **01:28** | **40.7** | **27.2** | **Ms 7.3** | **Ambraseys & Jackson (2000)** |
| 2) | 1912.08.10 | 09:23 | 40.8 | 27.5 | Ms 6.2 | Ambraseys & Jackson (2000) |
| 3) | 1912.08.10 | 18:30 | 40.6 | 27.1 | Mw 5.7 | Kondorskaya & Ulomov (1999) |
| **4)** | **1912.09.13** | **23:31** | **40.7** | **27.0** | **Ms 6.8** | **Ambraseys & Jackson (2000)** |
| 5) | 1912.10.21 | 09:31 | 40.5 | 27.1 | Mw 5.1 | Kondorskaya & Ulomov (1999) |
| 6) | 1912.10.21 | 23:40 | 40.5 | 27.1 | Mw 5.3 | Kondorskaya & Ulomov (1999) |

**Table 5.4 :** List of earthquakes compiled from historical documents. Times are Greenwich time. The location column corresponds to areas noted as the source of the shock in related document. Bursa, Keşan, Malkara, Lake Manyas and Lake Ulubat are sites apart from the fault and correspond to wrong interpretations of the authors.

| Date | Time | Location | Ref |
|---|---|---|---|
| 09.08.1912 | 01:28:46[a,c]<br>01:32:16[b] | Ganos, Dardanelles, | Mihailovic 1918[b], 1923 [c] 1927[a], |
| 09.08.1912 | 05:25:01 | Keşan, Tekirdağ, Malkara | Mihailovic 1918, 1923[c,] 1927 |
| 09.08.1912 | 06:10:02 | Ganos | Mihailovic 1918, |
| 09.08.1912 | 09:50:10 | Ganos, | Mihailovic 1918, |
| 09.08.1912 | 13:58:05 | Ganos | Mihailovic 1918, |
| 09.08.1912 | 18:58:20 | Ganos, | Mihailovic 1918, |
| 09.08.1912 | 22:11:15 | Ganos | Mihailovic 1918, |
| 10.08.1912 | 01:22:28 | Ganos | Mihailovic 1918, |
| 10.08.1912 | 09:23:46 | Hoşköy, Lake Manyas Lake Ulubat, and Bursa | Mihailovic, 1923, 1927, Macovei 1918 |
| 10.08.1912 | 14:13:10 | Ganos | Mihailovic 1918, |
| 10.08.1912 | 18:30:16 | Dardanelles, Lake Manyas Lake Ulubat, and Bursa | Mihailovic 1923, 1927, Macovei 1918 |
| 11.08.1912 | 07:20:43[a]<br>07:22:07[b] | South of Marmara, Marmara islands | Mihailovic 1918[b], 1927[a], |
| 13.09.1912 | 23:32:15[a,c]<br>23:34:45[b] | Hoşköy, Gulf of Saros | Mihailovic 1918[b], 1923[c], 1927 [a] |
| 14.09.1912 | 05:55:12 | Hoşköy, Gulf of Saros | Mihailovic 1918, |
| 16.09.1912 | 21:05:37[a]<br>21:08:12[b] | Gulf of Saros | Mihailovic 1918[b], 1927[a] |
| 17:09:1912 | 01:14:18 | | Mihailovic 1918, |

The main shock occurred on 9 August 1912 at 03:28:46 (LT). Macovei (1918) notes a source duration of 22 to 23 seconds; based on seismogram readings at the St. Benoit station (Istanbul) and Bucharest. A longer duration of 45 seconds is calculated from seismic recordings at the station of Jena (Hauptstation für Erbebenforschung, Jena). Ambraseys & Finkel (1987) notes a source duration of 40 seconds. Sadi (1912) reports also a duration of 30 to 40 seconds. It is notable that in several sources, the 9 August earthquake is described as three subsequent shocks with increasing quake and the last as the largest (Mihailovic, 1923, 1927, Macovei 1913, Sadi 1912). This might be related to arrival times of different types of waves (P, S and surface waves), or it may be associated to sub-events in a similar way that observed during the 17 August 1999 earthquake (Gülen et al., 2002). The main shock was followed by 4 large events on the day after. Two of them were estimated as M 6.20 and M 5.7 (Table 5.2). A second large shock occurred on 13 September 1912 at 23:31. The event is calculated as Ms 6.8 and caused also significant damage in the region (Ambraseys & Jackson, 2000). The size of this event implies that it is a separate large earthquake rather an aftershock and may have caused about ~30 km of surface rupture. Therefore, special attention has been given to bring out the characteristics of this event.

**Epicentre estimations**

The epicentres of the above mentioned shocks are not well constrained. Some estimations from seismologist of that time are available through historical documents (Mihailovic, 1919, 1927; Sidgreaves, 1912; Walker, 1912; Table 5.4). However, assessments are very rough and cluster within a radius of nearly 250 km. Most definitions give just an epicentral distance to the station or name a city located nearby. Although imprecise, better epicentre locations calculated by recent studies, which consider the fault setting are given in Table 5.2 (Fig 5.2). The epicentre of the 9 August shock is thought to be near Yörgüç. The aftershocks are located 10 to 30 km SW and NE of the main shock. The second main shock on 13 September is located north of Yeniköy. It is noteworthy that both types of sources (historical and recent) locate the 13 September shock to the east of the 9 August earthquake. This is a very important observation because the second shock constrains the western end for the 9 August fault rupture, which will be discussed at the end of this chapter.

**Table 5.5 :** Epicentre estimations of the 9 August and 13 September shocks from some seismic stations of that time ( Mihailovic, 1927, Walker, 1912). For locations of the station see Fig 5.2

| Station Names | 9 August 1912 | | 13 September 1912 | |
|---|---|---|---|---|
| | *Lat* | *Lon* | *Lat* | *Lon* |
| Tiflis | 41,8 | 27,8 | 42 | 27,4 |
| Pulkovo | 41 | 26,6 | 41,1 | 26,3 |
| Irkutsk | 41,5 | 28,5 | 39,3 | 28,1 |
| Jugendheim | 42,2 | 26 | -- | -- |
| Strasbourg | 40,06 | 27,4 | -- | -- |

## 5.3. Damage Distribution of the 9 August 1912 and 13 September 1912 Earthquakes

The destruction and loss of life is described in many sources (Sadi, 1912; Macovei, 1912, 1913; Mihailovic, 1918, 1927, Agamennone, 1912, Mâmâcânyam, 19??). However estimations of the loss vary widely from one and other. The most reliable source is considered to be Mihailovic, (1927). The damage and its distribution described and discussed by Ambraseys & Finkel (1987) relay primarily on the observations of Mihailovic (1927). Here, we summarize important parts of the damage and casualties caused by the two largest events; the 9 August and 13 September shocks based on Ambraseys & Finkel (1987) and Hecker (1920) (Fig. 5.2). No estimates are available of the total losses for the whole earthquake sequence in 1912. Therefore, the available damage descriptions are mainly related to the 9 August shock. The 13 September event is however described to a lesser extend, by minor sources (Hecker 1920).

### The 9 August 1912 shock damage

The Mürefte tremor was felt not only in the eastern Balkans, but also felt in Bucharest and Vienna (Macovei, 1912; Mihailovic, 1927; Ambraseys & Finkel, 1987). The damage was centred between Çanakkale (Dardanelles) and Tekirdağ, but also reached all the way to Istanbul, Edirne, Enez, Adapazarı, Ayvalık and Bursa (Ambraseys & Finkel, 1987; Mihailovic 1927). Heavy damage was recorded at Gaziköy, Hoşköy, Mürefte, Şarköy, Güzelköy, Mursallı, Yayaköy, Kavak, Gelibolu and Çanakkale (Fig 5.3). The maximum damage was localized between Tekirdağ and Mürefte which allowed to assigning a IX-X MSK maximum intensity near the Mürefte village. The earthquake struck at 03:30 a.m. local time and affected an area

containing 565,8000 people living in 122,400 houses (excluding Istanbul, Ambraseys & Finkel, 1987). The devastation of the shake killed 2800 and injured 7000 people. It totally destroyed 12600 houses, damaged 12100 beyond repair and caused serious damage to another 15,400 (Ambraseys & Finkel, 1987). The damage distribution is given in MSK scale in figure 5.2 and corresponds almost entirely to the 9 Aug. shock associated to a lesser degree to several fires which broke in the town and villages in the epicentral area.

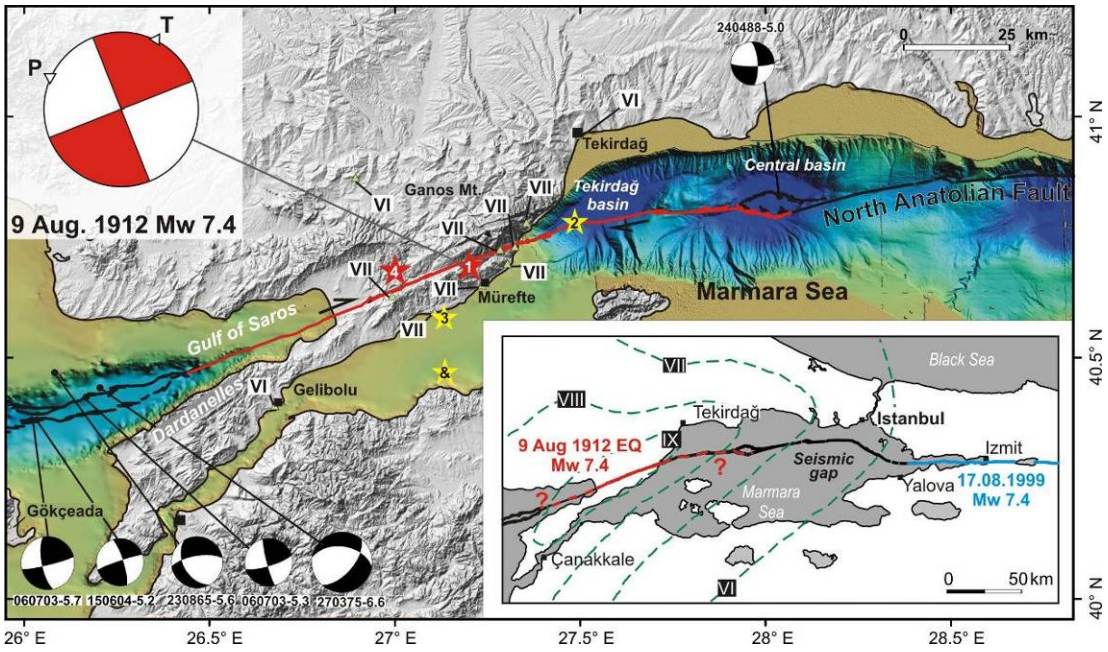


**Figure 5.2 :** The epicentre locations of the earthquakes in table 5.2 are indicated as red and yellow stars. Locations are in a rough estimate, particularly for the September shock, which was probably further west in the gulf. Numbers correspond to events in table 5.2,"&" stands for event 5 and 6. Intensity map of the August shock is given in the inset (after Ambraseys & Finkel, 1987), which indicates that the maximum damage is localized between Tekirdağ and Gelibolu peninsula. The damage distribution of the September shock, on the other hand, shows that maximum damage occurred near Mürefte (Roman numbers; Hecker, 1920). The damage distribution narrows the possible epicentre location of the September shock and implies that the shock should be in the shelf of the Gulf of Saros. Major fault complexities of the North Anatolian Fault on the offshore section are also visible (e.g. Central Basin, Tekirdağ basin, Ganos bend and the Saros basin.

**The 13 September shock damage**

Another large tremor occurred on 14 September 1912 (01:32). The event was recorded in at least 17 worldwide seismic stations and affected mainly the south-western part of the epicentral area of the 9 August event. Buildings that resisted to

the first shock with considerable damage were reduced to ruins while others suffered heavily between Tekirdağ and Çanakkale. The intensity is given for several localities with the maximum damage being assigned as VII MSK (Hecker, 1920). Figure 5.2 illustrates the damage distribution of the related source. There are no clear estimations on the total loss of the event and further information about damage is not available for this event. Most of the damage statistics were obtained before 13 September 1912, thus excluding the effects of the larger aftershock which were rather serious in the Gallipoli peninsula but not significant elsewhere (Ambraseys & Finkel, 1987).

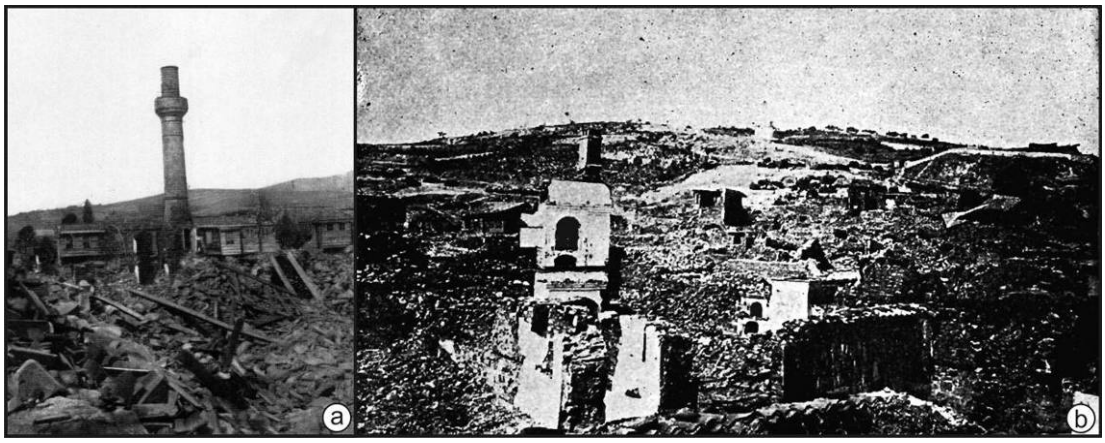


**Figure 5.3 :** Photographs showing the earthquake damage due to the 9 August shock. (a) minaret of a collapsed and burned mosque of Mürefte. (b) A view from Hoşköy showing total destruction.

### 5.4. Landslides, Liquefaction and other Co-seismic Phenomena

Surface faulting of the Mürefte earthquake was associated with remarkable amount of landslides. The sizes of the slides were considerably large and attracted the predominant interest of researchers among structures related to ground deformation (Sadi, 1912; Macovei 1913; Mihailovic, 1927). Several photographs document landslides mainly at two localities, at Ormanlı on northern slope of the Ganos Mt. and on the eastern slopes of the Kirazlı village (also partly on the slopes of the Kirazlı river). Other ground deformations are reported across a large area north east from Naibköy, Işıklar, Yenice, Barbaros and Yazı villages and another series of cracks are mentioned along the northwest of Esindik, Palamut, Isaklı and Yüllüce, Kadıköy and Saros (Mihailovic, 1923). The best documented landslides are at Ormanlı and Kirazlı.

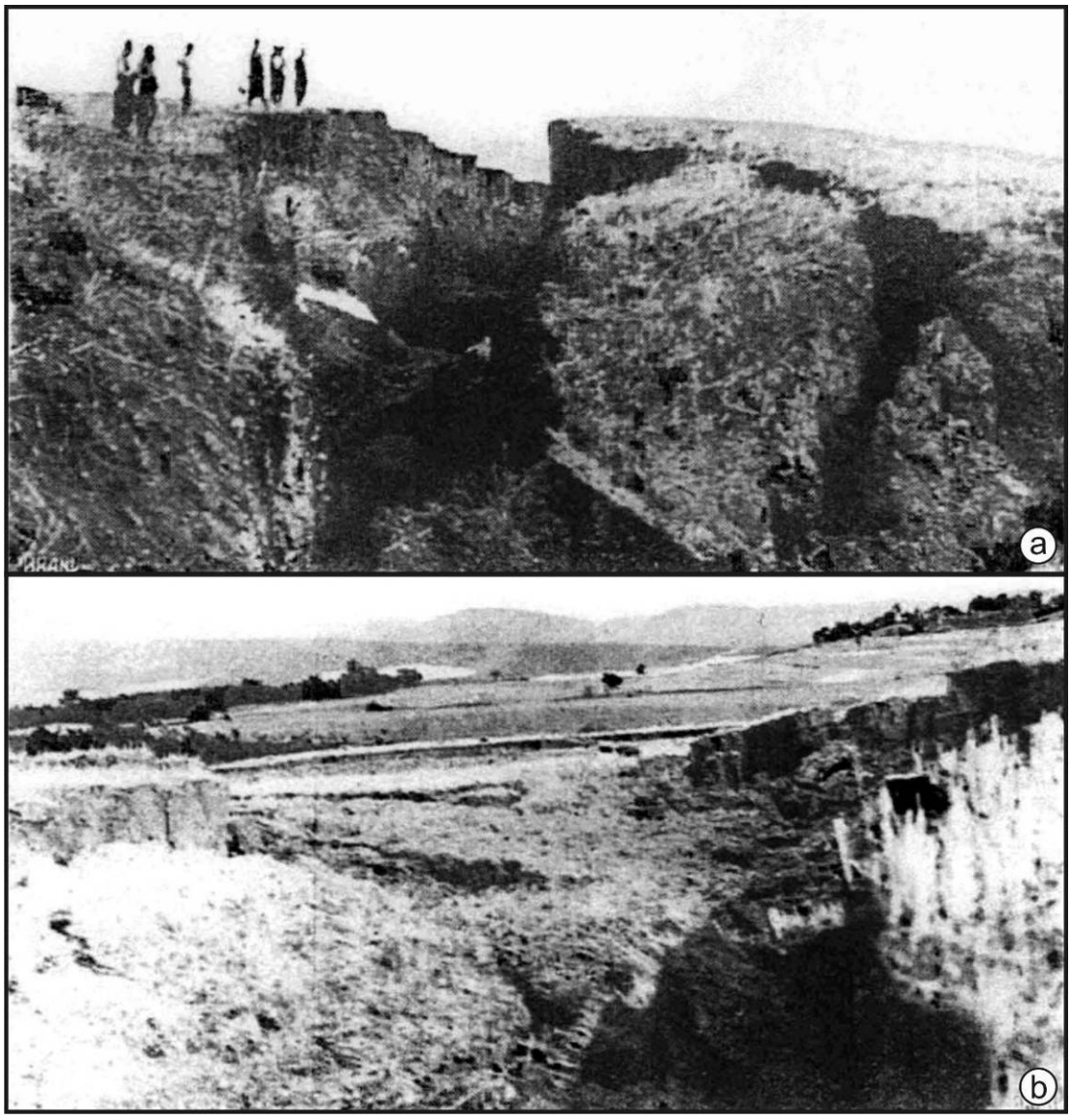


**Figure 5.4 :** a) A photograph showing a large landslide north of Ormanlı, which was reported by many sources (Sadi, 1912, Macovei, 1913; Mihailovic, 1927). b) A smaller landslide located close to Ormanlı

Ormanlı is a small village located 9 km north of the Ganos fault on the northern foothill of the Ganos Mt. One of the largest slides occurred close to this village and attracted interest of several researches. We read from Macovei (1913) that a large crack with a length of ~300m was located north of Ormanlı. The crack had an N-S orientation and an opening of 5-6 m decreasing towards south. He notes a second fracture in the same vicinity with an ellipsoidal structure of about 50 m. The cracks had N-S orientation too and the inner section of the structure sunk for 1-2 m. Both structures are documented with photographs (Fig. 5.4). The large cracks have also been documented and depicted in detail by Mihailovic (1927). He describes a series of cracks up to 347 m in length with a depth of 12 m and a gape of 6 m. Same

photographs are also given in his report. The geology of the southern limb of Ganos Mt. consists of Late Eocene–Early Oligocene shale of the Mezardere Formation, which are poorly consolidated sediments. The topography of this region expresses distinct characteristics of landslide morphology.

Kirazlı is a small village located 3 km south of the Ganos fault on the Panayir Hill. Mihailovic (1927) documents a 960-m-long large crack with an opening of 1.2 m and a depth of 7.5 m. Further descriptions are not available on the structure. This area consists of Upper Miocene massive and poorly consolidated sandstones of the Kirazlı Formation. Lower altitudes of region expose the Gazhanedere formation which is also poorly consolidated. These units experience landslides at stages of high ground water level. The 9 August shock triggered also landslides at these localities.

Ambraseys & Finkel (1987) report additional landslides triggered by the 13 September shock. Extensive sliding occurred on the central part of the Gelibolu (Gallipoli) peninsula; at Galata (Sütlüce) and Baberi (?). Landslides and rock falls due to the 13 September event aggravated much of the damage in this region.

Liquefaction has been reported at many parts of the Ganos and Gelibolu region. Widespread liquefaction occurred in the Saros bay, near Kavak, and along the Marmara coasts (Şarköy, Mürefte, Hoşköy and Gaziköy). The 13 September shock caused also some liquefaction in the Kavak river area and along the Saros coast and as well as in the valley of Ganos (Ambraseys & Finkel, 1987; Mihailovic, 1923).

Other events such as sudden dry outs of springs, or formations of new springs are also documented in the Ganos area (Macovei 1912). In Çanakkale (Dardanelles) hot water gushed out along the road between the Austrian and English consulates, where the earth is described to be opened (Agamennone, 1912, reviewed in Allen 1913). Beside, outflow of oil and formation of a crater like hole on the coast of Eriklice is reported by Macovei (1912, 1913) and Mihailovic (1927).

### 5.5. Coseismic Surface Faulting of the 9 August 1912 Earthquake

Extending from Gaziköy to the Saros bay , the onland section of the 1912 earthquake rupture has a length of 45 km with an average strike of N69°E. Detailed mapping shows that the rupture was nearly pure strike-slip, consisting of splays with variable lengths < 2 km, incorporated with step-overs, bends and mole tracks. Similar

descriptions were accessible in historical documents describing 50 m to 2 km of crack series with an orientation NE-SW, parallel to the mountain chain (Macovei, 1912). Measurements of co-seismic displacements ranged from 1.2 to 5.5 m. Contemporary documents indicate that the rupture zone was generally narrow (< 10 m), however in flat areas like the Gölcük and Kavak regions, the deformation zone was much larger, exceeding several hundred meters. Detailed mapping yield at least 3 sub-segments on the onland section. These segments are from east to west, the Güzelköy, Yeniköy and Saros segments. They range in length from 15-40 km and are bounded by right step-over basins.

### 5.5.1. The Güzelköy sub-segment:

The Güzelköy sub-segment is the easternmost onland rupture segment and is approximately 29 km long. Its eastern limit is determined by the Ganos bend; located 15 km offshore of Gaziköy. The western tip of the sub-segment is the Yörgüç basin that formed as a ~300-m-wide releasing bend. The mean orientation of the segment is N71°E and consists of 3 to 8-km-long sections which are sub-divided into shorter sections by right or left stepping jogs. Together with our slip measurements and those of Altunel et al. (2004), 30 sites allowed documenting the rupture geometry and co-seismic slip of the Güzelköy sub-segment (Fig. 5.5). The maximum slip along this segment is 5.5 m and is measured at Güzelköy and Yörgüç.

The segment is visible on the east at Gaziköy, where the land is densely inhabited and modified. As a result, a clear trace of the rupture is not preserved. However, contemporary studies illustrate several breaks distributed along the plain land and on northern slopes (Fig. 5.6, Mihailovic, 1927). Three groups of breaks are distinct in the sketch map. The first group consists of parallel SW-NE striking breaks. The second group includes fractures trending NW-SE and forming a significant angle to the prior. The last group of breaks are arc-like cracks located at the higher parts of the slopes. The SW-NE striking breaks are close and parallel to the Ganos fault suggesting that they represent the principle displacement zone. The second group are angular to the principle rupture zone and likely to be Riedel shear fractures.

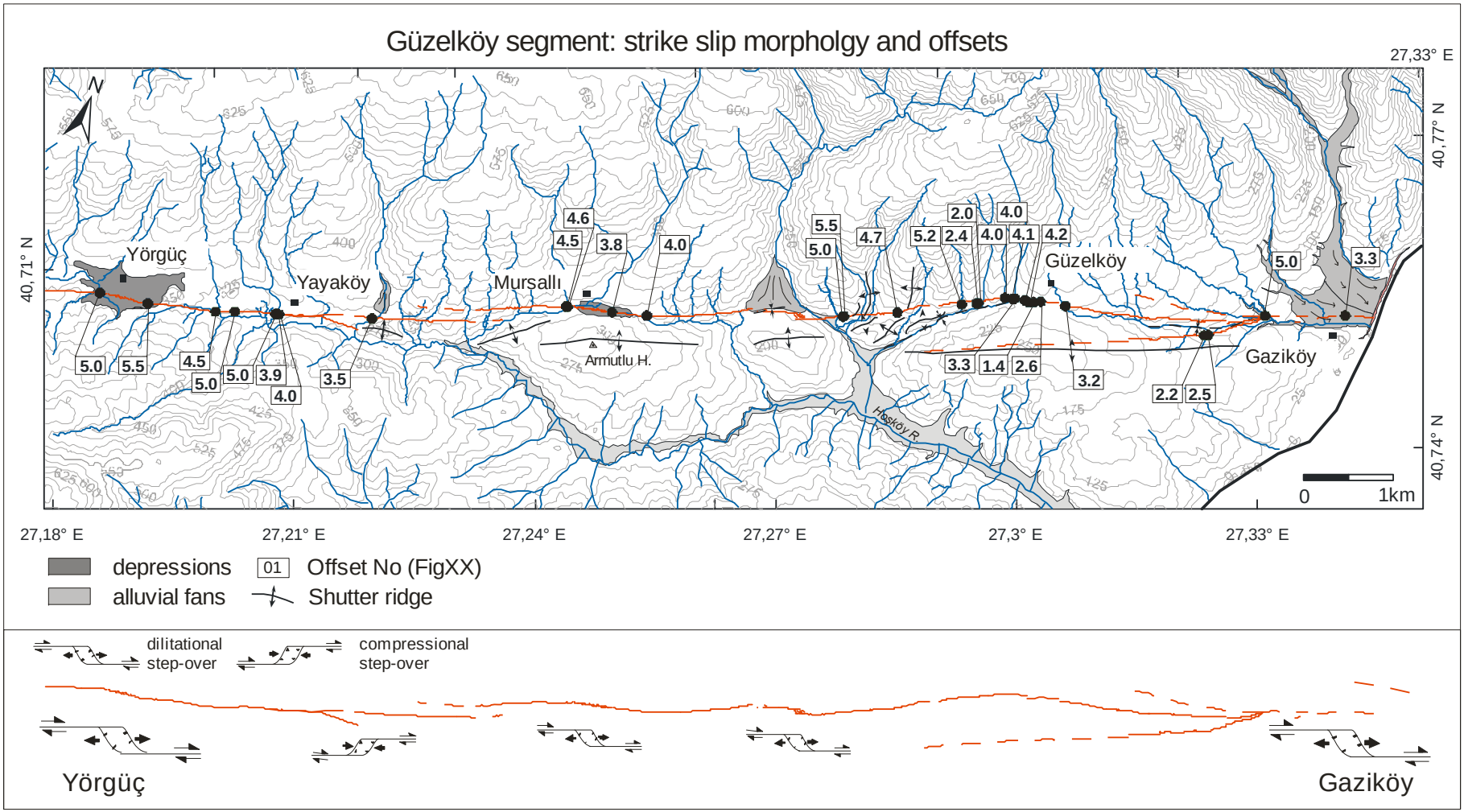


**Figure 5.5 :** The Güzelköy segment is located on the southern limb of Ganos Mountain and follows pre-existing topographic breaks at the base of the mountain. It generates shutter ridges, pressure ridge, stream offsets and sagpond. The N71°E average orientation of the fault varies ± 5°.

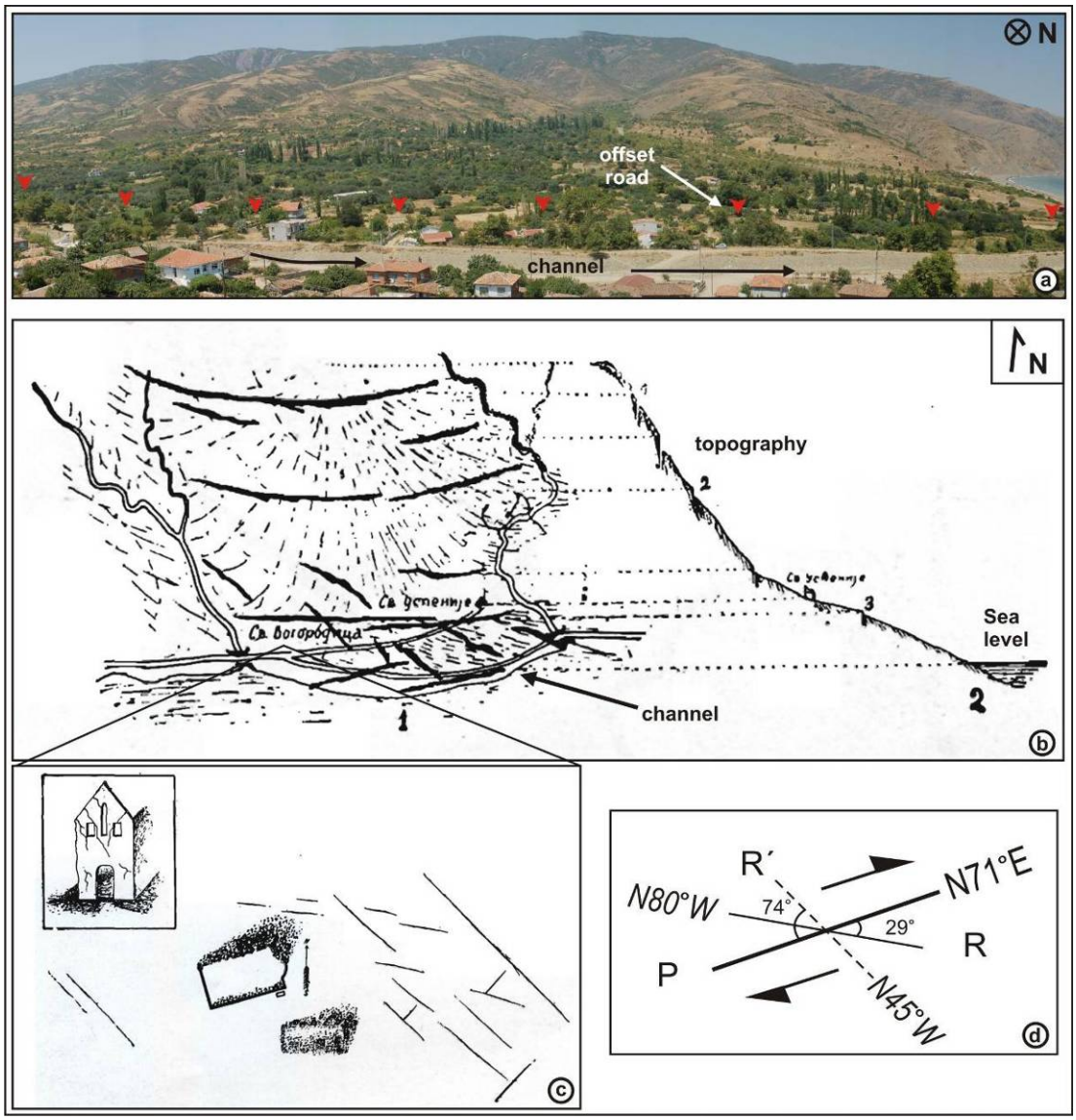


**Figure 5.6 :** Earthquake surface ruptures of the 9 August event in Gaziköy. a) A photo-mosaic of north side of Gaziköy. The Ganos fault runs sub-parallel the large channel following the margin of the alluvial fan. Detail on the road offset is given in Figure 5.7. (b) A map showing the north of Gaziköy; prepared right after the earthquake with a topographic cross-section to the right (from Mihailovic 1927). Surface ruptures and co-seismic deformation are drawn as thick black lines in the map. (c) A sketch from Mihailovic (1927) showing earthquake damage in a monastery. The arrow in the centre points to North. (d) Diagram illustrating the main and secondary faults and fractures in a shear zone. We consider the lines oblique to the principle rupture direction correspond to Riedel shears and secondary deformations (see text for detail).

A closer view to these structures is illustrated around a monastery at Gaziköy, where we see that their orientation resembles noticeably to R and R' shear fractures (Fig. 5.6); we note here that the sense of motion along these fractures is not mentioned in

the reports). The arc shaped breaks located on the slope of Ganos signify most probably secondary structures like tension cracks or slope failures.

Mihailovic (1927) reports a 2.5-km-long crack at Gaziköy consisting of short sections, which longest is 840 m with an opening of 50-60 cm and a depth of 1.80 m. He notes that the south-eastern block of this crack has subsided for 40 cm. The descriptions are confident with offshore observations along the western margin of the Tekirdağ basin. Similar section lengths and vertical offsets have been measured and described for the offshore section of the 1912 earthquake rupture (Armijo et al., 2005).

Two road displacements of 3.3 m and 5 m have been documented at Gaziköy 300 and 1200 m west from the coastline, respectively (Fig. 5.7). The former is on an old pavement road, most probably ancient. It displays a cumulative slip of ~12.7 m (The history of the Gaziköy village spans prior to the 1st c. B.C.; thus man-made structures may record multiple offsets).

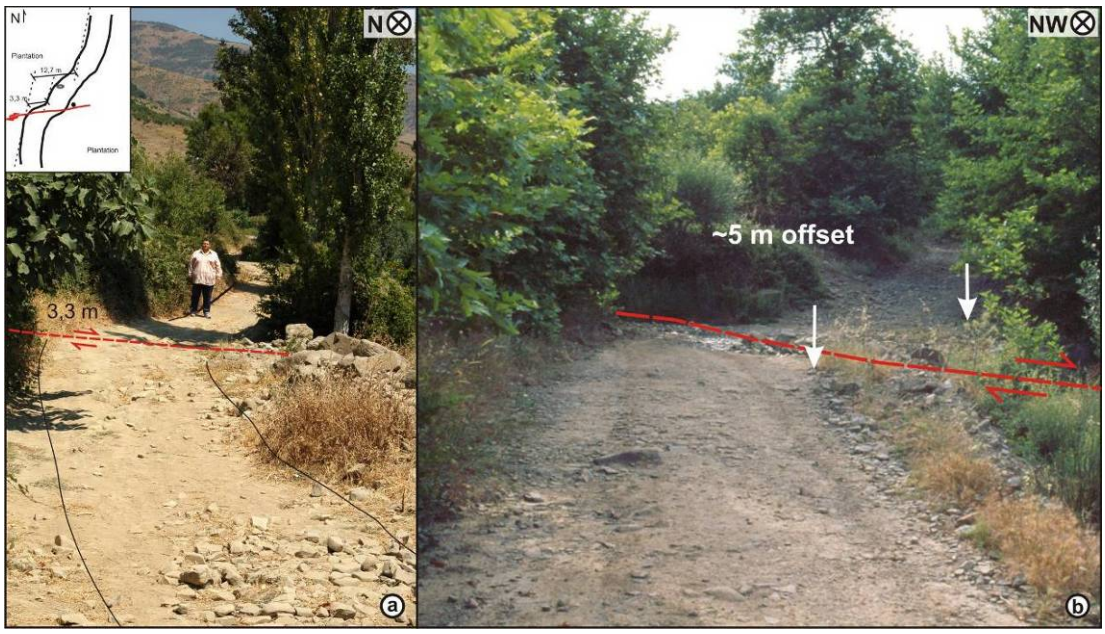


**Figure 5.7 :** Two road offset near Gaziköy. Location of a) is given in Figure 5.5. The road appears to be an ancient pavement. We measured 3.3 m of right-lateral co-seismic and 12.7 m cumulative displacement on this road. The inset illustrates the offset in map view. b) Another offset road (~ 5 m) located ~1 km to the west.

The Güzelköy segment bifurcates at a point about 2 km west from the coast line. The secondary branch strikes SW from the main branch and runs along the southern flank of a stream bed. NNW facing scarps are still well preserved in morphology at this

site (Fig. 5.8). The scarps have a left stepping patterns and climb towards the higher part of the valley side. We measure a vertical component of~ 0.5 m. However the total height of the scarp is 2-3 m and indicates successive earthquake faulting. The lateral movement has been extracted on a field limit and a stream as 2.2 m and 2.5 m respectively. This branch is visible for 2 km with a mean strike of N60°E before it crosses rural land and disappears. The main northern strand is morphologically better pronounced, forming steeper slopes on the northern valley wall. The fault trends about N72°E and is associated with several right steps. The slight subsidence in this area may be related to a shallow negative flower structure, since significant vertical component is not available all along the fault.


**Figure 5.8 :** A view of the southern branch of the 1912 earthquake rupture near the shore of Marmara Sea. Fault morphology and scarps associated with the event are still preserved between Gaziköy and Güzelköy. Here we measure a total scarp height of 2-3 m, 0.5 m being related to the 1912 event.

Contemporary documents note that breaks near Güzelköy extend for 7 to 8 km (Mihailovic, 1927). They consist of small section 500 to 600-m-long with an opening of 30 to 120 cm, and 1.3 to 2.8 m depth. A photograph of a crack near Güzelköy illustrates a strike-slip structure (Fig. 5.9). Descriptions on the location indicate that the image is taken south of the village, where the rupture crosses a 200-m-wide saddle. Villagers point this location for surface breaks. Here, the rupture constitutes several short right steps revealing a linear depression. Eleven adjacent cracks, reaching a total length of 2.5 km are reported by Mihailovic (1927) in this region. The cracks are 15-m-wide and have openings from 80 to 130 cm. The descriptions

point towards an en-echelon fault pattern diffused in a large zone, which is confident with the general fault geometry in the region.

Twelve co-seismic right lateral displacements have been measured by Altunel et al., (2004) at Güzelköy. The measurements correspond to field limits, walls, tree limits and streams. They display slips between 1.4 to 5 m (Fig 5.5, Table 5.5).

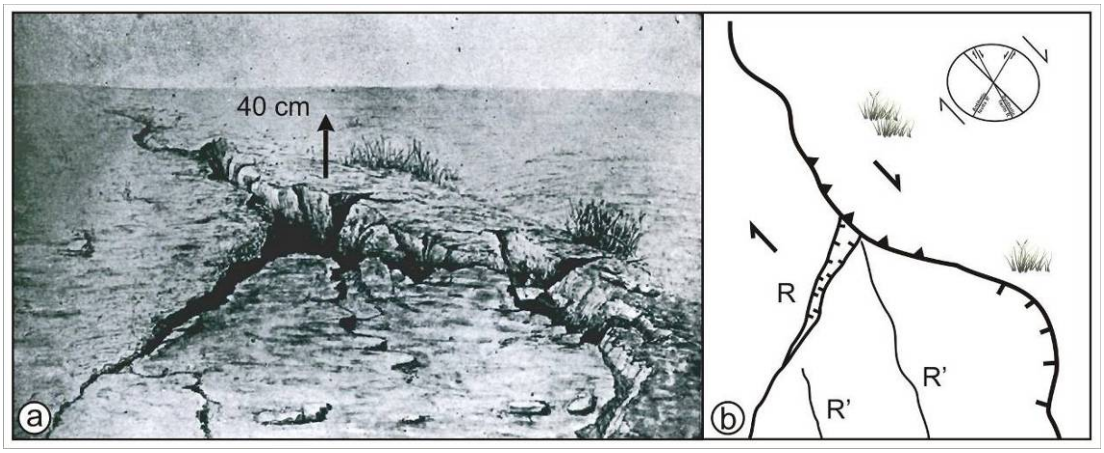


**Figure 5.9 :** a) a photograph showing cracks at Güzelköy (from Mihailovic, 1927). A sub-linear fracture is accompanied with other oblique openings. A 40 cm of uplift on one block is mentioned. We note that the uplift is not continuous all along the crack. b) map-view sketch of the structure. From the lower right, the main principle crack first curves to the right, then to the left; respectively the structure shows extensional and compressional character. Such deformation is typical on faults with right-lateral sense of slip. In addition, the orientation of the cracks on the lower part of image is in harmony with Riedel shears.

West of Güzelköy the rupture strikes N65°E and crosses several streams and ridges causing right lateral displacements between 2 – 5 m (Fig. 5.5). The 1912 rupture has been determined in trenches 2.3 km west of Güzelköy and by offsets of 5.5 m and 5 m on two paleo-streams (see p.134). Towards west, north of the Armutlu H., the fault runs along the edge of an alluvial fan. Here, an east facing slope is bounded by two parallel fault scarps accompanied by NW-SE striking minor scarps in between (Fig. 5.10). The geometry resembles a relay ramp revealed by right-stepping of the fault (Woodcock and Fischer, 1986).

Farther west, Altunel et al., (2000) measures 4 m of lateral displacement on a ridge. The rupture strikes N73°E near Mursallı and crosses the village on its south, where a ~300-m-long linear depression (saddle) is constituted due to right stepping of 50 m. Villagers point a ~0.7-m-high and 200-m-long scarp as the location of the 1912 rupture, (Fig. 5.11). The total height of the scarp is 1.5 - 2 m. Contemporary

photographs are also available for this site. Mihailovic (1927) describes 8-km-long and SW-NE oriented surface ruptures at Mursallı (Fig. 5.11). He mentions a saddle like structure with a height of 1.7 m as the location of the ruptures. The descriptions are identical and most probably correspond to the same locality. The rupture geometry, extracted from the photograph illustrates an en-echelon pattern with a clear principle deformation zone and a series of obliquely trending fractures, consistent with a right stepping faulting. Their orientation indicates that they are most probably R shear fractures and/or opening cracks. Similar rupture geometries were documented at several localities along the 1999 Kocaeli earthquake ($M_w$=7.4) rupture (Lettis et al., 2002).


**Figure 5.10 :** Partly preserved traces of the 1912 surface rupture are available east of Mursallı. The SW-NE trending fault constitutes a releasing step over. The inner part of the step is comprised by small NW-SE scarps. Such fault geometry is observed along strike-slip fault systems and are called relay ramps (after Woodcock and Fischer, 1986).

Altunel et al. (2004) and Altınok et al. (2003) report a co-seismic offset on the Mursallı road as 3.8 and 4.5 m, respectively (Fig. 5.12c). Using aerial photos (from the 1970's), a larger deflection of 16.5 ± 1 m is visible between two strait road sections. We may speculate that this may correspond to a cumulative movement of probably 4 events (This is possible since Mursallı is a village older than 800 years. On the western part of the saddle, a second road offset of 2.3 ± 0.5 m has been measured. The location corresponds to the tip of the southern segment, before it steps to the right, and therefore less slip is measured. After the step, farther southwest we

determined two stream offsets again with ~4.5 m of right lateral displacement (Fig. 5.13).

The rupture veers southward for ~12° where vegetation and hilly topography hides the trace of the rupture farther west between Mursallı and Yayaköy. Therefore, we rely on cumulative displacements and fault morphology to locate the rupture in this region. Offsets at Yayaköy, range between 4 and 5 m (Fig. 5.5) where we measure two road offset of 3.5 and 5 m, the latter showing also a cumulative displacement of 15 m (Fig. 5.12; Altunel et al., 2004)

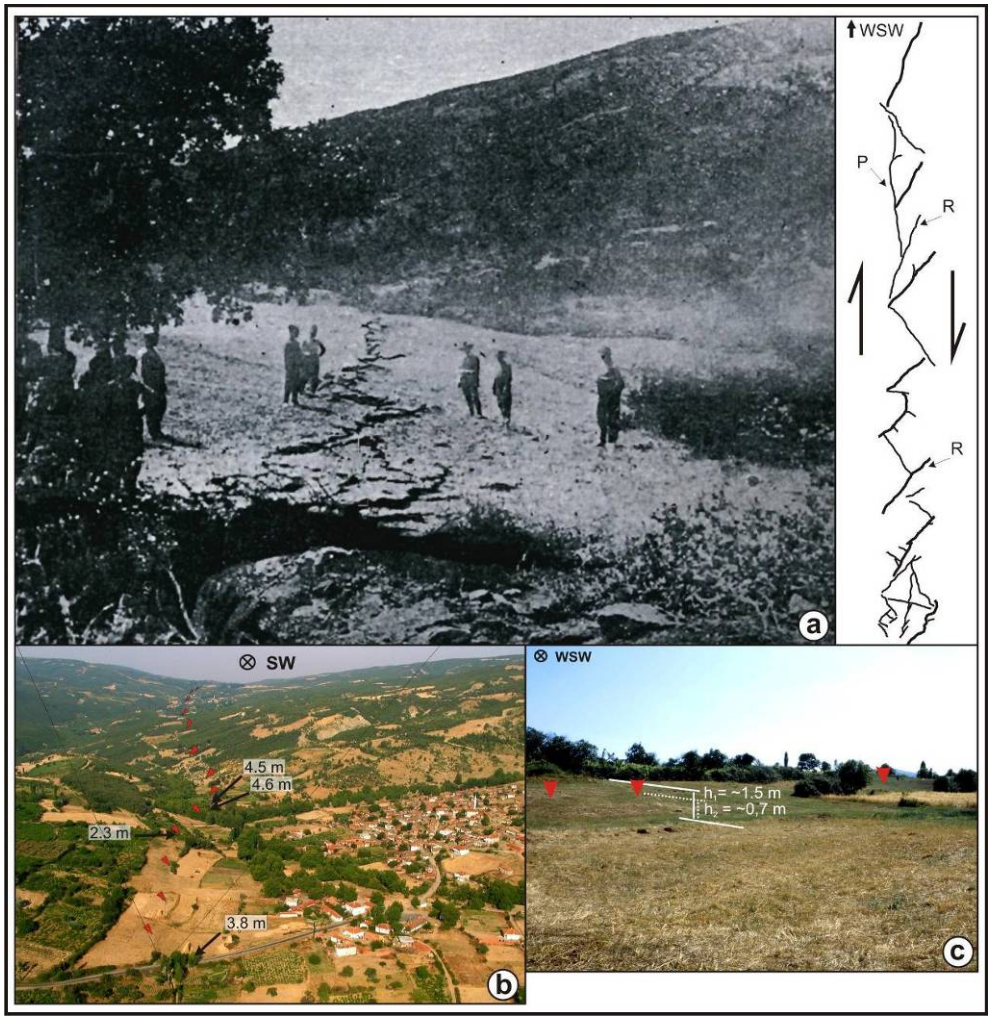


**Figure 5.11 :** Photographs showing the 1912 surface rupture and fault morphology around Mursallı. a) Coseismic surface faulting (from Mihailovic, 1927). The sketch map on the right is extracted from the photograph and illustrates the principle displacement zone and the Riedel fractures. b) Oblique aerial photo of the village (courtesy of S. Pucci). The rupture follows the linear depression located south of the village. Numbers show the amount of offsets measured. c) A fault scarp located between the two road offset. The 1.5-m-high cumulative scarp is constituted of a step of 0.7 m marking individual faulting events.

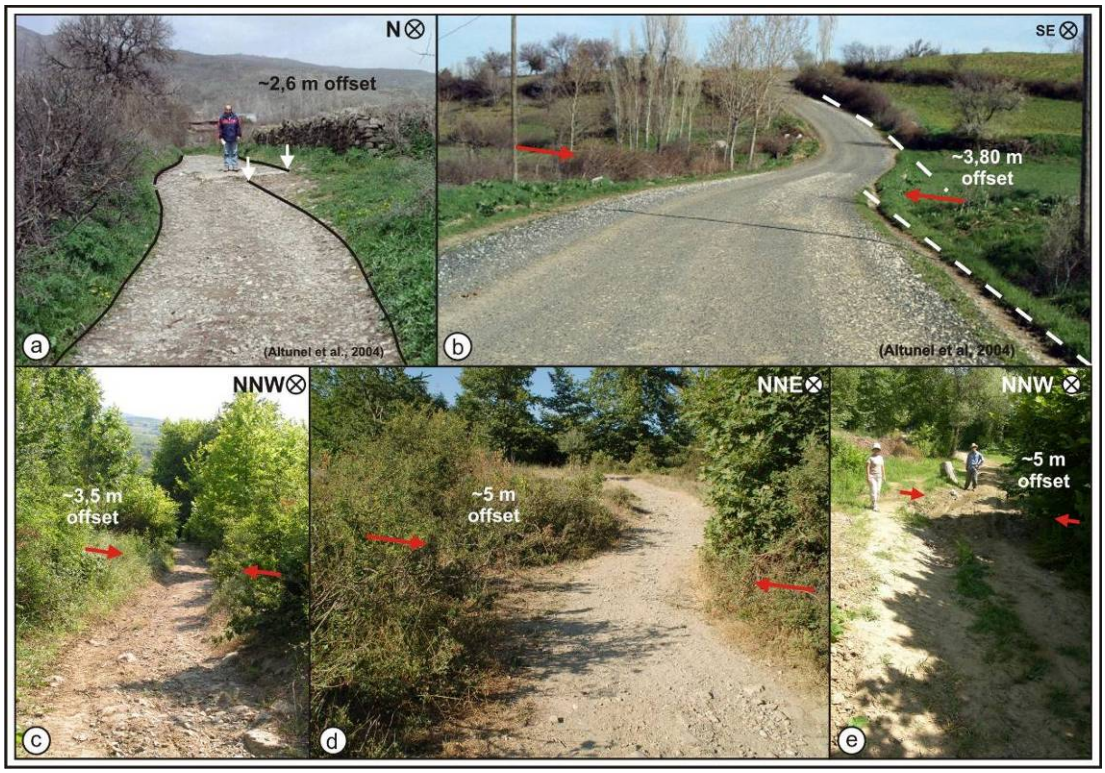


**Figure 5.12 :** Photographs showing coseismic offsets on roads. a) Güzelköy b) Mursallı: Measurements from the aerial photos of 1970's yield a cumulative displacement of 16.0 for the east-side and 16.9 m for the west-side of the road. c, d) Yayaköy e) Yörgüç. The roads show in general a deflection along a straight route and they are located on the fault. Although the offset parts are partly modified today, they general course of the road represent the co-seismic slip. Similar offsets and modifications can be observed along the 1999 earthquake road offsets (Emre et al., 2003).


**Figure 5.13 :** A photo-mosaic showing a well preserved co-seismic displacement on a stream segment; west of Mursallı. The linear stream bed is right-laterally shift for about 4.5 m.

Between Yayaköy and Yörgüç, the fault trends N75°E with a smooth bend, running along the northern flank of a valley where we observe a 0.5-m-high linear south facing scarp. We determined a prominent fresh depression at Yörgüç; a sagpond of 6 m wide and 15 m long which is most probably constituted by a single earthquake event. Villagers claim that this structure is what is left from the 1912 earthquake. The Güzelköy segment continues for a few hundred meters to the west until the releasing bend at Yörgüç.

### 5.5.2. The Yeniköy sub-segment

The Yeniköy sub-segment is 21 km long and bounded by the Yörgüç releasing bend on to the east and the Kavak step-over to the west. It displays minor branching and consists of discontinuous fault traces, noticeably longer than those along the Güzelköy segment. The length of the sections ranges between 4 and 6 km. The mean strike is N66°E, but it is associated with several left and right step-overs and a bend of nearly 10°. We measure 15 co-seismic displacements across streams, roads and field limits, ranging from 1.5 to 5.4 m. Contemporary reports document less evidence on surface faulting along this segment and information is mainly available through descriptions.

The segment displays a fairly straight linear geometry between Yörgüç and Gölcük. Evidence of recent surface faulting is small sagponds located on the back-tilted surfaces on northern slope of the Kocadüz Hill (503 m; see p. 61). The hilly and forestry topography of this region hinders clear evidence of surface ruptures on the morphology. The only coseismic displacement along this part was observed on a dirt road at Yörgüç (Fig. 5.12) where Altunel et al., (2004) measured an offset of 5 m at this locality. The most prominent geomorphologic feature associated with surface faulting along this fault section are two sag-ponds located 2.4 km east of Gölcük (see p. 61). Altınok et al. (2003) report a co-seismic offset of 4.5 m across a stream bed on the large valley floor between Yörgüç and Gölcük. Field observations suggest however that this apparent offset is most likely due to a landslide on the nearby alluvial fan.

Near Gölcük two contemporary photographs illustrate well a co-seismic scarp (Fig. 5.14). They show smooth warping on the ground instead of a mole track pattern typical of strike slip surface rupture, implying that here the slip has significant dip

slip component. Villagers claimed that prior to the earthquake the scarp was at a lower level and reached a 1.80 m height after the event (Mihailovic, 1927). Similar morphology was also observed along the 1999 Düzce earthquake rupture, where individual scarps with free faces 20–50 cm high lacerate obliquely a cumulative normal fault scarp 4 m high, as well with a 1.5 m lateral slip (Armijo et. al., 2005, see their figure 6). The scarp in Gölcük was probably generated with comparable rupture dynamics. The photograph in Figure 5.14b is taken on the plain land NE of Gölcük with a NE view towards the Gölcük stream.

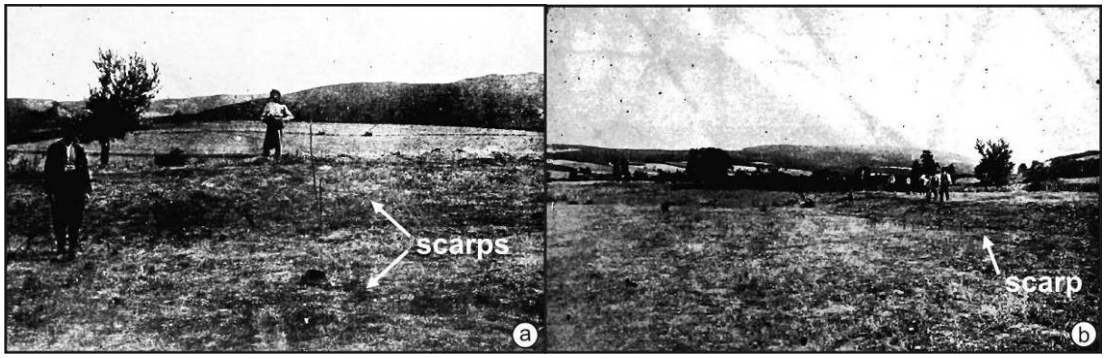


**Figure 5.14 :** Two contemporary photographs showing the earthquake scarp at Gölcük (from Mihailovic, 1927). The height of the scarp is reported as 1.8 m. The structures represent a warping rather than clear oblique faulting, but similar features were observed along the 1999 earthquake ruptures (see figure 6b in Armijo, et al., 2005)

The surface rupture creates a 200-m-wide pull-apart basin as a result of several extensional step-overs at Gölcük where Mihailovic (1927) reports cracks oriented NE-SW, SSW-NNE and NW- SE in series or as single cracks. He describes a 6-km-long surface break with minor divisions is reported at this locality. Indeed, the fault runs here, along the northern margin of a saddle parallel to the 5-km-long linear ridge (see p 61 & 63). Mihailovic describes another fracture of 1700-m-long with an opening of 2.3 m and a depth of 12 m. The breaks are accompanied with parallel WNW- ESE striking fractures spread over a wide area. These descriptions suggest an en-echelon surface break pattern due to step-over geometry. A subsidence of 80 cm is reported for the southern part of the ridge in the inner part of the step-over. A second group of cracks were reported within the valley floor of the Kavak River. They are oriented primarily SSW-NNE, but descriptions are insufficient to infer the origin of these fractures.

Towards west around Gölcük, the surface rupture shows runs through the fault zone that has a complex geometry comprising restraining and releasing bends and step-overs. The fault continues towards west with a strike of N61°E and crosses a valley that displays a cumulative offset of 181 m (see p 74). The area between Gölcük and Yeniköy has a dense vegetation cover and is a highly hilly region. As a result, the trace of the rupture is hardly preserved on this section, along which there are several deeply incised valleys and fault-parallel steep ridges. We observe three sagponds located 3 km east of Yeniköy that are aligned along an 80 m section, with increasing size towards west. The smallest pond most probably occurred during the 1912 event. We measured an offset of 2.5 m on a ridge next to the ponds (Fig. 5.15). Farther west the rupture forms a 10° restraining bend with a step of ~500 m.

Numerous coseismic offsets with significant amount of slip have been observed across the farm fields and streams between Sofuköy and Yeniköy. For example, Altunel et al. (2004) reported six coseismic displacements ranging between 4 and 5.5 m (Fig. 5.16). Mihailovic mentions distributed?? fractures orientated NE-SW parallel to the fault (i.e. N73°E) within the plain land between Sofuköy and Yeniköy. On the other hand, villagers claim two locations for surface breaks, one on the hill slope south of Sofuköy where we see the field limit offsets (Fig. 5.15) and one to the west and southwest of the village. They also claim a surface break running along the SW-NE striking linear crest of the Sofuköy ridge that continues into the valley located on the SW. Field observations yield that the fault consists of several branches at this vicinity. The 1912 surface rupture probably splayed into at least 2 branches. Altunel et al., (2004) measured a road offset of 5.2 m at Yeniköy and a stream offset of 4 m one kilometre further west that are located on separate branches. Detailed mapping shows that the fault forms a 200-m-wide releasing bend within 900 m. The orientation of the fault changes to N53°E and than back to N70°N gradually. Farther west of Yeniköy, the rupture can be hardly traced since the topography is smooth and lateral displacements are less distinct. We measured a minimum of 1.5 m displacement on a field limit. A small sagpond of 5 m x 2 m in size implies recent earthquake faulting. We determined a significant deflection on a linear road section about 300 m west of this sagpond. Altunel et al (2004) report a co-seismic slip of 4 m on a road adjacent to a large depression bounded by a 1.5-m-high fault scarp (Fig. 5.16) where we also measured a total slip of 15 m.

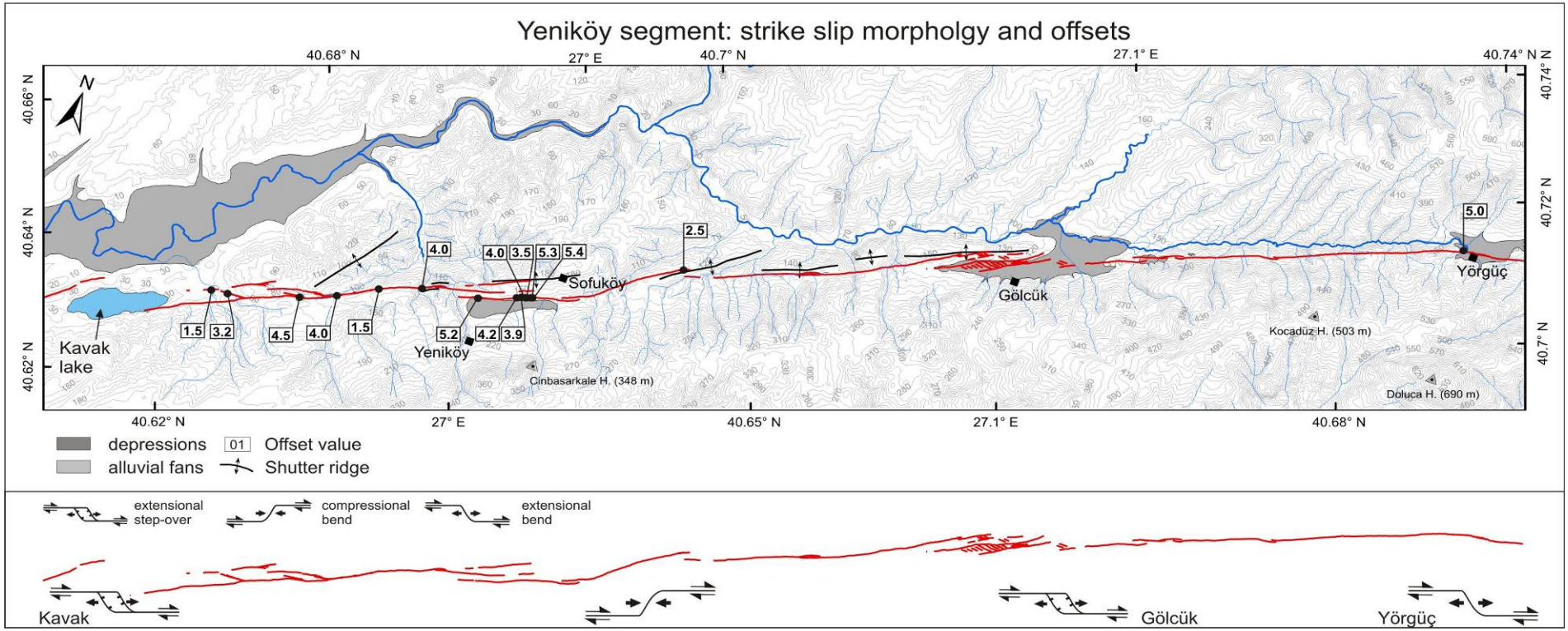


**Figure 5.15 :** The Yeniköy segment runs mostly along the northern limb of the Doluca Hill. Recent faulting is evident by stream, road and field offsets and sagponds. The mean strike is N66°E comprising bends of 10°.

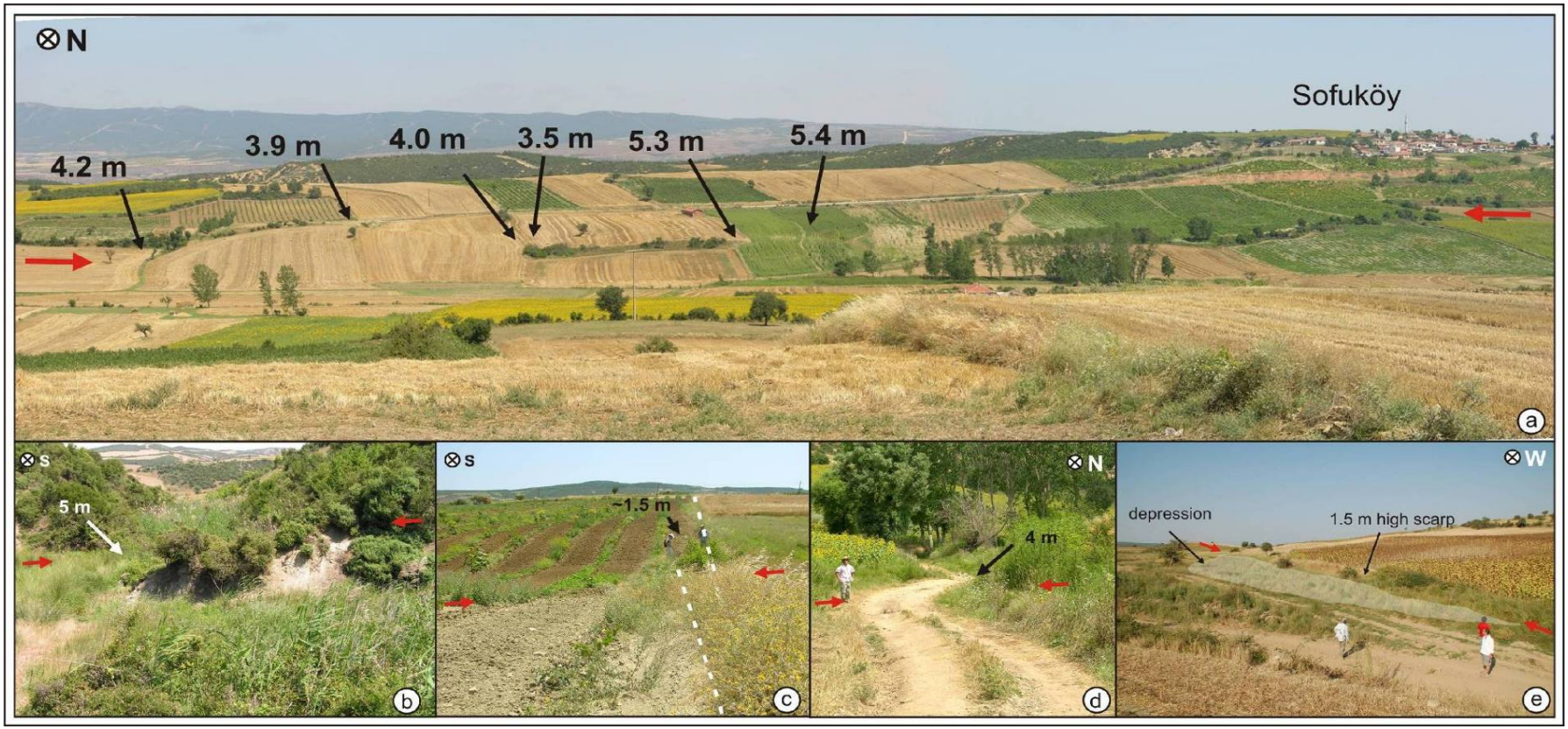


**Figure 5.16 :** The top figure shows well preserved offset field limits south of Sofuköy. A break in the hill slope is significantly, representing the 1912 earthquake scarp. Additional offsets have been documented west of Yeniköy. b) illustrates a fresh shutter ridge penetrating for 5 m into the stream bed. c) A poorly preserved field limit offset of 1.5 m. Although the offset is minor, faulting is evident by the sharp contact in the lithology adjacent to the fault. Note the difference in soil colour north and south of the fault. d) A road offset determined 2.5 km west of Yeniköy. The road shows a co-seismic offset of 4 m (Altunel et al, 2004) and a cumulative slip of 15 m.

The rupture runs further west crossing obliquely the Yeniköy-Kavak road. The topography towards west is fairly smooth and altered by agricultural activities and thus the presence of the fault is indicated by long linear saddles. The Yeniköy sub-segment reaches to the Kavak Lake where the fault makes a large step-over and jumps to the Saros sub-segment.

### 5.5.3. The Saros sub-segment

The onland portion of the Saros sub-segment is about 8 km-long and strikes approximately N66°E, running along the northern margin of a SW flowing stream on the flat land of the Evreşe plain. The fault appears to have a linear geometry and be localized in a narrow zone. The most obvious morphologic feature indicative of an active fault is a large sagpond located at the coast of Saros only (Fig. 4.19, p. 67). Traces of the 1912 rupture could not be observed since the marshy land is occupied with heavy vegetation. Here in this area, the 1912 earthquake faulting is only documented in trenches at Kavak and reported to be about 4.5 m by Rockwell et al, (2001, 2009; see p 176 for detail). Surface breaks at Kavak and close to the coast are reported in several historical accounts (Mihailovic, 1927; Sadi, 1912; Macovei 1912). Mihailovic (1927) describes large holes opened in the entire plain. Series of parallel cracks occurred in orientation SW-NE in the same orientation as the fault.

In conclusion, although the field support for the presence of the fault is rather weak, paleoseismic trenching and historical documents provide strong evidence that the 1912 earthquake ruptured the Evreşe plain at the Kavak region and continued for some distance into the Gulf of Saros.

## 5.6. Slip Distribution, Focal Mechanism, Fault Segmentation, and Rupture Dimension and Geometry

Slip Distribution: Ambraseys and Finkel (1987) suggest that surface ruptures during the 9 August 1912 earthquake present a maximum of 3 m right-lateral slip with a significant normal component. The offsets measurements of Altunel et al. (2004) are not evenly distributed all along the Ganos Fault since they cluster at some localities with gaps at the two tips around the Marmara and Saros coasts. In this study we provide additional slip measurements and fill these gaps by raising the number of measured sites from 31 to 45 along the fault (Fig. 5.17).

**Table 5.6 :** List of 44 co-seismic offsets measurements of the 9 August 1912 rupture. See appendix A2 for locations.

| Name | Km | 1912 | Error | Quality | Cumulative | Error | REFERENCE |
|---|---|---|---|---|---|---|---|
| Gaziköy – road 2 | 0.33 | 3.30 | 0.30 | 2 | 12.70 | 1.00 | This study |
| Gaziköy – road 1 | 1.22 | 5.00 | 0.50 | 3 | | | This study |
| Gaziköy - creek/field 1 | 1.90 | 2.50 | 0.30 | 2 | | | This study |
| Gaziköy - field 2 | 1.93 | 2.20 | 0.30 | 3 | | | This study |
| Güzel - Lstream East | 3.47 | 3.18 | 0.50 | | 17.80 | 0.50 | Altunel et al., (2004) |
| Güzel - pavement | 3.88 | 2.60 | 0.10 | | | | Altunel et al., (2004) |
| Güzel - Chanel | 3.94 | 1.40 | 0.12 | | | | Altunel et al., (2004) |
| Güzel - wall | 3.97 | 3.28 | 0.15 | | | | Altunel et al., (2004) |
| Güzel - Champ | 4.00 | 4.22 | 0.30 | | | | Altunel et al., (2004) |
| Güzel - tree limit | 4.03 | 4.05 | 0.20 | | 7.04 | 0.30 | Altunel et al., (2004) |
| Güzel - Stream West | 4.04 | 4.00 | | | 8.00 | | Altunel et al., (2004) |
| Güzel - Lstream West | 4.13 | 4.00 | | | 12.60 | 0.20 | Altunel et al., (2004) |
| Güzel - Stream bed1 | 4.41 | 2.00 | 0.30 | | | | Altunel et al., (2000) |
| Güzel -Stream bed2 | 4.48 | 2.40 | 0.30 | | | | Altunel et al., (2000) |
| Güzel - Stream bed3 | 4.55 | 5.20 | 0.30 | | | | Altunel et al., (2000) |
| Güzel - Stream 8 | 4.67 | 4.70 | 0.30 | | 12.10 | 0.30 | Altunel et al., (2004) |
| Güzel - paleostr - East | 5.64 | 5.51 | 0.50 | | 20.00 | 0.50 | Altunel et al., (2004) |
| Güzel - paleostr - West | 5.67 | 5.00 | 0.50 | | 8.40 | 0.50 | Altunel et al., (2004) |
| Mursalli - ridge | 8.17 | 4.00 | | | 26.00 | 1.00 | Altunel et al., (2000) |
| Mursalli - road | 8.56 | 3.80 | 0.20 | | | | Altunel et al., (2004) |
| Mursallı – stream | 9.06 | 4.60 | 0.40 | 1 | | | This study |
| Mursallı – stream | 9.07 | 4.50 | 0.40 | 1 | | | This study |
| Yayaköy – road East | 11.25 | 3.50 | 0.50 | 1 | | | This study |
| Yayaköy - Lstream | 12.40 | 4.00 | | | 12.50 | 0.50 | Altunel et al., (2004) |
| Yayaköy - Stream | 12.25 | 3.90 | 0.30 | | | | Altunel et al., (2004) |
| Yayaköy - road | 12.26 | 5.00 | | | 15.00 | 0.50 | Altunel et al., (2004) |
| Yaya W field | 12.79 | 5.00 | 0.50 | 1 | | | This study |
| Yayaköy stream | 13.10 | 4.50 | 0.50 | 1 | | | This study |
| Yörgüç - ridge | 13.77 | 5.50 | | | 11.00 | 0.50 | Altunel et al., (2000) |
| Yörgüç - road | 14.31 | 5.00 | 0.20 | | | | Altunel et al., (2000) |
| Sofuköy E sagpond | 27.28 | 2.50 | 0.30 | 2 | | | This study |
| Yeniköy - Field house | 29.80 | 5.40 | 0.20 | | | | Altunel et al., (2004) |
| Yeniköy - Field East | 29.82 | 5.30 | | | 10.60 | 0.50 | Altunel et al., (2004) |
| Yeniköy - Stream East | 29.87 | 3.57 | 0.20 | | 17.10 | 0.50 | Altunel et al., (2004) |
| Yeniköy - Field StrEast | 29.88 | 4.08 | 0.20 | | | | Altunel et al., (2004) |
| Yeniköy – tree | 29.93 | 3.90 | 0.10 | | | | Altunel et al., (2004) |
| Yeniköy - Stream West | 29.95 | 4.28 | 0.10 | | 35.00 | 0.50 | Altunel et al., (2004) |
| Yeniköy – road | 30.70 | 5.20 | 0.30 | | | | Altunel et al., (2004) |
| Yeniköy NNW | 31.63 | 4.00 | 0.20 | | 30.00 | 0.50 | Altunel et al., (2004) |
| W-Yeniköy field | 32.34 | 1.50 | | 1 | | | This study |
| W-Yeniköy road | 33.04 | 4.00 | 0.50 | 2 | 15.00 | 1.00 | This study |
| W-Yeniköy | 34.50 | 4.50 | 0.20 | | | | Altunel et al., (2004) |
| Kavak lake east2 | 34.84 | 3.20 | | 2 | | | This study |
| Kavak lake east1 | 35.12 | 1.50 | | 2 | | | This study |
| Kavak - trench | 42.91 | 4.50 | 0.20 | | 9.00 | 0.20 | Rockwell_etal_2002 |

Although the right-lateral offsets range from 1.4 to 5.5 m, most of them are greater than 3 m simply because only the large offsets are better preserved about 100 years after the earthquake. Offsets larger than 5 m were measured along the Güzelköy sub-segment where we also observe the maximum slip of 5.5 m. Large displacements reach to 5.4 m of right-lateral slip on the eastern tip of the Yörgüç sub-segment and at Yeniköy (Altunel et al., 2004).

Based on paleoseismic trenching studies on the Saros sub-segment near the coast, Rockwell et al., (2009) estimate a right-lateral offset of 4.5 m due to the 1912 earthquake. The overall slip distribution shows an average of 3 m with two peaks of 4.5 and 5 m at the western and eastern fault tips of Saros and Gaziköy, respectively. This implies that the 1912 rupture necessarily continued offshore into the Saros bay and Marmara Sea (Fig. 5.17).

Armijo et al. (2005) observe 6 ± 1 m right-lateral slip on a displaced ridge in the centre of the Tekirdağ sub-segment on the sea floor and attribute this to the 1912 earthquake. However, both the ridge and the scarp may as well include the penultimate faulting event at this location. Ustaömer et al. (2008) present an impressive fresh fault scarp that cuts the Saros shelf and the Saros basin further west showing ridges and stream channels with clear cumulative right-lateral offset that likely includes the 1912 event.

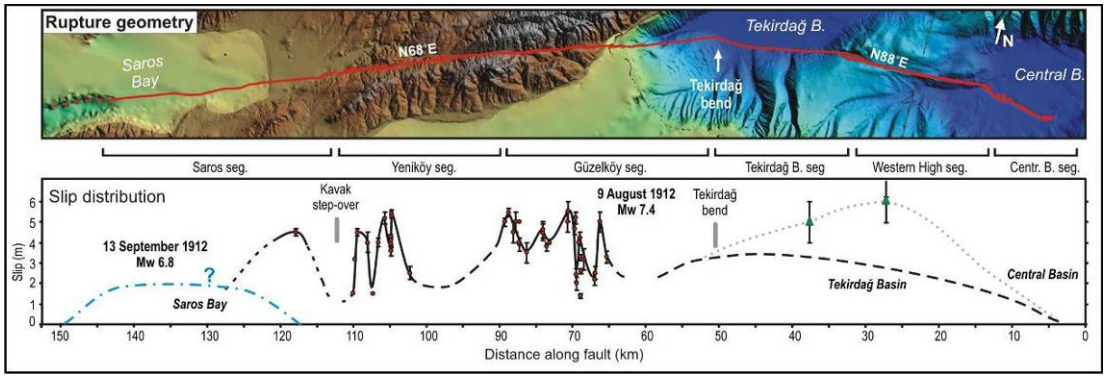


**Figure 5.17 :** Fault pattern of the Ganos segment and slip distribution of the 1912 earthquake sequence. Sub-segments along the fault zone indicate geometrical complexities. The 140 ± 20 km total fault length includes the 9 August and the 13 September earthquake ruptures. Offshore slip values (green triangles) in the Marmara Sea are from Armijo et al. (2005) which appear larger than the onland measurements as they may include a prior coseismic slip.

**Focal Mechanism:** We collected 73 historical seismic records from institutions worldwide in order to determine the seismic characteristics of the 9 August and 13 September 1912 earthquakes. P-wave polarities at 5 stations and field based N68°E fault strike allow us to construct the focal mechanism solution shown in Fig 5.3. The pure strike slip solution we obtained is in agreement with the known fault kinematics and slip measurements that do not show a significant vertical component.

**Geometrical complexities of the 1912 rupture:** Our detailed study on the onland fault geometry allows determining the segments of the Ganos fault. Here, we only summarize this pattern and use the fault geometry and related complexities in order to estimate a total length for the 1912 earthquake ruptures.

The N68°E trending fault onland is made of three sub-segments; from east to west, Güzelköy, Yeniköy and Saros that are separated by pull-aparts smaller than 1 km in width (Fig. 5.17). The Güzelköy sub-segment is about 30 km long and bounded to the east by the Tekirdağ bend and to the west by the Yörgüç releasing bend. West of the Yörgüç basin, the ~22-km-long Yeniköy sub-segment continues as a straight single fault forming a restraining bend west of the Gölcük pull-apart basin. The segment is limited to the west by the Kavak Lake (i.e., 550-m-wide pull-apart) at its western tip. West of Kavak Lake the fault runs into the Gulf of Saros where a 40-km-long submarine fault segment is observed.

The offshore fault scarps mapped by Armijo et al., (2005) and Ustaömer et al. (2008) suggest that the 1912 rupture extends offshore at both ends on submarine fault segments (Fig. 5.2, 5.17). Having a significant normal component, the Central Basin fault section is ~11 km long and trends N77°W. Trending N88°E the Western High sub-segment is about 20 km long and shows nearly pure strike-slip fault morphology. To the west of the Western High sub-segment is the 16-km-long Tekirdağ Basin sub-segment that runs along the southern boundary of the basin with a strike of N78°E and terminates at the Tekirdağ bend. The Saros sub-segment continues offshore as a fairly linear fresh scarp for about 30 km in the shelf, and terminates to the west at a ~50-km-long and 5-km-wide half-graben named the Saros Basin (Ustaömer et al., 2008; Fig. 5.2, 5.17).

The analysis of the onshore and offshore fault geometry indicates that the only major barriers to the earthquake rupture propagation are the Saros and Central pull-apart

basins (cf. Wesnousky, 2006). These barriers are comparable to the Çınarcık and Düzce basins that stopped the 1999 Izmit earthquake rupture propagation (Barka et al., 2002). On the contrary, Le Pichon et al. (2003) and Altinok et al. (2003) suggest the 9 August rupture stops at the Tekirdağ restraining bend.

**The total rupture length:** The size of the earthquake is given as Ms = 7.3-7.4 in previous studies (Ambraseys & Finkel, 1987; Ambraseys, 2001) which corresponds to a seismic moment 1.6 x1019 Nm (Ekström & Dziewonski, 1988). Using 2.5 m average slip, a fault width of 15-16 km and a shear modulus of 3 × 1011 dyne/cm2 the seismic moment yields 120 ±20 m rupture length (Aki, 1966, Kanamori, 1977). Similarly using the Ms 6.8 magnitude for the 13 September we deduce a 30 ± 10 km of rupture length for this event.

In addition, using seismic records of the 9 August and 13 September shocks we perform a deconvolution modelling and obtain a ~40 seconds source duration for the first shock (see p. 200 for detail). This implies a 120 ± 20 km-long rupture taking into account an average rupture velocity of 3 km/s. This is consistent with the earthquake size (Mw 7.4) and confirms that a significant portion of the earthquake rupture must be offshore (Fig. 5.17).

The total rupture length assessment should include both events and sums up to 150 ± 20 km. A rupture length of 120 km and the suggested eastern termination point from LePichon et al. (2003) and Altınok et al. (2003) for the 9 August shock requires the 13 September earthquake epicentre be located far west beyond the Dardanelles. However, such a scenario fails to explain the damage distribution given by Hecker (1920) and the epicentral location estimated by Ambraseys and Finkel (1987). Therefore, rather than towards the Saros Bay, the 9 August rupture must have propagated mostly into the Sea of Marmara and, once crossed the restraining bend, necessarily reached the Central Basin in agreement with Armijo et al. (2005) study. This implies a 150 ± 20 km total rupture length including (i) the three sub-segments in the Sea of Marmara (~ 65 km) beginning from the Central basin, (ii) the onland fault section (~ 45 km) and (iii) the Saros Bay sub –segment (~ 40) limited by the Saros pull-apart basin.

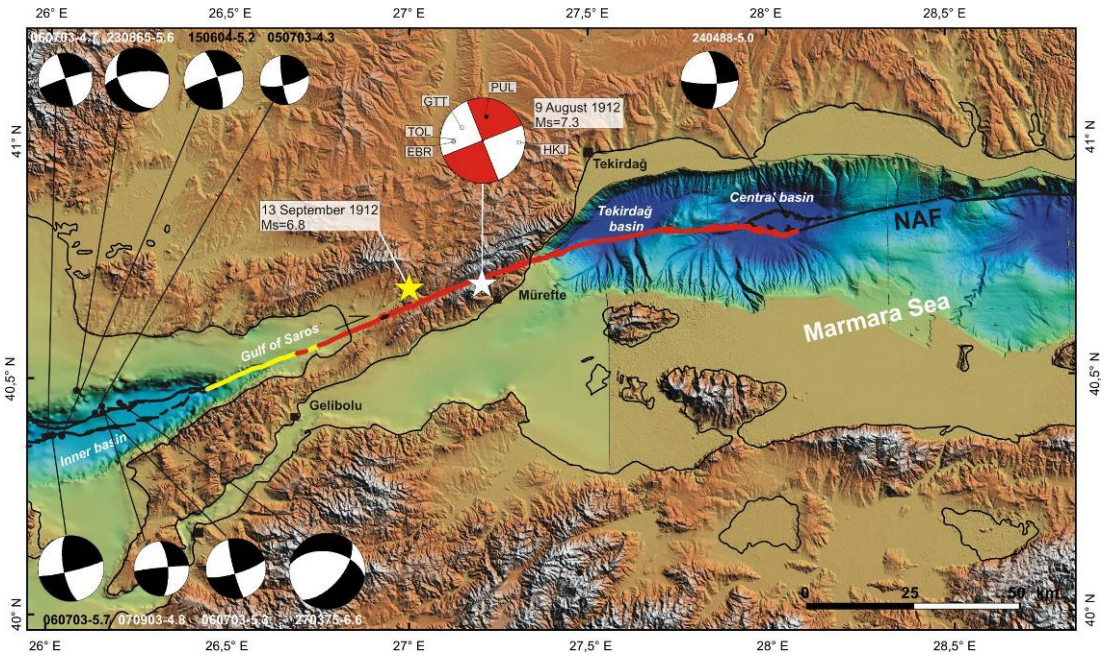


**Figure 5.18 :** We provide a focal mechanism for the 9 August 1912 Mürefte earthquake constrained by P-wave polarities at 5 stations and field based azimuth of N68°E for a pure strike-slip fault. The suggested mechanism is consistent with other strike-slip solutions for the eastern and western part of the Ganos fault. The red and yellow lines indicates the suggested 9 August and 13 September surface ruptures, respectively.

Therefore, the eastern termination of the 9 August 1912 rupture and the western termination of the 1999 earthquake rupture (Cakir et al., 2003) imply a minimum 100-km-long seismic gap in the Sea of Marmara (Fig 5.3). This fault length suggests an earthquake size M>7 that should be taken into account in any seismic hazard assessment for the Istanbul region.

## 6. PALEOSEISMOLOGY ALONG THE GANOS FAULT

Paleoseismology is a relatively young earth science branch in active tectonic studies that investigates past earthquakes in geological deposits (Wallace, 1999; McCalpin 1996). Surface rupture of significantly large earthquakes can be buried and preserved at sites where depositional conditions are present. Trenching at appropriate sites may expose past surface ruptures and will allow establishing the faulting event chronology for a fault section. Paleoseismological studies are better constrained if correlated with a completed historical catalogue that allows the calibration of past faulting events identified in trenches. Historical documents clearly note that many urban places, in and around the Ganos region, were struck several times by large earthquakes (M>7). The evidences are based mainly on coseismic damage and lack of any geological evidence. Hence the precise earthquake locations are approximate and in consequence the related fault sections can not be well identified. This is particularly difficult in regions where faults are offshore; such as the Sea of Marmara region. However, the damage and descriptions of those large earthquakes imply that they were associated with surface ruptures and significant amount of co-seismic slip ($\bar{U}$>0.5 m).

The historical seismicity section (p. 34) outlined that at least 16 earthquakes have considerably affected the study area since BC 360.

- -360
- -287
- 50
- 447
- 477 (484)
- 740
- 824
- 926
- 1063
- 1343
- 1344
- 1354
- 1509
- 1659
- 1766a
- 1766b
- 1912

The epicentral areas for most of these events are not well established. The best determined event is the 1912 Mürefte earthquake, which surface ruptures are evident along the inland section of the Ganos fault. However the locations of the earlier events are not well constrained and require further investigation.

In this work, we use paleoseismic trenching in order to document faulting events of past earthquakes in the Ganos region. Intensive mapping along the Ganos fault allow us constraining the earthquake rupture of 9 August 1912 Mürefte earthquake. The earthquake fault geomorphology is critical for paleoseismic site selection in order to determine the timing and co-seismic slip of past faulting events. We selected three sites (Güzelköy, Yeniköy and Yörgüç), where we expected to observe evidence of past surface faulting within a continuous late Pleistocene and Holocene stratigraphy. The trench sites were chosen in order to obtain an evenly distributed location along the 45 km inland fault section. The easternmost trenching study was conducted at Güzelköy. Towards west, two sites were investigated, at Yörgüç and Yeniköy located in the central section of the Ganos fault (Fig. 6.1). Our paleoseismic investigations complement prior paleoseismic studies conducted at Saros site located on the westernmost fault section (Rockwell et al., 2001, 2009).

Each trench site and related analysis is presented separately in the following paragraphs.

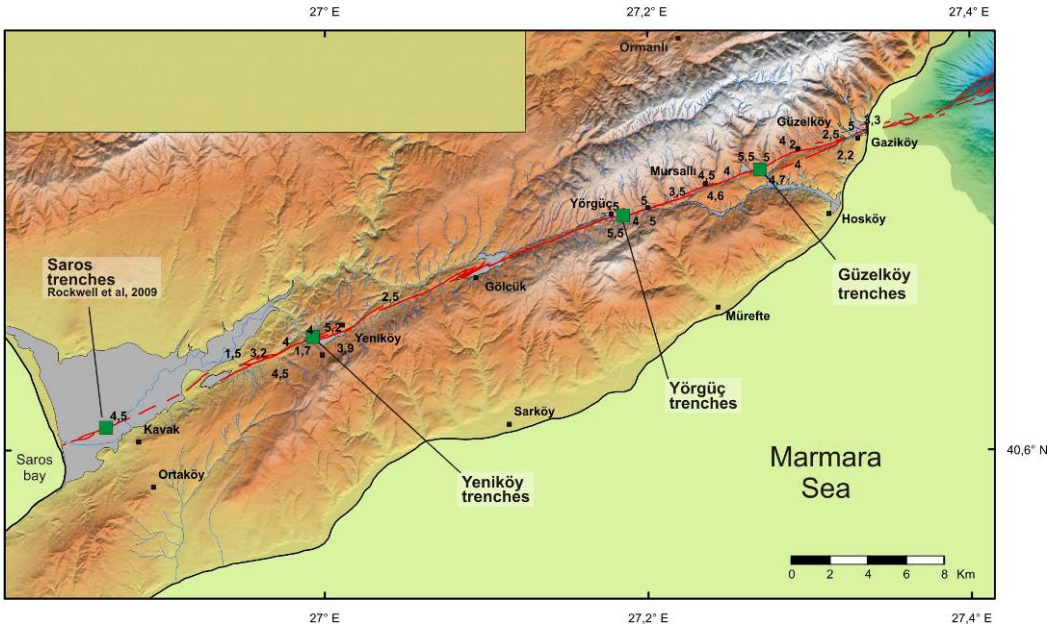


**Figure 6.1 :** The 1912 earthquake caused significant surfaces ruptures along the inland section, which allowed determining suitable sites for paleoseismic trenching. Trench sites are indicated with green boxes. Number next to the fault correspond to right lateral coseismic offsets of the 1912 event.

## 6.1. The Güzelköy Trench Site

The Güzelköy paleoseismic site located ~5.8 km west of the Marmara coastline belongs to the eastern Ganos fault section. Between Gaziköy – Güzelköy several markers document the active deformation of the North Anatolian Fault by shutter-ridges, streams offsets and scarps (Fig. 6.2, 6.3). Here, the fault zone is approximately 200 m wide and splays into three strands; ~1 km east of the trench site. Cumulative displacements of stream beds and ridges indicate that the slip occurs dominantly on the northern most strand. Detailed mapping enabled to determine evidence of recent earthquake faulting, such as continuous fresh fault scarps and co-seismic offsets of the 1912 earthquake rupture. Offset measurements at the trench site yield 5.5 m maximum coseismic displacement.

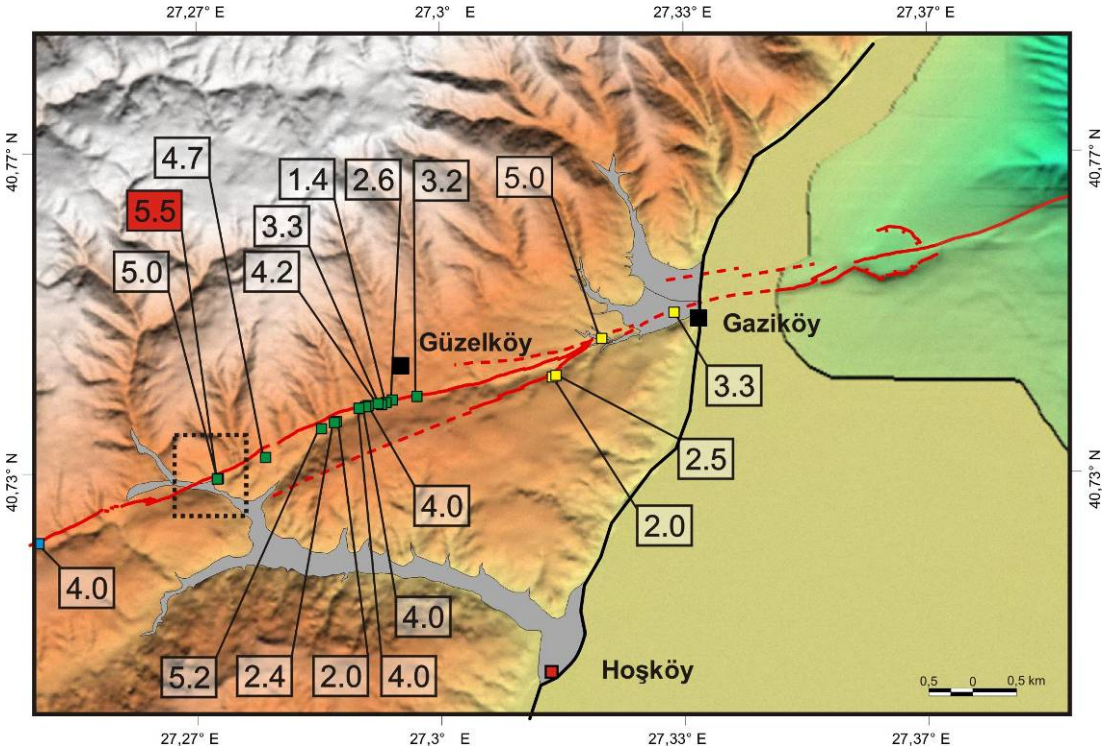


**Figure 6.2 :** Fault map of Güzelköy region showing the fault splays, co-seismic slip (white boxes, meter) of the 1912 earthquake and the location of the trench site (dashed black line). Offset measurements of Altunel et al., are given as green boxes, yellow boxes correspond to measurements from this study.

### 6.1.1. Earthquake geomorphology and paleoseismic site selection

The selected site consists of two main parallel and sporadic stream channels flowing nearly north-south on ~ 20° slope upstream and ~ 10° downstream (Fig. 5 a). The geology of the site consists mainly of Oligocene - Eocene flyschs and turbidites of

the southern limbs of the Ganos Mountain. The streams and related eroded material (mainly alluvial deposits and slope debris) are deflected and dammed by a ~ 150-m-long and ENE-WSW trending shutter ridge made of flyschs. The western stream shows a small deflection and incision on the flat lying alluvial units. The eastern stream channel presents a significant incision of nearby hills with an alluvial fan and a larger deflection than the western stream. Although the alluvial fan buries all geomorphic structures, the fault zone is here precisely traced from the two deviated streams and a displaced substratum ridge block of the crest in between streams (Figure 6.3).

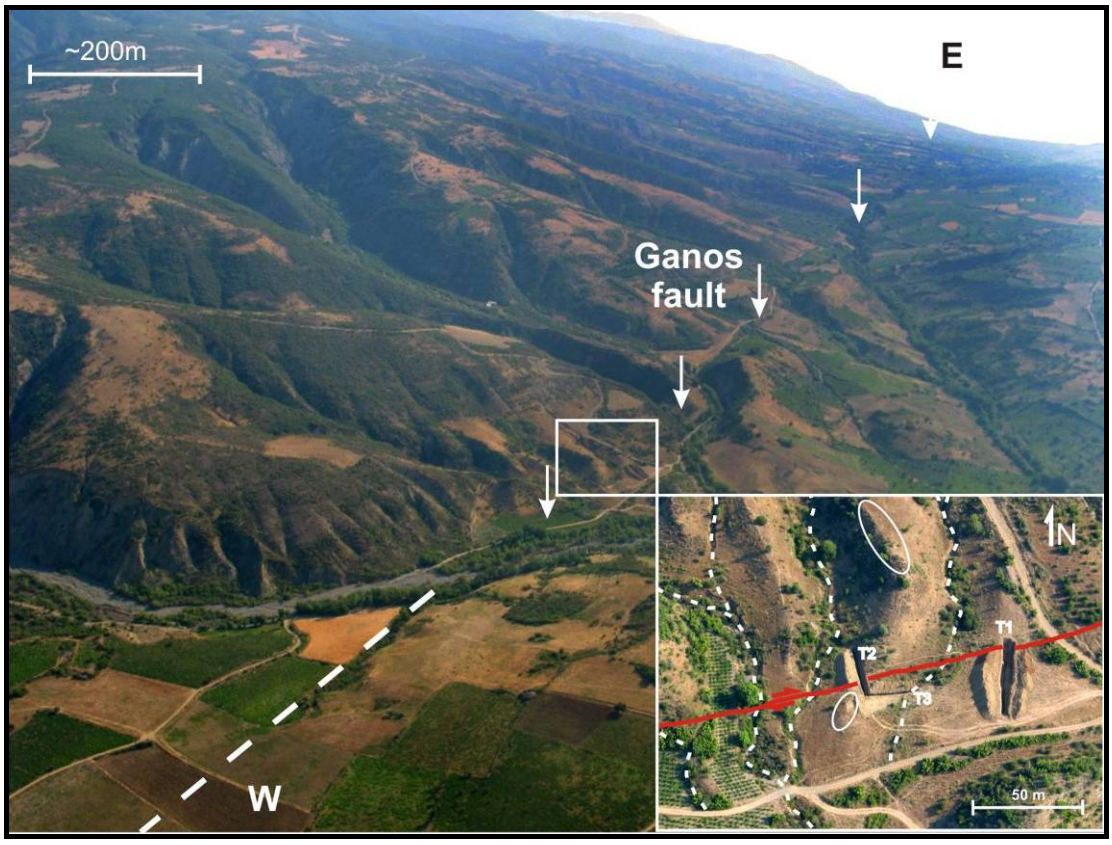


**Figure 6.3 :** Aerial photo of the Gaziköy-Güzelköy section of the NAF. The Ganos fault (white arrows) offsets several streams and ridges in the region. The trench site is given in the inset, where the stream offsets (dashed lines) and the ridge offsets (ellipses) are indicated. The two streams west of T2 show a good example of how stream bed capturing may occur by successive right-lateral motion. Additional lateral slip will connect the eastern stream to the southern channel, as observed south to the fault. (Aerial photo by Puchi, S.)

A micro-topographic survey with up to 9000 levelled points (of channel edges and centres, hill crests, flat and slope areas, and shutter ridge) was conducted at the site using a Wild TC1800 total station (Fig. 6.5). Data was collected with an array of ~

0.5 m to document all the morphological characteristics associated with past fault movements. The channel boundaries that are well preserved in the morphology allows to measure 10.5 ±0.5 m and 19 ±1.5 m of cumulative right-lateral offset for the western and eastern streams, respectively. In addition, the displaced basement block ridge provides 29 ±1.5 m of right-lateral cumulative slip. Taking into account the fault zone and the shutter ridge position, the eastern stream alluvial fan deposits indicate the potential for recording past channel successive offsets and well preserved paleoseismic data. The present-day erosional and depositional conditions of the site determine the three dimensional trenching scheme that enables the documentation of successive earthquake faulting and related offset.

### 6.1.2. Paleoseismic trenching

We have excavated 7 trenches near the eastern stream of the Güzelköy site and in between the hill slope (to the north) and the shutter ridge to the south (Fig. 6.4). Each trench-wall grid was also levelled in order to correlate the stream offset with the buried offset features and to obtain a 3D view of trench-walls with respect to the fault zone and associated geomorphology. Trenches T1, T2 and T4 are north-south trending and dug across the fault (Fig. 6.4) in order to pinpoint the fault location in relation with the micro-topography and stream deviations, and study the repeated fault movements and their relation to colluvial wedges. Trenches T3, T5, T6 and T7 are ENE-WSW to E-W trending and dug parallel to the fault zone in order to study the stream channel deposits and deflection as a function of the successive fault movements. All trenches display coarse to fine alluvial sedimentary units and slope debris material that provide the potential for recording the successive earthquake faulting. We present below the stratigraphic layers of alluvial and slope deposits for both the cross-cutting and parallel trenches (Table 6.1).

**Stratigraphic succession:**

Trench 1 was dug on the left bank of the eastern stream and across a small scarp that may correspond to a remnant of the 1912 rupture. The trench is 35-m-long and deep enough to reveal a ~ 5-m thick succession of alluvial coarse, fine gravels and sandy silty units. Trench 1 revealed a complex fault zone with several rupture branches and associated colluvial deposits. We logged in detail the northern trench section close to the fault.

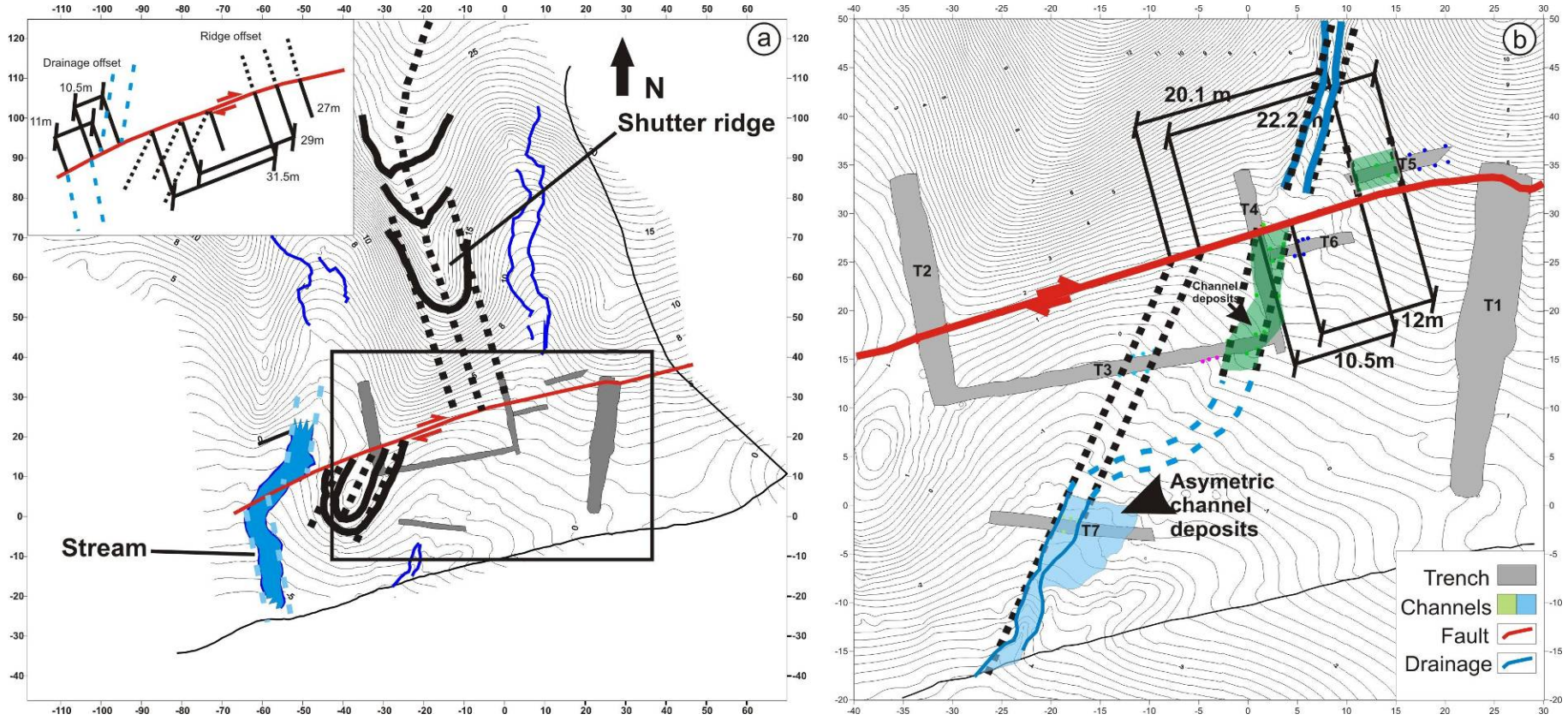


**Figure 6.4 :** The image on the left shows the topographic map of the area obtained by micro-topo survey with 9000 points. A cumulative offset of 10.5 ± 05 m and 29 ± 1.5 m is measured on the stream and ridge, respectively. The image to the right gives a closer view to the trench site, where fault and trench locations and related offset of determined structures are given.

A massive red sandy-silt deposit with clasts lying on a white sandy clay (unit **w** in figure 6.7) is visible at the trench bottom and north to the fault zone (Fig. 6.6, 6.7). South of the fault zone, unit **g** made of clasts in reddish sandy-silt covers unit **s** and corresponds to a minimum 1-m-thick colluvial deposits with the matrix probably resulting from a re-worked unit s. Units a, c, and d correspond to an accumulation of colluvial wedges with less than 0.5 m thickness near the fault zone and may result from fault scarp degradation. Units b, e and f are colluvial deposits made of sandy gravel mixed with alluvial deposit (small channels) and with 0.2 to 0.5-m constant thickness across the fault zone. Unit e which is a light colluvial unit with clay layers overlain by sandy clay deposits shows some materials within the fault zone. Unit f is made of mixed colluvial deposits with sandy-silty layers with alluvial fine gravel and channel structures down-slope. The succession of colluvial units that appears next to the fault zone illustrates the previous faulting episodes.

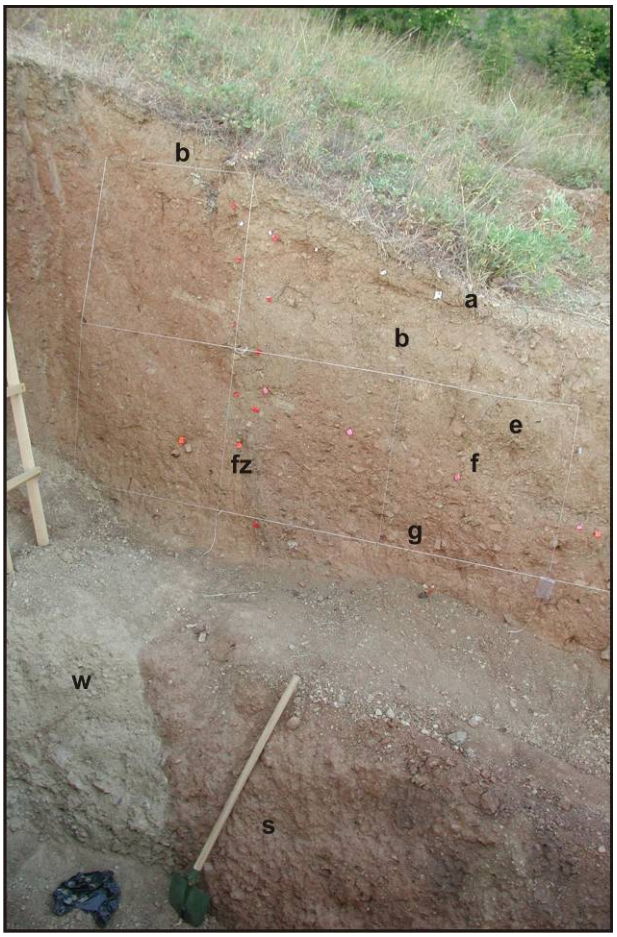


**Figure 6.5 :** The eastern trench wall of T1 showed clear evidence of past earthquake faulting and related colluvial sediments.

Trench T2 is ~25-m-long and located across the fault in between the displaced basement block and the hill slope (Fig. 6.2, 6.3). The trench log shows north of the fault zone mainly unit s (massive red sandy-silt similar facies of the unit in trench T1) and south of the fault zone a 1.5-m-thick lacustrine deposits (fine and laminated silty-clay layers, unit x3) overlaying unit x2 made of laminated sandy-clay with intercalated coarse gravels and unit x1 with well stratified coarse alluvial deposits (Figure 6.7). Unit x3 is overlain by unit d, a ~ 0.1 m-thick laminated light clay that ends the lacustrine sedimentation. The lacustrine deposits rapidly wedge-out near the

main fault zone and further south across a secondary fault which suggest a tectonic control of sedimentation on a small pull-apart basin. The stratigraphic succession continues with unit c made of stratified fine gravel laying conformably on unit x3 and they both show a significant tilt (~ 20°) towards the nearby main fault zone fault (fz in Figure 6.7). Unit b consists in loose sandy gravel with small channels and

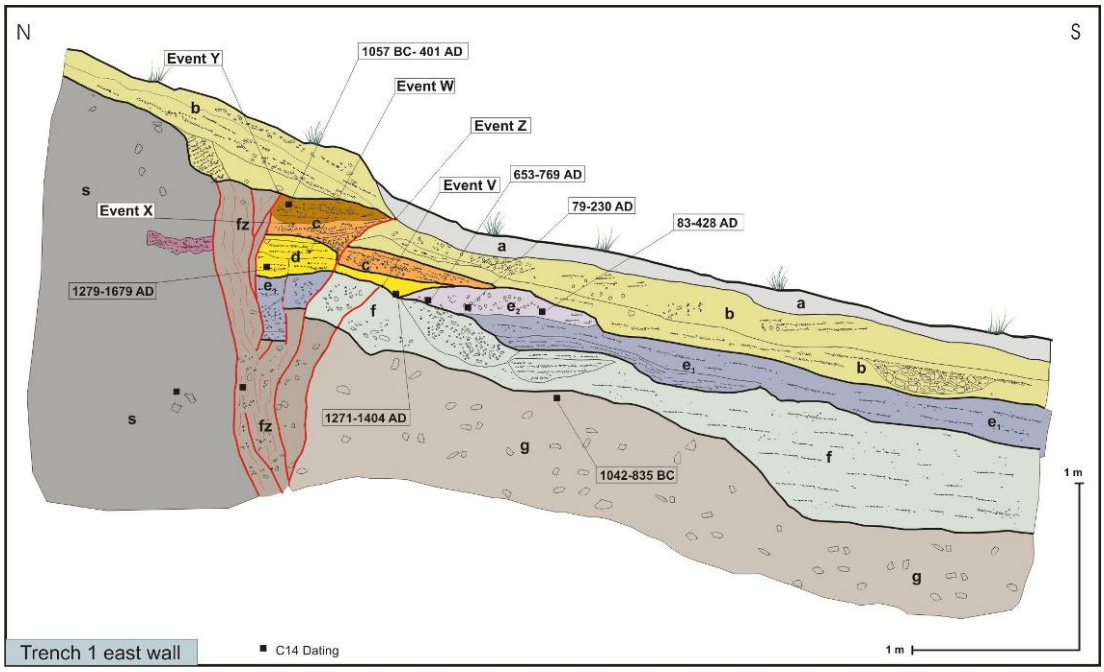


**Figure 6.6 :** Trench log of the eastern wall of T1 showing the fault zone, earthquake ruptures and related colluvial wedges.

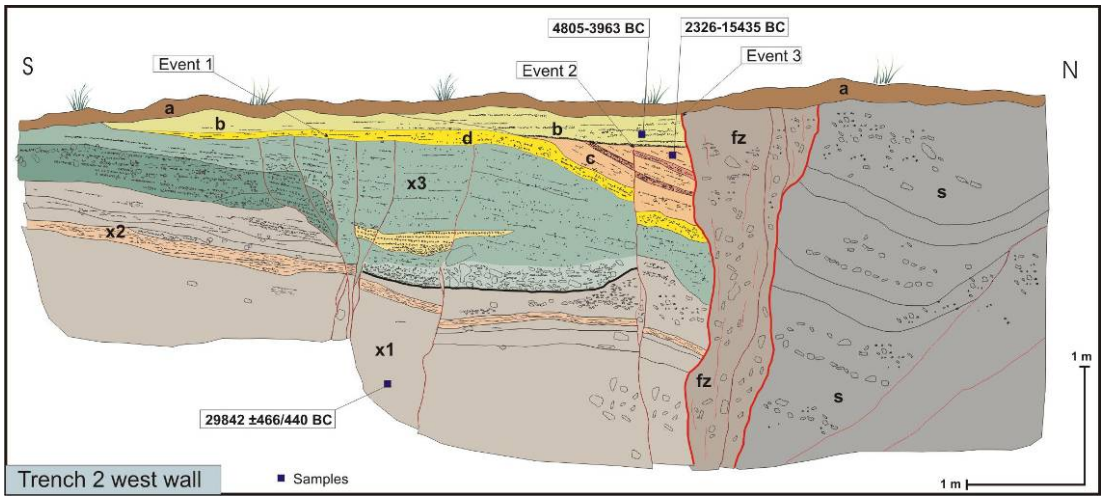


**Figure 6.7 :** The western trench wall of T2 showed a larger fault zone compared to the one in T1. Several faulting events are evident in this trench, however contamination in the charcoal samples did not allow obtaining proper radiocarbon dating results.

covers with unconformity units x3, d and c. The fault zone is here ~ 4 m wide and consists in the main fault zone fz and several branches that affect alluvial and lacustrine deposits (unit x3).

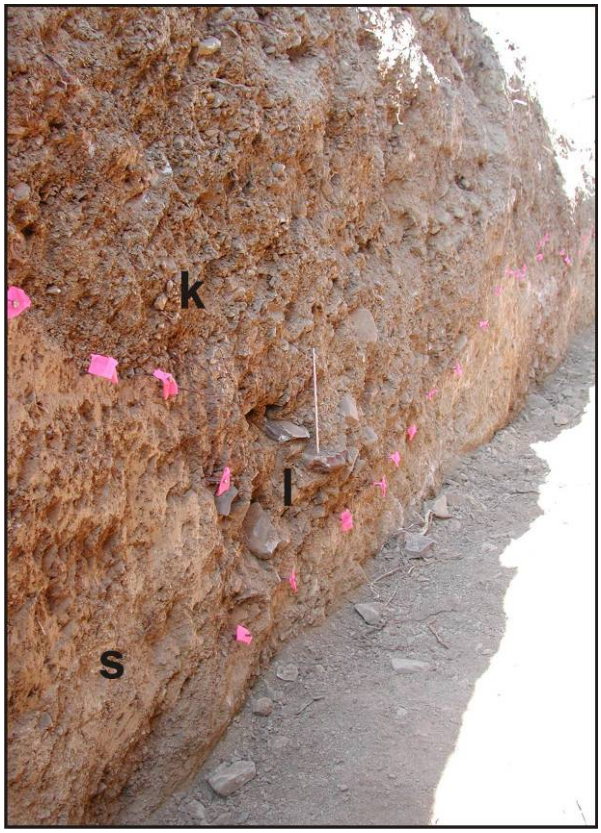


**Figure 6.8 :** The asymmetric channel geometry is clearly visible in T3. The light coloured unit s is truncated by the reddish units l and k.

Trenches T3 to T7 display channel structures. Trench T3 is ~40-m-long parallel and close (~ 2 m) to the fault, connects T4 with T2 and displays a sharp unconformity of a buried channel on the massive red sandy-silt (unit s). The paleo-channel is asymmetric (deepest units close to the east) and shows a succession of coarse gravel at the base (unit l, Fig. 6.8) overlain by well-sorted fine and coarse gravel layers (unit k) and fine gravels mixed with sandy layers of overlapping small channels (unit j Fig. 6.8). Trench T4 is ~20-m-long also dug across the fault and shows a ~ 2-m-thick well-sorted fine and coarse gravel deposits mixed with sandy layers of small channels (unit j) overlapping the massive red sandy-silt (unit s). The fault sharply limits colluvial deposits to the north from ~ 1.5-m-thick fine gravel deposits (unit j) to the south (also visible in trench T6). Fault branches visible at the trench base are overlain by unit j. At the top of trench wall, the fault zone is buried by young channel deposits.

Trench T5 is ~ 13-m-long, parallel and the only excavation located in the northern fault compartment (Fig. 6.5). Field observations on the left bank alluvial terrace and related coarse pebble and gravel leaded us to infer the existence of a buried channel east of the stream. In fact, the trench log of Figure 6.10 shows a paleo-channel with coarse gravels at the base (unit l) and stratified and well-sorted fine and coarse gravels (unit k) and fine gravels mixed with sandy layers of small channels (unit j)

overlapping with colluvial deposits. The channel incised in the massive red sandy-silt deposit with clasts (unit s) and is overlain by a succession of colluvial deposits that also cover a remnant alluvial terrace. Trench T6 is also parallel to the fault but dug immediately south (~ 1 to 2 m) of the fault as traced from T1, T2 and T4 (Fig. 6.5). The trench exhibits a succession of ~ 1.5-m-thick paleo-channel deposits incising the massive red sandy-silt deposit with clasts (unit s, Fig. 6.11). Within the channel, the lowermost deposit is made of coarse gravel and pebble (unit l) overlain by well-sorted fine and coarse gravels (unit k). On the top, unit j made of fine gravels mixed with sandy layers of small channels truncates considerably unit s. Trench T6 is ~ 10-m-long nearly orthogonal to and cutting T4 with unit j having a similar texture and structure in both trenches.

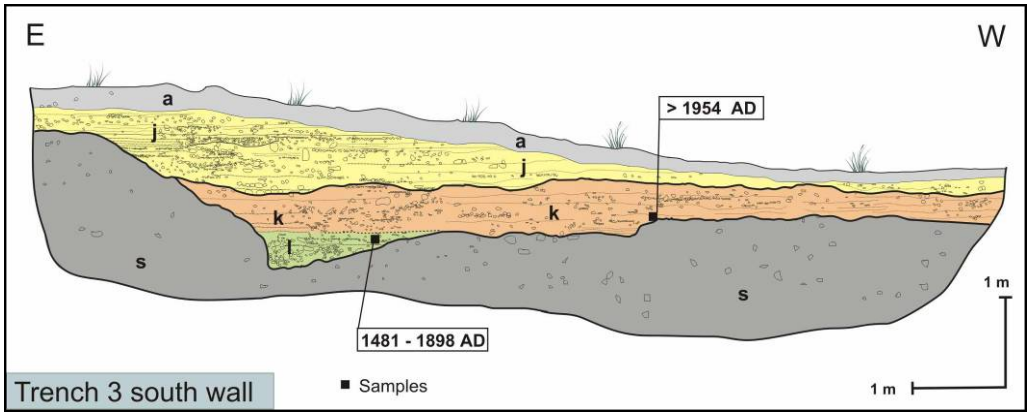


**Figure 6.9 :** Log of trench T3 illustrating the asymmetric channel geometry. See figure 6.4 for location.

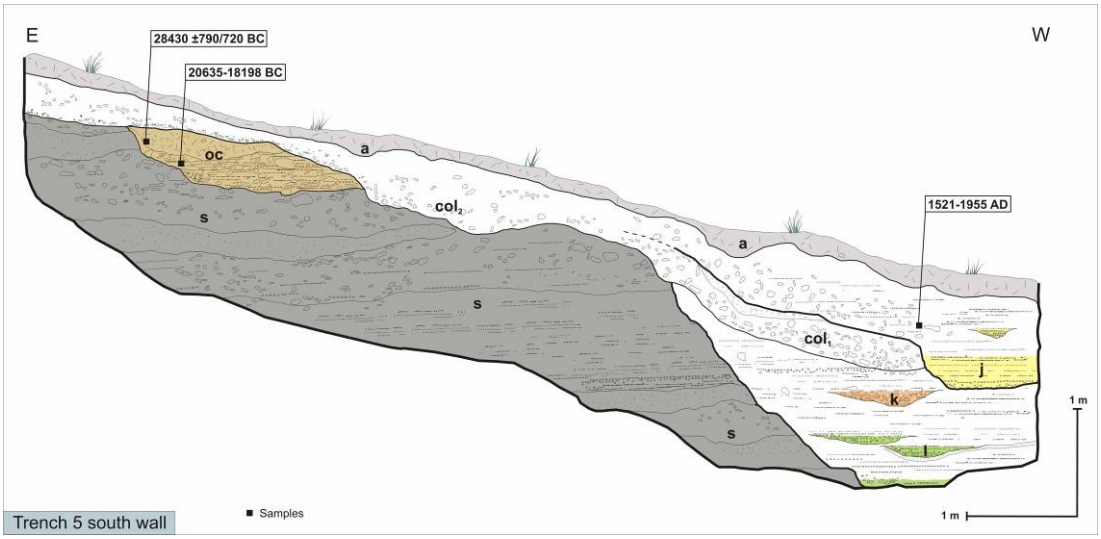


**Figure 6.10 :** T5 is located to the north of the fault and exposes a buried channel comparable with channel observed in T3, T4, T6 and suggests 11 ±1 m right-lateral offset.

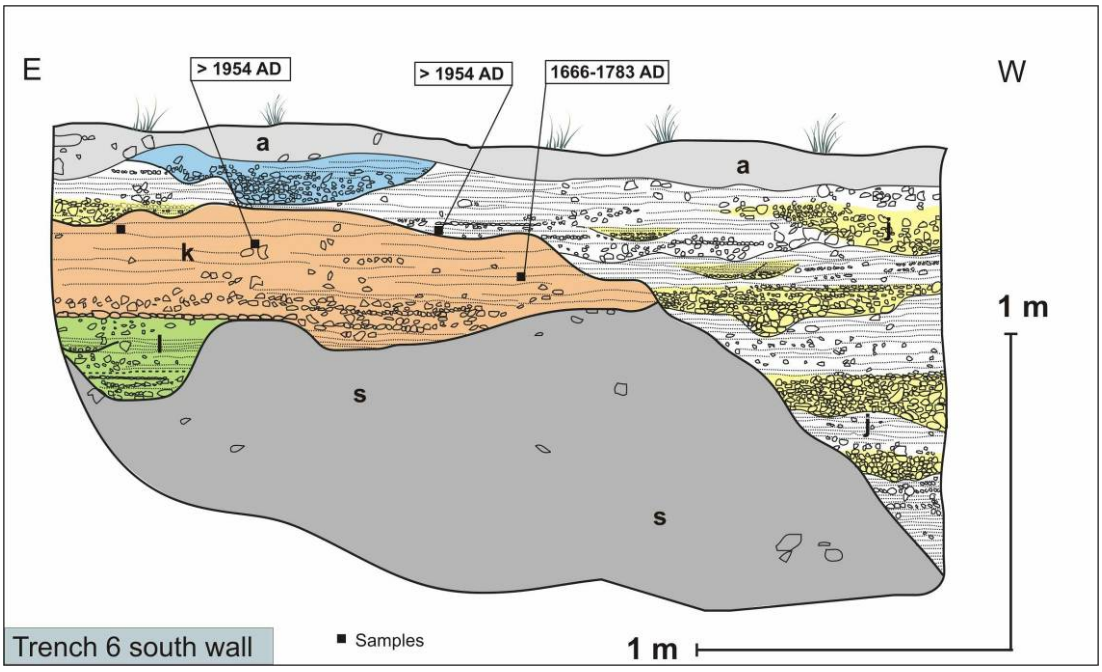


**Figure 6.11 :** T6 is located south to the fault and shows the offset part of the buried channel.

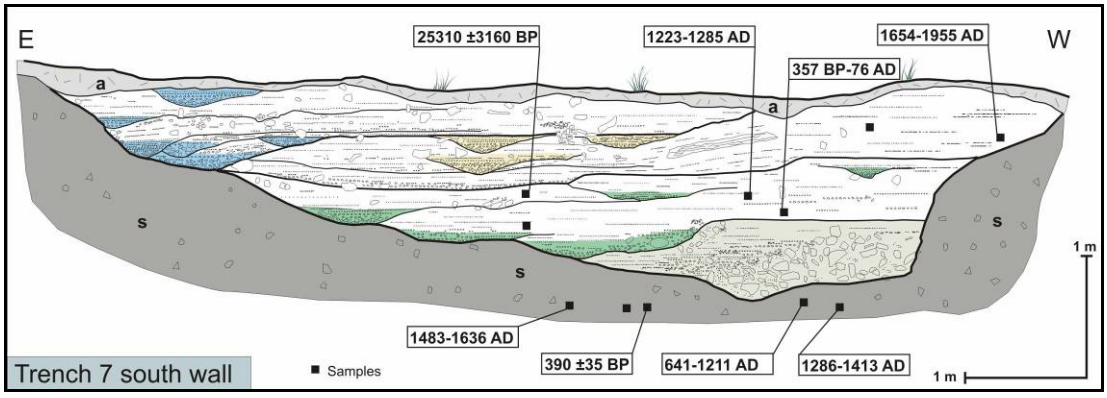


**Figure 6.12 :** T7 is the southernmost fault parallel trench. The trench walls exposed an asymmetric channel geometry and eastward migrating channel deposits. Several samples were collected and dated from to determine the age of the channel.

T6 was also dug proceeding eastward beginning from T4 in order to meet the edge of alluvial deposits and channel and related unit s below (Fig. 6.5, 6.11). The geometry of channels as deduced from both walls of trenches T3, T4 and T6 suggests the existence of two parallel channels and related alluvial fans also indicated by units l, k overlapped by unit j. The objective was also here to compare channel deposits and related offset of eastern edges between channels in T5, T6 and T3 (Fig. 6.9, 6.10, 6.11).

**Table 6.1 :** List of units observed in the trenches and their descriptions.

| Unit | Description |
|---|---|
| **a** | Soil |
| **b** | colluvial unit, light, loose, sandy gravel; alluvial deposit (small channels) |
| **c** | Reddish colluvial wedge and stratified fine gravel |
| **d** | sandy gravel with mixed light silty layers |
| **$e_1$** | Light colluvial unit with clay layers |
| **$e_2$** | Sandy clay |
| **f** | Mixed sandy-silty unit alluvial fine gravel (channel) |
| **g** | clasts in reddish sandy-silt |
| **s** | Massive red sandy-silt with clasts |
| **fz** | Fault zone with shear fabric (oriented clasts and gravel) |
| **j** | Well-sorted fine and coarse gravel unit (uppermost channel deposit) |
| **k** | Stratified alluvial deposit (with channels) |
| **l** | lowermost channel unit (coarse gravel) |
| **oc** | Old channel unit (coarse gravels) |
| **col** | Colluvial deposit (clast in sandy-silt) in trench 5 |
| **s** | Massive red sandy-silt with clasts |

**Paleoearthquake analysis and faulting events**

The paleoseismic study aimed here to correlate the successive earthquake faulting in cross-cutting trenches with the right-lateral offset as observed from deflected stream channels. The timing of successive faulting episodes is constrained using 25 dated samples of charcoal fragments pieces and organic-rich sediment. Table 6.2 shows the analytical characteristics of 39 samples, their corresponding unit in Figures 6.5-6.11, and the radiocarbon dating. All radiocarbon dating (Table 6.2) are calibrated using

2σ age-range and 95.4% probability density using Oxcal v4.0 (Bronk Ramsey, 2001) programme and INTCAL98 calibration curve of Stuiver and Rymer (1998).

**Trench T1**

Trench T1 shows near the surface the most recent faulting event and fault scarp that may likely correspond to surface rupture of the 9 August 1912 earthquake. The shear zone is ~ 0.5-m-thick and appears as several fault branches that show a positive flower structure and reverse faulting geometry. The trench log reveals the succession of colluvial wedge units d and c next to the fault zone resulting from past surface rupturing events, similarly to unit a that postdate the 1912 earthquake. Colluvial unit b made of light loose sandy gravel mixed down-slope with alluvial deposit (small channels) truncates previous deposits and shows ~ 0.25 m vertical separation on the fault which can be correlated with event Z (1912 earthquake). Unit c is a reddish colluvial wedge with sorted fine gravels faulted by event Y and buried by unit b. The timing of event Y is difficult to infer because of the probably reworked detrital charcoal present in sample TG1-E11 and related old age (BC 1057 – AD 401, Table 6.2).Unit c probably results from the erosion of a previous fault scarp and the faulting event that affects colluvial wedge d corresponds to event X.

Unit d made of well stratified sandy gravels mixed with colluvium and light silty layers provides two consistent radiocarbon ages AD 1271-1404 and AD 1279-1679 that predate events X, Y and Z. Unit d which has a distinct texture and colour may result from fault scarp degradation and faulting event W. Colluvial units f and e are comparable to unit b and their constant thickness across the fault indicates that they do not result from fault scarp degradation. However, colluvial units e and f are faulted by event V and buried by unit d.

The uppermost layers of e (unit e2) provide two consistent C14 ages AD 79-230 and AD 83-428 and AD 653-769 that predate faulting event V. Near the fault zone, the gap in sedimentation of e2 may correspond to a lack of earthquake record. Although the erosional surface between units f and g may also indicate the probable occurrence of a significant sedimentary truncation and erase of earthquake record, the uppermost layers of unit g provides the radiocarbon age BC 1042-835 that also predates past faulting events indentified in trench T1.

**Table 6.2 :** List of collected samples and related radiocarbon dating results.

| Sample Name | Trench Unit | Amount of Carbon (mg) | d13C (%) | Radio-carbon age (BP) | Uncertainty ( ± years) | Calibrated age (+=AD) 2σ range | |
|---|---|---|---|---|---|---|---|
| TG1-E03 | g | 3,77 | -24,72 | 2802 | 39 | -1042 | -835 |
| TG1-E07 | e | 0,24 | -24,18 | 1760 | 75 | 83 | 428 |
| TG1-E08 | d | 0,3 | -32,75 | 660 | 55 | 1271 | 1404 |
| TG1-E09 | e | 1,34 | -24,09 | 1330 | 25 | 653 | 769 |
| TG1-E10 | d | 0,1 | -34,88 | 450 | +140/-130 | 1279 | 1679 |
| TG1-E11 | c | 0,05 | -30,51 | 2290 | +310/-300 | -1057 | 401 |
| TG1-E12 | e | 3,47 | -24,9 | 1865 | 30 | 79 | 230 |
| TG2-W01 | x1 | 1,26 | -22,56 | 29840 | +470/-440 | - | - |
| TG2-W06 | | 0,96 | -23,83 | 2395 | 40 | -759 | -390 |
| TG2-W15 | b | 0,13 | -24,57 | 5550 | 200 | -4805 | -3963 |
| TG2-W16 | c | 0,08 | -24,33 | 1770 | +1580/-1320 | -23261 | -15435 |
| TG3-S100 | l | 0,32 | -25,35 | 235 | 60 | 1481 | 1898 |
| TG3-S102 | | 0,19 | -25,99 | >1954 | | | |
| TG4-E02 | | 0,3 | -29,69 | 535 | 45 | 1304 | 1443 |
| TG4-W01 | | 5,7 | -24,79 | 345 | 20 | 1480 | 1635 |
| TG4-W01 | | 3,5 | 22,45 | 340 | 20 | | |
| TG4-W03 | | 0,69 | -24,59 | 1720 | 70 | 130 | 524 |
| TG5-S01 | oc | 0,27 | -29,74 | 17960 | +440/-420 | -20635 | -18198 |
| TG5-S02 | oc | 0,58 | -25,03 | 28430 | +790/-720 | | |
| TG5-S03 | j | 0,24 | -25,95 | 180 | 60 | 1521 | 1955 |
| TG6-N01 | k | 1,3 | -22,87 | 155 | 30 | 1666 | 1783 |
| TG6-N02 | | 0,1 | -31,30 | >1955 | | | |
| TG6-N03 | | 0,45 | -29,55 | >1954 | | | |
| TG6-N04 | | 1,6 | -27,63 | >1954 | | | |
| TG6-S01 | | 3,0 | -25,50 | >1955 | | | |
| TG6-S06 | | 3,5 | -24,99 | >1954 | | | |
| TG6-S06 | | 0,87 | -25,28 | >1954 | | | |
| TG6-S07 | | 1,9 | -26,76 | >1954 | | | |
| TG7-S02b | | 0,1 | -30,75 | >1955 | | | |
| TG7-S02b | | 1,3 | -24,14 | 390 | 35 | | |
| TG7-S03 | | 3,27 | -28,91 | 345 | 25 | 1483 | 1636 |
| TG7-S03 | | 0,73 | -27,03 | 640 | 45 | 1483 | 1636 |
| TG7-S04 | ? | 5,0 | -25,13 | 765 | 20 | 1223 | 1285 |
| TG7-S05 | | 0,3 | -28,67 | 2080 | 80 | -357 | 76 |
| TG7-S05 | | 0,2 | -26,71 | 2360 | 90 | -357 | 76 |
| TG7-S06 | | 0,1 | -26,95 | 1130 | +160-150 | 641 | 1211 |
| TG7-S07 | | 0,3 | -31,02 | 620 | 55 | 1286 | 1413 |
| TG7-S08 | j | 2,68 | -25,27 | 200 | 25 | 1654 | 1955 |
| TG7-S09 | | 0,11 | -29,71 | 25310 | +3160/-2260 | | |

A more satisfactory result of paleo-earthquake timing from trench T1 is the occurrence of most recent three faulting events X, Y and Z and related faulted colluvial deposits d, c and a, respectively. The dating of young colluvial deposits in trench T1 suggests the occurrence of three faulting events since AD 1271-1404 (sample TG1-E08, Table 6.2).

The uppermost layers of e (unit e2) provide two consistent C14 ages AD 79-230 and AD 83-428 and AD 653-769 that predate faulting event V. Near the fault zone, the gap in sedimentation of e2 may correspond to a lack of earthquake record. Although the erosional surface between units f and g may also indicate the probable occurrence of a significant sedimentary truncation and erase of earthquake record, the uppermost layers of unit g provides the radiocarbon age BC 1042-835 that also predates past faulting events indentified in trench T1. A more satisfactory result of paleo-earthquake timing from trench T1 is the occurrence of most recent three faulting events X, Y and Z and related faulted colluvial deposits d, c and a, respectively. The dating of young colluvial deposits in trench T1 suggests the occurrence of three faulting events since AD 1271-1404 (sample TG1-E08, Table 6.2).

**Trench T2**

Trench T2 exposes an impressive set of fault branches next to the main fault made of a ~ 0.5-m-thick shear zone with oriented gravels and pebbles, breccias and gouge zone that indicate several episodes of faulting activity. South to the main fault zone, a graben like structure filled with the lacustrine unit x3 displays several fault branches is buried below unit d. Near the main fault zone, another fault branch affects north dipping layers of unit d and c which are buried below unit b. At the surface, unit b is faulted by the main fault zone. Although trench T2 exhibits a thick stratigraphic succession with different fault branches all collected samples provide old ages (see Table 6.2 & Figure 6.7) and unfortunately do not allow us to determine the timing of successive faulting events.

**Channel offset and right-lateral faulting events:**

An old channel geometry can be traced across the fault zone and southward using the precise location of the channel edges throughout the alluvial fan deposits (Fig. 6). From north to south, trenches T5, T6 and T4, T3 and T7 show a buried channel that represents an abandoned stream incision due to the successive fault movements.

When matching the eastern edges of buried channels in trenches T5 and T6 located on both sides and close to the fault, total station measurements indicate a cumulative right-lateral offset of ~ 11 m which includes the 1912 displacement at this site. This cumulative amount of slip is very comparable to the 10.5 ±0.5 m measured on the nearby western stream (Fig 6.5). Both trenches provide radiocarbon ages of channels with AD 1521-1955 for T5 and 1666-1783 for T6 and suggest that the cumulative slip took place from AD 1666 to AD 1912. Assuming a maximum 5.5 m slip par event as a characteristic displacement as observed during the 1912 earthquake at this site, we infer that last two earthquakes Z and Y occurred since AD 1666 and may be correlated with the 1659 or 1766 and 1912 large events of the historical catalogue (Ambraseys, 2002).

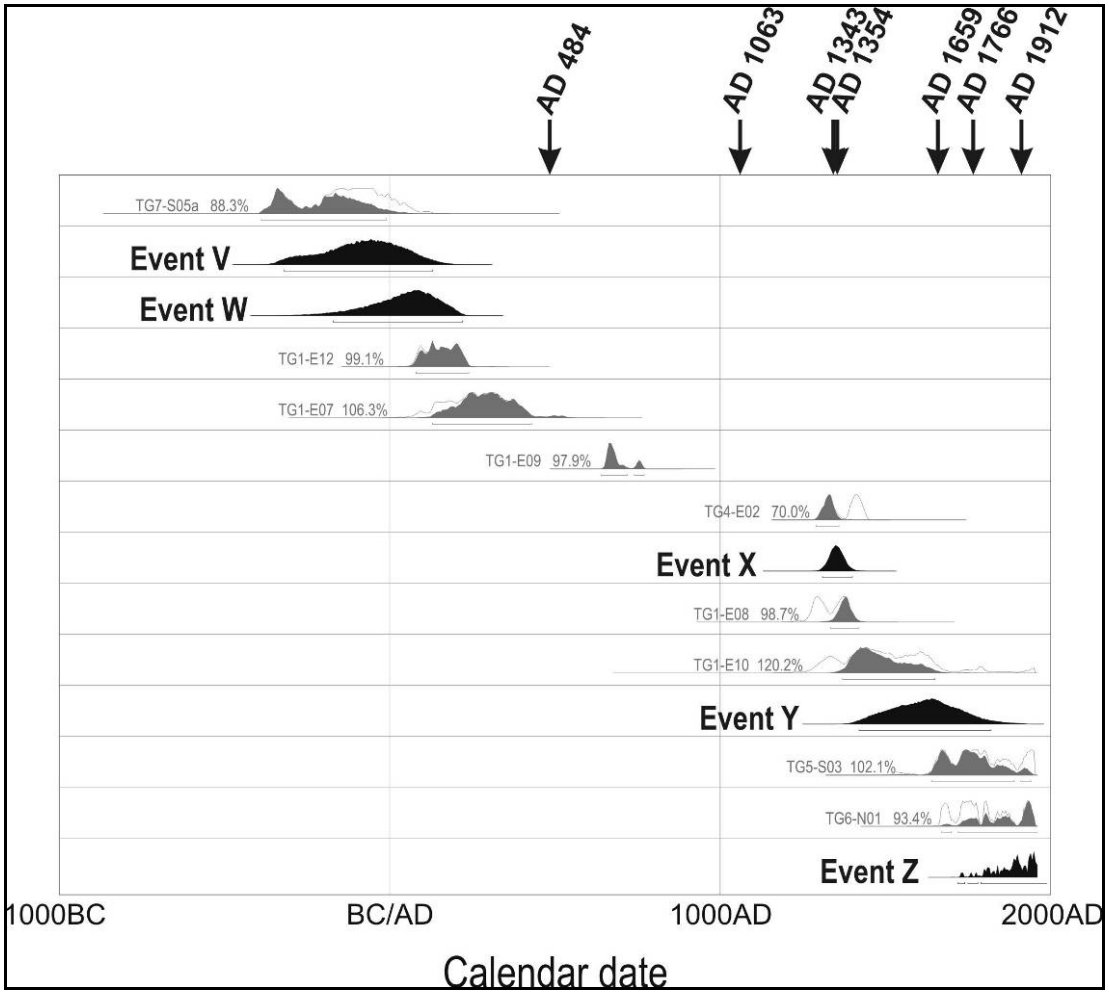


**Figure 6.13 :** Calibrated radiocarbon age of samples and probability density of events determined in the trenches.

Furthermore, the eastern edge of channel in trench T3 is located ~ 5 m west of the channel in trench T6 (Fig. 6.5). Taking into account that sample TG3-S100 collected

in unit 1 of channel in trench T3 provides an age AD 1481-1898 and that sample TG4-E02 yields an age AD 1304-1443, it suggests that the additional ~ 5 m slip between channels T6 and T3 took place after AD 1304 and may correspond to the earthquake event X which may be correlated with the 1343 large event of the historical catalogue (Ambraseys, 2002). The total cumulative right-lateral offset of ~ 16 m between T5 and T3 may correspond to faulting events X, Y and Z that took place since AD 1304 and imply 22.9 mm/yr slip rate (for the last 700 years).

Trench T5 and T7 exhibit paleo-channels that mark the maximum cumulative right-lateral offset along the fault. The total right-lateral offset estimated from the eastern edge, central position and western edge of each channel section yields an average 21 ±1.5 m (Fig. 6.3). The oldest age BC 357 – AD 76 of sample TG7-S05 collected within the lower channel deposits in Trench 7 that may be correlated with the ~ 29 m of cumulative right-lateral offset of the basement block ridge yield 12.5 mm/yr. Taking into account that the age AD 1223 – 1285 of sample TG7-S04 collected within the channel deposits in Trench 7 may predate the total ~ 21 m cumulative right-lateral offset, we obtain a maximum 26.9 mm/yr slip rate (for the last 781 years). However, if we combine with the results of trench T1 and the dating of the last three events X, Y and Z taking place after AD 1271 and related cumulative right-lateral displacement from paleo-channel of trenches T5, T4 and T3 we obtain an average 21.8 mm/yr slip rate (for the last 733 years).

### 6.1.3. Results of the Güzelköy site

The combined study of geomorphology with micro-topography and paleoseismic trenching provides some constraints on the timing of successive faulting and related past earthquakes along the eastern section of the Ganos fault. The Güzelköy paleoseismic site is located on a fault section where the maximum coseismic slip reaching 5.5 m is collocated with a well preserved 29 ±1.5 m cumulative fault offset of the basement ridge block outcrop and two stream incisions. Using total station the measured offsets on stream incisions indicate 10.5 ±0.5 m and 21 ±1.5 m for the western stream and eastern paleo-channels, respectively. The ±1.5 m uncertainty is estimated from the eastern paleo-channel edges and centres, and basement ridge block. The error bar of the western stream offset is better constrained because the

stream incision is sharp and edges are linear due to the stream entrenchment on a slope morphology (Fig. 6.3, 6.5).

The paleoseismic results from trenches indicate the occurrence of five faulting events (V, W, X, Y and Z) identified mainly from buried ruptures and the successive colluvial wedge deposits d, c and a in trench T1 and from the right-lateral offset of buried paleo-channel visible in trenches T5, T6, T4, T3 and T7. Faulting events X, Y and Z in trench T1 dated post AD 1271 – 1404 (from colluvial wedge d) can be well correlated with the 16 ±1.5 m lateral offset of paleo-channel dated post AD 1304 – 1443 measured in parallel trenches T5, T6 and T3 located immediately north and south to the fault. This correlation reflects the consistency between the 5 to 5.5 m coseismic characteristic slip (as measured for the 1912 event at this site) obtained from the cumulative offset of paleo-channel from trenches T5 and T3 reaching three times the 1912 slip and the three faulting events X, Y and Z identified in trench T1. A noteworthy observation is the similar ~ 10 m right-lateral offset measured from the paleo-channel in T5 and T6 and the western stream deflection that amounts two characteristic slip events. The occurrence of five paleo-earthquakes predated by unit e (AD 79 – 230 and AD 83 – 428) can be correlated with the 21 ±1.5 m total offset of paleo-channels in trenches T5, T6, T4, T3 and T7. Taking into account the ~ 16 m cumulative offset of paleo-channel of trenches T5 and T3 and related maximum age AD 1304 from trench T4 we obtain an average 22.9 mm/yr right-lateral slip rate along the fault. If the maximum age AD 1271 of unit d in trench T1 predates faulting events X, Y and Z and related ~ 16 m characteristic slip events we obtain an average 21.8 mm/yr slip rate. These slip rate estimates are to be related with the maximum characteristic slip comparable to the 5 to 5.5 m right-lateral slip of the 1912 earthquake at the Güzelköy site. Using trench results near Saros Bay and assuming 4.5 m average characteristic slip for historical earthquakes of the past 1600 years, Rockwell et al. (2009) calculate 15.8 (+7.3/-3.8) mm/yr. However, the cumulative slip is inferred from a list of historical large events that may not be correct for the Saros Bay site. Our estimated slip rates from paleo-earthquakes (and related characteristic slip) in trenches and measured paleo-channel offset are consistent with the 22 – 26 mm/yr right-lateral slip obtained from ~ 17 years GPS measurements (McClusky et al., 2000; Reilinger et al., 2006).

Faulting events V, W, X, Y, Z identified from trench T1 may well be correlated with the historical large earthquakes reported in the seismicity catalogue of the Marmara Sea region (Ambraseys, 2002). Except for the 1912 event, the difficulty is to assign the rupturing event Y to either the 1659 or 1766 earthquakes, and event X to either the 1343 or 1354 earthquakes. Furthermore, the uncertainty in dating related to the poor organic and charcoal content of samples probably due to the fast alluvial accumulation in channels and the slope environment that favour detrital charcoal, prevented us to resolve the age of paleo-earthquakes at the Güzelköy site. The dating of event W from unit e2 of trench T1 (AD 79-230, AD 83-428 and AD 653-769) and from the earlier fault offset younger than BC 357 – AD 76 can possibly be correlated with the damaging 484 earthquake in Gelibolu (Table 3; Ambraseys and Finkel, 1987). If the record of faulting event is complete in our paleoseismic trenches for the last 2000 years it implies that a period of quiescence may have taken place from 484 to 1343-1354 earthquake events, and that the 1063 earthquake took place along another fault segment of the NAF.

## 6.2. The Yeniköy Site

### 6.2.1. Earthquake geomorphology and site selection

The Yeniköy trench site is on the western part of the Ganos fault at 1 km northwest from the Yeniköy village (Figure 6.1 & Figure 6.14). The site corresponds to the western section of the 1912 Yeniköy sub-segment (see p. 124). Here, the fault zone corresponds to a ~300-m-wide step-over with minimum three branches showing offsets of ridges and valleys. The trench site is on the northernmost and youngest branch. This fault strand shows steep slopes, clear-cut offsets of young streams, sagponds, and distinct fault scarps indicating recent earthquake faulting. In addition, the 1912 earthquake rupture has been well indentified along this section with several right lateral offsets of 4-5 ± 0.7 m and an apparent fault scarp. At this location we observed cumulative right lateral displacements of a shutter ridge and an S-N flowing stream (Fig. 6.14). The 1912 rupture crosses the Köy creek and the northern limit of its depositional bank between the stream and the shutter ridge (Figure 6.15)

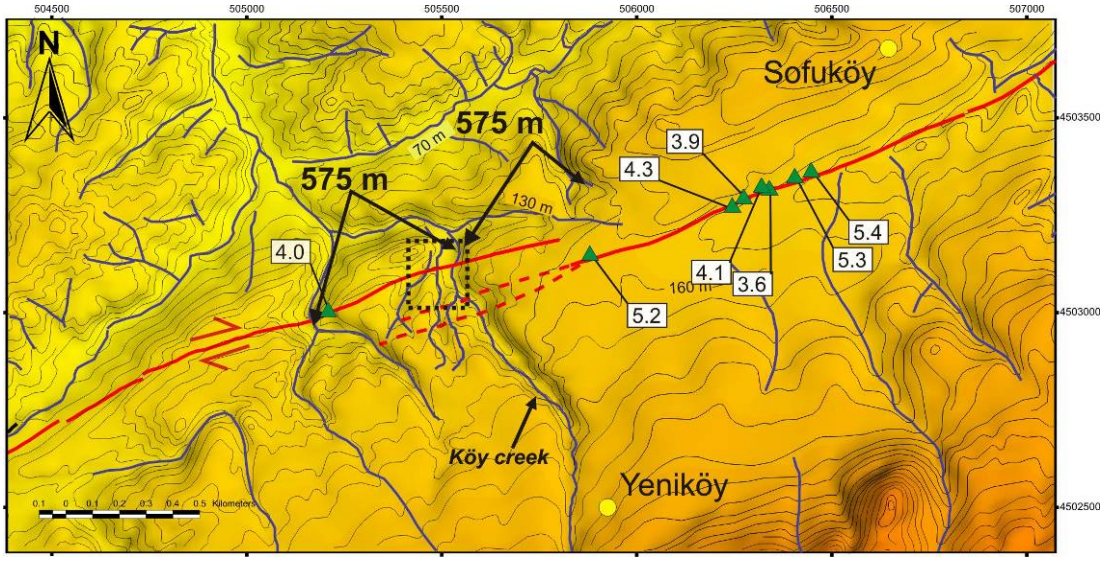


**Figure 6.14 :** The Yeniköy trench site (dashed black line) is located at a step-over of the Ganos fault (red lines). The Ganos fault and the 1912 earthquake rupture is well documented in that region. Co-seismic offsets range from 4-5 m (white boxes) between Yeniköy and Sofuköy.

Some preliminary observations yielded to classify this place as a potential trench site: (1) The 1912 earthquake rupture is well mapped along this section and shows evidence of 4 to 5 m co-seismic displacements. (2) The shutter ridge, the cumulative young stream offset and a fresh fault scarp indicate recent successive earthquake faulting and testify that the northernmost branch bears the most recent faulting events. (3) The alluvial terrace deposits that cumulate against the fault scarp may bury and preserve past earthquake ruptures. We assume that for each co-seismic offset the stream would be dammed and give rise to temporary flooding events and deposition on the bank; and (5) The terrace riser limited to the south by the fault may be preserved north of the fault on the left bank.

In order to strengthen our site selection, we conducted a GPR survey. We investigated the fault zone and search for buried structures which could help resolving the precise fault location. 3 of 4 profiles were taken orthogonal and 1 parallel to the fault trend (Figure 6.16). Preliminary analysis of the GPR profiles yield to determine two pairs of discontinuities parallel to the fault trend and were interpreted as two fault splays (indicated in red Fig. 6.16). The absence of prominent fault morphology within the terrace has been related to agriculture. However, the northern part of profiles crossing the fault shows ruptured units (reflectors) and confirms the fault mapping (Figure 6.17).

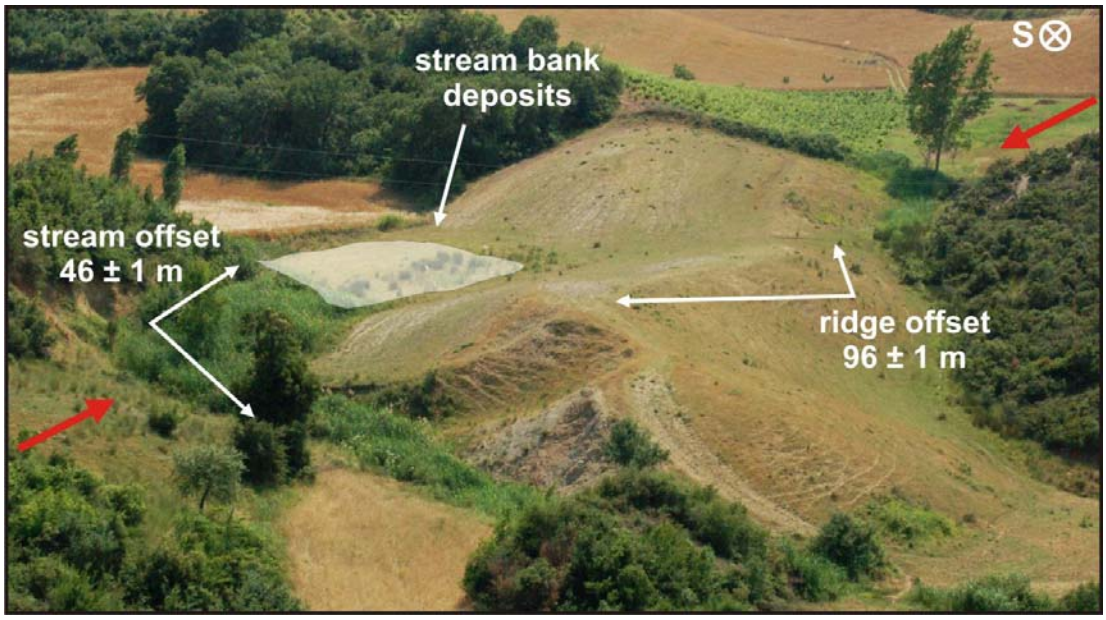


**Figure 6.15 :** The Yeniköy trench site is located ~2 km southwest of the Yeniköy village. Here, two right-lateral cumulative offsets of 46 ± 1 m and 96 ± 1 which show the long-term activity of the NAF. White arrows indicate the displacement, red arrows shows the orientation of the fault. At the east of the shutter ridge sediments of the stream bank deposit against the fault scarp and show the potential to bury surface ruptures.

Before trenching, we performed micro-topographic survey using Trimble Differential GPS to establish a detailed relief map (0.5 to 1.0 m resolution) of the site and estimate cumulative right-lateral offset of the shutter-ridge and the stream. A total of 5500 topographic points have been collected to build the topographic map given in Figure 6.16. The survey allowed measuring 46 ± 1 m right lateral cumulative displacement on the Köy creek segment and 96 ± 1 m for the ridge offset. As shown in Figure 6.16 the smaller offset was taken using the straight stream segment and related incision south of the fault and the preserved linear part of the stream valley to the North. The ridge offset is estimated using the eastern slope of the shutter ridge north to the fault (which corresponds to the same stream incision) with the eastern slope of the ridge west of the stream and south of the fault.

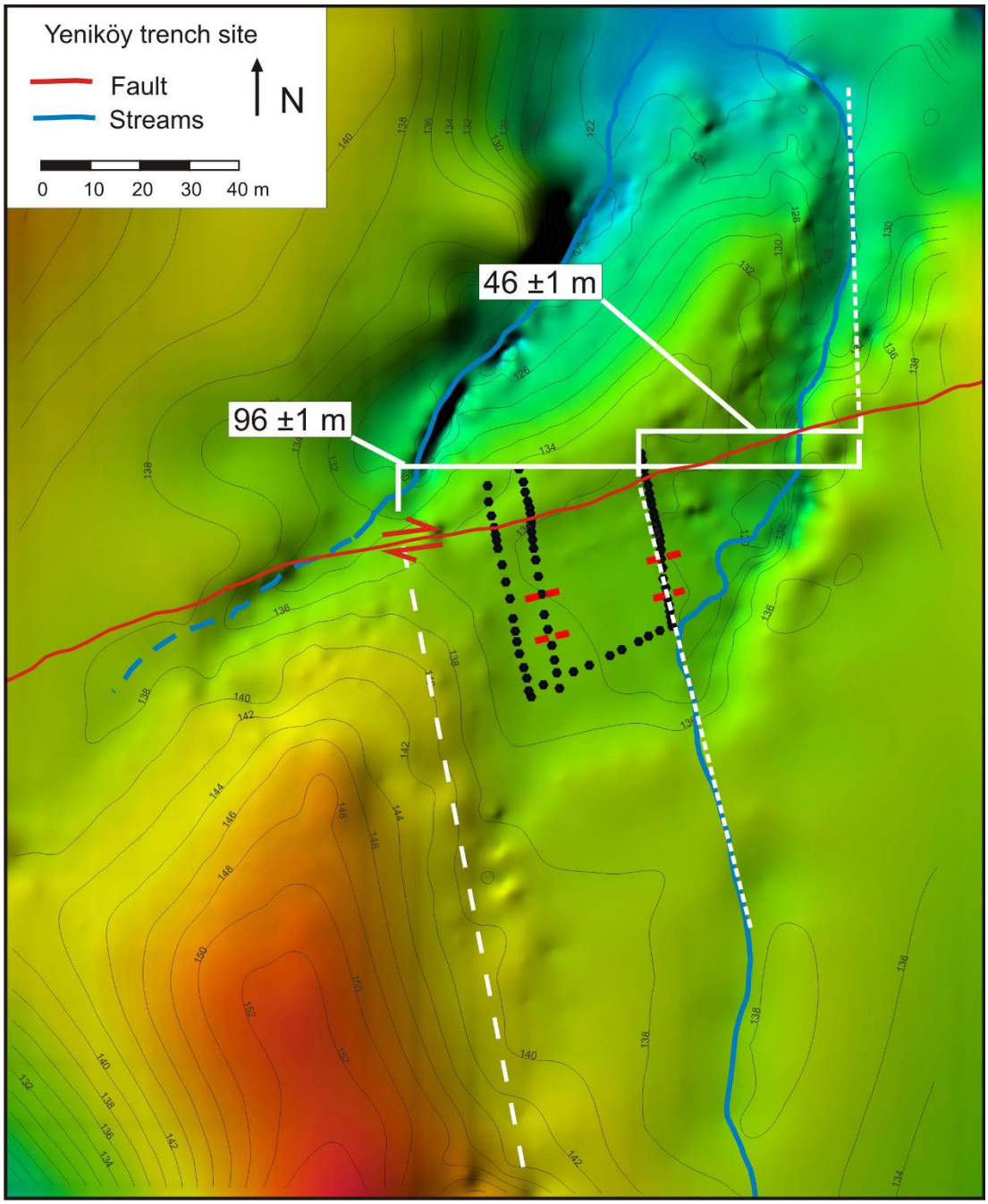


**Figure 6.16 :** Digital elevation model has been obtained from 5500 DGPS data points. The map shows the 96 ± 1 m and 46 ± 1 m ridge and stream offset, respectively. Black dots represent GPR profile locations. The faults identified from GPR profiles (prior to excavation) are in Fig 6.17.

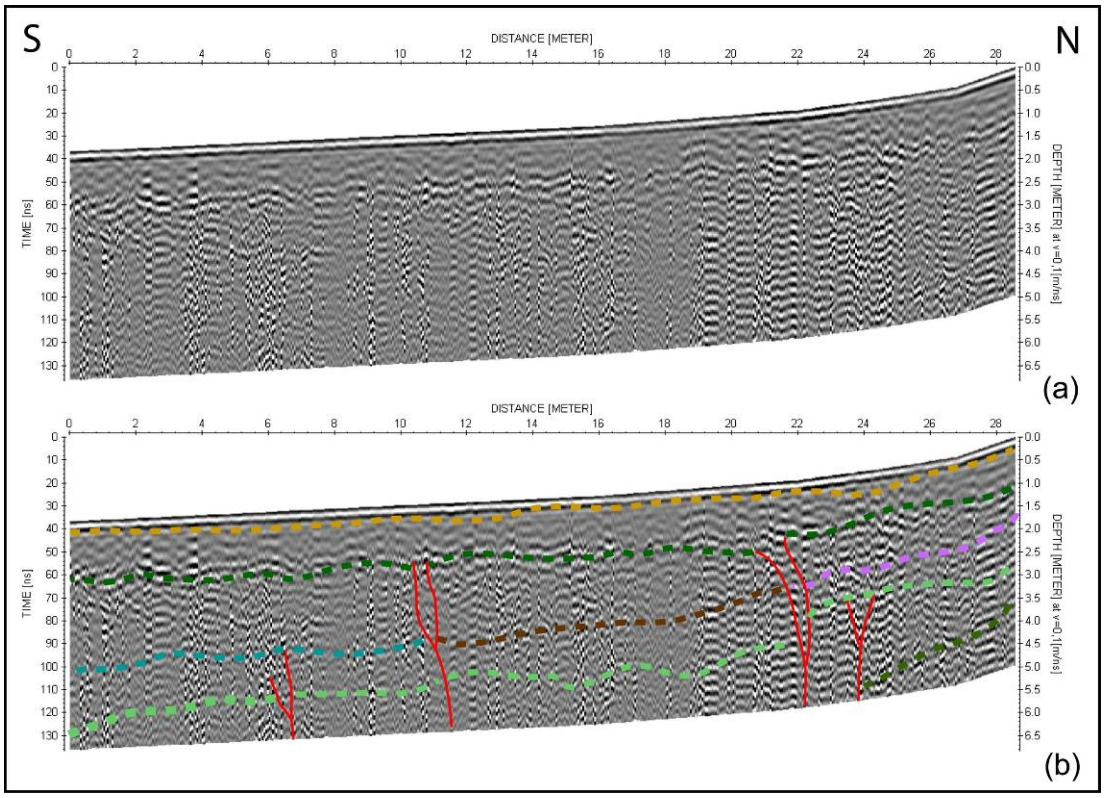


**Figure 6.17:** The processed GPR profile (a) and the interpreted profile (b) show on the top continuous reflectors (yellow line). Structures interpreted as faults are indicated as red solid lines to the north of the profile below the yellow line. The profile corresponds to the western N-S profile in Fig 6.16.

### 6.2.2. Paleoseismic trenching

We excavated 5 trenches within the alluvial terrace and the western bank of the Köy creek; 3 trenches T1, T2 and T4 are across and 2 others T3 and T5 are parallel to the fault (Figure 6.18). Orthogonal trenches were dug to investigate fault location and past faulting events, whereas the two parallel trenches were opened to locate the spatial distribution of the terrace riser north and south from the fault.

Each trench wall was logged using a 1 m wall grid; near the fault zone a grid of 0.5 m has been used for more accuracy. Nearly 1800 photographs were taken with a Nikon D50 digital camera using 28 mm focal length. Canon Photostich Software was used to construct the photo-mosaics for each trench wall. All tectonic and sedimentary structures on the walls were mapped using these photo-mosaics. Subsequent to the logging procedure 120 samples mainly of charcoal and organic matter were collected for isotopic (radiocarbon) dating of the sedimentary deposits.

Finally before closing the trenches, we levelled the trench margins, the fault zones exposed in trenches, the terrace riser and the related channels exposed in the trenches with total station in order to constrain a 3D view of the site. We also collected additional topographic points to improve the earlier previous micro-topographic map.

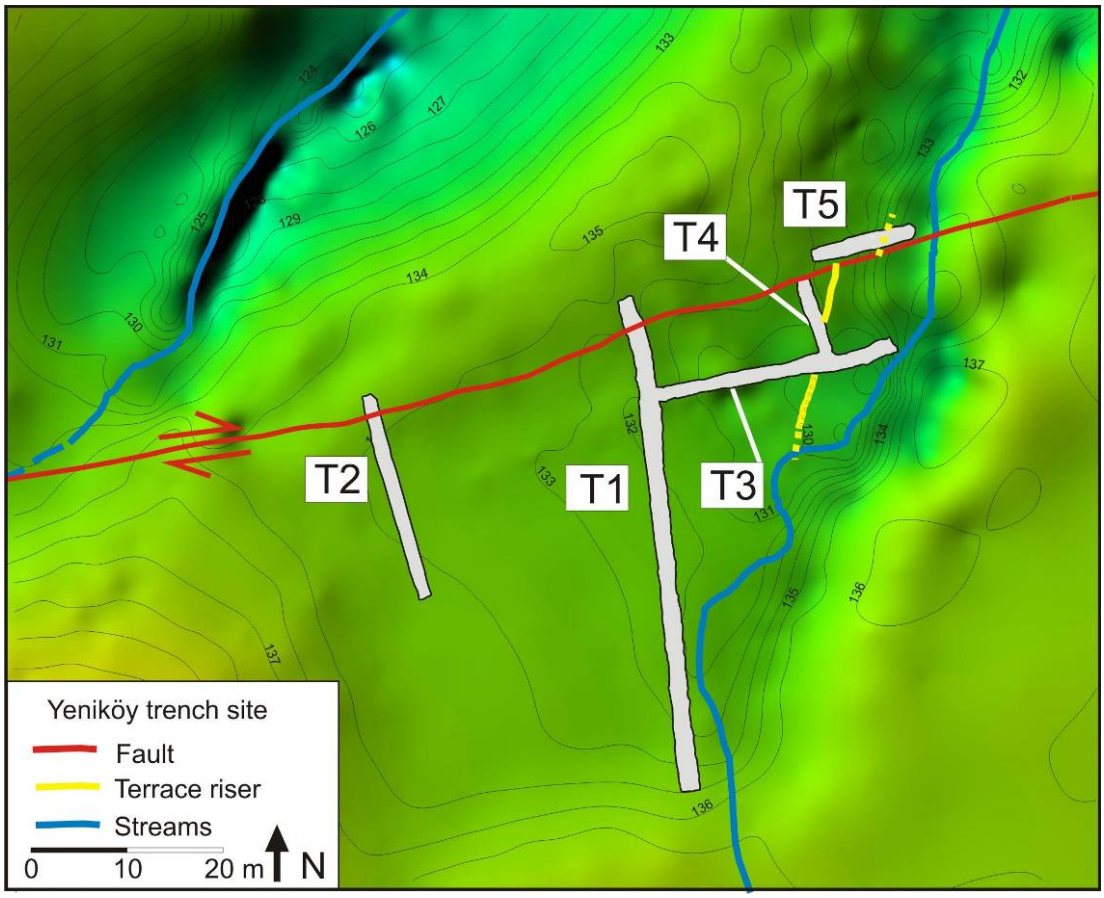


**Figure 6.18 :** Closer view of the paleoseismic site and trench locations. T1, T2 and T4 allowed locating the fault zone and past faulting events. T3 and T5 were dug to check the spatial distribution of the channel deposits and also allowed to drain the high ground water in T1.

All trenches show sedimentary deposits with comparable stratigraphy made of colluviums, massive clays and alluvial deposits (Table 6.3). Trenches across the fault scarp display different lithology with a clear contact that corresponds to shear zone. In general, the northern part exhibits successive colluvial deposits, whereas the southern part shows thick massive clay layer as bottom unit. Both units are reworked sediments from the Oligocene shale and sandstones whereas the well stratified and overlaying alluvial deposits derive from the Miocene beach facies deposits. In the following section we present the stratigraphy of 6 main depositional units (Table 6.3) as logged in trenches.

**Stratigraphic succession:**

Trench T1 is 50-m-long on the alluvial terrace and across the fault scarp (Figure 6.18). The average depth of the trench was limited to 1.5 m due to high ground water level. However, the trench depth was sufficient to expose the stratigraphic succession including the stream channel deposits. In Figure 6.19 and Figure 6.20, we observe a ~ 1-m-wide fault zone with several rupture branches affecting colluvial wedges and a paleosol. We logged the fault zone of the western wall of T1 in detail to document the stratigraphy of the site and faulting events. The trench bottom is a colluvium (Co) made of silty clay deposits with clasts that show minor difference on the two fault compartments. North of the fault, the Co is layered and shows ~ 20° to 30° southward tilting (Fig. 6.19, 6.20). The 1.5-m-thick Co is overlain by a reddish clay unit ($Rp_2$) whereas south of the fault Co is massive and shows no stratigraphy. Close to the fault zone a bluish clayey silt unit (Bc) is located within Co and exposes liquefaction features (intercalated sand blows). Southward, Co is interfingering with alluvial deposits (Flv in Fig. 6.19) visible all along the trench walls. At the trench bottom, the alluvial deposits interfinger with Co and moving to the top they overlay the Co and show well stratified sedimentary units with channels and northward migrating sequence. The top units are $Sl_1$ and $Sl_2$, which correspond to the soil development. $Sl_1$ is deposited on a smooth slope and thickens towards south where it interfingers with $Sl_2$, indicating that they deposited at the same time. Two reddish shear zones are distinct on the western wall (Fc, Fd and Fe).

Trench T2 dug across the fault is ~2-m-deep and 22-m-long., located ~ 20 m west of T1 (Figure 6.21, 6.22, 6.23). We logged the northern first 9 m of the two trench walls, which expose several fault branches and related sedimentary deposits. Both walls show similar stratigraphy and a clear contact along a shear zone and faulted units with different stratigraphic characteristics. The trench bottom on the north consists of a light-brown massif clay unit (**Brc**), which shows several fault branches. Brc contains sparsely scattered clasts of sandstones with alternating size of 1-20 cm. The unit hold no organic matter which prevented us to collect any sample for $^{14}C$ dating. Brc is at least 90 cm thick and is capped by **Bc**, which is a southward tilted 10-cm-thick bluish clayey-silt layer comparable to Bc in T1. Bc pinches out towards south but is faulted into several pieces. Unit **Co** is deposited conformably on top of

Bc and is also faulted. Both, Co and Brc are overlain by unit **Rp**, which is a 10-cm-thick reddish, oxidized, clay layer, deposited on top of an erosional surface.

**Table 6.3 :** List of stratigraphic units exposed on the trench walls and their lithologic descriptions.

| Unit | Description |
|---|---|
| **$Sl_1$** | Soil |
| **$Sl_2$** | Soil |
| **$Sl_3$** | Grey-yellow silt and clay with scattered clasts |
| **Rc** | Reddish-brown clay |
| **Sc** | Brown-grey clayey silt |
| **Scl** | Stratified grey clayey silt |
| **Bsc** | Dark brown-grey silty clay |
| **Flv** | Coarse to fine, well sorted medium rounded clasts forming a typical sequence of fluvial stratigraphy with horizontal- and cross-bedding and channels |
| **Fss** | Unconsolidated grey-yellow stratified sand |
| **Fgs** | Grey massive cemented silt with thin clay layer and some gravels |
| **Fbc** | Coarse to fine, well sorted medium rounded consolidated clasts with horizontal- and cross-bedding and channels |
| **Fsc** | Reddish massive silty clay with increasing silt content towards east |
| **Ysc** | light yellow, clayey silt with scattered gravels content and some bioturbations |
| **Rp** | dark red, oxidized massive clay, well consolidated, with pockets of caliche |
| **$Rp_2$** | reddish oxidized clayey silt |
| **Bc** | Bluish-grey silty clay with scattered gravel content |
| **Co** | silty clay deposits with coarse gravels |
| **Brsc** | Brown massive clay with very few medium rounded poorly sorted gravel content |
| **Brc** | Light brown massive clay with poorly rounded medium sorted scattered gravels. |

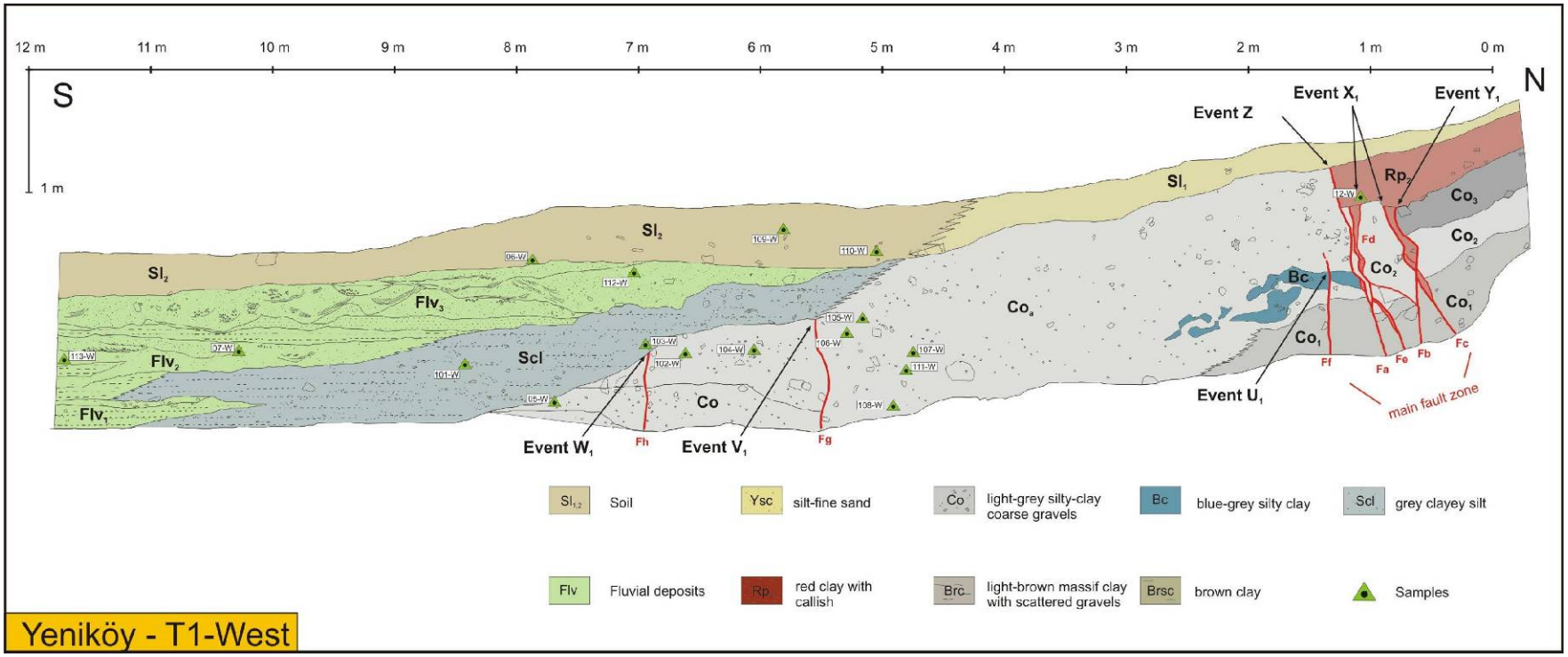


**Figure 6.19 :** The trench log of T1 illustrates a main fault zone with several rupture branches. Additional branches are observed towards south (Fh & Fg). The trench exposed a colluvial stratigraphy overlain by a alluvial sequence. The 1912 earthquake rupture is indicated as Event Z.

The unit comprises some small size gravels and patches of caliche. On top of Rp lies a massif wedge shaped sand deposit (**Ysc**) with 1 m maximum thickness. Ysc consists partly of sand and some pebbles and includes some bioturbation. The unit is most probably deposited on a slope adjacent to a small basin margin. Ysc derives most probably from the Miocene beach sand formation which represents the southern geology of the Ganos fault. Ysc is visible on both trench walls of T2 but it is not observed in the other trenches. South of the fault, a minimum 1.5 m thick massif clay unit (Brsc) forms the basement (Fig. 6.22, 6.23). It consists mainly of clay with gravels of sandstones ranging from 1-20 cm in size, infrequently distributed. The gravel content indicates that the unit is deriving from the Oligocene formation. Brsc is rich in organic matter and allowed us to collect 35 charcoal samples. The unit is overlain unconformably by a clayey silt deposit, which probably correspond to a little pond. At the southern end of T2 we notice a fluvial channel which is comparable to unit Flv in T1. The uppermost unit is $Sl_2$ which is 20- 40-cm-thick and covers all units within the trench.

Trench T3 is 24-m-long and was dug parallel to the fault. It exposes the eastward sedimentation of Flv in T1 and allows tracing the spatial distribution of the terrace riser. In parallel, the trench served as an outlet channel to drain the high ground water in T1. We have not logged T3 however the margins of the terrace riser and the trench were levelled with a total station.

Trench T4 is 8-m-long and 1 m deep located ~15 m east of T1 and across the fault (Fig. 6.24). T4 exposed some part of the terrace riser and the fault zone. We logged in detail the northern 7 m of the west wall. The stratigraphy was similar to T1 and T2. The bottom unit is Brc, which is covered by a sequence of colluvial deposits ($Col_{1\text{-}5}$). The alluvial deposit Flv interfingers with $Col_4$ and shows a northward migrating sequence as observed in T1. The stratigraphy of T4 is very comparable with T1. We determined two fault branches that mainly cut unit Brc and $Col_{1\&2}$.

T5 is 10-m-long and nearly 2-m-deep and located on the northern part, parallel to the fault (Fig. 6.18). We opened the trench to expose the northern part of the stream channel corresponding to the terrace riser. We logged the southern and northern walls of the trenches (Fig. 6.25, 6.26). The trench walls expose a colluvial basement Col overlain by a westward migrating channel sequence.

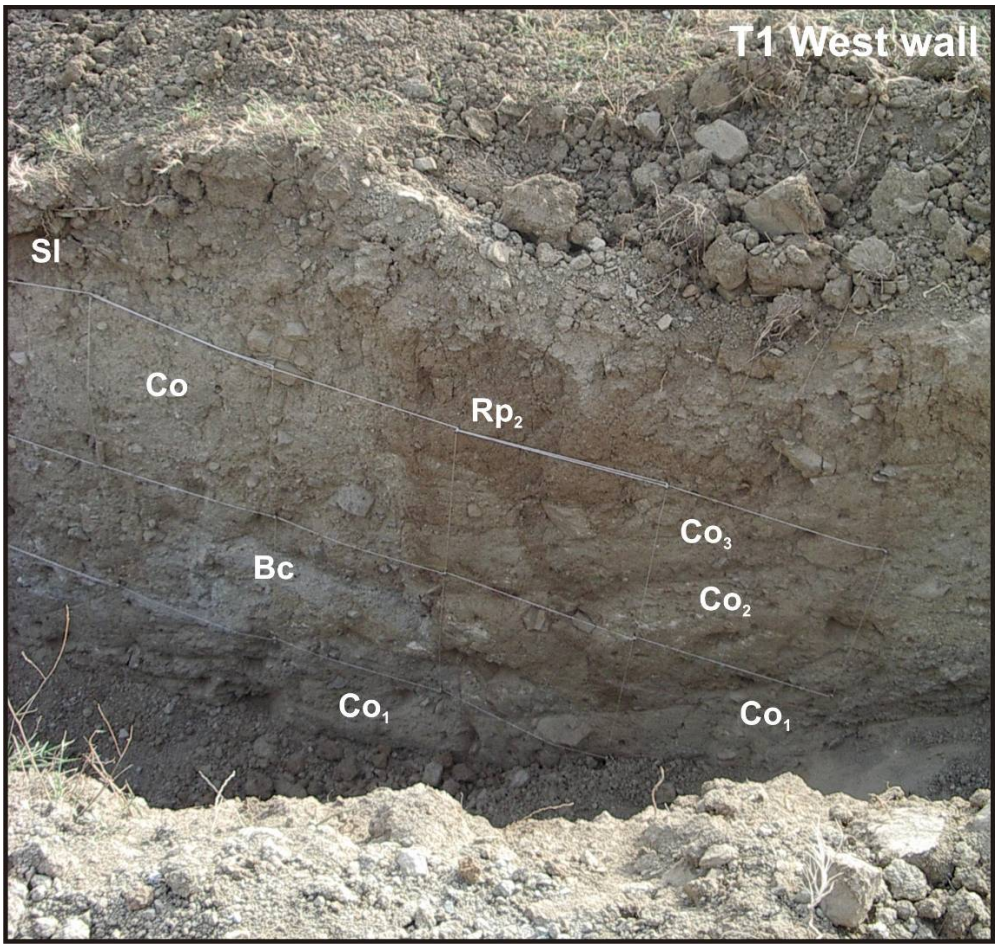


**Figure 6.20 :** The photograph of the western wall of T1 showing the fault zone (Vertical reddish strips that correspond to shear zones). The trench wall exposes intensely faulted colluvial (Co and Bc) and paleosol units (RP2; see text for details).

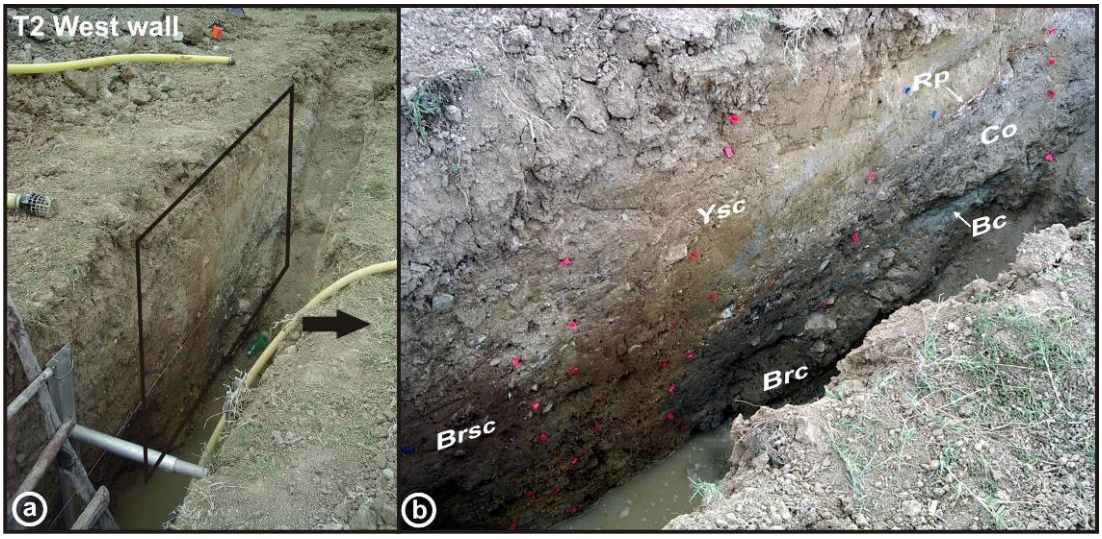


**Figure 6.21 :** Photographs showing the western wall of trench T2. The fault zone limits two different basement deposits. The south is composed of clay deposits (Brsc) and the north of the fault is made of colluvial deposits (Brc and Co).

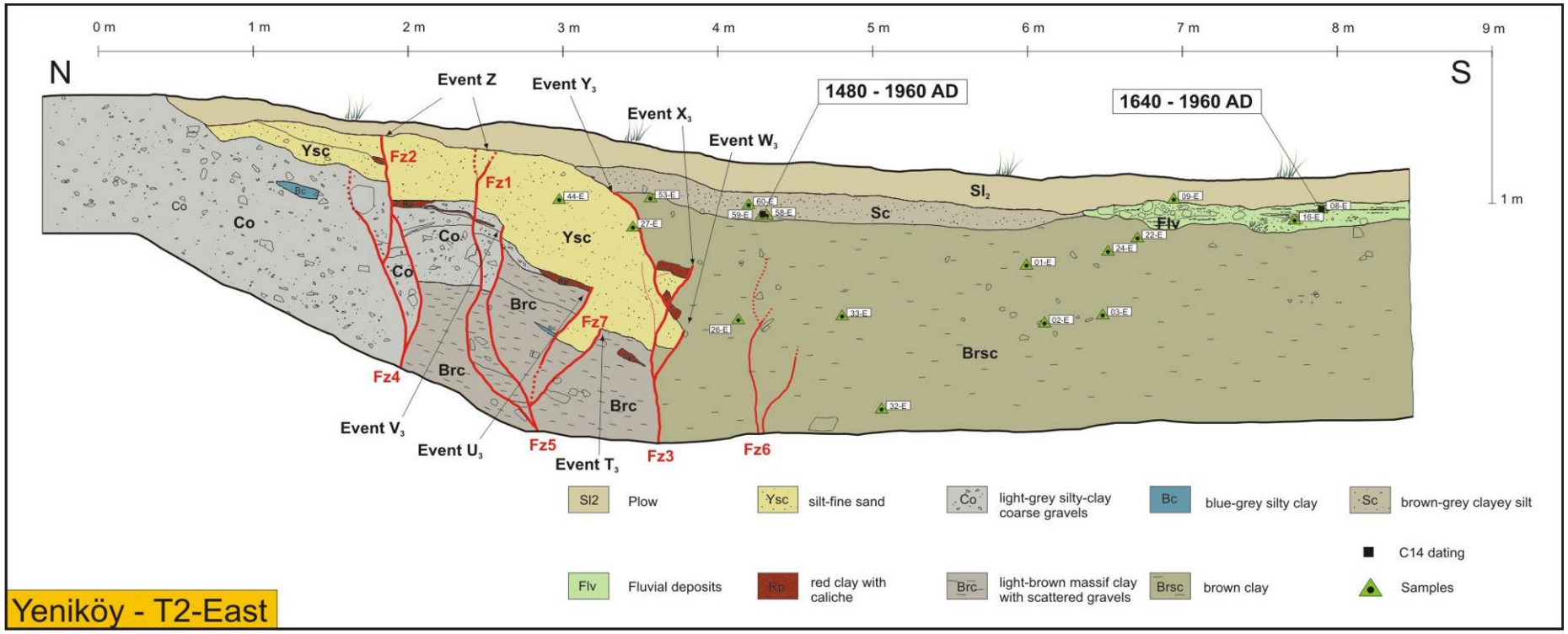


**Figure 6.22 :** Eastern trench log of T2 showing seven faulting events. The correlation with the western wall showed that event W3and X3 are not present on the western wall.

**Paleoearthquake analysis and faulting events**

The trench walls display fault zones and provide evidence of several faulting events. The sedimentary deposits indicate the successive faulting consistent with the fault scarp location, stream and ridge offsets. In order to characterize the timing of past earthquakes, we dated 14 charcoal fragments out of 120 samples from trenches T2 and T5. Figure 6.24 shows the C14 dating results calibrated using Oxcal v4.0 with 2σ age-range and 95.4% probability density (Reimer et al., 2004; Bronk Ramsey, 2005).

**Trench T1**

T1 exposes on the south facing slope of the shutter-ridge a ~1-m-wide main fault zone that can be interpreted as a result of successive faulting events.

Event Z: The uppermost faulted unit is $Rp_2$. In figure 6.19 the fault branch Fa truncates, $Co_1$, $Co_2$, Bc and $Rp_2$ and is buried by the soil $Sl_1$, which corresponds to the most recent deposit. Therefore, we consider that this event may be related with the 1912 earthquake rupture.

Event $Y_1$: Unit $Rp_2$ buries Fb, Fc and Fd, and postdates the corresponding faulting events. Unit $Co_1$ and $Co_2$ are faulted by Fb, Fc and Fd. In addition Fb offsets the reddish shear zone of Fc for 3-5 cm, hence necessarily postdates Fc. $Co_3$ faulted by Fb and not by Fc confirms that $Co_3$ may postdate Fc. Hence, it can be suggested that Fb may correspond to a prior event or to the penultimate event of the 1912 rupture. However, we cannot confirm this concluding remark because we have no dating of $Rp_2$ and $Co_3$.

Event $X_1$: Fc and Fd buried by $Rp_2$ affect $Co_1$ and $Co_2$ but not $Co_3$. Hence, Fc and Fd characterize a faulting event prior to $Co_3$ and event $Y_1$.

In addition, we observe two fault branches within the colluvium $Co_a$ south of the main fault zone (Fig. 6.19). Fg and Fh cut into younger units of $Co_a$ below the well stratified Scl. Fh that offsets the contact between Co and $Co_a$ and is buried by Scl may correspond to another event older than event Z. Furthermore, Fg that also affects Co and $Co_a$ limits to the north Co and shows an upper termination below Scl but coincident with the interfingering between Scl and $Co_a$. The northern limit of Co by Fg and coincidence with the interfingering may correspond to another faulting event older than Z but younger than the event observed on Fh. Based on this stratigraphic relationship we may conclude that Fg and Fh occurred after event Ff and correspond

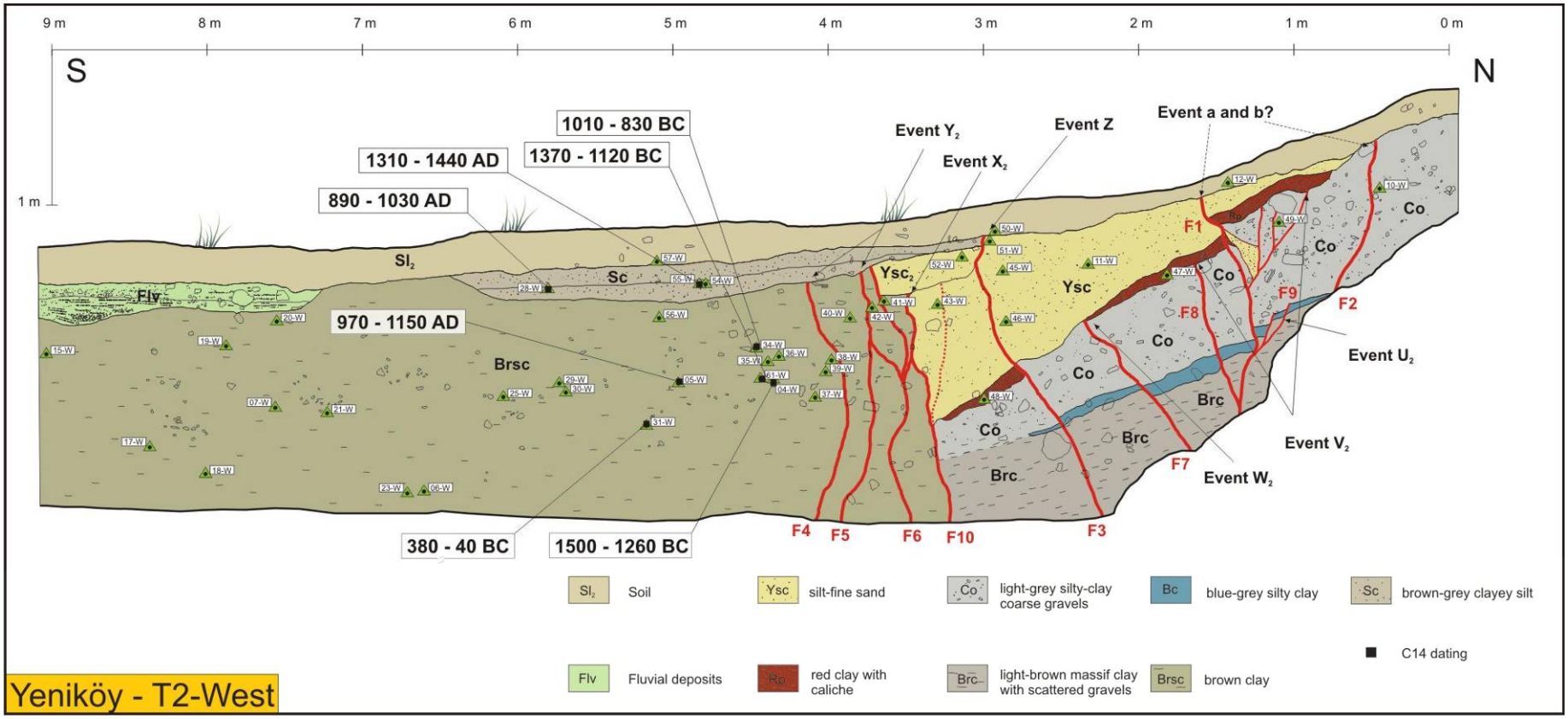


**Figure 6.23 :** Western trench log of T2 showing six faulting events. The correlation with the western wall showed that event V2and U2 are not present on the western wall. C14 dating of unit Brsc that postdates all events yield and calibrated age of 1500 – 830 BC. Event Z corresponds to the 1912 rupture

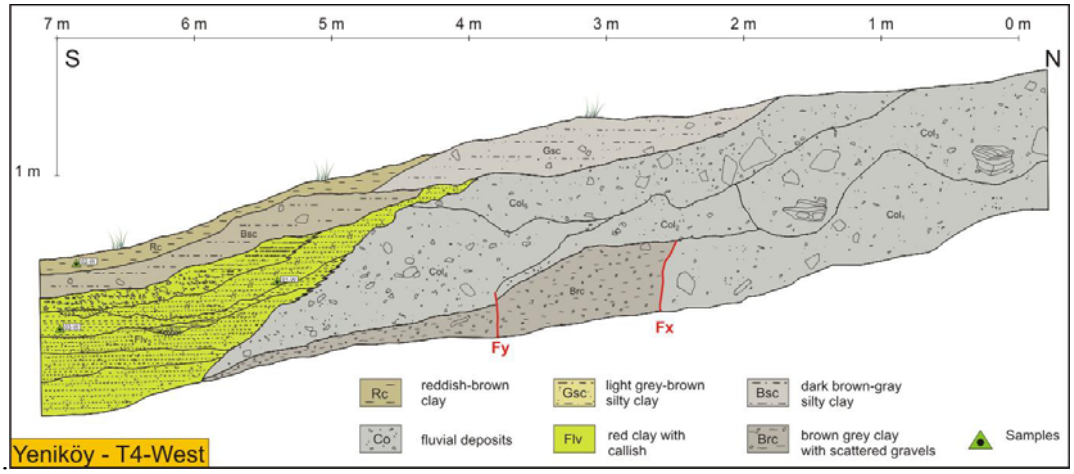


**Figure 6.24 :** Logs of T4 shows the channel stratigraphy and its relations to the fault. Logs of T5 illustrate the stratigraphy north of fault. Dating of channel deposits yield and minimum age of 840–590 BC for the oldest unit.

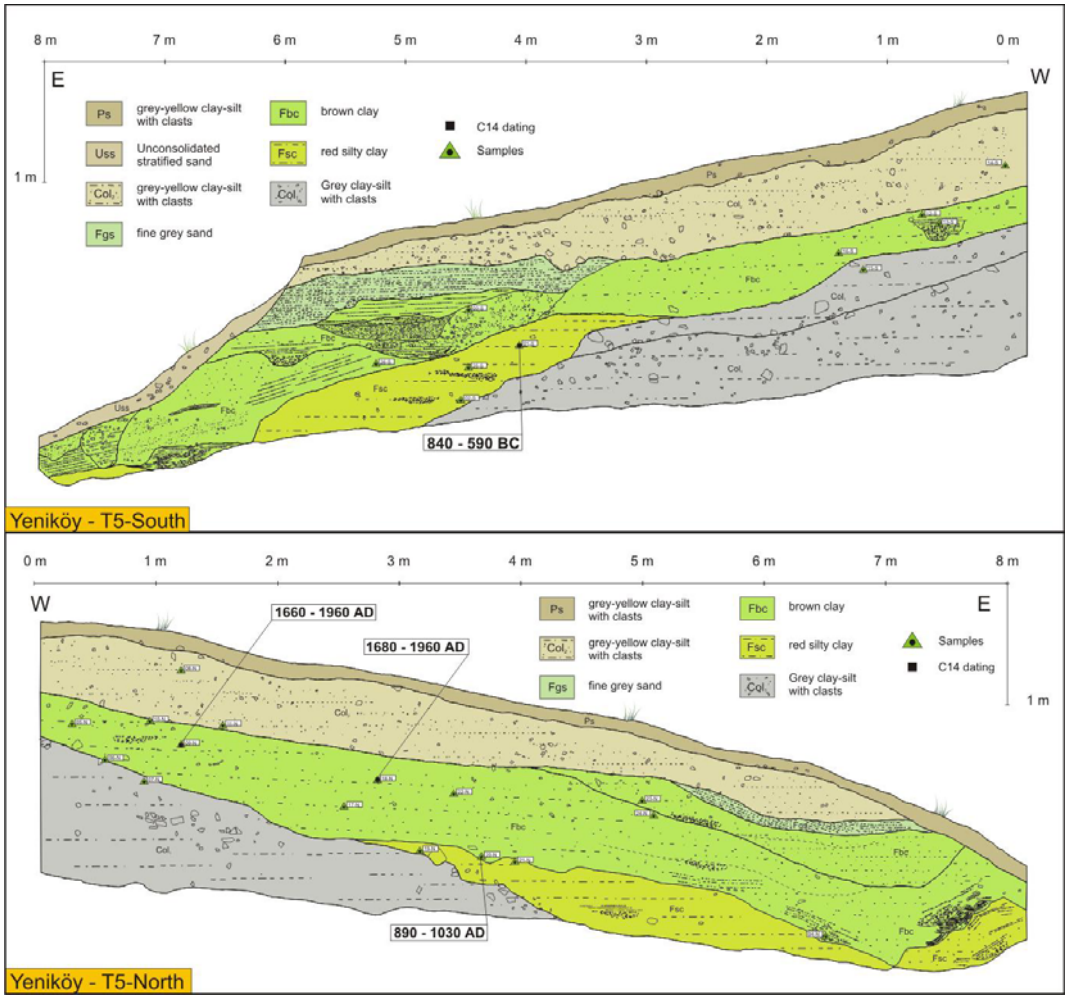


**Figure 6.25 :** The logs of T5 illustrate the channels deposits of the Köy creek. The fluvial unit (Fsc) represents almost the lowermost deposits of the creek. A combined calibration of the two charcoal samples from the top of Fsc yield an date of 120 AD - 250 AD. Hence a minimum age of ~2000 years can be estimated for the creek (see text for detail).

to one or two events. Ff offsets unit Bc and postdates these units. However, the main erosional limit between Scl and units $Co_a$-Co shows that an important truncation of sedimentary units which may contain faulting events took place after deposition of $Co_a$.

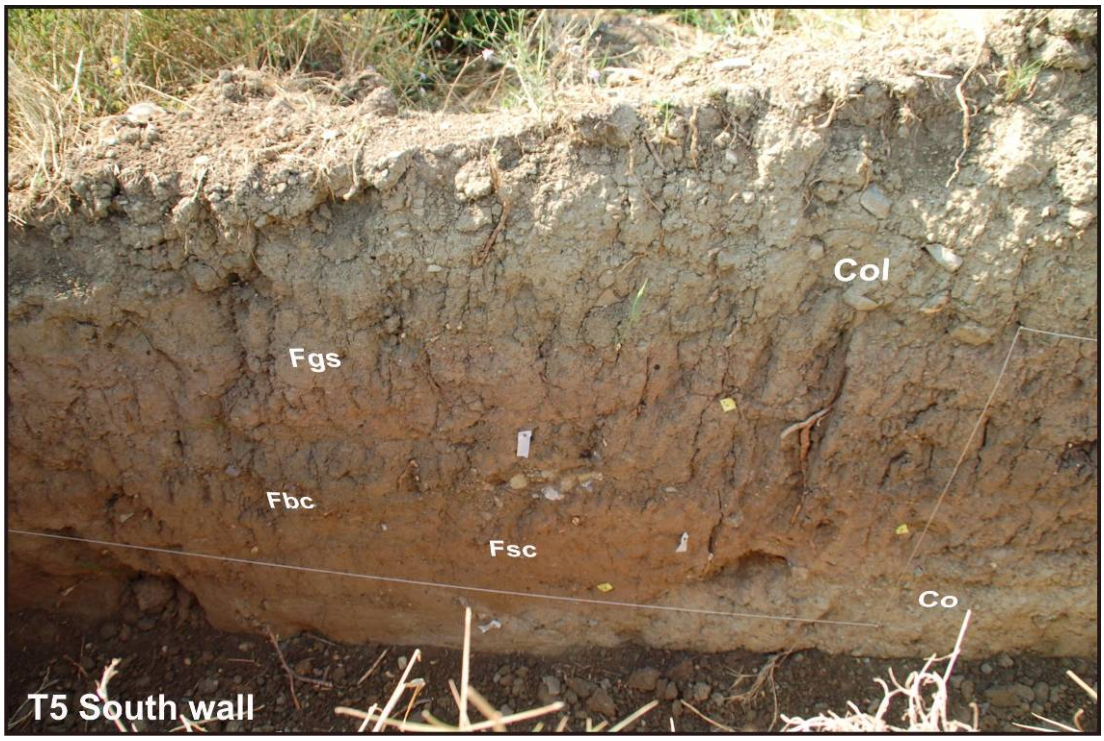


**Figure 6.26 :** A photograph showing the southern trench wall of T5. The reddish units (Fgs, Fbc, and Fsc) are channel deposits overlaying on top of a colluvium indicated as Co. Fsc represents the oldest deposits of the Köy creek. Radiocarbon dating of charcoal samples from T5 allowed determining a minimum age for the channel deposits (see text for detail).

Bc shows a clear liquefaction characteristics and closely located to the fault zone. It was not possible to determine if this liquefaction was tectonically or gravitationally induced. If it occurred by tremor of near by faulting it may represent the oldest event in T1.

We collected 17 charcoal samples from trench T1 but we did not analyze any unit.

**Trench T2**

Event Z: The faulting event is observed on both trench walls. On the western wall three fault splays marked as F1, F2 and F3 rupture all units, but $Sl_2$. The same is observed n the eastern wall with branches Fz3, Fz3 and Fz5. The base of $Sl_2$ buries the faults and corresponds to the event horizon. The faulting event is therefore

bracketed between $Sl_2$ and Sc. C14 dating of Sc that yield a youngest calibrated age 1310 – 1440 AD and 1480 – 1960 A.D. (sample 55-W and 58-E, Fig. 6.22, 6.23) provide a maximum age for Event Z.

**Table 6.4 :** 15 samples were collected from the Yeniköy trenches. Radiocarbon dating results are given below.

| Sample Name | Trench unit | Nature | Radiocarbon age (BP) | Uncertainty ± years | Calibrated age (+=AD) 2s range | |
|---|---|---|---|---|---|---|
| YK-T2-W55 | Sc | charcoal | 540 | 30 | 1325 | 1440 |
| YK-T2-W28 | Sc | charcoal | 1060 | 30 | 900 | 1030 |
| YK-T2-E08 | Flv | charcoal | 190 | 30 | 1660 | 1960 |
| YK-T2-W46 | Ysc | charcoal | 9250 | 60 | -8570 | -8300 |
| YK-T2-W04 | Brsc | charcoal | 3130 | 50 | -1490 | -1260 |
| YK-T2-W31 | Brsc | charcoal | 2150 | 60 | -360 | -40 |
| YK-T2-W61 | Brsc | charcoal | 2985 | 30 | -1290 | -1120 |
| YK-T2-W05 | Brsc | charcoal | 1015 | 30 | 985 | 1150 |
| YK-T2-W34 | Brsc | charcoal | 2770 | 35 | -980 | -830 |
| YK-T2-E59 | Brsc | charcoal | 250 | 50 | 1520 | 1960 |
| YK-T5-N18 | Bc | charcoal | 115 | 30 | 1690 | 1940 |
| YK-T5-N09 | Bc | charcoal | 150 | 30 | 1670 | 1960 |
| YK-T5-S01 | Rsc | charcoal | 2600 | 35 | -810 | -590 |
| YK-T5-N20 | Rsc | charcoal | 1060 | 30 | 900 | 1030 |

Taking into account the analysis of historical catalogues three large earthquakes (1343 or 1344 or 1354, 1659 or 1766 and 1912) occurred in this time frame. If we consider that the two samples are from the middle part of the 25 cm thick Sc it is likely that the event horizon is much younger than the sample date. Since we know that the most recent surface faulting affected this site, Event Z in trench may be correlated with the 1912 earthquake. However, the base of $Sl_2$ is an erosional surface that truncates all previous sedimentary units and related fault splays and removed the earthquake record.

Prior events: Faults F4, F5 and F6 cut through Brsc, are covered by Sc and correspond to Event $Y_2$. Here again, F4, F5, and F6 are splay ruptures predating Sc and postdating Brsc. This can be compared with branch Fz3 and event $Y_3$ on the eastern trench wall. The unconformable contact between Brsc and Sc indicates that

the faults may be related to one or more faulting event. Other faulting events are older and recorded within the colluvial part of T2. We can suggest a relative order of occurrence among the ruptures for both trench walls. Rupture F10 on the west-wall, affects Ysc and all units below while it is buried by $Ysc_2$ and characterizes Event $X_2$ which is not observed on the eastern wall. Fz3 on the east wall ruptures Brc, Ysc, $Rp_2$, affects younger sediments of Brsc and corresponds to Event $X_3$. A branch of Fz3 affects Brc, Ysc and older deposits of Brsc. Therefore it is interpreted as a separate event (Event $W_{3)}$. F7 displaces Brc, Bc, Co and the tip of unit Rp. This event ($W_2$) can be correlated with the rupture branches Fz8 or Fz9 that affect the same units and the related Event $U_3$ or $V_3$ on the eastern wall. Another rupture branch is F8 which cuts unit Brc, Bc and Co, and is buried by Rp and indicates faulting Event $V_2$. The rupture splays F9 show faulting of units Brc, Bc, and the base of colluvial unit Co. Faulting Event $U_2$ took place after deposition of Brc and Bc but also during the deposition of the first layers of Co.

**Trench T4**

Trench T4 exposed two fault branches indicated as Fx and Fy. Fy is faulting Brc and $Co_2$, while Fx cuts Brc and $Co_1$. This implies that Fx occurred prior to Fy. Both events are within basement units; therefore we did do any dating to determine the timing of the events.

**Channel offset and right-lateral faulting events:**

Trench T5 was excavated parallel to the fault, on its North. The purpose was to expose the northern continuation of the terrace riser located south to the fault. The stratigraphy in T5 showed buried channels below 1 m of the surface. The northern part of the terrace riser was not observed in the trench. However, we exposed the base and nearly the lowest sediments of the 46 ± 1 m offset Köy creek. Radiocarbon dating from unit Fbc (sample 20-S) and Fsc (sample 01-S) yield calibrated calendar ages 890 – 1030 AD and 840 – 590 BC, respectively. Sample 20-S is taken nearly from the top of unit Fsc and corresponds to the minimum age of the channel. Taking into account the 46 ±1 m right-lateral offset and the age of the channel, we may deduce a maximum 17 ± 0.7 mm/yr slip rate for last 2700 years of the Ganos fault.

**Summary of Yeniköy trench results:**

The Yeniköy site was selected as a potential trench location based on geomorphological investigations. At a large scale the fault zone is well identified thanks to clearly visible scarps, stream offsets and shutter-ridges. 1912 co-seismic offsets are evident along strike, at close distances to site (Figure 6.14). GPR profiles showed shallow fault like structures fitting with the 1912 surface ruptures. We determined 5 events in trench T1, a minimum of 6 events in trench T2 and 2 in T4. The 1912 earthquake is inferred in T1 and T2. Although, prior events could not all be dated we deduce that a total of 10 events occurred at this site. Indeed, prior to 1912 and after 1310 (lower bracket of calibrated age of sample 55-W, Table 6.4) the historical catalogue reports the occurrence of two earthquakes which may correspond to 1343 or 1344 or 1354 and 1659 or 1766. The comparison between east and west walls of trench T2 shows that additional two faulting events that occurred prior to Event $Y_2/Y_3$ and after Event $V_2$ affecting colluvium Ysc and Brsc on the east wall, are not observed on the west wall. The 10 faulting events identified in trenches post-date the oldest units (Brsc and Brc) and corresponding youngest radiocarbon age 1010 BC – 830 BC.

The excavation of channel deposits of the Köy creek allowed constraining an age for the stream and obtain a slip rate for this section of the NAF. The oldest age of the lowermost unit of channel deposits yield a calendar date 840 – 590 BC (Rsc sample 01-S) and gives a minimum age for the channel. Taking this minimum age and the 46 ± 1 m right-lateral stream offset we obtain 17 ± 0.7 mm/yr slip rate for the last 2840 years. Co-seismic offset measurements along the 1912 rupture showed that the earthquake caused 4-5 m right-lateral displacements at Yeniköy. If a characteristic offset behaviour of 4-5 m is applied to the 46 ± 1 m stream offset we can deduce that this cumulative offset corresponds to 10 ± 1 events, which is similar to the number of events determined in our trenches.

## 6.3. The Yörgüç Site

### 6.3.1. Earthquake geomorphology and site selection

The Yörgüç trench site located on the central part of the Ganos fault, ~1 km east from the Yörgüç village corresponds to the Güzelköy sub-segment of the 1912 earthquake rupture (Fig. 6.1). The fault zone is localized in this region within a

narrow valley, 10 to 50 m in width. The 1912 rupture is visible in this area where we clearly observe fault scarps, stream offset, road offsets, and sag-ponds. Co-seismic displacements were measured along this fault and reaches 4.5 m. Two sites were excavated at Yörgüç. The first is located in a releasing bend area, (Trench T2 & T1 in figure 6.27) and the second site is located farther west, where the fault zone is getting narrower (Trench T3 in figure 6.27).

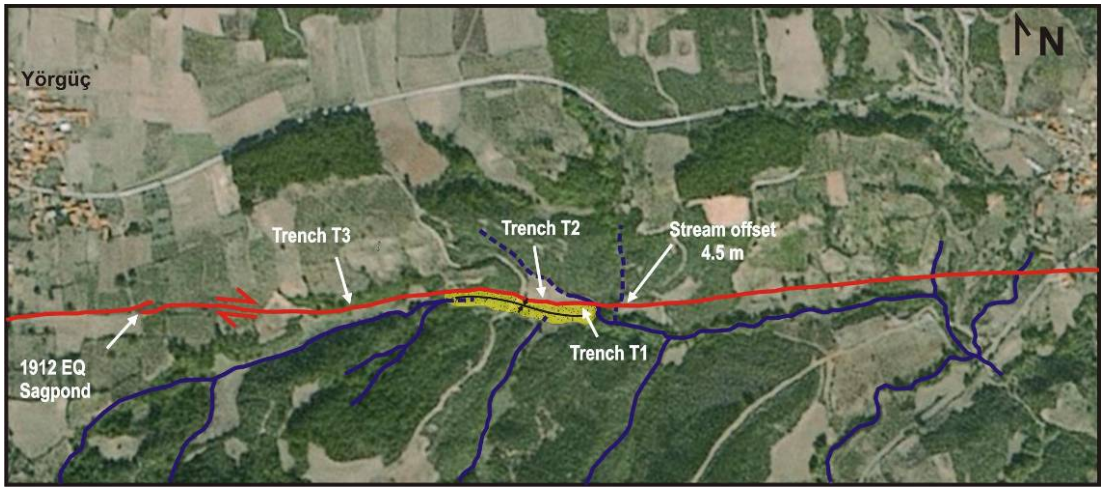


**Figure 6.27 :** The Yörgüç trench sites are located east of Yörgüç. The Ganos fault forms a small releasing bend at this locality. Streams sub-parallel and perpendicular to the fault carry fine to medium clasts into the basin (yellow), which deposit on top of the fault.

The nearby streams erode Miocene sandstones and carry fine to medium size sediments into the basin and burry the fault located at the northern margin. This condition allows co-seismic ruptures to be preserved within the geologic record.

### 6.3.2. Paleoseismic trenching

#### Trench 1 & 2

Trench T1 is 15 m long and 1.5 m deep and dug from the northern basin margin towards south and exposed the contact between basement units and basin deposits (Fig. 6.27, 6.28). The ground water level was nearly at 1 m depth and caused stability problems (the wall collapsed), when trench depth reached 1.5 m. The fault zone consists of very loose fine material causing instant collapse and prevented us to do any observation within the fault zone.


**Figure 6.28 :** View of the location of T1 at the eastern end of the basin. Red lines indicate the most-possible location of the fault zone. The presence of unconsolidated units and high ground-water level caused instability within the trench and walls collapsed when reached the fault zone.

We opened a second trench towards west were we expected lower ground-water level and more compact sedimentation. T2 is ~50-m-long and 1.7-m-deep showing a cross-cut of the basin sediments (Fig. 6.27). Trench walls were stabilized using hydraulic shores.

**Stratigraphic succession and paleoearthquake analysis**

Trenches T1 and T2 exposed comparable stratigraphy. All units are reworked material of the Miocene Kirazlı formation, which is composed of a beach facies deposit. The stratigraphy in T2 points towards a regressive sequence of fine sediments representing probably a lacustrine to marsh environment. The base of T2 (at 1.5 m depth) is made of three units; a, b and c (Fig 6.28). Unit a is a yellow-grey massif silty sand deposit and is unconsolidated. It interfingers laterally to a greenish-yellow sandy-silty clay unit (b). Unit b interfingers towards south with unit c which consists of greenish massif clay. units a to c, probably correspond pond sediments from the basin margin to the centre, respectively. A brown silty clay deposit (d) conformly overlays a, b and c. The contact between unit d and unit e is erosional. Unit e is brownish-grey clay overlain on the top by the soil unit. This stratigraphy is nearly continuous all along the trench. Towards south, we found a piece of cloth within unit e at ~60 cm depth which designate a modern age of maximum 30 years. This indicates a young and rapid sedimentation that do not include past earthquakes. In contrast, the northern part of the trench shows less sedimentation accompanied by fault related structures.

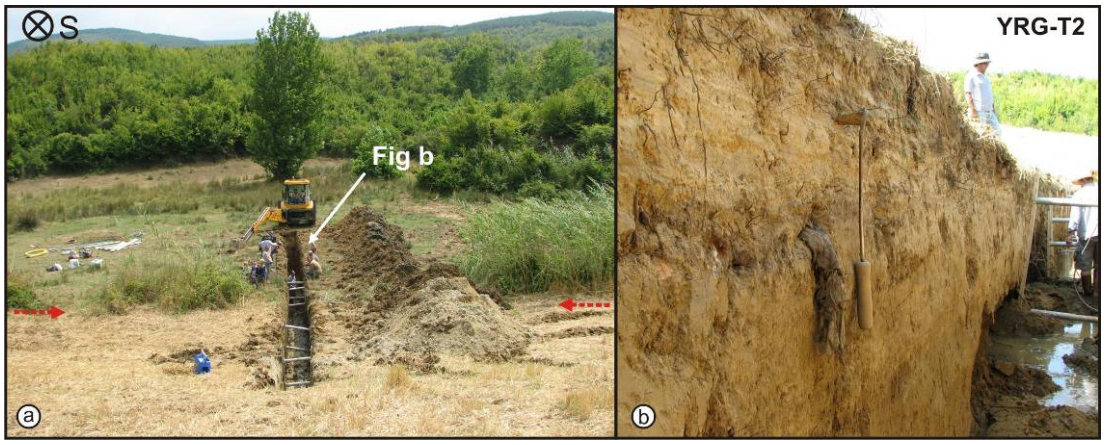


**Figure 6.29 :** View to the south of trench T2. Red lines indicate the most-possible location of the fault zone. The trench exposed an intercalation of fine to medium coarse sediments showing well stratification. At the southern end of the trench we determined a piece of textile buried nearly 60 cm below surface. The printings of the textile indicate a very recent age (probably no more than 30 years). This implies a minimum 2 cm/yr sedimentation rate for the central part of the basin and requires a trench-depth of 1-2 m for the most recent event (1912 earthquake).

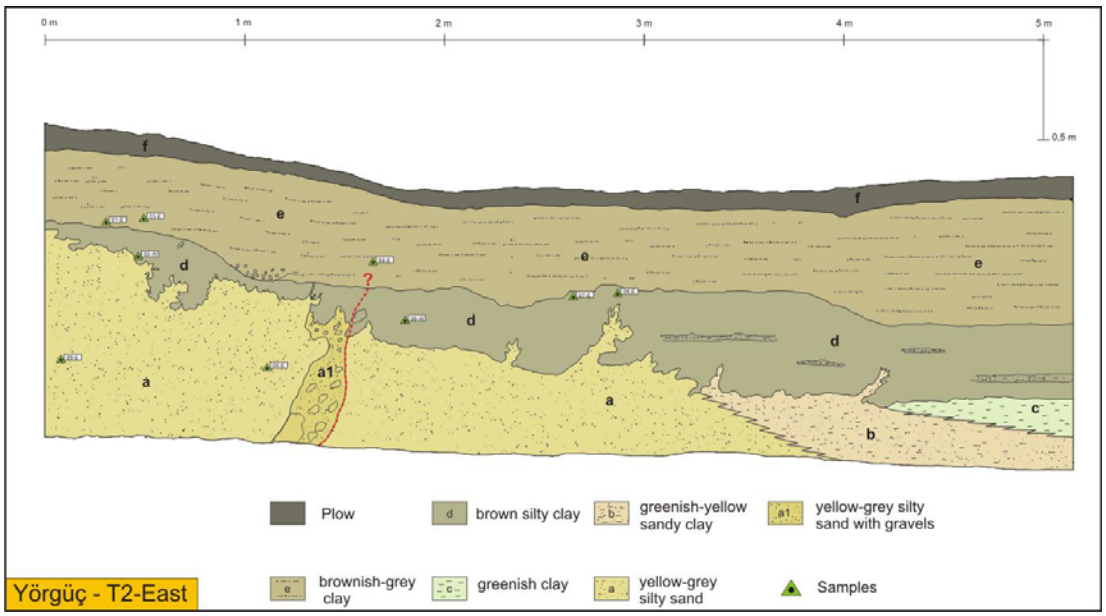


**Figure 6.30 :** The analysis of the eastern trench wall of T2 yield evidence for one faulting event associated with liquefaction structures, most possibly due to the 1912 earthquake.

**Trench 3**

In order to obtain a succession of older events we decided to open a third trench further west, apart from the releasing basin. Here, we dug a 15-m-long, 3-m-deep trench, where sediment accumulation occurs mostly by wash out from the adjacent

valley slope during high rainfall and a stream flowing parallel to the valley (Fig. 6.29).

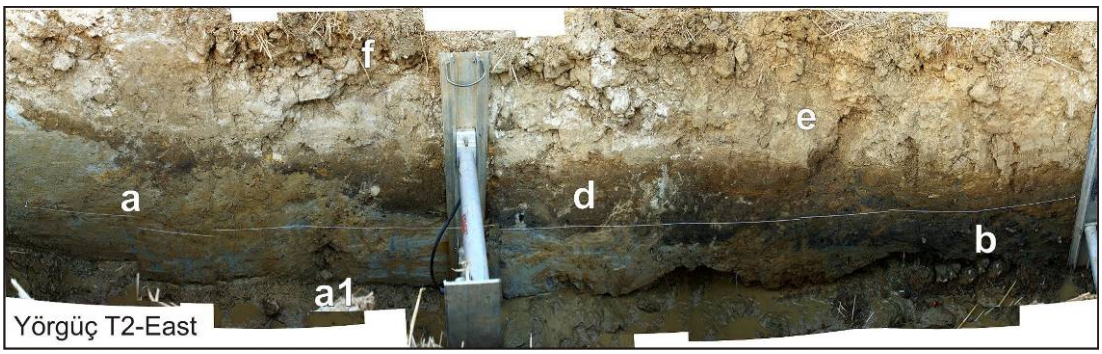


**Figure 6.31 :** The photo-mosaic of east wall of T2 shows flame structures along the contact between the light unit a and dark unit d.

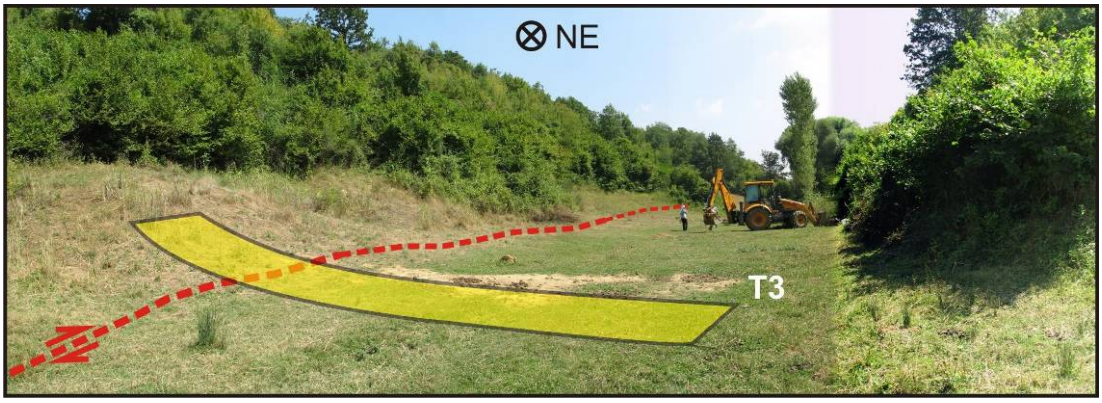


**Figure 6.32 :** View of trench location T1. The fault zone is localized here in a very narrow valley with steeps slopes. During high rainfalls sediments are washed out from the slopes and accumulate within the valley. Small streams may associate from time to time within this process, as observed in the trench wall.

T3 exposed a well stratified sedimentation (Fig 6.30) where the sequence starts with unit a at the base made of scattered coarse gravels within a massive yellow clayey silt matrix. Unit b that overlays unit a has a similar lithology but with abundant amount of muscovite. The lower unit b which shows an erosional surface on the top, is overlain by a well stratified sequence of clay, silt, and fine sand intercalation. Unit c is composed of silty clay and unit d is made of silt with mica content. The upper units (e and f) show intercalation with seasonal variation in deposition, where medium to fine sand (f) deposit in summer by abrupt small flooding events and silty clay (e) material deposits in winter time when wet conditions are more dominant in the area. Unit e and f are organic rich material and bear bioturbation. Close to the top

the sequence is truncated by channel deposits and colluvial units (g1 and g2). The uppermost unit is composed of fine to medium grained soil.

**Table 6.5 :** List of units and description of sediments determined in trench 3.

| Unit | Description |
|---|---|
| **s** | Fine grained soil |
| **g** | Light brown clayey silt, consolidated |
| **f** | Yellow silty fine sand |
| **e** | Greenish-brown clay with mica and silt, consolidated |
| **d** | Yellow silt with mica content |
| **c** | Brownish, dark grey silty clay |
| **b** | Yellow clayey silt with a few scattered gravels. Clasts contain mica |
| **a** | Yellow clayey silt with abundant scattered coarse gravels. |

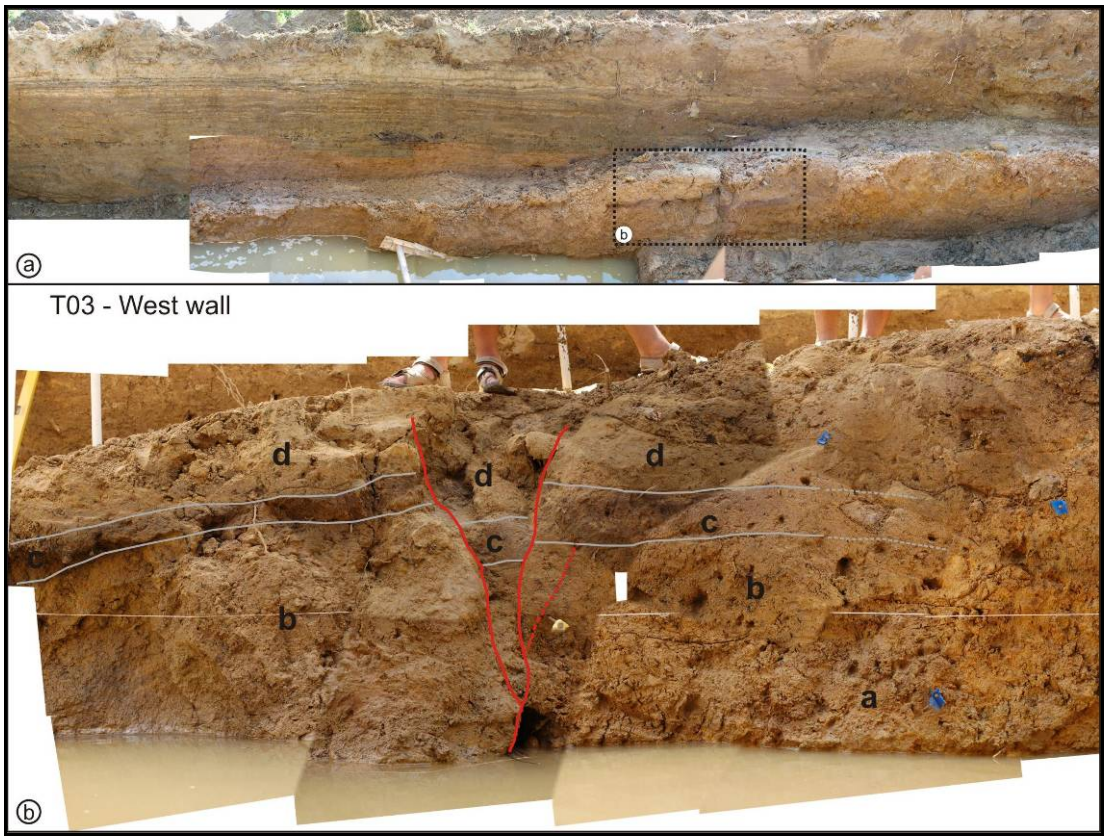


**Figure 6.33 :** The photo-mosaic shows the stratigraphy of the western wall of T3. Horizontally stratified sediments deposited on top of a clayey basement indicate a regressive sequence (a). We determined one faulting event cutting through unit a, b, c, and d and showing a negative flower structure (b). This event is overlain by unit f. The stratigraphy allowed collecting several charcoal samples for C14 dating (see Table 6.6).

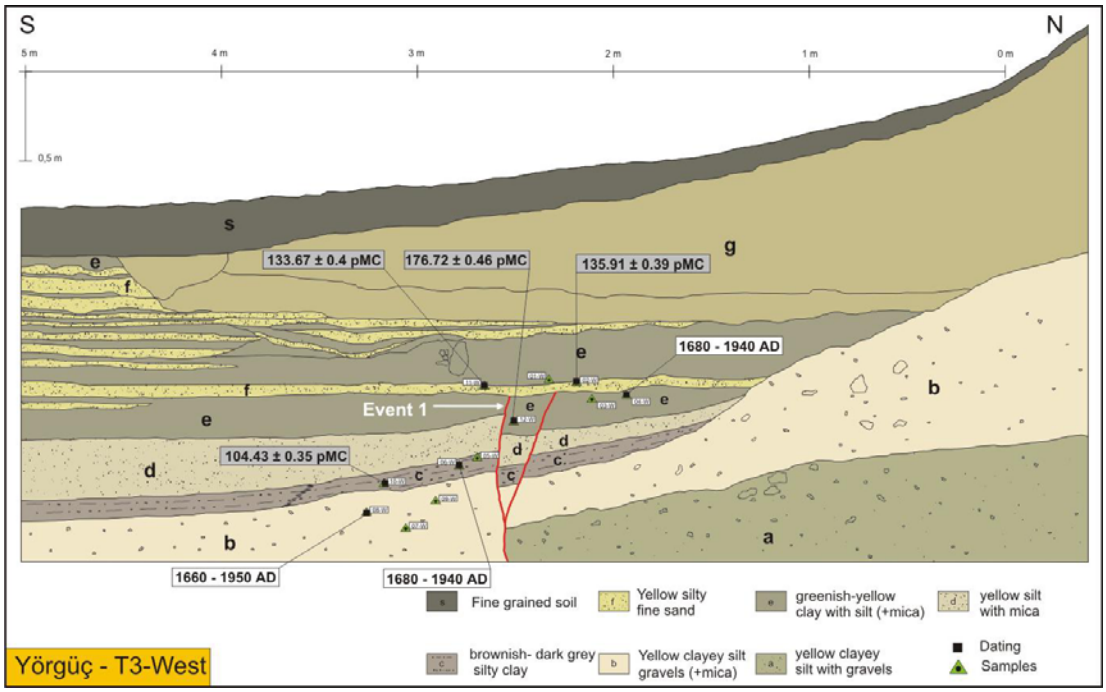


**Figure 6.34 :** Trench log of T3 illustrate a successive basin stratigraphy deposited on top of basement units a and b. We determined a faulting event, most probably related to the rupture of the 1912 earthquake. White and grey boxes correspond to C14 dating results. Samples indicated with grey boxes yield modern age, and are labelled with the percentage of modern carbon (C14/C, pMc).

**Paleoearthquake analysis**

Since trench T1 had instability problems we could not observe and describe any faulting event.

Two structures are distinct in trench T2. The southern and northern edges of unit a1 have a vertical sharp contact with the southern limit most likely due to faulting. The vertical structure of gravel deposits and the undulated top unit suggest an injection of coarse gravels within a matrix made of unit a. The contact between the lower most units a, b and c, and the marsh unit d shows distinct flame structures, typical of liquefaction processes (McCalpin, 1996). Since the flame structures and injected unit a1 affects unit d overlain very recent deposit unit e, we may consider the injection as a liquefaction structure associated with the 1912 earthquake.

In trench T3 we identified one faulting event close to the bottom of the trench (Fig. 6.31). A rupture branch with one splay that affect unit a, b, c, d and e are overlain by unit f. The fault limits unit a to the south and shows ~10 cm vertical separation affecting unit c, d and e. The relationships between the fault and successive units

indicate that two faulting events occurred at this site after deposition of unit a and b. Indeed the thickness of unit next to the fault and the different thickness of unit b suggest the occurrence of a faulting event probably before the erosional surface of unit b. The second faulting event affects the erosional surface, unit c, d and e. Calibrated C14 dating from units b, c and e1 provide 1660-1950 AD, 1680-1940 AD and 1680 – 1950 AD, respectively. The first faulting event occurred before unit b. The second faulting event affects unit e1 and is buried by unit f. Both events are younger than 1660AD.

### 6.3.3. Results of Yörgüç trench site:

The trenches opened at Yörgüç were located nearly at the central onland part of the Ganos fault. The excavated basin is a depo-centre fed by several streams and located at a small releasing bend. Three trenches allowed documenting the site stratigraphy and one faulting event.

In trench T1, stability problems caused the trench walls to collapse and obstructed us to document faulting events.

Trench T2 allowed us to expose a 1.7 m deep section of the stratigraphy. One faulting event associated with liquefaction structures is determined in T2. On the southern part of the trench we determined a fabric with printings nearly at 60 cm depth. The age of cloth piece is most probably modern, maximum 30 years, which indicates sedimentation is very rapid in this basin with a rate of ~2 cm/yr. Older events than the 1912 must be buried located fairly deeper than was excavated. To manage with the shallow ground water level and instability problems requires better equipment, preparation and a larger budget, which was not present in this campaign.

Trench 3 was opened at a locality were we expected lower sedimentation rates. A 3-m-deep trench showed a well stratified geologic record. We determined one faulting event at nearly 2.5 m depth. C14 dating yield modern dates indicating also rapid sedimentation, hence we consider the event observed in the trench corresponds most probably to the 1912 earthquake rupture.

The Yörgüç restraining basin, where we opened T1 and T2 is a suitable site for trenching were we observed evident for faulting, tremor induced liquefaction and good continuous stratigraphy. We consider this site has the potential to expose

several historical faulting events if can be excavated deeper up to 5-6 m with sufficient equipment for draining the ground water and stabilizing the trench walls.

## 6.4. The Saros Site (Rockwell et al., 2001 & 2009)

### 6.4.1. Earthquake geomorphology and site selection

The Saros site is located within the Evreşe plain, at the westernmost onland section of the Ganos fault. The fault strikes here through highly cultivated flat area. The fault morphology, particularly the 1912 rupture is poorly preserved in this area. Two large linear depressions are most evident structures along the strike of the fault; the Kavak Lake and a large sagpond at the coast of Kavak (Fig. 6.33). The fault cuts the Kavak river bank deposits, which potentially have a good geologic record.

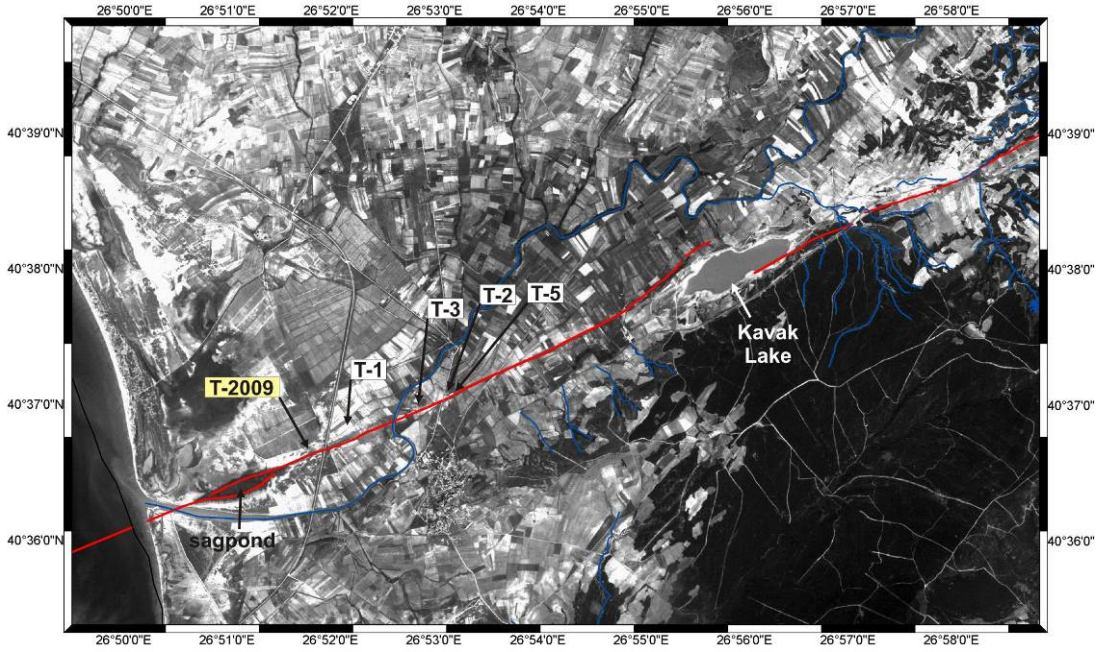


**Figure 6.35 :** The SPOT5 image of the Evreşe plain shows the location of trench sties with respect to the fault (red line). Prominent fault morphologies are two linear depression, the Kavak Lake and the sagpond at the coast. The trenches are located between these two structures within the bank deposits of the Kavak River (blue line). White boxes indicate trenches of Rockwell et al., (2001) and yellow box Rockwell et al., (2009).

### 6.4.2. Trench results of Rockwell et al., (2001)

Rockwell et al., (2001) opened 5 trenches at several sites along this section of the fault and identified 5 historical earthquake ruptures (Fig. 6.33). Their trench T-1 is located on the western bank of the Kavak River and exposed well-bedded

stratigraphy on both sides of the fault (Fig. 6.34). The comparison of individual units presented a mismatch across the fault which has been interpreted due to lateral slip. They identified four main units in T-1 showing evidence of 2 faulting events. The highest event in the stratigraphy truncates units 4, 3 and partly 2 and is capped by a thin layer of unit 2. A second event truncates the same stratigraphy as event 1, however it breaks only up to the middle portion of unit 2 (Fig. 6.34). Both events occurred during the deposition of unit 2, however at different times. C14 dating of unit 2 yield a calibrated age of A.D. 1446 (2σ age range: A.D. 1405-1634). Other two samples from unit 3 provided inconsistent ages; the upper sample dated to 2000 BC, while the lower yield a calibrated date of A.D. 1415. Based on these dating results Rockwell et al (2001), concluded that the two faulting events in T-1 post-date A.D. 1446 and may correspond to the earthquakes of 1509/1766 and 1912.

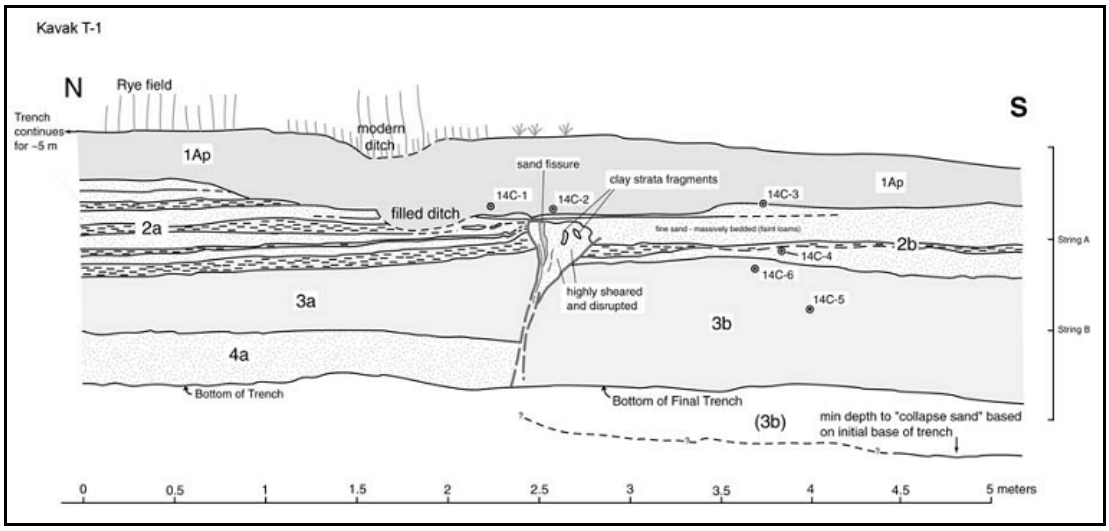


**Figure 6.36 :** Log of trench T-1 where two faulting events were determined (Rockwell et. al., 2001).

Trenches T2 and T5 were excavated east of the Kavak river within a year interval. They exposed a well-stratified section of sediments that record multiple earthquake rupture events and showed thicker sediment accumulation on the southern, down-throw side of the fault (Fig. 6.35 & 6.36). Five earthquake ruptures have been recognized in the upper 1.5 m of T-2 and T-5. Event 1 shears up to the base of the modern A horizon in trench T-2, but not in T-5. This events is unconstraint by radiocarbon dates, but has been correlated with the 1912 earthquakes because it penetrates into the uppermost soil part. Event 2 is considered to be occurred after the deposition of units G1 and F and is observed in both trenches. Unit D overlays the

fault scarps and is the event horizon. The age of this event is constrained with a comparison of events in T-1, because unit G5 was dated to A.D. 1020 which is considered to be too old for the event. Subsequently event 2 has been interpreted as one of the earthquakes of 1766 or 1509. Event 3 is also determined in both trenches. It truncates unit G4 but is overlain by unit G3. Radiocarbon dating of unit G4 and G2 yield older ages, therefore the age of event 3 is constrained to be younger than A.D. 1020 (unit G5).

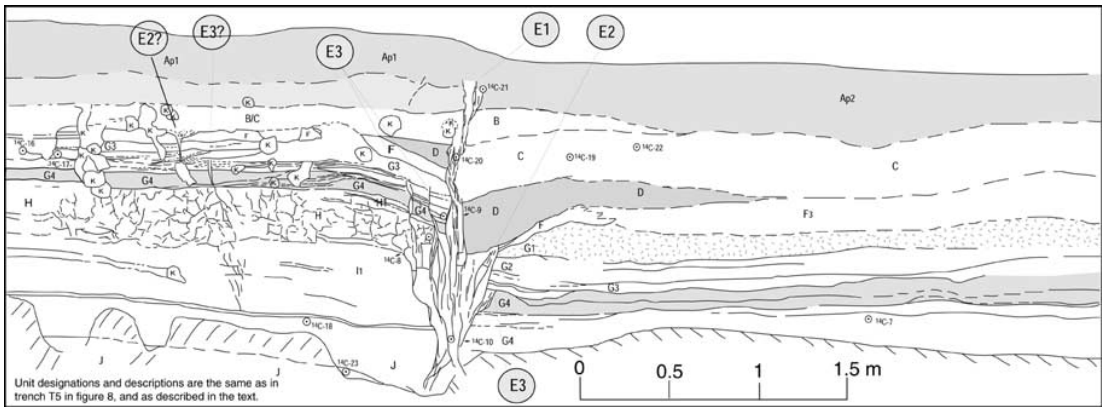


**Figure 6.37 :** Log of trench T-2 where three faulting events were determined (Rockwell et. al., 2001).

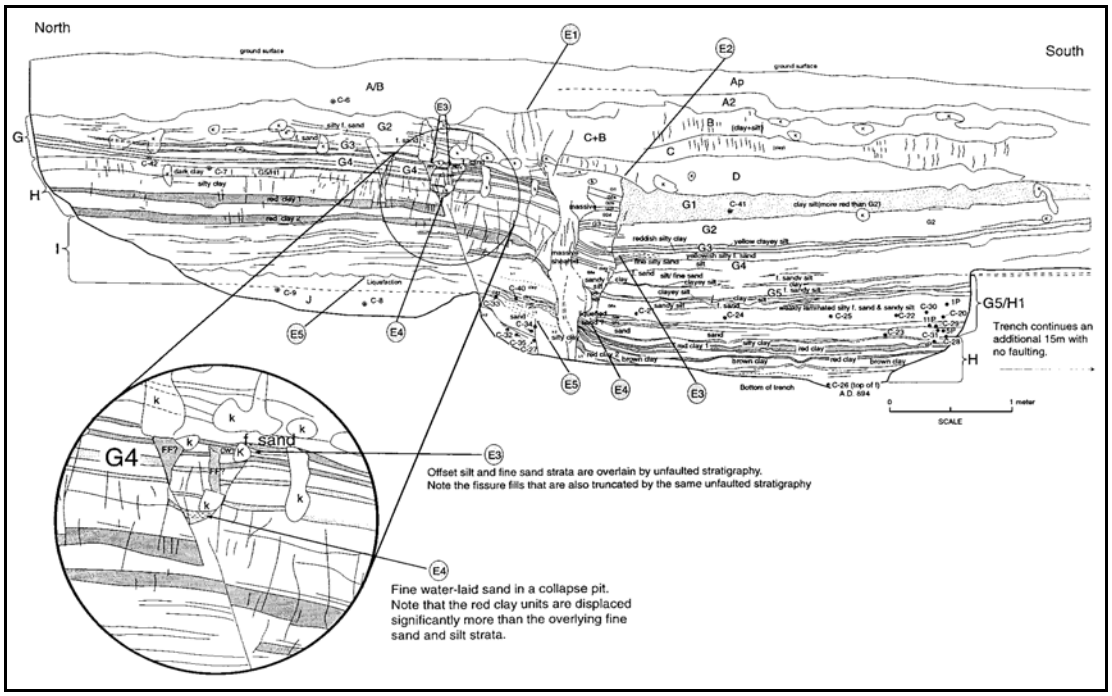


**Figure 6.38 :** Log of trench T-5 where four faulting events were determined (Rockwell et. al., 2001).

This event is interpreted as either the 1509 earthquake or one of the events of the 1343, 1344 and 1354 sequence. Event 4 is determined in T-5 and displaces unit H, but is overlain by unit G5. Unit H is dated to be younger than A.D. 791 and maybe as young as A.D. 1003. Unit G5 yield ages no older than A.D. 965 – 1163. Two possibilities are proposed for the age of this event. Taking the maximum age of unit H the event is considered to correspond to the earthquake in A.D. 824. However the mean age of H yield A.D. 894, in this case all four events post-date A.D. 900 and may correspond to earthquakes ca. 1350, 1509, 1766 and 1912.

**Trench results of Rockwell et al., (2009)**

Rockwell et al., (2009) opened 26 trenches east of the sagpond, where they identified an abandoned channel to the Kavak River that crosses the fault at a high angle. The site is known to have ruptured during the 1912 earthquake associated with lateral spreading and liquefaction (Ambraseys & Finkel, 1987; Mihailovic, 1927; Macovei, 1913).

Trenching at this site allowed documenting historical ruptures and resolving slip on the channel-fan complex. The trenches exposed a succession of young sediments. A distinctively clean, well-sorted channelized sand unit (Unit 200) is used as an offset marker. Dating results for units from 10-190 ranged from A.D. 600-1955, with no order in the section. Therefore, the entire section from unit 200 to surface is considered to be deposited in the past 350 years. Dating for unit 200 made from several samples constrain a larger uncertainty from about 1490-1530. This results that all samples constrain the sand to the past 500 years. Sample T6-43 from the channel is said to be no older than A.D. 1655. Therefore its age is constrained as A.D. 1655.

Two large surface ruptures were observed in T6, represented by liquefaction, brittle faulting, tilting, fissures and a narrow trough filled with sediments. Fractures extending to the base of unit 190 indicate a faulting event, which is overlain by well bedded stratigraphy of units 160-190. A massive fine sand unit, which is affected by liquefaction derived from a base unit, is overlain by unit 190. A depression is filled by units 160-190. The depression is interpreted as a direct result of surface rupture prior to 1912. The 1912 is represented by rupture and liquefaction of units 190 up to

160, to the base of 150. Units 110-150 accumulated within a trough along the fault. Unit 50 fills against scarp and 10-30 deposited after scarp.

Other trenches opened east of the highway exposed evidence for two earthquake ruptures (located 10 m next to Rockwell et al., (2001) trench T-1). Fractures extending up to unit 200 are overlain by ejecta 191 that derived from 200. Massive clean sand fills the main fault zone. The timing of the faulting is interpreted when unit 200 was on surface. Second event is represented by fractures displacing all units up through 160, including 191. Other liquefactions have been related with this event. Unit 100-130 fill against the scarp. Unit10-50 bury the scarp. The two events have been related with 1766 and 1912.

The fan represented by unit 200 is deflected downstream. The reconstruction of the fan apex and the deepest part of the channel resolved an offset of 9 ±1 m. A secondary smaller channel also reconstruct to a secondary fan apex and the margins of the channel. This amount of displacement is considered to represent two earthquake faulting events, which are interpreted to be the 1766 and 1912 event. Each event is estimated to have a slip of 4-5 m.

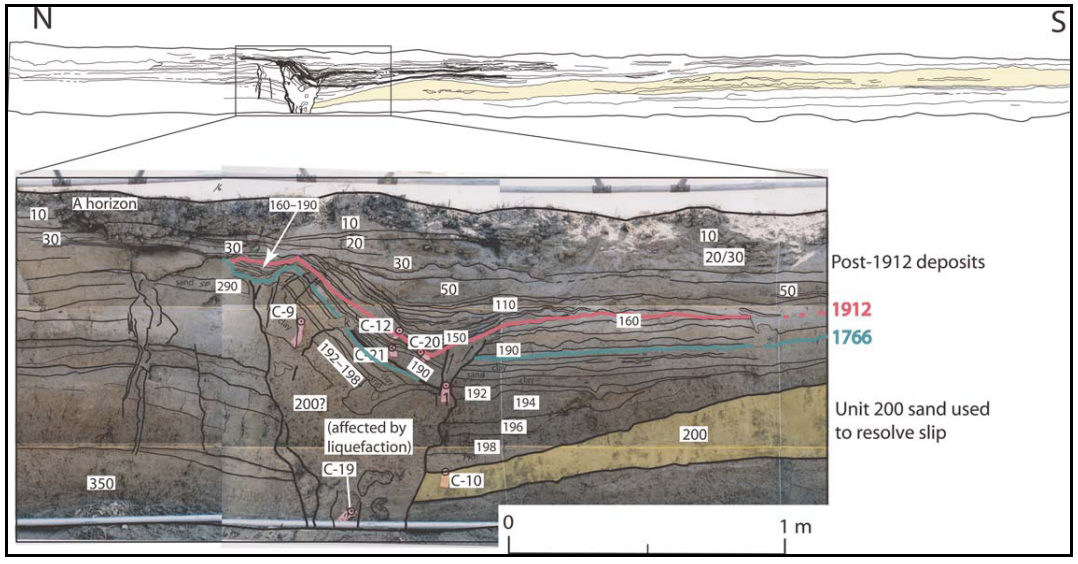


**Figure 6.39 :** Log of the eastern trench wall of T-6. The coloured lines represent the 1912 and 1766 event horizons. The unit 200 sand is the yellow shaded unit in the top diagram.

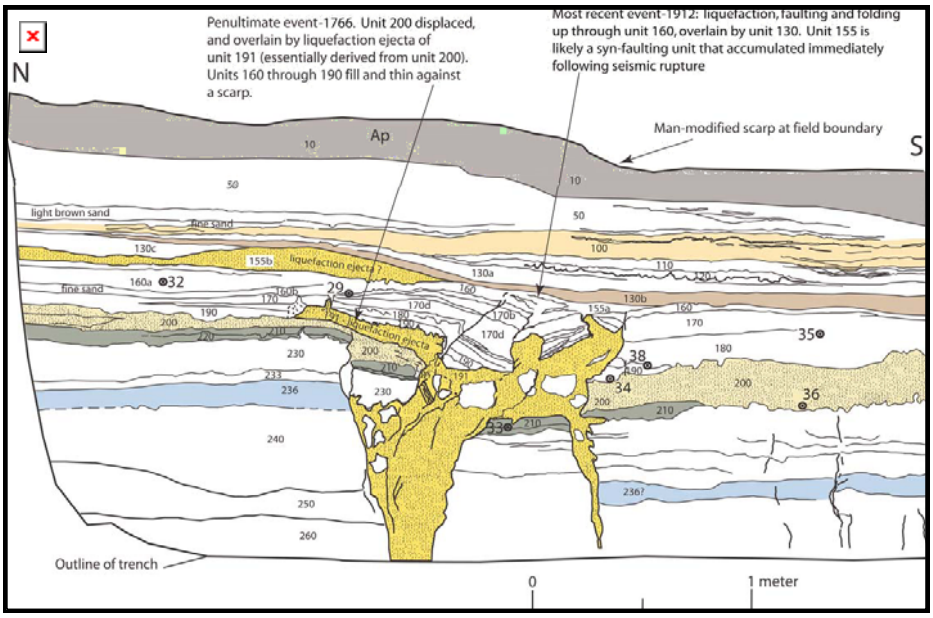


**Figure 6.40 :** Log of the eastern trench wall of T-25

The Saros trenches may not show clear evidence of 1912 related faulting however the 9 m laterally displaced channel deposits are younger than A.D. 1600. Two are known for this time The penultimate event of 1912 is either the 1659 or the 1766 and no other earthquake is known for that region. Co-seismic slip measurements of the 1912 earthquake yield offset ranging from 3 to 5.5. Considering a characteristic slip behaviour of 4.5 m for the Saros region, the 9 m.

## 6.5. Trenching Results along the Ganos Segment

The combined study of geomorphology with micro-topography and paleoseismic trenching provides some constraints on the timing of successive faulting and related past earthquakes of the westernmost segment of the North Anatolian Fault. Together with the studies of Rockwell et al., (2001 & 2009), four sites showed evidence of five earthquake events associated with significant amount of lateral slip along on the eastern, central and western parts of the Ganos fault for the last 2000 years. Historical earthquakes corresponding to that time frame are given in (Table 6.6). The listed events caused substantial damage in and around the Ganos region and may have caused surface faulting along the 45 km inland section of the Ganos fault.

**Table 6.6 :** List of historical earthquakes that affected the Ganos region.

| Date (y, m, d) | Ms | $I_o$ | Localities with heavy damage | Lat | Lon | Ref. |
|---|---|---|---|---|---|---|
| 477.08.25/ 484.09.00 | 7.2 | IX* | Çanakkale, Gelibolu, Saros | 40.8 | 29.5 | 1 |
| 1063.09.23 | 7.4 | IX** | Saros, Mürefte, Tekirdağ, İstanbul | 41.0 | 29.0 | 2 |
| 1343.10.18 | 7 | VIII** | İstanbul | 41.0 | 29.0 | 2 |
| 1344.11.06 | ? | IX** | Tekirdağ, İstanbul, | 40.7 | 27.4 | 2 |
| 1354.03.01 | 7.4 | X** | Çanakkale, Gelibolu, Saros, Tekirdağ | 40.6 | 26.9 | 2 |
| 1659.02.17 | 7.2 | | Tekirdağ | 40.5 | 26.4 | 2 |
| 1766.05.22 | 7.4 | | Istanbul, Bosphorus, Gulf of Mundaya, Bursa, Izmit, Tekirdağ | 41.0 | 29.0 | 2 |
| 1766.08.05 | 7.4 | | Bozcaada, Çanakkale, Gelibolu, Saros, Tekirdağ | 40.6 | 27.0 | 2 |
| 1912.08.09 | 7.3 | X | Gelibolu, Saros, Tekirdağ | 40.7 | 27.2 | 4 |
| 1912.09.13 | 6.9 | VII | Gelibolu, Saros, Mürefte | 40.7 | 27.0 | 5 |

### 6.5.1. Historical Seismicity

The analysis of past earthquakes in trenches at Güzelköy, Yörgüç, Yeniköy and Saros (site 1 & 2), yield comparable results (Table 6.7). The maximum number of events is observed at Güzelköy and Yeniköy, 5 and 6 respectively. Two trenches at Saros (2001) show 3 to 4 faulting events. The trenches at Yörgüç and Saros (2009) exposed 2 events. The difference is related to the time span of the exposed geologic records in the trenches. The 5 faulting events at Güzelköy postdate 1043 – 835 BC, which is very comparable with the 6 faulting events identified at Yeniköy postdating 1500 – 830 BC. The events may be younger because ages correspond to a maximum value. The ages of the 4 events recognized in the Saros trenches (Rockwell et al., 2001) are no older than A.D. 791 and may include the events observed at Güzelköy and Yeniköy. Similarly, the two events at Yörgüç and trenches in Saros (Rockwell et al., 2009) which postdate A.D. 1600 can be incorporated in the 6 events.

The timing of some events are well constrained by event horizons and units lain conformably above and below the event horizon that are dated with radiocarbon dating. The correlation of age constrained faulting events with the historical seismic catalogue is given in Table 6.7. The 1912 earthquake is observed at all trench sites with significant amount of faulting and related lateral slip. The penultimate event is identified at Güzelköy and at Saros (Trench T6). At Saros, the related dating puts the event post A.D. 1600 (unit 200), while at Güzelköy it dates post A.D. 1271 (unit d).

**Table 6.7 :** A comparison of trenches, observed number of events and their correlation with historical earthquakes at 4 sites (*Rockwell et al., 2001; **Rockwell et al., 2009)

| Site | | | Güzel-köy | Yeniköy | | Yörgüç | | Saros* (2001) | | | Saros** (2009) | |
|---|---|---|---|---|---|---|---|---|---|---|---|---|
| *Trenches* | | | *T1* | *T1* | *T2* | *T2* | *T3* | *T-1* | *T-2* | *T-5* | *T-6* | *T-25* |
| *Number of observ. EQ's* | | | 5 | 6 | 6-8 | 1 | 2 | 2 | 3 | 4 | 2 | 2 |
| *Historical EQ's* | *Ms* | $I_o$ | *Comparable EQ's* | | | | | | | | | |
| 477.08.25/484.09.00 | 7.2 | IX | ★? | | | | | | | | | |
| 824.05.05 | | VIII | | | | | | | | | | |
| 1063.09.23 | 7.4 | IX | | | | | | | | | | |
| 1344.11.06 | ? | IX | ★ | | | | | | | | | |
| 1354.03.01 | 7.4 | X | | | | | | | | | | |
| 1659.02.17 | 7.2 | | ★ | | | | | | | | ★ | |
| 1766.08.05 | 7.4 | | | | | | | | | | | |
| 1912.08.09 | 7.3 | X | ★ | ★ | ★ | ★ | ★ | ★ | ★ | ? | ★ | ★ |

Two historical events are known after 17th century affecting the Ganos-Saros region, the 1659 and 1766 earthquake. This event is either the 1659 or the 1766. The uncertainty in radiocarbon dating did not allow determining the corresponding historical earthquake. At Güzelköy unit d postdates actually two events prior to 1912. Therefore the second faulting event occurred pre 15-16th century and post 1271 (unit d). Here again the time frame coincides with two historical earthquakes, the 1344 and 1354 which we are not able to distinguish with the present C14 results. Another faulting event identified at Güzelköy (T1) is no older 79 A.D. Considering the stratigraphy the event is inferred to be the 484. The geologic record of 1063 is either eroded or the earthquake did not rupture this section of the Ganos fault.

### 6.5.2. Slip rate estimations from paleo-channels and other offset streams

The combination of geomorphic analysis and trenching results provides constrains on estimating the slip rate of the North Anatolian Fault at the Ganos region. Using paleo-channel and stream offsets and dated units from trenches we calculated slip rates for the Güzelköy and Yeniköy sites. At Güzelköy two paleo-channels offset for 16 m and 21 m yield 22.3 ± 0.5 mm/yr for the last ~700 years and 26.9 mm/yr for the last 781 years, respectively. In addition, dating from the lowermost units of the 46 ± 1 m offset stream at Yeniköy provided a maximum 17 mm/yr slip rate for the last 2840 years. From the trenches at Saros, Rockwell et al., (2009), calculated 15.8 mm/yr slip rate assuming a characteristic 4.5 m co-seismic slip for the last 6 events.

GPS velocities for this region reach 20 to 26 mm/yr (Mc Clusky et al, 2000; Reilinger et al., 2006). This value however is higher than geologic rates estimated at Yeniköy and Saros, but similar to the rate at Güzelköy. The slip rate estimations from Yeniköy and Saros sites are comparable (16-17 mm/yr) and are 5 to 10 mm/yr lower than Güzelköy. Bearing in mind the co-seismic slip distribution of the 1912 surface rupture it may be noticed that the co-seismic displacement was also significantly larger at Güzelköy than at Yeniköy and Saros. The co-seismic slip was measured as maximum (5.5 m) at Güzelköy, while near Yeniköy and at Saros the slip was 4.5 m. This observation suggests the idea of characteristic fault behaviour during earthquakes and may explain the discrepancy between geodetic velocity measurements and geologic slip rates. In addition, the 1912 slip distribution showed that the fault geometry plays a significant role in displacement. This was also observed along the 1999 earthquake rupture where the slip significantly decreased at step-over areas (Barka et al., 2002). The fault structure near Yeniköy shows a releasing step-over geometry, which would also explain the relatively low slip rate.

### 6.5.3. Recurrence interval of earthquakes in the Ganos region

Paleoseismic trenching revealed the presence of at least 8 faulting events along the Ganos fault. Eight historical earthquakes causing damage in the Ganos-Saros region are given in Table 6.6. Although with limited age constrain, the last three events are well documented in trenches at Güzelköy (T1) and Saros (T-6) which correspond to the 1912, 1766 or 1659 and 1344 or 1354 earthquakes. The uncertainty for the latter two events derives from the ambiguity of source estimations for historical earthquakes, which rely mostly on damage distribution. The 1766 and 1659 caused damage in the Ganos region, but the damage of the prior event extents eastwards towards Istanbul and the damage of the 1659 extends towards the Saros bay. Therefore they may correspond to rupture events situated next to each other. The same situation is present for the 1344 and 1354 earthquake, of which the 1354 affected the Ganos and Saros and the 1344 the Ganos and Tekirdağ regions. Such earthquake sequences are likely to occur along the North Anatolian Fault, as was experienced in 1999 (Barka et al., 2002; Akyüz et al., 2002). However, trenching along the Ganos fault shows that the two earthquakes of each sequence did not occur on the same fault section (at Güzelköy and Saros).

Two earthquake scenarios for the last six events which are thought to have ruptured the Ganos fault are given in Table 6.8. Scenario 1 yields five intervals ranging from 239 to 340 years with an average recurrence interval of 285 ± 36 years, whereas the five intervals in Scenario 2 range from 146 to 422 years and give an average recurrence interval of 285 ± 93 years. The last three faulting events at Güzelköy and the last ten events at Yeniköy are constrained by a lower boundary of 1271 A.D and 900 B.C, respectively. These results are in accordance with the obtained recurrence interval. In addition, at Saros Rockwell et al. (2009) suggests a 280 ±110 year interval.

The 1766 earthquake is attributed to the Ganos fault (Ambraseys, 2002), however other studies suggest and offshore location in the Sea of Marmara (Altınok et al., 2003; Yaltırak, 2009). In Scenario 2 the interval between 1766 and 1912 is nearly %50 shorter than the suggested recurrence interval. Taking into account the ~24 mm/yr GPS velocity for the western part of the North Anatolian Fault (Reilinger et al., 2006), and the 16 to 22 mm/yr geologic slip rates for the Ganos region (Rockwell et al., 2009 and this study) the 146 year time interval would allow a stress concentration of 2.5 to 3.5 m (Table 6.9). The arguments for an offshore location for the 1766 are mainly based on the inference that this value is nearly the half of the maximum offset of the 1912 (5.5 m; Altınok et al., 2003; Yaltırak, 2009). It should be noted that this may be possible if the earthquakes along the Ganos fault are not characteristic and co-seismic slip varies among subsequent events. However we know from the trenches at Güzelköy and Saros that each of the last two events produced 4 to 5 m displacement. Therefore we have more evidence to consider a characteristic slip model.

**Table 6.8 :** Two earthquake recurrence scenarios are suggested from the trenching and historical catalogue analysis.

| **Scenario 1** | | **Scenario 2** | |
|---|---|---|---|
| **Earthquakes (date)** | **Interval (years)** | **Earthquakes (date)** | **Interval (years)** |
| 484 | | 484 | |
| 824 | *340* | 824 | *340* |
| 1063 | *239* | 1063 | *239* |
| 1344/1354 | *286 ±5* | 1344/1354 | *286 ±5* |
| 1659 | *305* | 1766 | *422* |
| 1912 | *253* | 1912 | *146* |
| ***Mean recurrence:*** | ***285*** | ***Mean recurrence:*** | ***285*** |
| *Standard Dev.:* | *36* | *Standard Dev.:* | *93* |

Another critical assumption is whether the accumulated strain energy is totally released during an earthquake or if some of the energy may be preserved. In Scenario 2 the interval between the 1354, 1766 and 1912 is 422 and 146 years respectively. 422 years imply ~8 m of strain accumulation, while 146 years store 2.5 m slip (Table 6.9). If the characteristic slip behaviour is preserved the 1766 event would have released only 5.5 m o slip and 2.5 m would be retained for the next event. During the following 146 years 2-3 m slip would be added and the 1912 maximum co-seismic would be achieved.

**Table 6.9 :** Considering two average slip rates we calculate the slip accumulation for the suggested recurrence interval. Similarly we calculate the required time to accumulate the average and maximum slip value of the 1912 earthquake that we assume to represent the characteristic behaviour of the Ganos fault.

| **Recurrence interv.** | **Accumulated slip for 17 mm/yr** | **Accumulated slip for 24 mm/yr** |
|---|---|---|
| ***285 years*** | 4,8 m | 6,8 m |
| **Characteristic co-seismic slip** | **Geologic slip rate (17 mm/yr)** | **Geodetic velocity (24 mm/yr)** |
| ***5.5 m*** *(max)* | 324 years | 229 years |
| ***2.5 m*** *(mean)* | 146 years | 104 years |
| ***2.0 m*** *(mean)* | 118 years | 83 years |

A simpler and preferred solution is considering characteristic and periodic fault behaviour. Then the 285 years earthquake recurrence implies 5 to 6 m of slip accumulation per event, which is comparable with the 1912 slip distribution and the offsets measured for the last two events.

As a result it is essential to enlarge the current paleoseismic data along the Ganos fault with new sites where precise dating of the above mentioned events is possible; particularly to refine the relation and location between the 1344, 1354, 1659, 1766 and 1912 events. In addition a longer detailed event chronology would allow the confirm the result for more recent events.

# 7. HISTORICAL SEISMOGRAM ANALYSIS OF THE 1912 EARTHQUAKE SEQUENCE

## 7.1. Introduction

The 1912 Mürefte earthquake occurred at an early stage of seismological research. At that time, earthquake recording was accomplished by primitive seismographs which were continuously experimented and developed. Different from today's standardized seismometers, stations were operating with various types of seismographs; i.e. Milne-, Ewing-, Omori-, Bosch-Omori-, Imamura-, Vasca sismica-, Rebeur-Ehlert-, Agamennone-, Galitzin-, Wiechert-, Vincentini-, Grablovitz-, Mainka-instruments. All were functioning with different characteristics but were recording seismic waves. The value of these recordings can not be ignored because they are the only source for the seismic parameters of earthquakes of that time. The 1912 earthquakes were also registered by several of these instruments. The contemporary analyses of old seismograms predate fundamental developments in quantitative seismology and are therefore very primitive. However, present techniques and methods in modern seismology allow comprehensive analysis of the earthquake phenomena (Kanamori, 1988; Kanamori and Brodsky, 2004). A reanalysis of old seismograms, integrated with modern methods may provide key information for kinematics and seismic parameters of the 1912 earthquakes (Batllo et al., 2008). Therefore we collected seismograms of the largest shocks of the 1912 earthquake sequence.

## 7.2. The Collection Procedure of Historical Seismograms

As an essential and initial step to collect the historical seismograms we investigated the number and location of seismic stations active in 1912. The Seismological Archives Working Group of the International Association of Seismology and Physics of Earth Interior (IASPEI) provide a list of stations around the world operating between 1889 and 1920. The list shows that 143 stations were active with at least one seismograph in 1912. Figure 7.1 illustrates the distribution of the stations. It is noticeable that most stations were located in Europe and United States. The stations

cluster mostly towards northwest and west of the epicentre. However several stations are also present on the east and southeast. We contacted several seismological institutions and observatories and requested historical seismograms for the events given in Table 7.1. We collected 73 seismic records of the 9 August and 13 September shocks. The majority of the records are from European stations located northwest and west of the epicentre. However, we also received recordings from Japan, Australia and Russia which correspond to the East, Southeast and North of the epicentre. Most of the records were obtained from the SISMOS database established by the *Istituto Nazionale di Geofisica e Vulcanologia* INGV. The database is a unique free online archive where historical seismograms were available in raster format with a minimum resolution of 600 dpi.

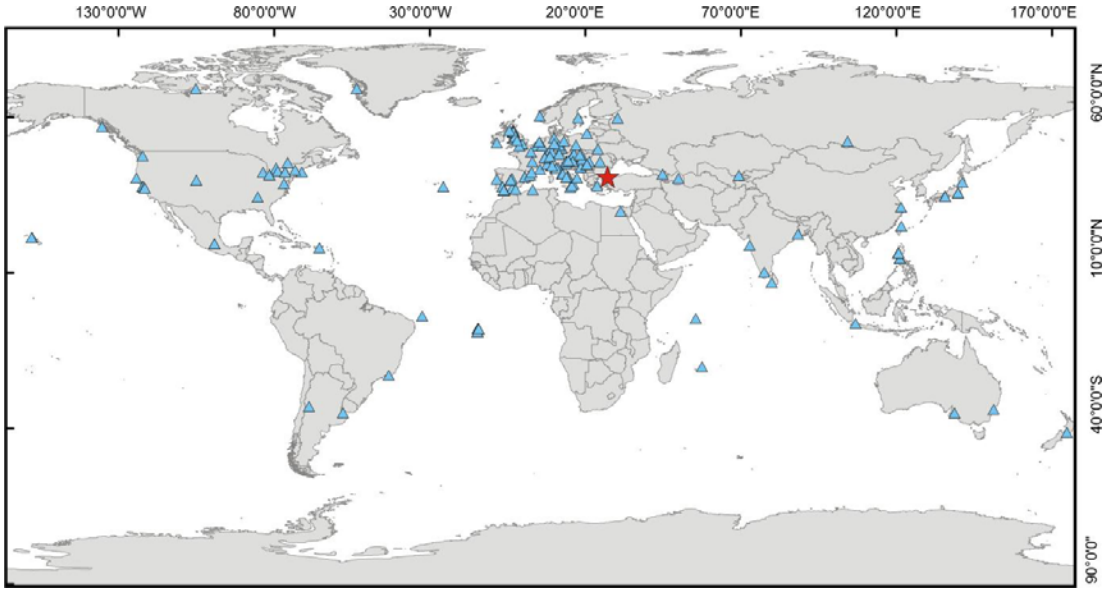


**Figure 7.1 :** Distribution of the 143 stations (blue triangles) that were operating in year 1912. The red star indicates the epicentre area for 1912 events.

**Table 7.1 :** List of earthquakes of the 1912 sequence for which seismograms were requested (see also Fig 7.3).

| Date | Time (GMT) | Ms | Lat | Lon |
|---|---|---|---|---|
| 1912.08.09 | 01:29 | 7.4 | 40.70 | 27.20 |
| 1912.08.10 | 09:23/23:31 | 6.2 | 40.80 | 27.50 |
| 1912.08.10 | 18:30 | 5.3 | 40.60 | 27.10 |
| 1912.09.13 | 09:23 | 6.8 | 40.70 | 27.00 |

From the SISMOS database we downloaded more than 100 seismograms that cover the recording period of the events given in Table 7.1. We noticed that some seismographs did not register the events, while another nearby station or even adjacent instrument had a significant record. We consider that this is related to different instrument characteristics or adjustments. Together with direct requests we obtained 56 and 17 registrations of the 9 August and 13 September shocks, respectively (Table 7.2 & 7.3).

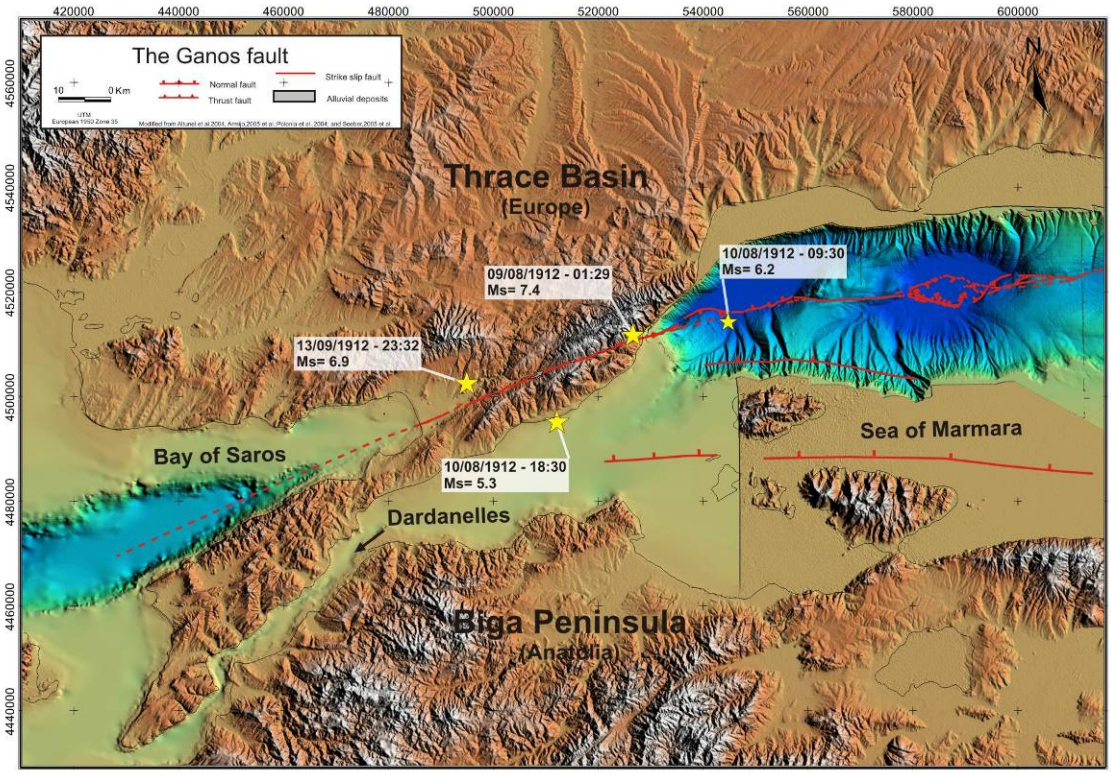


**Figure 7.2 :** Location of earthquakes given in Table 7.1 (after Ambraseys, 2002)

### 7.3. Record Selection and Instrument Characteristics

As mentioned previously, different types of instruments were present at the time of the earthquake and recording characteristics varied not only among different types of instruments but also among the same seismograph. Basically all instrument record seismic oscillations using an arm as a pendulum and record on a paper media (i.e. smoked paper, photometric paper). The paper media is usually attached on drum which turns with a constant velocity (Fig 7.2). In parallel, the recording arm/needle moves laterally (perpendicular to the drum turn direction) allowing a continuous helicoidally. registration from one edge to the other of the paper media. However several parts and parameters of the described system vary among instruments.

**Table 7.2 :** List of seismograms for the 9 August 1912 earthquake.

| No | Country | City | Station Code | Component | Seismograph |
|---|---|---|---|---|---|
| 1 | Australia | Sydney | RIV | E-W | Wiechert |
| 2 | Australia | Sydney | RIV | N-S | Wiechert |
| 3 | Australia | Sydney | RIV | E-W | Mainka |
| 4 | Australia | Sydney | RIV | N-S | Mainka |
| 5 | Georgia | Tbilisi | TIF | N-S | Galitzin |
| 6 | Georgia | Tbilisi | TIF | E-W | Galitzin |
| 7 | Germany | Göttingen | GTT | E-W | Wiechert |
| 8 | Germany | Göttingen | GTT | N-S | Wiechert |
| 9 | Germany | Göttingen | GTT | Z | Wiechert |
| 10 | Germany | Jena | JEN | E-W | Wiechert |
| 11 | Germany | Potsdam | POT | E-W | Wiechert |
| 12 | Germany | Potsdam | POT | N-S | Wiechert |
| 13 | Italy | Chiavari | CHV | E-W | ? |
| 14 | Italy | Chiavari | CHV | N-S | ? |
| 15 | Italy | Chiavari | CHV | E-W | ? |
| 16 | Italy | Chiavari | CHV | N-S | ? |
| 17 | Italy | Firenze | FIR | E-W | ? |
| 18 | Italy | Firenze | FIR | N-S | ? |
| 19 | Italy | Ischia | IC1H | N-S | Vasca sismica |
| 20 | Italy | Ischia | IC1H | E-W | Vasca sismica |
| 21 | Italy | Ischia | IS1H | N-S | Vasca sismica |
| 22 | Italy | Ischia | IS1H | E-W | Vasca sismica |
| 23 | Italy | Taranto | TA1H | E-W | Wiechert |
| 24 | Italy | Taranto | TA1H | N-S | Wiechert |
| 25 | Japan | Tokyo | HGJ | E-W | Omori |
| 26 | Japan | Tokyo | HGJ | E-W | Omori |
| 27 | Japan | Tokyo | HGJ | E-W | Omori |
| 28 | Japan | Tokyo | HGJ | N-S | Omori |
| 29 | Japan | Tokyo | HGJ | E-W | Ewing |
| 30 | Japan | Tokyo | HGJ | Z | Imamura |
| 31 | Japan | Tokyo | HGJ | E-W | Imamura |
| 32 | Japan | Tokyo | HGJ | N-S | Imamura |
| 33 | Netherlands | de Bilt | DBN | N-S | Galitzin, Wiechert, Bosch |
| 34 | Netherlands | de Bilt | DBN | E-W | Galitzin, Wiechert, Bosch |
| 35 | Norway | Bergen | BER | Hor. | Bosch-Omori |
| 36 | Norway | Bergen | BER | Hor. | Bosch-Omori |
| 37 | Russia | Irkutsk | IRK | E-W | ? |
| 38 | Russia | Irkutsk | IRK | N-S | ? |

**Table 7.2 :** (continued) List of seismograms for the 9 August 1912 earthquake.

| | | | | | |
|---|---|---|---|---|---|
| 39 | Russia | Pulkovo | PUL | E-W | ? |
| 40 | Russia | Pulkovo | PUL | N-S | ? |
| 41 | Russia | Pulkovo | PUL | Z | ? |
| 42 | Spain | Ebro | EBR | NW-SE | Grablovitz |
| 43 | Spain | Ebro | EBR | NE-SW | Grablovitz |
| 44 | Spain | Ebro | EBR | N-S | Vincentini |
| 45 | Spain | Ebro | EBR | E-W | Vincentini |
| 46 | Spain | Ebro | EBR | Z | Vincentini |
| 47 | Spain | Toledo | TOL | E-W | Bosch |
| 48 | Spain | Toledo | TOL | N-S | Bosch |
| 49 | Spain | Toledo | TOL | E-W | Agamennone |
| 50 | Spain | Toledo | TOL | N-S | Agamennone |
| 51 | Spain | Toledo | TOL | Z | Agamennone |
| 52 | Spain | Toledo | TOL | E-W | Milne |
| 53 | Spain | Toledo | TOL | E-W | Rebeur-Ehlert |
| 54 | Sweden | Uppsala | UPP | E-W | |
| 55 | Sweden | Uppsala | UPP | N-S | |
| 56 | United Kingdom | Paisley | PAI | Hor. | Milne |

**Table 7.3 :** List of seismograms for the 13 September 1912 earthquake.

| No | Country | City | Station | Component | Seismograph |
|---|---|---|---|---|---|
| 1 | Italy | Chiavari | CHV | E-W | ?A |
| 2 | Italy | Chiavari | CHV | N-S | ?A |
| 3 | Italy | Ischia | IC1H | N-S | Vasca sismica |
| 4 | Italy | Ischia | IC1H | E-W | Vasca sismica |
| 5 | Italy | Ischia | IC1H | N-S | ? |
| 6 | Italy | Ischia | IC1H | E-W | ? |
| 7 | Italy | Ischia | IS1H | N-S | Vasca sismica |
| 8 | Italy | Ischia | IS1H | E-W | Vasca sismica |
| 9 | Italy | Ischia | IS1H | N-S | ? |
| 10 | Italy | Ischia | IS1H | E-W | ? |
| 11 | Italy | Taranto | TA1H | E-W | Wiechert? |
| 12 | Italy | Taranto | TA1H | N-S | Wiechert? |
| 13 | Italy | Taranto | TA1H | E-W | Wiechert? |
| 14 | Italy | Taranto | TA1H | N-S | Wiechert? |
| 15 | Norway | Bergen | BER | Hor.? | Bosch-Omori |
| 16 | Spain | Ebro | EBR | NW-SE | Grablovitz |
| 17 | Spain | Ebro | EBR | NE-SW | Grablovitz |

A proper analysis of historical seismograms requires knowing certain instrument parameters:

- To = natural period of the pendulum in seconds
- V = amplification
- ε = damping coefficient
- r = solid friction of the registering needle given in millimetres
- Turning speed of the seismogram (drum).
- Lateral velocity of the recording arm.
- Others

These parameters are available in the bulletins of seismological stations or are enclosed to seismograms. However, in most cases the essential parameters are not accessible, because they are not registered, lost or insufficiently noted. To avoid complications due to missing instrument information we decide to apply the Empirical Green Function (EGF) approach by Vallee (2004); suggested by Bouchon M. (personal communication, 2005). Therefore we selected stations from which we could obtain registrations of at least two events; the 9 August , the 13 September and/or other events on 10 August (Fig. 7.3). Among 73 seismograms only records from Bergen (BER), Ebro (EBR), Ischia (IC1H), Chiavari (CHV) and Taranto (TA1H) contained comparable signal pairs (Appendix 3A).

**Bergen (BER) – Norway**

Three seismograms recorded by a Bosch instrument were collected from the Bergen station. Two of the records are the East and North horizontal components of the 9 August shock (exact components information of records are missing). The third record corresponds to the 13 September shock. It is also a horizontal component, but if east or north is not known. All registrations have a clearly visible signal which can be followed from start point until the end. The minute marks of the instrument are also distinct.

**Ebro (EBR) – Spain**

Two different instruments, Grablovitz and Vincentini recorded the 9 August and 13 September shock at Ebro station. The Grablovitz seismograph registered the northwest and northeast horizontal components. The signal is apparent for both events. The 9 August shock was recorded fully by both components with only a small missing part towards the end. However the 13 September shock is only noticeable on the northwest component with minor amplitudes. The minute marks

are clear to read. The Vincentini seismograph registers three components; east, north and vertical component. The east and west components show a apparent signal for the 9 August shock, however the vertical component shows only a minor oscillation. The signal of the 13 September is readable for the east and north components, but the vertical component did not register any movement. Minute marks are easily accessible on for both events.

**Taranto (TA1H) – Italy**

The seismograms of the Taranto station are from a Wiechert instrument. Three earthquake registration were obtained from this station; 9 August, 10 August and 13 September. All seismograms have a clear signal with a complete record of all events. The 9 August record is clipped at high amplitudes because the oscillating arm reached the registration limits of the instrument when surface waves arrive. However the bodies waves are well recorded in the signal and may be of use.

**Chiavari (CHV) – Italy**

When the Chiavari station was established in 1909 four seismographs were operating in the observatory; two Agamennone seismographs, a vertical pendulum built by Bianchi and an Alfani seismograph (Ansaloni, 2006). The seismograms we collected are from the SISMOS database and instrument information are missing on the records. Therefore we could not identify to which instrument these recordings belong. Based on the presence of two components (most probably horizontal) we consider that the registrations belong to a Agamennone instrument. Two seismograms for the 9 August and 13 September shocks were available. The signals for both events are clear visible. The signal of the 9 August shock is shifted on one component, while the other component and the signals for 13 September are well registered.

**Porto d'Ischia (IS1HD) – Italy**

The Ischia records belong to the 9 August and 13 September shocks, registered by a horizontal pendulum. The 9 August signal is incomplete for both components. The signal breaks when the first high amplitude is registered. This occurs when the recording arm is displaced over its maximum amplitude, which is in this record caused most probably by surface waves. The first wave train however is well

recorded on at least one component which could be of use. The signal of the 13 September shock is complete and readable for both components.

Important note: The Ischia and Chiavari records were very recently obtained and could not be included into the digitization and modelling process.

### 7.4. Characteristics of Recording System, Signal Deformation and Correction Procedure

The standard mechanism of primitive seismographs is based on an oscillating arm with a needle at the end that registers seismic movements on a smoked paper placed on a turning cylinder. The needle is fixed at the extremity of an arm and the needle movement corresponds to the intersection between a cylinder and a sphere. This geometry induces a curved deformation of the signal (Fig 7.3, Schlupp, 1996). The curvature is worst in case of great amplitude signal and occurs due to the finite arm length and finite radius of the cylinder bearing the smoked paper (Pintora & Quintiliani, 2007). Furthermore, the equilibrium position of the arm is usually not aligned with the seismogram trace. This adds an inclination to the signal (Fig. 7.3, Schlupp, 1996). To correct the finite distortion we use Teseo2 software which offers a function that creates a corrected path from a curved one. The algorithm in Teseo2 is from Cadek, (1987), while the code was originally written in FORTRAN by Schlupp (1996). The algorithm needs some parameters, while a few of them are suggested. Some of these parameters can be measured or calculated directly from the seismogram. The drum speed and lateral velocity can be retrieved by measuring the distance between the minute marks on the signal and the distance between two parallel signals, respectively. The drum speed range is fixed by the type of the instrument, therefore measurements should not exceed the common range for the instrument. For instance, Wiechert seismographs turn speed range from 10 to 30 mm/min, while the lateral speed is constant at 4.5 mm/min. The radius of the drum (r), the arm length (R), and the distance from the rotating arm axe to the driving cylinder axe (a) depends on the type of instruments and can be retrieved from manufacturer catalogues. In cases where arm length (R) is not available, an approximate value can be deduced from signals where high amplitudes show distinct curvature; best in high frequency signals. If we simplify the recording system, the curve represents basically an arc of a circle. Using tangents to the circle the point of rotation of the arm can be recovered (Fig. 7.3).

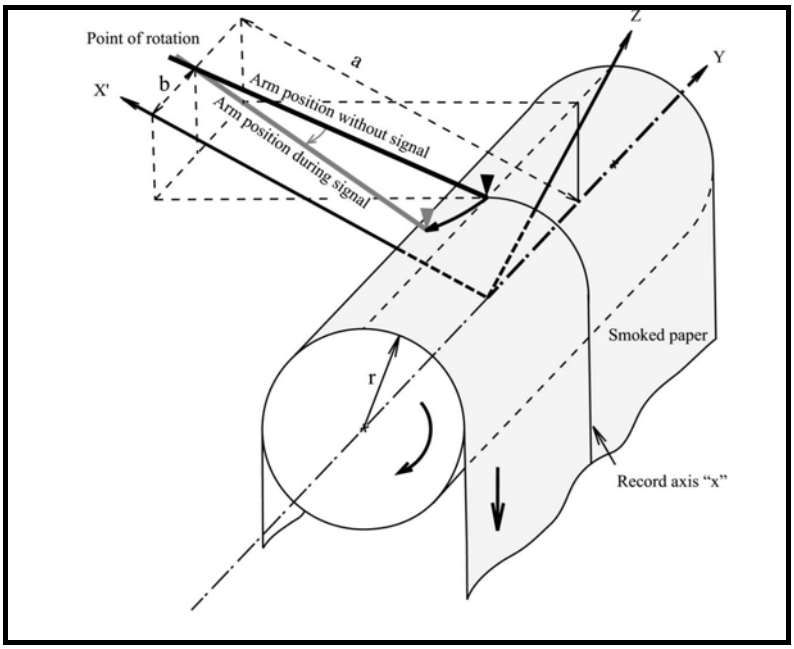


**Figure 7.3 :** The mechanical recording schema of old seismograph and important parameters of components used for signal corrections (Schlupp, 1996).

- R = length of the writing arm, from its rotating axis to the tip of the needle
- r = radius of the drive cylinder bearing the smoked paper
- a = distance from the rotating arm axis to the driving cylinder axis
- b = shift of the arm axis, in millimetres, to the base line on the smoked paper
- d = minute length on the original record in millimetres
- x(i) = coordinate to transform in seconds for time axis
- y(i) = coordinate to transform in millimetres for amplitude axis

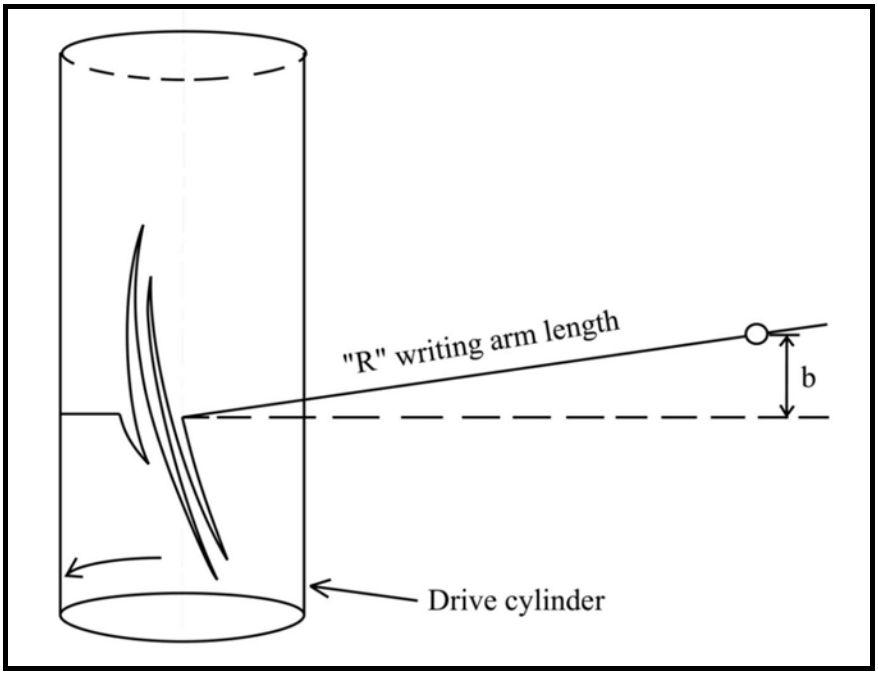


**Figure 7.4 :** Illustration showing how curvature occurs during recording and which parameters are important for correction (Schlupp, 1996)

In cases where the recording arm is not aligned to the signal, the shift of the arm can be deduced with the same geometric approach. As the first step of the digitization procedure we scanned all obtained seismograms with 600 to 1200 dpi resolution and saved in TIFF format. Seismograms downloaded from the SISMOS database are also at 1200 dpi resolution and in TIFF file format. During scanning a common rotation occurs while placing the seismogram into the scanner. Therefore we aligned all signals by rotating them to a fixed horizontal reference line using graphic software Photoshop. To digitize the signal we use Teseo2 software that is a plug-in designed for the free graphic software GIMP. The signal is redrawn as a path (vector). Afterwards we initiate the Curvature Correction function and input the following parameters for the related seismograms; paper speed, lateral speed, arm length, arm shift and cylinder radius.

Geometric corrections were essential particularly for the Bergen and Taranto records. Figure 7.5, 7.6 and 7.6 show the original and corrected records for seismic signals of the 9 August and 13 September from both stations. The corrected signals are exported as sac formats for signal modelling.

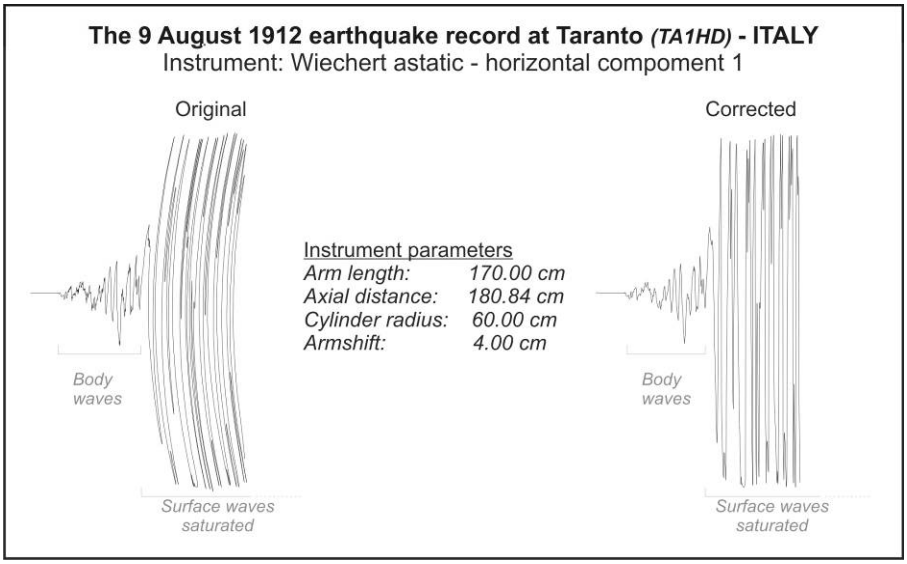


**Figure 7.5 :** The original and corrected seismogram of the 9 August 1912 earthquake recorded at Taranto station – Spain.

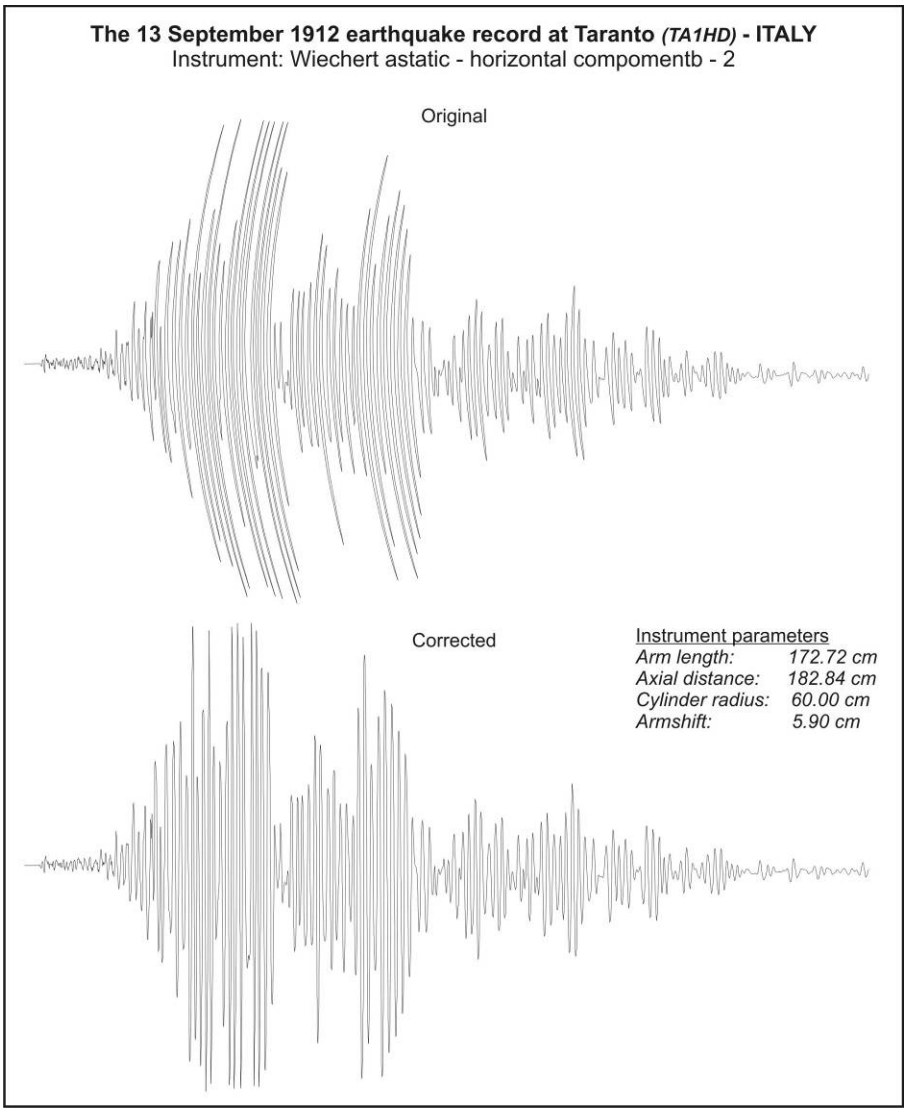


**Figure 7.6 :** The original and corrected seismogram of the 13 September 1912 earthquake recorded at Taranto station – Spain.

As a result we established digitized and corrected seismic signal for 3 stations; Ebro, Taranto and Bergen (seismograms of Ischia and Chiavari were not retrieved at that time). The number of corrected digital signals for the 9 August, 10 August and 13 September shocks are 9, 6 and 7, respectively; 22 in total.

## 7.5. Signal Processing and modelling

The modelling of historical seismic signals require additional parameters to be input in the process. Some necessary parameters are:

- To = natural period of the pendulum in seconds
- V = amplification
- ε = damping coefficient

These parameters can be obtained from bulletins or are sometimes indicated on the seismogram it's self. In most cases this information is difficult to access because the bulletins of the time of the event are missing or not indicated in related documents. Two avoid complications due to missing instrument information we apply the Empirical Green Function (EGF) approach by Vallee (2004) as suggested by Bouchon M. (personal communication, 2005). This technique uses the signal of a smaller event to model the Green function of the main earthquake. The request for the smaller event is to be at least one degree in magnitude smaller than the mainshock and to have a similar location and focal mechanism (Valleé & Di Luccio, 2005). In addition, since the events are recorded by old fashioned seismographs other prerequisites are identical instruments, recording component and device adjustments for any chosen pairs. The technique described by Valleé (2004), stabilizes the classical deconvolution between the mainshock and the EGF in order to obtain more reliable Relative Source Time Functions (RSTFs). If these RSTFs, are obtained at various azimuths they can give information on the source process itself. With this objective we digitized seismograms for the 1912 earthquake sequence.

The processing step was accomplished with the contribution of Martin Valleé, who kindly applied his method on the corrected 22 signals in sac format.

### 7.6. Results on the Seismogram Analysis

Due to limitations by the applied method and majorly because of limitations (insufficiency) of signal corrections our modelling revealed reliable results only for the Taranto station.

The signals of the 9 August and 13 September shocks of Taranto station provides a relative source time function (Fig. 7.7). The modelling indicate that the moment ration between the 9 August and 13 September shocks is about 30 which corresponds to 1 degree difference in magnitude (i.e., Mw 6.4 for the second shock) and infer 40 sec. for the 9 August source duration (7.7).

The 40 second source duration obtained from the relative source time function implies ~ 120 km coseismic rupture length if an unilateral rupture propagation at 3 km/sec is attributed to the 9 August earthquake. The source duration and suggested rupture length is comparable with the size of the shock (Mw = 7.4).

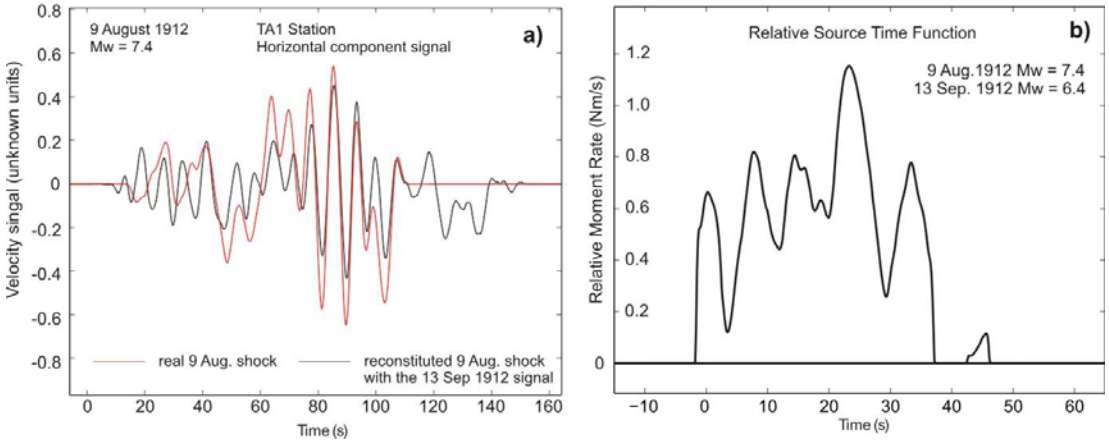


**Figure 7.7 :** Results of the signal processing using 13 September shock to model the Green Function of the 9 August shock. a) comparison of real and modelled signal of the 9 August shock, b) Relative Source Time Function of the two earthquakes indicating 40 second rupture duration for the 9 August event.

In addition to the modelling, we use P-wave polarities at 5 stations to construct a focal mechanism for the 9 August 1912 earthquake. The vertical component seismograms from Göttingen (GTT), Toledo (TOL), Ebro (EBR), Pulkovo (PUL) and Hongo (HGJ) and field based N68°E fault strike allow us to construct the focal mechanism solution shown in figure 5.18. The pure strike slip solution we obtained is in agreement with the known fault kinematics and slip measurements.

## 8. CONCLUSION AND RECOMMENDATIONS

We investigated the structural and tectonomorphic characteristics of the Ganos fault and the co-seismic deformation related to the 9 August 1912 Mürefte earthquake; as well as its source characteristics. For that purpose, the entire onland fault zone has been mapped at a 1/25.000 scale using field observation and remote sensing software and data. The surface rupture and related co-seismic displacements of the 9 August 1912 Mürefte earthquake are documented at several localities. In addition the instrumental recordings of the 1912 earthquake sequence are collected in order to extract source characteristics of the largest shocks. We applied paleoseismic trenching at 3 sites in order to document the 1912 earthquake and prior events along the Ganos fault. Here, we summarize results of the related chapters and provide an overall conclusion on the characteristics of the westernmost onland extension of the North Anatolian Fault.

**1a** - Geomorphic analysis along the 45-km-long onland section of the Ganos fault allowed documenting typical structures of right lateral strike slip faulting; i.e. step-overs, pull-aparts, bends, pressure ridges, offset ridges, shutter ridges and stream displacements. Cumulative displacements determined at 69 localities and tectonic reconstructions provide insight of the long term and short term deformation characteristic of the Ganos fault segment. A classification of the stream offsets and correlations with climatic events deduced from Black Sea sea level curves showed well correlations of consecutive 5 cumulative slip groups (from 70 to 300 m) with subsequent sea level rise periods at 4 ka, 10.2 ka, 12.5 ka, 14.5 ka and 17.5 ka. Slip rate estimations yield a constant slip rate of 17.9 mm/yr for the last 20.000 years and a variable slip rate of 17.7 mm/yr, 17.7 mm/yr, 17.9 mm/yr and 18.9 mm/yr for the last 10.2 ka, 12.5 ka, 14.5 ka and 17.5 ka respectively. The results are similar with slip rates obtained from the paleoseismic trenching sites in this study (18 - 27 mm/yr). Although indirectly dated, these values provide for the first time a slip rate for the Ganos fault; the westernmost section of the North Anatolian Fault. Studies along the eastern parts of the North Anatolian Fault yield rates 15 to 25 mm/yr that

are comparable with our estimations (Puchi et al., 2008, Kozaci et al., 2007 & 2009, Hubert-Ferrari et al., 2002). Furthermore, over the short period, geodetic measurements suggest 17 to 26 mm/yr strain accumulation along the North Anatolian Fault that are in the same range as the geologic rates (Kahle et al., 1998; Straub et al., 1997; McClusky et al., 2000; Reilinger et al., 1997 & 2006).

**1b** - The suggested 9 km valley offset based on morphologic analysis has important implications on the age of the western part of the North Anatolian Fault. Şengör et al, (2005) and Le Pichon et al., (2001) show an 4 ±1 m offset feature in the Sea of Marmara which they assume to be the total offset of North Anatolian Fault in this area. Using an average constant slip rate of 19 mm/yr they extract a 200 ka age for the North Anatolian Fault in the Sea of Marmara. A substantiation of a 9 ± 1 km offset along the Ganos fault would suggest necessarily an older age for the North Anatolian Fault as also proposed by Armijo et al (1999).

**2 a** – We provide detailed field and seismological data for the 9 August 1912 Mürefte earthquake ($M_s$=7.3) and emphasize the presence of a second large shock on 13 September 1912 ($M_s$=6.8) with an epicentral region to the west of the first main shock. The 9 August shock was responsible of severe destruction ($I_o$ = X) between Tekirdag and Çanakkale, while the 13 September caused $I_o$ = VII damage west of Gaziköy and along the Gallipoli peninsula. Surface breaks have been recorded along the entire 45-km-long onland section of the Ganos fault. Co-seismic offsets at 45 sites provide a maximum slip of 5.5 m which was previously suggested as 3 m (Ambraseys & Finkel et al, 1987). 5 m right-lateral displacement was measured on the eastern coast and 4.5 m on the western coast (Rockwell et al., 2009). We extend the slip measurements of Altunel et al., (2004) from 31 localities to 45 with a better distribution along the fault. The offset distribution indicates that a certain length of the rupture is offshore; in the Saros bay and Sea of Marmara. Combined with submarine fresh fault scarps and offsets (Armijo et al., 2005; Ustaömer et al., 2008) we suggest a 150-km-long earthquake segment that consist of minimum of 4 sub-segments limited by geometrical complexities in which the Saros Trough and the Central Marmara basin are the largest and may serve as barriers to arrest rupture propagation.

**2b)** The magnitude and related seismic moment suggests 120 ± 20 km and 30 ± 10 km rupture length for the 9 August and 13 September shocks, respectively (Aki, 1966, Kanamori, 1977). In addition, the 40 second source duration obtained from relative source time function for the 9 August event implies 120 km rupture length considering 3 km/s unilateral rupture propagation, which consistent with the earthquake size ($M_w$ 7.4). The total 150 ± 20 km rupture length deduced from the earthquake magnitude is equivalent to the size of the earthquake segment determined from onland and offshore morpho-tectonic analysis.

**2c)** Based on prior epicentre estimations, damage distribution, field observation, seismological data and contemporary document we locate the 13 September epicentre between the Saros Trough and Kavak and think it ruptured the adjacent fault section of the 9 August rupture. Considering a rupture length of 120 km and the suggested eastern termination point from Le Pichon et al. (2003) and Altınok et al. (2003) for the first shock requires the 13 September earthquake epicentre be located far west beyond the Dardanelles. However, such a scenario fails to explain the damage distribution given by Hecker (1920) and the epicentral location estimated by Ambraseys and Finkel (1987). Therefore, rather than towards the Saros Bay, the 120-km-long 9 August rupture must have propagated mostly into the Sea of Marmara and necessarily reached the Central Basin in agreement with Armijo et al. (2005) study. This implies a 150±20 km total rupture length including (i) the three sub-segments in the Sea of Marmara (~ 65 km) beginning from the Central basin, (ii) the onland fault section (~ 45 km) and (iii) the Saros Bay sub –segment (~ 40) limited by the Saros pull-apart basin. Therefore, the eastern termination of the 9 August 1912 rupture and the western termination of the 1999 earthquake rupture (Cakir et al., 2003) imply a minimum 100-km-long seismic gap in the Sea of Marmara (Fig 5.3). This fault length suggests an earthquake size M>7 that should be taken into account in any seismic hazard assessment for the Istanbul region.

**3a** - The combined study of geomorphology with micro-topography and paleoseismic trenching provides some constraints on the timing of successive faulting and related past earthquakes. We identified a total of 8 faulting events in trenches at Güzelköy, Yörgüç and Yeniköy. Together with the studies of Rockwell et al., (2001 & 2009), the four sites show comparable evidence of five earthquake

events associated with significant amount of lateral slip along on the eastern, central and western parts of the Ganos fault for the last 2000 years. The 5 faulting events at Güzelköy postdate 1043 – 835 BC, which are very comparable with the 6 faulting events identified at Yeniköy postdating 1500 – 830 BC. The ages correspond to a maximum value hence events are necessarily younger. The ages of the 4 events recognized in the Saros trenches (Rockwell et al., 2001) are no older than A.D. 791 and may include the events observed at Güzelköy and Yeniköy. Similarly, the two events at Yörgüç and trenches in Saros (Rockwell et al., 2009) which postdate A.D. 1600 can be incorporated in the 5 events.

**3b)** The comparison of constrained event ages with the historical catalogue allows restricting the timing of the earthquakes. Seven large shocks are known to affect this region after A.D.; i.e. 1912, 1766, 1659, 1354, 1344, 1063, and the 484 earthquakes. The 1912 earthquake is observed at all trench sites with significant amount of faulting and related lateral slip. The penultimate event is identified at Güzelköy and at Saros (Trench T6) which is related either the 1659 or the 1766 earthquakes. Prior events were only observed at Güzelköy site. A faulting event dated as pre 15-16$^{th}$ century and post 1271 coincides with two historical earthquakes., which is either the 1344 or 1354 earthquake. The last two faulting events no older than 79 A.D, which may be related to the 1063 and 484 earthquakes. Since we observed 5 events in all trenches with some age constrain for the last 2000 years we suppose that all above mentioned faulting events ruptured the entire onland section.

**3c)** The combination of geomorphic analysis and trenching results provides constrains on estimating the slip rate of the North Anatolian Fault at the Ganos region. At Güzelköy two paleo-channels offset for 16 m and 21 m yield 22.3 ± 0.5 mm/yr for the last ~700 years and 26.9 mm/yr for the last 781 years, respectively. At Yeniköy dating from the lowermost units of the 46 ± 1 m offset stream provided a maximum 17 mm/yr slip rate. From the trenches at Saros, Rockwell et al., (2009), calculated 15.8 mm/yr slip rate assuming a characteristic 4.5 m co-seismic slip for the last 6 events.

**3d)** A combined study of historical catalogues and paleoseismic trenching may allow constraining the earthquake recurrence interval for the Ganos region. Eight historical earthquakes causing damage in the Ganos-Saros region are the. 1912, 1766, 1659,

1354, 1344, 1063, 824 and 484 events. The uncertainty for the earthquakes from 12$^{th}$ to 16$^{th}$ century derives from the ambiguity of source estimations for historical earthquakes. The 1766 and 1659 may correspond to rupture events situated next to each other. The same may be valid for the 1344 and 1354 earthquakes. Such earthquake sequences are recently observed along the North Anatolian Fault (i.e. 1999 earthquakes Barka et al., 2002; Akyüz et al., 2002). Important here is that, if the event pairs would rupture the same segments we would observe them in the trenches, which is not the case. Therefore they must have ruptured at adjacent segments of the Ganos fault.

We suggest two earthquake recurrence scenarios for the last six events. Scenario 1 yields five intervals ranging from 239 to 340 years with an average recurrence interval of 285 ± 36 years and encompasses the 1912, 1659, 1354/1344, 824, 484 events. Whereas the five intervals in Scenario 2 range from 146 to 422 years and give an average recurrence interval of 285 ± 93 years and includes the 1912, 1766, 1354/1344, 824, 484 events. These results are in accordance with the 280 ±110 year recurrence intervals suggested by Rockwell et al. (2009). The decision if the 1766 or the 1659 is the penultimate event of the 1912 earthquake is critical, but difficult to resolve. The 280 years recurrence interval is sufficient to accumulate 5.5 m lateral slip considering a 19 mm/yr constant slip rate (which are values consistent with our slip rate estimations from paleoseismology and geomorphology and maximum co-seismic slip observations for the 1912 earthquake). An evaluation for the last 6 events along the Ganos fault should prefer Scenario1 if a characteristic earthquake behaviour and periodic recurrence interval is considered (Schwartz and Coppersmith, 1984). On the other hand Scenario 2 could be valid if a non-periodic recurrence interval is attributed for this section of the North Anatolian Fault. In this scenario it should be noted that the periods between the earthquakes before and after the 1766 are 422 and 146 years respectively. A 19 mm/yr constant slip rate would cause 8 m of strain accumulation pre 1766, and 2.7 m post 1766. If each earthquake along the Ganos fault causes similar size of events the maximum slip should be comparable and correspond to 5.5 m. If we consider that 5.5 m slip occurred during the 1766 earthquake 3 m of slip would have remained. Therefore, the following period of 146 years is sufficient to complete the slip to 5 m and may have triggered the 1912

**4a)** 61 historical seismogram recordings have been collected for the 9 August, 10 August and 13 September 1912. Comparable pairs have been digitized using TESEO software and analyzed to extract information for rupture duration and propagation, focal mechanism and epicentre.

**4b)** We collected 73 historical seismic records from institutions worldwide in order to determine the seismic characteristics of the 9 August and 13 September 1912 earthquakes. P-wave polarities at 5 stations and field based N68°E fault strike allow us to construct the focal mechanism solution shown in Fig 5.3,. The pure strike slip solution we obtained is in agreement with the known fault kinematics and slip measurements that do not show a significant vertical component.

The Ganos fault; although short and limited by two seas at it two ends shows typical features of right lateral strike slip faulting that may allow improving our understanding of fault mechanism in short and long term. Offsets are evident at various scales (10 to 9000 m). We were able to date some of the small displacements (> 50 m) and obtained comparable slip rates. However the larger offsets are indirectly dated and should be confirmed with absolute dating methods. Particularly, if the suggested offset groups are dated the obtained slip rates would yield an average rate independent of fault geometry and related cumulative slip distribution.

The complex seismic history, if carefully studied with more paleoseismic trenching can shed more light to our understanding on the behaviour of earthquake segments and their periodicy of earthquake production.

The available seismic parameters of the 1912 earthquake will play a key role in evaluating paleoseismic results and the slip rate estimations.

## REFERENCES


**Agamennone, G.,** 1912. Il disastroso terremoto nel bacino occi-dentale del Mar di Marmara, . In *Estrato della 'Rivista di Astronomiae Scienze affini'*, pp. 3-8.

**Aki, K.,** 1966. Generation and propagation of G waves from the Niigata earthquake of June 16, 1964. II. Estimation of earthquake moment, released energy, and stress-strain drop from the G wave spectrum, *Bull. Earthquake Res. Inst. Tokyo Univ*, Vol. **44**, pp. 73-88.

**Aksu, A. E., Hiscott, R. N., Kaminski, M. A., Mudie, P. J., Gillespie, H., Abrajano, T. and Yasar, D.,** 2002. Last glacial-Holocene paleoceanography of the Black Sea and Marmara Sea: stable isotopic, foraminiferal and coccolith evidence, *Marine Geology*, Vol. **190**, no. 1-2, pp. 119-149.

**Aksu, A. E., Hiscott, R. N. and Yasar, D.,** 1999. Oscillating Quaternary water levels of the Marmara Sea and vigorous outflow into the Aegean Sea from the Marmara Sea-Black Sea drainage corridor, *Marine Geology*, Vol. **153**, no. 1-4, pp. 275-302.

**Aksu, A. E., Yaltırak, C. and Hiscott, R. N.,** 2002. Quaternary paleoclimatic-paleoceanographic and tectonic evolution of the Marmara Sea and environs, *Marine Geology*, Vol. **190**, no. 1-2, pp. 9-18.

**Akyüz, H. S., Hartleb, R., Barka, A., Altunel, E., Sunal, G., Meyer, B. and Armijo, R.,** 2002. Surface Rupture and Slip Distribution of the 12 November 1999 Duzce Earthquake (M 7.1), North Anatolian Fault, Bolu, Turkey, *Bulletin of the Seismological Society of America*, Vol. **92**, no. 1, pp. 61-66.

**Allen, C. G.,** 1913. Review: Il Disastroso Terremoto nel Bacino Occidental del mar di Marmara: by G. Agamennone, *Bulletin of the Seismological Society of America*, Vol. **3**, no. 2, pp. 93-94.

**Allen, C. G.,** 1913. Review: Il Servizio Sismico in Grecia, nei Balcani e nell' Impero Ottomano: by G. Agamennone, *Bulletin of the Seismological Society of America*, Vol. **3**, no. 2, pp. 94-94.

**Allen, C. R.,** 1969. Active faulting in northern Turkey, *Div. Geol. Sci. Calif. Inst. Tech.*, Vol. **Contr. No. 1577**, p. 32.

**Altınok, Y., Alpar, B. and Yaltırak, C.,** 2003. Şarköy - Mürefte 1912 Earthquake's Tsunami, extension of the associated faulting in the Marmara Sea, Turkey, *Journal of Seismology*, Vol. **7**, no. 3, pp. 329-346.

**Altunel, E., Barka, A. A. and Akyüz, H. S.,** 2000. Slip distribution along the 1912 Mürefte-Şarköy earthquake, the North Anatolian Fault, Western Marmara. In *The 1999 Izmit and Düzce Earthquakes: Preliminary Results*, pp. 341-349.

**Altunel, E., Meghraoui, M., Akyüz, H. S. and Dikbas, A.,** 2004. Characteristics of the 1912 co-seismic rupture along the North Anatolian Fault Zone (Turkey): implications for the expected Marmara earthquake, *Terra Nova*, Vol. **16**, no. 4, pp. 198-204.

**Ambraseys, N. N.,** 1970. Some characteristic features of the Anatolian fault zone, *Tectonophysics*, Vol. **9**, no. 2-3, pp. 143-165.

**Ambraseys, N. N.,** 2002a. Seismic sea-waves in the Marmara Sea region during the last 20 centuries, *Journal of Seismology*, Vol. **6**, no. 4, pp. 571-578.

**Ambraseys, N. N.,** 2002b. The Seismic Activity of the Marmara Sea Region over the Last 2000 Years, *Bulletin of the Seismological Society of America*, Vol. **92**, no. 1, pp. 1-18.

**Ambraseys, N. N.,** 2006. Comparison of frequency of occurrence of earthquakes with slip rates from long-term seismicity data: the cases of Gulf of Corinth, Sea of Marmara and Dead Sea Fault Zone, *Geophysical Journal International*, Vol. **165**, no. 2, pp. 516-526.

**Ambraseys, N. N. and Finkel, C. F.,** 1987. The Saros-Marmara earthquake of 9 August 1912, *Earthquake engineering & structural dynamics*, Vol. **15**, no. 2, pp. 189-211.

**Ambraseys, N. N. and Finkel, C. F.,** 1991. Long-term seismicity of Istanbul and of the Marmara Sea region, *Terra Nova*, Vol. **3**, no. 5, pp. 527-539.

**Ambraseys, N. N. and Finkel, C. F.,** 1995. *The Seismicity of Turkey and adjacent areas: A Historical Review, 1500-1800*, Eren Yayıncılık, İstanbul.

**Ambraseys, N. N. and Jackson, J.,** 1998. Faulting associated with historical and recent earthquakes in the Eastern Mediterranean region, *Geophysical Journal International*, Vol. **133**, no. 2, pp. 390-406.

**Ambraseys, N. N. and Zatopek, A.,** 1969. The Mudurnu Valley, West Anatolia, Turkey, earthquake of 22 July 1967, *Bulletin of the Seismological Society of America*, Vol. **59**, no. 2, pp. 521-589.

**Andrieux, J., Över, S., Poisson, A. and Bellier, O.,** 1995. The North Anatolian Fault Zone: distributed Neogene deformation in its northward convex part, *Tectonophysics*, Vol. **243**, no. 1-2, pp. 135-154.

**Armijo, R., Meyer, B., Hubert, A. and Barka, A.,** 1999. Westward propagation of the North Anatolian fault into the northern Aegean: Timing and kinematics, *Geology*, Vol. **27**, pp. 267-270.

**Armijo, R., Meyer, B., Hubert, A. and Barka, A.,** 2000. Westward propagation of North Anatolian fault into the northern Aegean:Timing and kinematics: Comment and Reply: REPLY, *Geology*, Vol. **28**, no. 2, pp. 188-189.

**Armijo, R., Meyer, B., Navarro, S., King, G. and Barka, A.,** 2002. Asymmetric slip partitioning in the Sea of Marmara pull-apart: a clue to propagation processes of the North Anatolian Fault, *Terra Nova*, Vol. **14**, no. 2, pp. 80-86.

**Armijo, R., Pondard, N., Meyer, B., Uçarkus, G., Lepinay, B. M. d., Malavieille, J., Dominguez, S., Gustcher, M.-A., Schmidt, S., Beck, C., Çagatay, N., Çakir, Z., Imren, C., Eriş, K., Natalin, B., Özalaybey, S., Tolun, L., Lefevre, I., Seeber, L., Gasperini, L., Rangin, C., Emre, O. and Sarikavak, K.,** 2005. Submarine fault scarps in the Sea of Marmara pull-apart (North Anatolian Fault): Implications for seismic hazard in Istanbul, *Geochemistry Geophysics Geosystems*, Vol. **6**, p. Q06009.

**Aydın, A. and Kalafat, D.,** 2002. Surface Ruptures of the 17 August and 12 November 1999 Izmit and Duzce Earthquakes in Northwestern Anatolia, Turkey: Their Tectonic and Kinematic Significance and the Associated Damage, *Bulletin of the Seismological Society of America*, Vol. **92**, no. 1, pp. 95-106.

**Bahr, A., Arz, H. W., Lamy, F. and Wefer, G.,** 2006. Late glacial to Holocene paleoenvironmental evolution of the Black Sea, reconstructed with stable oxygen isotope records obtained on ostracod shells, *Earth and Planetary Science Letters*, Vol. **241**, no. 3-4, pp. 863-875.

**Bahr, A., Lamy, F., Arz, H., Kuhlmann, H. and Wefer, G.,** 2005. Late glacial to Holocene climate and sedimentation history in the NW Black Sea, *Marine Geology*, Vol. **214**, no. 4, pp. 309-322.

**Barka, A. A.**, 1992. The North Anatolian fault zone, *Annales Tectonicae*, 164-195.

**Barka, A.,** 1985. Geology and tectonic evolution of some Neogene-Quaternary basins in the North Anatolian fault zone. In *Ketin Symposium Spec. Publ. Geol. Soc.*, pp. 209-227.

**Barka, A.,** 1996. Slip distribution along the North Anatolian fault associated with the large earthquakes of the period 1939 to 1967, *Bulletin of the Seismological Society of America*, Vol. **86**, no. 5, pp. 1238-1254.

**Barka, A., Akyuz, H. S., Altunel, E., Sunal, G., Cakir, Z., Dikbas, A., Yerli, B., Armijo, R., Meyer, B., de Chabalier, J. B., Rockwell, T., Dolan, J. R., Hartleb, R., Dawson, T., Christofferson, S., Tucker, A., Fumal, T., Langridge, R., Stenner, H., Lettis, W., Bachhuber, J. and Page, W.,** 2002. The Surface Rupture and Slip Distribution of the 17 August 1999 Izmit Earthquake (M 7.4), North Anatolian Fault, *Bulletin of the Seismological Society of America*, Vol. **92**, no. 1, pp. 43-60.

**Barka, A., Akyuz, H. S., Cohen, H. A. and Watchorn, F.,** 2000. Tectonic evolution of the Niksar and Tasova-Erbaa pull-apart basins, North Anatolian Fault Zone: their significance for the motion of the Anatolian block, *Tectonophysics*, Vol. **322**, no. 3-4, pp. 243-264.

**Barka, A. and Gülen, L.,** 1988. New constraints on age and total offset of the North Anatolian fault zone: implications for tectonics of the Eastern Mediterranean region. In *Melih Tokay Symposium, Spec. Publ. Middle-east Techn. Univer.*, pp. 39-65.

**Barka, A. A. and Gülen, L.,** 1989. Complex evolution of the Erzincan Basin (eastern Turkey), *Journal of Structural Geology*, Vol. **11**, no. 3, pp. 275-283.

**Batllo, J., Stich, D. and Macia, R.,** 2008. Quantitative Analysis of Early Seismograph Recordings. In *Historical Seismology, Interdisciplinary Studies of Past and Recent Earthquakes 2*, Modern Approaches in Solid Earth Sciences, pp. 385-402.

**Bergougnan, H.,** 1975. Relations entre les édifices pontique et taurique dans le nord-est de l'Anatolie, *Bulletin de la Société géologique de France, nspécial:" Alpes maritimes franco-italiennes et Apennin septentrional", Paris*, Vol. **17**, no. 6, pp. 1045-1057.

**Bigourdan, M.,** 1918. Note de Michailovic Jelenko-Resultats des études sur le tremblement de terre d'aout et de septembre 1912 sur la mer de Marmara - 1918, *Acad. Scien. France.*

**Bouchon, M. and Martin, V.,** 2003. Observation of Long Supershear Rupture during the Ms=8.1 Kunlunshan (Tibet) Earthquake, *Science*, Vol. **301**, pp. 824-826.

**Bouchon, M., Toksöz, M. N., Karabulut, H., Bouin, M.-P., Dietrich, M., Aktar, M. and Edie, M.,** 2002. Space and Time Evolution of Rupture and Faulting during the 1999 Izmit (Turkey) Earthquake, *Bulletin of the Seismological Society of America*, Vol. **92**, no. 1, pp. 256-266.

**Bozkurt, E.,** 2001. Neotectonics of Turkey – a synthesis, *Geodinamica Acta*, Vol. **14**, p. 18.

**Carton, H., Singh, S. C., Hirn, A., Bazin, S., Voogd, B., Vigner, A., Ricolleau, A., Cetin, S., Ocakoglu, N., Karakoc, F., Sevilgen, V. and Carton, H.,** 2007. Seismic imaging of the three-dimensional architecture of the Cinarcik Basin along the North Anatolian Fault, *J. Geophys. Res.*, Vol. **112**, no. B06101.

**Chery, J. and Vernant, P.,** 2006. Lithospheric elasticity promotes episodic fault activity, *Earth and Planetary Science Letters*, Vol. **243**, no. 1-2, pp. 211-217.

**Crampin, S. and Evans, R.,** 1986. Neotectonics of the Marmara Sea region of Turkey, *Journal of the Geological Society*, Vol. **143**, no. 2, pp. 343-348.

**Cunningham, W. D. and Mann, P.,** 2007. Tectonics of strike-slip restraining and releasing bends, *Geological Society, London, Special Publications*, Vol. **290**, no. 1, pp. 1-12.

**Çağatay, M. N., Eriş, K., Ryan, W. B. F., Sancar, Ü., Polonia, A., Akçer, S., Biltekin, D., Gasperini, L., Görür, N., Lericolais, G. and Bard, E.,** 2009. Late Pleistocene–Holocene evolution of the northern shelf of the Sea of Marmara, *Marine Geology*, Vol. **265**, no. 3-4, pp. 87-100.

**Çağatay, M. N., Görür, N., Algan, O., Eastoe, C., Tchapalyga, A., Ongan, D., Kuhn, T. and Kuşçu, I.,** 2000. Late Glacial-Holocene palaeoceanography of the Sea of Marmara: timing of connections with the Mediterranean and the Black Seas, *Marine Geology*, Vol. **167**, no. 3-4, pp. 191-206.

**Çağatay, M. N., Görür, N., Polonia, A., Demirbag, E., Sakinc, M., Cormier, M. H., Capotondi, L., McHugh, C., Emre, O. and Eris, K.,** 2003. Sea-level changes and depositional environments in the Izmit Gulf, eastern Marmara Sea, during the late glacial-Holocene period, *Marine Geology*, Vol. **202**, no. 3-4, pp. 159-173.

**Çakır, Z., Barka, A., Chabalier, J.-B. d., Armijo, R. and Meyer, B.,** 2003. Kinematics of the November 12, 1999 (Mw=7.2) Düzce Earthquake Deduced from SAR Interferometry, *Turkish Journal of Earth Sciences*, Vol. **12**, pp. 105-118.

**Dewey, J. F. and Şengör, A. M. C.,** 1979. Aegean and surrounding regions: Complex multiplate and continuum tectonics in a convergent zone, *Geological Society of America Bulletin*, Vol. **90**, no. 1, pp. 84-92.

**Dewey, J. W.,** 1976. Seismicity of Northern Anatolia, *Bulletin of the Seismological Society of America*, Vol. **66**, no. 3, pp. 843-868.

**Dizer, M. and Izgi, C.,** 1987. Kandilli Rasathanesinde Mevcut Elyazması ve Eski Takvimlerde Kayıtlı Depremler.

**Dolukhanov, P. M. and Arslanov, K. A.,** 2009. Ecological crises and early human migrations in the Black Sea area, *Quaternary International*, Vol. **197**, no. 1-2, pp. 35-42.

**Ergintav, S., Burgmann, R., McClusky, S., Cakmak, R., Reilinger, R. E., Lenk, O., Barka, A. and Özener, H.,** 2002. Postseismic Deformation near the Izmit Earthquake (17 August 1999, M 7.5) Rupture Zone, *Bulletin of the Seismological Society of America*, Vol. **92**, no. 1, pp. 194-207.

**Erinç, S.,** 1973. Türkiyenin şekillenmesinde Neotektoniğin rolü ve jeomorfoloji-jeodimanik ilişkiler. In *Cumhurriyetin 50. yılı Yerbilimleri Kongresi*, pp. 1-12.

**Eriş, K. and Çağatay, N.,** 2008. Marmara Denizi'nde son buzul döneminden günümüze deniz seviyesi değişimleri, *İTÜ Dergisi*, Vol. **7**, no. 6, pp. 13-23.

**Eriş, K. K., Ryan, W. B. F., Çagatay, M. N., Sancar, U., Lericolais, G., Ménot, G. and Bard, E.,** 2007. The timing and evolution of the post-glacial transgression across the Sea of Marmara shelf south of Istanbul, *Marine Geology*, Vol. **243**, no. 1-4, pp. 57-76.

**Ferry, M., Meghraoui, M., Karaki, N. A., Al-Taj, M., Amoush, H., Al-Dhaisat, S. and Barjous, M.,** 2007. A 48-kyr-long slip rate history for the Jordan Valley segment of the Dead Sea Fault, *Earth and Planetary Science Letters*, Vol. **260**, no. 3-4, pp. 394-406.

**Flerit, F., Armijo, R., King, G. C. P., Meyer, B. and Barka, A.,** 2003. Slip partitioning in the Sea of Marmara pull-apart determined from GPS velocity vectors, *Geophysical Journal International*, Vol. **154**, no. 1, pp. 1-7.

**Gautier, P., Brun, J.-P., Moriceau, R., Sokoutis, D., Martinod, J. and Jolivet, L.,** 1999. Timing, kinematics and cause of Aegean extension: a scenario based on a comparison with simple analogue experiments, *Tectonophysics*, Vol. **315**, no. 1-4, pp. 31-72.

**Gazioğlu, C., Gökaşan, E., Algan, O., Yücel, Z., Tok, B. and Doğan, E.,** 2002. Morphologic features of the Marmara Sea from multi-beam data, *Marine Geology*, Vol. **190**, no. 1-2, pp. 397-420.

**Görür, N., Cagatay, M., Sakinc, M., Sümengen, M., Sentürk, K., Yaltirak, C. and Tchapalyga, A.,** 1997. Origin of the Sea of Marmara as Deduced from Neogene to Quaternary Paleogeographic Evolution of its Frame, *International Geology Review*, Vol. **39**, no. 4, pp. 342-342.

**Grünthal, G.,** 1993. European macroseismic scale 1992. In *Cahiers du Centre Européen de Géodynamique et de Séismologie*, pp. 1-79.

**Guidoboni, E. and Comastri, A.,** 2005. *Catalogue of earthquakes and tsunamis in the Mediterranean area from the 11th to the 15th century*, Istituto Nazionale di Geofisica e Vulcanologia, Rome.

**Guidoboni, E., Comastri, A. and Traina, G.,** 1994. *Catalogue of ancient earthquakes in the Mediterranean area up to the 10th century*, Istituto Nazionale di Geofisica e Vulcanologia, Rome.

**Gutzwiller, O.,** 1923. *Beitraege zur Geologie der Umgebung von Merfete am Marmara-Meere*, Emil Birkhauser & Cie, Basel.

**Gülen, L., Pınar, A., Kalafat, D., Özel, N., Horasan, G., Yılmazer, M. and Işıkara, A. M.,** 2002. Surface Fault Breaks, Aftershock Distribution, and Rupture Process of the 17 August 1999 Izmit, Turkey, Earthquake, *Bulletin of the Seismological Society of America*, Vol. **92**, no. 1, pp. 230-244.

**Hartleb, R. D., Dolan, J. F., Akyuz, H. S., Dawson, T. E., Tucker, A. Z., Yerli, B., Rockwell, T. K., Toraman, E., Cakir, Z., Dikbas, A. and Altunel, E.,** 2002. Surface Rupture and Slip Distribution along the Karadere Segment of the 17 August 1999 Izmit and the Western Section of the 12 November 1999 Duzce, Turkey, Earthquakes, *Bulletin of the Seismological Society of America*, Vol. **92**, no. 1, pp. 67-78.

**Hartleb, R. D., Dolan, J. F., Akyuz, H. S. and Yerli, B.,** 2003. A 2000-Year-Long Paleoseismologic Record of Earthquakes along the Central North Anatolian Fault, from Trenches at Alayurt, Turkey, *Bulletin of the Seismological Society of America*, Vol. **93**, no. 5, pp. 1935-1954.

**Hecker, O.**, 1920. Mitteilungen über Erdbeben im Jahre 1912, Hauptstation für Erdbebenforschung, Jena, früher in Strassburg.

**Hempton, M. R.,** 1987. Constraints on Arabian Plate Motion and Extensional History of the Red Sea, *Tectonics*, Vol. **6**, pp. 687-705.

**Hiscott, R. N., Aksu, A. E., Mudie, P. J., Marret, F., Abrajano, T., Kaminski, M. A., Evans, J., Çakıroglu, A. I. and Yasar, D.,** 2007. A gradual drowning of the southwestern Black Sea shelf: Evidence for a progressive rather than abrupt Holocene reconnection with the eastern Mediterranean Sea through the Marmara Sea Gateway, *Quaternary International*, Vol. **167-168**, pp. 19-34.

**Holmes, A. W.,** 1961. A stratigraphic review of Thrace. In *Turkish Petroleum Corporation unpubl techn rep 368*, pp. 1-56.

**Hubert-Ferrari, A. l., Armijo, R., King, G., Meyer, B. and Barka, A.,** 2002. Morphology, displacement, and slip rates along the North Anatolian Fault, Turkey,*Journal of Geophysical Research*, Vol. **107**, no. B10, pp. 2235.

**Hubert-Ferrari, A., Barka, A., Jacques, E., Nalbant, S. S., Meyer, B., Armijo, R., Tapponnier, P. and King, G. C. P.,** 2000. Seismic hazard in the Marmara Sea region following the 17 August 1999 Izmit earthquake, *Nature*, Vol. **404**, no. 6775, pp. 269-273.

**Huhmann, M., Kremenetski, K. V., Hiller, A. and Brückner, H.,** 2004. Late quaternary landscape evolution of the upper Dnister valley, western Ukraine, *Palaeogeography, Palaeoclimatology, Palaeoecology*, Vol. **209**, no. 1-4, pp. 51-71.

**IASPEI**, 2004, International Association of Seismology and Physics of the Earth's Interior *Working Group on Seismological Archives Report*

**Issar, A.,** 2003. *Climate changes during the Holocene and their impact on Hydrological systems*, Cambridge University Press,

**Izmailov, Y. A.,** 2005. Evolyutsiya geografiya poberezhii Azovskogo I Chernogo morei, *Geo, Sochi*.

**İmren, C., Le Pichon, X., Rangin, C., Demirbag, E., Ecevitoğlu, B. and Görür, N.,** 2001. The North Anatolian Fault within the Sea of Marmara: a new interpretation based on multi-channel seismic and multi-beam bathymetry data, *Earth and Planetary Science Letters*, Vol. **186**, no. 2, pp. 143-158.

**İzdar, E.**, 1959. Beitrage zur Geologie der Umgebung von Tepeköy, *Diplomarbeit*,

**İzzi, S.,** ???? Târih. In *EİY Or. 3918 BM*.

**Kanamori, H.,** 1977. The Energy Release in Great Earthquakes, *Journal of Geophysical Research*, Vol. **82**, 20, pp. 2981–2987.

**Kanamori, H.,** 1988. Importance of historical seismograms for geophysical research, *Historical seismograms and earthquakes of the world*, pp. 16–33.

**Kanamori, H. and Brodsky, E. E.,** 2004. The physics of earthquakes, *Reports on Progress in Physics*, Vol. **67**, no. 8, pp. 1429–1496.

**Karabulut, H., Roumelioti, Z., Benetatos, C., Ahu Komec, M., Ozalaybey, S., Aktar, M. and Kiratzi, A.,** 2006. A source study of the 6 July 2003 (Mw 5.7) earthquake sequence in the Gulf of Saros (Northern Aegean Sea): Seismological evidence for the western continuation of the Ganos fault, *Tectonophysics*, Vol. **412**, no. 3-4, pp. 195-216.

**Karaca, M., Deniz, A. and Tayanç, M.,** 2000. Cyclone track variability over Turkey in association with regional climate, *International Journal of Climatology*, Vol. **20**, no. 10, pp. 1225-1236.

**Kaymakci, N., Aldanmaz, E., Langereis, C., Spell, T. L., Gurer, O. F. and Zanetti, K. A.,** 2007. Late Miocene transcurrent tectonics in NW Turkey: evidence from palaeomagnetism and 40Ar-39Ar dating of alkaline volcanic rocks, *Geological Magazine*, Vol. **144**, no. 2, pp. 379-392.

**Keller, E. A., Pinter, N. and Green, D. J.,** 1996. *Active tectonics: earthquakes, uplift, and landscape*, Prentice Hall New Jersey,

**Ketin, I.,** 1948. Über die tektonisch-mechanischen Folgerungen aus den großen anatolischen Erdbeben des letzten Dezenniums, *International Journal of Earth Sciences*, Vol. **36**, no. 1, pp. 77-83.

**Ketin, İ.,** 1957. Kuzey Anadolu Deprem Fayı, *İTÜ Dergisi*, Vol. **15**, no. pp. 49-52.

**Ketin, I.,** 1966. Tectonic units of Anatolia (Asia Minor), *Maden Tetkik ve Arama Enstitusu. Dergisi*, Vol. **66**, pp. 23–34-23–34.

**Ketin, I.,** 1969. Uber die nordanatolische Horizontalverschiebung, *Bull. Min. Res. Explor. Inst. Turkey*, Vol. **72**, pp. 1-28.

**Ketin, İ.,** 1976. San Andreas ve Kuzey Anadolu Faylari arasında bir karşılaştırma, *Türkiye Jeoloji Kurumu Bülteni*, Vol. **19**, pp. 149-154.

**Koçyiğit, A.,** 1989. Suşehri basin: an active fault-wedge basin on the North Anatolian Fault Zone, Turkey, *Tectonophysics*, Vol. **167**, no. 1, pp. 13-29.

**Konca, A. Ö., LePrince, S., Avouac, J.-P. and Helmberger, D. V.**, 2009. Fault Trace and Rupture Process of 1999, Mw7.1 Düzce Earthquake from Analysis of SPOT, GPS, InSAR, Strong-Motion and Teleseismic Data, *62. Geological Kurultai of Turkey*, Ankara, 13−17 April 2009,

**Kondo, H., Awata, Y., Emre, O., Dogan, A., Ozalp, S., Tokay, F., Yildirim, C., Yoshioka, T. and Okumura, K.,** 2005. Slip Distribution, Fault Geometry, and Fault Segmentation of the 1944 Bolu-Gerede Earthquake Rupture, North Anatolian Fault, Turkey, *Bulletin of the Seismological Society of America*, Vol. **95**, no. 4, pp. 1234-1249.

**Kondorskaya, N. V. and Ulomov, V. I.,** 1999. Special catalogue of earthquakes of the Northern Eurasia (SECNE).

**Kozacı, Ö., Dolan, J. F. and Finkel, R. C.,** 2009. A late Holocene slip rate for the central North Anatolian fault, at Tahtaköprü, Turkey, from cosmogenic 10Be geochronology: Implications for fault loading and strain release rates,*Journal of Geophysical Research*, Vol. **114**, no. B01405,

**Kozacı, Ö., Dolan, J., Finkel, R. and Hartleb, R.,** 2007. Late Holocene slip rate for the North Anatolian fault, Turkey, from cosmogenic 36Cl geochronology: Implications for the constancy of fault loading and strain release rates, *Geology*, Vol. **35**, no. 10, pp. 867-870.

**Kürçer, A., Chatzipetros, A., Tutkun, S. Z., Pavlides, S., Ate, z. and Valkaniotis, S.,** 2008. The Yenice-Gönen active fault (NW Turkey): Active tectonics and palaeoseismology, *Tectonophysics*, Vol. **453**, no. 1-4, pp. 263-275.

**Langridge, R. M., Stenner, H. D., Fumal, T. E., Christofferson, S. A., Rockwell, T. K., Hartleb, R. D., Bachhuber, J. and Barka, A. A.,** 2002. Geometry, Slip Distribution, and Kinematics of Surface Rupture on the Sakarya Fault Segment during the 17 August 1999 Izmit, Turkey, Earthquake, *Bulletin of the Seismological Society of America*, Vol. **92**, no. 1, pp. 107-125.

**Le Pichon, X., Rangin, N., Chamot-Rooke, C. and Şengör, A. M. C.,** 2003. The North Anatolian fault in the Sea of Marmara, *Journal of Geophysical Research*, Vol. **108**, no. B4, pp. 2179-2179.

**Le Pichon, X., Şengör, A. M. C., Demirbağ, E., Rangin, C., Imren, C., Armijo, R., Görür, N., Çağatay, N., Mercier de Lepinay, B. and Meyer, B.,** 2001. The active Main Marmara Fault, *Earth and Planetary Science Letters*, Vol. **192**, no. 4, pp. 595-616.

**Lettis, W., Bachhuber, J., Witter, R., Brankman, C., Randolph, C. E., Barka, A., Page, W. D. and Kaya, A.,** 2002. Influence of Releasing Step-Overs on Surface Fault Rupture and Fault Segmentation: Examples from the 17 August 1999 Izmit Earthquake on the North Anatolian Fault, Turkey, *Bulletin of the Seismological Society of America*, Vol. **92**, no. 1, pp. 19-42.

**Macovei, G.,** 1912. Sur La Tremblement De Terre De La Mer De Marmara Le 9 Aout 1912, *Bull. sect. sci. acad. Rumanie*, Vol. **1**, pp. 9-18.

**Macovei, G.,** 1913. Aspura Cutremurului de Pamant dela Mare de Marmara dela 9 August 1912, *Academia Romana, Publicatiunile Adamachi V.*, Vol. **33**, pp. 260-273.

**Major, C. O., Goldstein, S. L., Ryan, W. B. F., Lericolais, G., Piotrowski, A. M. and Hajdas, I.,** 2006. The co-evolution of Black Sea level and composition through the last deglaciation and its paleoclimatic significance, *Quaternary Science Reviews*, Vol. **25**, no. 17-18, pp. 2031-2047.

**Mâmâcânyam, E.,** 19?? Mürefte civarı büyük zelzele ve yangını garib destanı, R. Sukâyân Matbaası, p. 45.

**Mann, P.,** 2007. Global catalogue, classification and tectonic origins of restraining- and releasing bends on active and ancient strike-slip fault systems, *Geological Society, London, Special Publications*, Vol. **290**, no. 1, pp. 13-142.

**McCalpin, J.,** 1996. *Paleoseismology*, Academic Press, San Diego.

**McClusky, S., Balassanian, S., Barka, A., Demir, C., Ergintav, S., Georgiev, I., Gürkan, O., Hamburger, M., Hurst, K., Kahle, H., Kastens, K., Kekelidze, G., King, R., Kotzev, V., Lenk, O., Mahmoud, S., Mishin, A., Nadariya, M., Ouzounis, A., Paradissis, D., Peter, Y., Prilepin, M., Reilinger, R., Sanli, I., Seeger, H., Tealeb, A., Toksöz, M. N. and Veis, G.,** 2000. Global Positioning System constraints on plate kinematics and dynamics in the eastern Mediterranean and Caucasus, *Journal of Geophysical Research*, Vol. **105**, no. B3, pp. 5695–5719.

**McHugh, C. M. G., Gurung, D., Giosan, L., Ryan, W. B. F., Mart, Y., Sancar, U., Burckle, L. and agatay, M. N.,** 2008. The last reconnection of the Marmara Sea (Turkey) to the World Ocean: A paleoceanographic and paleoclimatic perspective, *Marine Geology*, Vol. **255**, no. 1-2, pp. 64-82.

**McHugh, C. M. G., Seeber, L., Cormier, M.-H., Dutton, J., Cagatay, N., Polonia, A., Ryan, W. B. F. and Gorur, N.,** 2006. Submarine earthquake geology along the North Anatolia Fault in the Marmara Sea, Turkey: A model for transform basin sedimentation, *Earth and Planetary Science Letters*, Vol. **248**, no. 3-4, pp. 661-684.

**McKenzie, D.,** 1972. Active Tectonics of the Mediterranean Region, *Geophysical Journal of the Royal Astronomical Society*, Vol. **30**, no. 2, pp. 109-185.

**Meade, B. J., Hager, B. H., McClusky, S. C., Reilinger, R. E., Ergintav, S., Lenk, O., Barka, A. and Ozener, H.,** 2002. Estimates of Seismic Potential in the Marmara Sea Region from Block Models of Secular Deformation Constrained by Global Positioning System Measurements, *Bulletin of the Seismological Society of America*, Vol. **92**, no. 1, pp. 208-215.

**Meghraoui, M. and Crone, A. J.,** 2001. Earthquakes and their preservation in the geological record, *Journal of Seismology*, Vol. **5**, no. 3, pp. 281-285.

**Melinte-Dobrinescu, M. C., Suc, J.-P., Clauzon, G., Popescu, S.-M., Armijo, R., Meyer, B., Biltekin, D., Çağatay, M. N., Uçarkuş, G., Gwénaël, J., Fauquette, S. and Çakır, Z.,** 2009. The Messinian Salinity Crisis in the Dardanelles region: Chronostratigraphic constraints, *Palaeogeography, Palaeoclimatology, Palaeoecology*, Vol. **278**, no. 1-4, pp. 24-39.

**Mihailovic, J.,** 1918. Resultats des études sur le tremblement de terre d'aout et de septembre 1912 sur la mer de Marmara, pp. 784 - 787.

**Mihailovic, J.,** 1923. Le mecanisme des mouvements sismiques dans la mer de Marmara , Belgrade, 108, 54-63, September, 1923. , *Bulletin de l'Academie royale des Sciences de Serbie, Belgrad*, Vol. **108**, pp. 54-63.

**Mihailovic, J.**, 1923. Mehanizam Trusvih pokreta ha Mramornom Moru, *GLASA*, Srpske Kraljevske Akademije, Belgrad.

**Mihailovic, J.,** 1927. Memoir-Sur les Grands Tremblement de Tere de la Mer de Marmara, pp. 215 - 222.

**Mihailovic, J.,** 1927. Trusne katastrofe na Mramornome moru. In *Posebno izdan. srpse akad nauka 16*, p. 1-303.

**Mihailovic, J.,** 1933. La séismicite de la Thrace, de mer de Marmara et de l'Asie Mineur. In *Monograph. et Travaux Sci. Inst. Seism.*

**Mudie, P. J., Rochon, A. and Aksu, A. E.,** 2002. Pollen stratigraphy of Late Quaternary cores from Marmara Sea: land-sea correlation and paleoclimatic history, *Marine Geology*, Vol. **190**, no. 1-2, pp. 233-260.

**Okay, A. İ., Demirbağ, E., Kurt, H., Okay, N. and Kuşcu, İ.,** 1999. An active, deep marine strike-slip basin along the North Anatolian fault in Turkey, *Tectonics*, Vol. **18**, no. 1, pp. 129-147.

**Okay, A. İ., Kaşlılar-Özcan, A., İmren, C., Boztepe-Guney, A., Demirbag, E. and Kuşcu, İ.,** 2000. Active faults and evolving strike-slip basins in the Marmara term Sea, northwest Turkey: a multichannel seismic reflection study, *Tectonophysics*, Vol. **321**, no. 2, pp. 189-218.

**Okay, A. I., Satır, M., Zattin, M., Cavazza, W. and Topuz, G.,** 2008. An Oligocene ductile strike-slip shear zone: The Uludağ Massif, northwest Turkey—Implications for the westward translation of Anatolia, *GSA Bulletin*, Vol. **120**, no. 7-8, pp. 893-911.

**Okay, A. I., Siyako, M. and Bürkan, K. A.,** 1991. Geology and tectonic evolution of the Biga Peninsula. In *Special Issue on Tectonics, Bulletin of the Technical University* pp. 191-255.

**Okay, A. I. and Tüysüz, O.,** 1999. Tethyan sutures of northern Turkey, *Geological Society, London, Special Publications*, Vol. **156**, no. 1, pp. 475-515.

**Okay, A. I., Tuysuz, O. and Kaya, S.,** 2004. From transpression to transtension: changes in morphology and structure around a bend on the North Anatolian Fault in the Marmara region, *Tectonophysics*, Vol. **391**, no. 1-4, pp. 259-282.

**Özalaybey, S., Ergin, M., Aktar, M., Tapırdamaz, C., Biçmen, F. and Yörük, A.,** 2002. The 1999 Izmit Earthquake Sequence in Turkey: Seismological and Tectonic Aspects, *Bulletin of the Seismological Society of America*, Vol. **92**, no. 1, pp. 376-386.

**Öztin, F.,** 1987. 9 Agustos 1912 Şarköy-Mürefte depremi, *Deprem Araştırma Bülteni*, Vol. **56**, pp. 91-127.

**Palyvos, N., Pantosti, D., Zabci, C. and D'Addezio, G.,** 2007. Paleoseismological Evidence of Recent Earthquakes on the 1967 Mudurnu Valley Earthquake Segment of the North Anatolian Fault Zone, *Bulletin of the Seismological Society of America*, Vol. **97**, no. 5, pp. 1646-1661.

**Pantosti, D., Pucci, S., Palyvos, N., De Martini, P. M., D'Addezio, G., Collins, P. E. F. and Zabci, C.,** 2008. Paleoearthquakes of the Duzce fault (North Anatolian Fault Zone): Insights for large surface faulting earthquake recurrence, *Journal of Geophysical Research*, Vol. **113**, no. B01309.

**Parke, J. R., White, R. S., McKenzie, D., Minshull, T. A., Bull, J. M., Kuşcu, I., Görür, N. and A.M.C., Ş.,** 2002. Interaction between faulting and sedimentation in the Sea of Marmara, western Turkey,*Journal of Geophysical Research*, Vol. **107**, no. B11, p. 2286.

**Pavoni, N.,** 1962. Die Nordanatolische Horizontalverschiebung, *International Journal of Earth Sciences*, Vol. **51**, no. 1, pp. 122-139.

**Peyron, O., Guiot, J., Cheddadi, R., Tarasov, P., Reille, M., de Beaulieu, J.-L., Bottema, S. and Andrieu, V.,** 1998. Climatic Reconstruction in Europe for 18,000 YR B.P. from Pollen Data, *Quaternary Research*, Vol. **49**, no. 2, pp. 183-196.

**Pfannenstiel, M.,** 1944. Diluviale Geologie des Mittelmeergebietes: die diluvialen Entwicklungstadien und die Urgeschichte von Dardanellen, Marmara Meer und Bosphorus, *Geologische Rundschau*, Vol. **34**, pp. 342-334.

**Pınar, A., Honkura, Y. and Kuge, K.,** 2001. Seismic activity triggered by the 1999 Izmit earthquake and its implications for the assessment of future seismic risk, *Geophysical Journal International*, Vol. **146**, no. 1, pp. F1-F7.

**Pınar, N.,** 1953. Preliminary note on the earthquake of Yenice-Gonen, Turkey, March 18, 1953, *Bulletin of the Seismological Society of America*, Vol. **43**, no. 4, pp. 307-310.

**Pucci, S.**, 2006. The Düzce segment of the North Anatolian Fault Zone (Turkey): Understanding its seismogenic behavior through earthquake geology, *PhD Thesis*, Earth Sciences, Perugia

**Pucci, S., De Martini, P. M. and Pantosti, D.,** 2008. Preliminary slip rate estimates for the Düzce segment of the North Anatolian Fault Zone from offset geomorphic markers, *Geomorphology*, Vol. **97**, no. 3-4, pp. 538-554.

**Ramrath, A., Zolitschka, B., Wulf, S. and Negendank, J. F. W.,** 1999. Late Pleistocene climatic variations as recorded in two Italian maar lakes (Lago di Mezzano, Lago Grande di Monticchio), *Quaternary Science Reviews*, Vol. **18**, no. 7, pp. 977–992.

**Ramsey, C. B.,** 2001. Development of the radiocarbon calibration program, *Radiocarbon*, Vol. **43**, no. 2A, pp. 355–363.

**Reid, H. F.,** 1910. The Mechanics of the Earthquake, The California Earthquake of April 18, 1906, Report of the State Investigation Commission,, *Carnegie Institution of Washington, Washington, DC*, Vol. **2**.

**Reilinger, R. E., McClusky, S. C., Oral, M. B., King, R. W., Toksöz, M. N., Barka, A. A., Kınık, I., Lenk, O. and Şanlı, I.,** 1997. Global Positioning System measurements of present-day crustal movements in the Arabia-Africa-Eurasia plate collision zone, *Journal of Geophysical Research*, Vol. **102**, no. B5, pp. 9983–9999.

**Reilinger, R. E., McClusky, S., Vernant, P., Lawrence, S., Ergintav, S., Cakmak, R., Ozener, H., Kadirov, F., Guliev, I., Stepanyan, R., Nadariya, M., Hahubia, G., Mahmoud, S., Sakr, K., ArRajehi, A., Paradissis, D., Al-Aydrus, A., Prilepin, M., Guseva, T., Evren, E., Dmitrotsa, A., Filikov, S. V., Gomez, F., Al-Ghazzi, R. and Karam, G.,** 2006. GPS constraints on continental deformation in the Africa-Arabia-Eurasia continental collision zone and implications for the dynamics of plate interactions, *Journal of Geophysical Research*, Vol. **111**, no. B05411.

**Rockwell, T. K., Barka, A., Dawson, T., Akyüz, S. and Thorup, K.,** 2001. Paleoseismology of the Gazikoy-Saros segment of the North Anatolia fault, northwestern Turkey: Comparison of the historical and paleoseismic records, implications of regional seismic hazard, and models of earthquake recurrence, *Journal of Seismology*, Vol. **5**, no. 3, pp. 433-448.

**Rockwell, T. K., Lindvall, S., Dawson, T., Langridge, R., Lettis, W. and Klinger, Y.,** 2002. Lateral Offsets on Surveyed Cultural Features Resulting from the 1999 Izmit and Duzce Earthquakes, Turkey, *Bulletin of the Seismological Society of America*, Vol. **92**, no. 1, pp. 79-94.

**Rockwell, T. K., Ragona, D., Seitz, G., Langridge, R., Aksoy, M. E., Ucarkus, G., Ferry, M., Meltzner, A. J., Klinger, Y., Meghraoui, M., Satir, D., Barka, A. and Akbalik, B.,** 2009. Palaeoseismology of the North Anatolian Fault near the Marmara Sea: implications for fault segmentation and seismic hazard, *Geological Society, London, Special Publications*, Vol. **316**, no. 1, pp. 31-54.

**Ryan, W. B. F. and Cita, M. B.,** 1987. The nature and distribution of Messinian erosional surfaces; indicators of a several-kilometer-deep Mediterranean in the Miocene, *Marine Geology*, Vol. **27**, pp. 193-230.

**Sadi, D. Y.,** 1912. Marmara Havzasının 26-27 Temmuz Hareket-i Arzı 15 Eylül 1328, *Resimli Kitap Matbaası, İstanbul*, pp. 45.

**Sakınç, M. and Bargu, S.,** 1989. İzmit Körfezi güneyindeki Geç Pleyistosen(Hreniyen) çökel stratigrafisi ve bölgenin neotektoıiik özellikleri, *Türkiye Jeoloji Bülteni*, Vol. **32**, pp. 51-64.

**Saltık, O.,** 1974. arköy-Mürefte sahaları jeolojisi ve petrol olanakları,. In *TPAO Arama Grubu Arşivi 879*, pp. 24.

**Schlupp, A.**, 1996. Neotectonique de la Mongolie Occidentale analysee a partir de donnees de terrain, sismologiques et satellitaires, *PhD Thesis,* IPGS, Strasbourg

**Schwartz, D. P. and Coppersmith, K. J.,** 1984. Fault Behavior and Characteristic Earthquakes: Examples From the Wasatch and San Andreas Fault Zones, *Journal of Geophysical Research*, Vol. **89**, no. B7, pp. 5681-5698.

**Schwartz, D. P. and Sibson, R. H.**, 1989. Fault Segmentation and Controls of Rupture Initiation and Termination, *USGS open-file report*, United States Geological Survey, no: **89-315,** Proc. Conf. XLV, Palm Springs, California.

**Seeber, L., Emre, O., Cormier, M. H., Sorlien, C. C., McHugh, C. M. G., Polonia, A., Ozer, N. and Cagatay, N.,** 2004. Uplift and subsidence from oblique slip: the Ganos-Marmara bend of the North Anatolian Transform, western Turkey, *Tectonophysics*, Vol. **391**, no. 1-4, pp. 239-258.

**Sekiguchi, H. and Iwata, T.,** 2002. Rupture Process of the 1999 Kocaeli, Turkey, Earthquake Estimated from Strong-Motion Waveforms, *Bulletin of the Seismological Society of America*, Vol. **92**, no. 1, pp. 300-311.

**Şengör, A. M. C.,** 1979. Mid-Mesozoic closure of Permo-Triassic Tethys and its implications, *Nature*, Vol. **279**, no. 5714, pp. 590-593.

**Şengör, A. M. C.,** 1979. The North Anatolian transform fault: its age, offset and tectonic significance, *Journal of the Geological Society*, Vol. **136**, no. 3, pp. 269-282.

**Şengör, A. M. C., Görür, N. and Şaroğlu, F.,** 1985. Strike-slip deformation basin formation and sedimentation: strike-slip faulting and related basin formation in zones of tectonic escape: Turkey as a case study, *Soc. Econ. Paleontol. Mineral. Spec. Publ*, Vol. **37**, no. pp. 227-264.

**Şengör, A. M. C., Okan, T., Caner, İ., Mehmet, S., Haluk, E., Naci, G., Xavier Le, P. and Claude, R.,** 2005. The North Anaotlian Fault: A New Look, *Annual Review of Earth and Planetary Sciences*, Vol. **33**, pp. 37-112.

**Şengör, A. M. C. and Kidd, W. S. F.,** 1979. Post-collisional tectonics of the Turkish-Iranian plateau and a comparison with Tibet, *Tectonophysics*, Vol. **55**, no. 3-4, pp. 361-376.

**Şengör, A. M. C. and Yılmaz, Y.,** 1981. Tethyan evolution of Turkey: A plate tectonic approach, *Tectonophysics*, Vol. **75**, no. 3-4, pp. 181-241.

**Seymen, İ.,** 1975. *Kelkit vadisi kesiminde Kuzey Anadolu Fay Zonunun tektonik özelliği,* İTÜ Maden Fak. Yay., Istanbul.

**Shimazaki, K. and Nakata, T.,** 1980. Time predictable recurrence model for large earthquakes, *Geophysical Research Letters*, Vol. **7**, no. 4, pp. 279-282.

**Sidgreaves, W.,** 1912. The earthquake in Turkey on August 1912, *Nature*, Vol. **89**, no. 2233, pp. 607.

**Sieh, K.,** 1996. The repetition of large-earthquake ruptures, *Proceedings of the National Academy of Sciences of the United States of America*, Vol. **93**, no. 9, pp. 3764–3771.

**Smith, A. D., Taymaz, T., Oktay, F., Yuce, H., Alpar, B., Basaran, H., Jackson, J. A., Kara, S. and Simsek, M.,** 1995. High-resolution seismic profiling in the Sea of Marmara (Northwest Turkey); late Quaternary sedimentation and sea-level changes, *GSA Bulletin*, Vol. **107**, no. 8, pp. 923-936.

**Straub, C., Kahle, H.-G. and Schindler, C.,** 1997. GPS and geologic estimates of the tectonic activity in the Marmara Sea region, NW Anatolia, *Journal of Geophysical Research*, Vol. **102**, no. B12, pp. 27587–27601.

**Stuiver, M., Reimer, P. J. and Braziunas, T. F.,** 1998. High-precision radiocarbon age calibration for terrestrial and marine samples, *Radiocarbon*, Vol. **40**, no. 3, pp. 1127–1151

**Sümengen, M. and Terlemez, İ.,** 1993. Güneybatı Trakya yöresi Eosen çökellerinin stratigrafisi, *Maden Tetkik Arama Dergisi*, Vol. **113**, no. pp. 17-30.

**Sümengen, M., Terlemez, I., Şentürk, K. and Karaköse, C.**, 1987. Gelibolu yarımadası ve güneybatı Trakya havzasının stratigrafisi, sedimentolojisi ve tektoniği, *MTA raporu*, Ankara.

**Tabban, A. and Ateş, R.**, 1976. 9 Agustos 1912 Şarköy-Mürefte Depremi Çalısmaları Ön Raporu, T.C. Imar ve İskan Bakanlığı, Deprem Arastırma Enstitüsü Baskanlığı, Ankara.

**Tan, O., Tapırdamaz, M. C. and Yörük, A.,** 2008. The Earthquake Catalogues for Turkey, *Turkish J. Earth Sci*, Vol. **17**, no. 2, pp. 405-418.

**Tibi, R., Bock, G., Xia, Y., Baumbach, M., Grosser, H., Milkereit, C., Karakisa, S., Zunbul, S., Kind, R. and Zschau, J.,** 2001. Rupture processes of the 1999 August 17 Izmit and November 12 Düzce (Turkey) earthquakes, *Geophysical Journal International*, Vol. **144**, no. 2, pp. F1-F7.

**Toksöz, M. N., Shakal, A. F. and Michael, A. J.,** 1979. Space-time migration of earthquakes along the North Anatolian fault zone and seismicity gaps, *Pure and Applied Geophysics*, Vol. **117**, pp. 1258-1270.

**Turgut, S., Siyako, M. and Dilki, A.,** 1983. Trakya havzasının jeolojisi ve hidrokarbon olnakları, *Türkiye Jeoloji Kurultayı Bülteni*, Vol. **4**, pp. 35-46.

**Tüysüz, O., Barka, A. and Yiğitbaş, E.,** 1998. Geology of the Saros graben and its implications for the evolution of the North Anatolian fault in the Ganos-Saros region, northwestern Turkey, *Tectonophysics*, Vol. **293**, no. 1-2, pp. 105-126.

**Uçarkuş, G., Armijo, R., Çakır, Z., Schmidt, S. and Meyer, B.**, 2008. Recent Earthquake Breaks at the Sea of Marmara Pull-apart (North Anatolian Fault), *Eos Trans. AGU* San Francisco, 15-19 December,

**Uçarkus, G., Armijo, R., Pondard, N., Meyer, B. and Çakir, Z.**, 2006. The Eastern Marmara pull-apart junction (North Anatolian Fault) and its relation to the submarine end of the 1999 Izmit earthquake rupture, *Geophysical Research Abstracts*, 08807-08807.

**Ünal, O. T.**, 1967. Trakya jeolojisi ve petrol imkanları, Türkiye Petrolleri Anonim Ortaklığı, Ankara.

**Url-1** <*http://sismos.rm.ingv.it/*> accessed at 12.06.2009

**Utkucu, M., Nalbant, S. S., McCloskey, J., Steacy, S. and Alptekin, O.,** 2003. Slip distribution and stress changes associated with the 1999 November 12, Düzce (Turkey) earthquake (Mw= 7.1), *Geophysical Journal International*, Vol. **153**, no. 1, pp. 229-241.

**Vallée, M.,** 2004. Stabilizing the Empirical Green Function Analysis: Development of the Projected Landweber Method, *Bulletin of the Seismological Society of America*, Vol. **94**, no. 2, pp. 394-409.

**Vallée, M. and Luccio, F. D.,** 2005. Source analysis of the 2002 Molise, southern Italy, twin earthquakes (10/31 and 11/01), *Geophysical Research Letters*, Vol. **32**, no. L12309.

**Walker, W. G.,** 1912. Turkish Earthquake of September 13, *Nature*, Vol. **90**, no. 2241, p. 163.

**Wallace, R. E.,** 1990. *The San Andreas Fault System, California*, U.S. Geological Survey Professional Paper 1515, Govt. Print. Off.

**Watzov, S.,** 1914. Tremblements de terre en Bulgarie pendant l'année 1912, *Publ. Ins. Meteorol. Central. Sofia*.

**Wesnousky, S. G.,** 2006. Predicting the endpoints of earthquake ruptures, *Nature*, Vol. **444**, no. 7117, pp. 358-360.

**Woodcock, N. H. and Fischer, M.,** 1986. Strike-slip duplexes, *Journal of Structural Geology*, Vol. **8**, no. 7, pp. 725-735.

**Wright, T., Parsons, B. and Fielding, E.,** 2001. Measurement of Interseismic Strain Accumulation Across the North Anatolian Fault by Satellite Radar Interferometry, *Geophysical Research Letters*, Vol. **28**, no. 10, pp. 2117-2120.

**Yaltırak, C.,** 1995. Gaziköy-Mürefte (Tekirdağ) arasının sedimenter ve tektonik özellikleri - Sedimantary and Tectonic characteristics of the between Gaziköy-Mürefte (Tekirdağ), *TPJD Bülteni*, Vol. **C.6**, pp. 93-112.

**Yaltırak, C.,** 1996. Tectonic history of the Ganos fault system (in Turkish with English abstract), *Turkish Association of Petroleum Geologist Bulletin*, Vol. **8**, no. 1, pp. 137-156.

**Yaltırak, C. and Alpar, B.,** 2002. Kinematics and evolution of the northern branch of the North Anatolian Fault (Ganos Fault) between the Sea of Marmara and the Gulf of Saros, *Marine Geology*, Vol. **190**, no. 1-2, pp. 351-366.

**Yaltırak, C., Sakınç, M. and Oktay, F. Y.,** 2000. Westward propagation of North Anatolian fault into the northern Aegean:Timing and kinematics: Comment and Reply: COMMENT, *Geology*, Vol. **28**, no. 2, pp. 187-188.

**Yaltırak, C., Sakınç, M., Aksu, A. E., Hiscott, R. N., Galleb, B. and Ulgen, U. B.,** 2002. Late Pleistocene uplift history along the southwestern Marmara Sea determined from raised coastal deposits and global sea-level variations, *Marine Geology*, Vol. **190**, no. 1-2, pp. 283-305.

**Yanko-Hombach, V. and Dolukhanov, P. M.,** 2007. *The Black Sea flood question*, Springer,

**Yeats, R. S., Sieh, K. E. and Allen, C. R.,** 1997. *The geology of earthquakes*, Oxford University Press,

**Yilmaz, Y.,** 1993. New evidence and model on the evolution of the southeast Anatolian orogen, *Geological Society of America Bulletin*, Vol. **105**, no. 2, pp. 251-271.

**Yoshioka, T.,** 1996. Evolution of fault geometry and development of strike-slip basins: Comparative studies on the transform zones in Turkey and Japan, *The Island Arc*, Vol. **5**, no. 4, pp. 407-419.

**Zattin, M., Okay, A. I. and Cavazza, W.,** 2005. Fission-track evidence for late Oligocene and mid-Miocene activity along the North Anatolian Fault in south-western Thrace, *Terra Nova*, Vol. **17**, no. 2, pp. 95-101.

**Zhang, P., Mao, F. and Slemmons, D. B.,** 1999. Rupture terminations and size of segment boundaries from historical earthquake ruptures in the Basin and Range Province *Tectonophysics*, Vol. **308**, no. 1-2, pp. 37-52.

**APPENDICES**

## APPENDIX A1 – HISTORICAL SEISMICITY

Historical catalogs note more than 150 earthquakes, for the Marmara region, since the 5th century B.C. This section contains a selection of these earthquakes. The selection is based on which segments of the NAF might have been ruptured during the event. Only earthquakes which link to either to the Ganos fault, or to its neighboring segments have been taken into consideration. Please refer to Guidoboni et al (1994, 2005) and Ambraseys and Finkel (1995) for further information.

### B.C 427 Dec : Marmara Ereğlisi ( )

This is an earthquake thought to be at Perinthus (Marmara Ereğlisi). It is mentioned in the fourth book of Hippocrates' Epidemics:

*"4.21. During the winter solstice, a large star. On the fifth and sixth following, earthquake. When we were in Perinthus the asthmatic woman, Antigenes' wife, who did not know whether she was pregnant. She had red patches on her skin…"*

There is a disagreement of the date of the earthquake. Capelle, (1924) dates it to B.C. 427, whereas Deichgraber, (1933) relates it with the epidemic in Perinthus at B.C. 399-5. Though an astronomical event is mentioned, a more precise date has not been established up to date.

The lack of further detail, such as descriptions of damage or loss of live might be because the event was not destructive. However, an earthquake which causes many losses can be a good reason for an epidemic in the region. The poor information available, does not allow us to make any interpretation about the event.

### B.C. 360: (≥ VIII ≤ X) Çanakkale, Ereğli (1)

This is an event related to Ophryneum (near Çanakkale) and Heraclia Pontica (Ereğli, Black Sea). Information is based on two accounts. The first is mentioned in a trial by Demosthenes; the Greek rhetorician. Demosthenes wrote in Contra Apaturium:

*"…After these events, then, a terrible tragedy struck Parmenion, O judges. For while he was living at Ophryneum, having fled from his country, there was an earthquake in Chersonese, so his house collapsed and his wife and children were killed…"*

The earthquake mentioned here caused a house (and probably more) to collapse in Ophryneum. Aristotle makes in Meteorologica general remarks about earthquakes and mentions probably the same earthquake.

*"…Furthermore, the most violent earthquake take place where the sea is subjected to currents and the land is of a porous and cavernous kind. That is why they also occur in the Hellespont. Examples of such events have occurred in our lifetime. Thus an earthquake which occurred in certain places only ceased when the clouds broke and the wind which had driven them moved away, as happened recently near Heraclea Pontica…"*

Heraclea Pontica is an ancient city located at Ereğli on the Black Sea cost. The date of Aristotle's remark is unclear and the adverb "recently" makes the date more arguable. However his remark of the fire in Ephesus (B.C. 356) allows constructing an approximate date.

**B.C 287: (≥ IX ≤ XI) Ortaköy (Saroz) (1)**

An earthquake occurred at Lysimachia (Ortaköy-Saros). The event affected the Gelibolu region and is described by the Latin historian Justin. Though Justin is thought to have lived in the 2nd-3rd century (AD) the date he provided for the earthquake can be well established.

*"…At about this time, there was an earthquake in the region of the Hellespont in the Chersonese, but it was the city of Lysimachia, founded by the king Lysimachus twenty-two years earlier, which was worst, affected, being reduced to ruins. This was a bad omen for Lysimachus and his house, for it not only caused havoc in the regions where it was felt, but was also a portent of his own fall from power."*

The foundation of Lysimachia is in 309 B.C. and Justin is mentioning that the earthquake occurred 22 years after the foundation, which gives us 287 B.C. The description designates an extensively destructive event, which causes a city to ruin totally.

This earthquake could be most probably either in the Saros bay, or on the western part of the Ganos fault.

**c.50 : Dardanelles (1)**

Flavius Philostratus, who is a Greek sophist, lived between 172 and 250 mentions the event in his book "The Life of Apollonius" He states an earthquake affected Hellespont (Dardanelles).

*"At one time the cities on the north side of the Hellespont were struck by earthquakes and Egytpians and Chaldeans (in this context wizards) went begging abouth through them to collect money, pretending that they needed ten talents to offer sacrifices to Earth and Poseidon. And the cities began to contribute under the stress of fear, partly out of their common funds and partly out of private. But the imposters refused to offer the sacrifices in behalf of their dupes unless the money was deposited in the banks.*

*Now the sage determined not to allow the peoples of the Hellespont to be imposed upon; so he visited their cities, and drove out the quacks who were making money out of the misfortunes of others, and when he divined the causes of the supernatural wrath, and by making such offerings as suited each case averted the visitation at small cost, and the land was at rest.…"*

No evidence of destruction is available, however the description of the fear of habitants indicate presumably a large shock. The earthquake might have occurred in the Saros bay.

**447 Jan 26: (≥ IX ≤ XI), Ms = 7.2; Istanbul, Thrace, Dardanelles, Gelibolu, Iznik, Kocaeli (1)**

A very destructive earthquake ruined many places in and around Constantinople (Istanbul), Nicomedia (Iznik), and Bithynia (Thrace). Information about the event is available by several sources; therefore the date is also well established. Ambraseys and Finkel, (1991) indicate that this shock was preceded by another damaging shock on Jan 26, which caused the main destruction in Constantinople.

Damage and distribution: Marcellinus records damage in Istanbul: *"…many recently rebuild walls…collapsed together with fifty-seven towers… …huge blocks of stones in a building and a number of status collapsed in the Forum Tauri……many cities were reduced to ruins"*

Evagrius verifies the causes of the earthquake around Istanbul and extends it's affects to Bithynia (Thrace), Hellespont (Dardanelles) and Phrygia. He remarks a collapsed long wall in Chersonese (Gelibolu) and states that many villages were reduced to ruins. Though his descriptions are in an exaggerated mode, he is pointing events which could be linked to surface rupture, cracks, landslide and tsunami. However he is not giving locations for these phenomena's.

Malalas signifies an earthquake caused destruction in Constantinople (Istanbul) but also in Nicomedia (Kocaeli). He specifies that Nicomedia was almost ruined and was flooded by the sea.

In the Chronicon Paschale walls are reported to be collapsed in Constantinople (Istanbul).

The destruction explained in the accounts expands to a very wide region; from Hellespont to Nicomedia, which is not very credible. The size of the event seems to be open to question.

Loss of live: Marcellinus portrays a high number of death: *"...starvation and noxious smell killed thousands of people and cattle..."* However the Chronicon Paschale counters this information partly. *"...For amidst such great peril he did not kill anyone."* Though Marcellinus points on thousands of death he does not say they died because of the destruction, moreover due to after affects of the earthquake.

Seismotectonic interpretation: Considering the damage distribution and that most of the damage is centered in Istanbul, the earthquake appears to have occurred within the Sea of Marmara; presumably in the central part of the sea. Ambraseys and Finkel, (1991), relates the destruction in Constantinople to the shock on Jan 26. They indicate damage in Hellespont and Bithynia and propose an epicentral area in the central basin. However in more recent studies Ambraseys revises its location, and puts the 447 shock next to the Sapanca lake (Ambraseys, 2002a, 2006). For such a wide damage distribution it is hard to argue about which segment of the NAF has ruptured.

**460 : (≥ VIII ≤ IX) Erdek, Thrace, Dardanelles (1)**

An earthquake which affected mainly Cyzicus (near Erdek), but also Thrace and Hellespont (Dardanelles). The event is based on two accounts; Marcellinus and Evagrius.

Damage and distribution: Marcellinus reports that Cyzicus was destroyed partly. Evagrius expands the destruction to Thrace and Hellespont and records that Cyzicus was ruined completely. However his information is lacking of further description of the damage.

The presence of insufficient information to damage and a number of deaths and injuries, it is not possible to infer any size of the earthquake. However existing data indicate the earthquake may have occurred on the southern branch of the North Anatolian Fault.

**477/478/480 Sep 24/25/26: (IX), Ms = 7.3; Dardanelles, Thrace, Istanbul, Kocaeli, Gölcük (1)**

Several accounts exist for this event, providing damage information over a wide area (Marcellinus, Malalas, Chronicon Paschale, Theophanes, Cedrenus, Great Chronographer). Ambraseys, (2002a, (2006; Ambraseys and Finkel, (1991) dates the event to 26 Sep. 478. The exact date of the event is not clearly identified; however it can be placed in 26 Sep 477 or 478.

Damage and distribution: Marcellinus reports that some gates, churches and the statue of Theodosius collapsed in Constantinople (Istanbul). A similar destruction at Constantinople is expressed by the Great Chronographer. However he is making a more devastated picture, writing that all the towers were collapsed and many houses were destroyed after a 30 day period with shocks. The Anonymous Ecclestical History affirms such a level of destruction too, as do Cedrenus and Theophanes.

The Great Chronographer refers a rise of the sea, which causes damage to some houses, in Constantinople. He is also pointing extensive damage at the Dardanelles region:

*"...The earthquake continued for 30 days... ...Also in the reign of Zeno, a strong earthquake occurred, causing substantial damage. For in the Hellespont area it damaged most of the cities of Abydus and Lampsacus, and in Thrace it reduced Callipolis and Sestus to ruins, as well as most of Ttenedos; and 50 towers of the Long Walls were also demolished, and all those who had fled there were buried in them. In the area around Sestus a sort of mud welled up from the earth and immediately became stiff and solid".*

Malalas writes that beside Constantinople, Nicomedia (Kocaeli) and Helenopolis (Karamürsel-Gölcük) suffered from the earthquake. Ambraseys and Finkel, (1991) point out that the major destruction was in Nicomedia and Helenopolis.

Loss of live: Many accounts point that a high number of people have died, so that Constantinople started to stink and caused noxious exhalations. Many people were buried under their houses. Nevertheless a clear number can not be obtained.

Seismotectonic interpretation: Based on the catalog of Guidoboni et al., (1994), the most affected city is to be Constantinople, hence the epicenter could be within the central part of the Sea of Marmara. On the other hand Ambraseys, 2002a, 2006; Ambraseys and Finkel, 1991 consider that the major destruction was in Nicomedia and Helenopolis and place the shock near Gölcük. In the text of the Great Chronographer it is not clear whether the earthquake affecting Dardanelles is the same, which struck Istanbul or it is a separate event occurred within the 30 day period of aftershocks. Theophanes says this is the second shock hitting Constantinople. Hermann, (1962) considers there were two events and places the second to 488. The damage distribution covering a wide area from Nicomedia to Hellespont can be due to 2 main shocks, similar as in 1766.

**543 Sep 6 : (IX); Erdek (1)**

Cyzicus was struck by a destructive earthquake. The date of the event is not very well obtained. The earthquake demolished half of Cyzicus (near Erdek), (Malalas). This might be an event occurred on the southern branch of North Anatolian Fault.

**557 Dec 14/23: (IX-X), Ms = 6.9; Istanbul (1)**

This is an earthquake which is described to have demolished Constantinople (Istanbul). Panic and heavy damage is described by several accounts (Agathias, Malalas, Theophanes and others).

Damage and distribution: The two main walls of Constantinople have been collapsed. Several churches suffered extensive damage, like St. Samuel, Theotocos at Perala, St. Vicentus and St. Sophia. The dome of St. Sophia was badly damaged and resisted only for one year before it collapsed (The Great Chronographer, Pseudo-Dionysius, Theophanes and Cedrenus). Several column and statues were overturned (Malalas, Theophanes). Rhegium (Küçükçekmece) was reduced to ruins and almost no building remained safe.

Most authors record the damage only in Constantinople. They provide no information about the surrounding of the city. Information is only available in the Life of St. Symen the Stylite the Younger, where Nicomedia (Izmit), Nicea (Iznik) and others cities of Illyria is written to be damaged.

Loss of live: Aghiatas says “large number of people perished in the disaster”. On the other hand, other authors mention only fear and panic of people, who have

apparently survived. Some point that others were rescued even after two-three days under the ruins. They either discard the deaths or don't bother because their number is not very high.

Seismotectonic interpretation: The aftershocks continued for 10 days, which relatively short for a large earthquake which caused so much damage in Istanbul. Beside, the distribution of damage is unclear. There is evidence of destruction in Constantinople and Rhegium. However the damage in Nicomedia, Nicea and other cities of Illyria is mentioned only in one account and is not described. Beside, the same account placed the event to 554, which causes uncertainty. Considering that the evident damage is centered in Constantinople, the earthquake could be a similar event like the 1894-Istanbul earthquake. Ambraseys, 2002a, 2006; describes the same damage based on the same sources but places the event off shore of Küçükçekmece.

**740 Oct 26: (≥ IX ≤ XI), Ms = 7.1; Istanbul, Kocaeli, Iznik (1)**

Constantinople, Nicomedia and Nicea were affected by this earthquake. The date of the event is well obtained. The accounts Theophanse, Georgius Monachus and Nicephorus provide information on the damage mainly in Istanbul.

Damage distribution: The main walls collapsed in Constantinople. St Irene is mentioned among many churches which were damaged; some were destroyed to their foundations. Nicomedia (Izmit) and Praenetus (Karamürsel) suffered heavily; only one church survived in Nicea (İznik). The sea invaded some of the land.

In Thrace some villages were destructed, but further information about the western extension of the damage is not available.

Loss of life: Many people were killed by the disaster and the ones who survived had to move out of the city.

Seismotectonic interpretation: The aftershocks continued for 12 moths, which may be because the event was large. The damage occurred in Istanbul and on the East and South of the city (Niceomedia and Nicea). Ambraseys and Finkel, 1991; puts the shock in the Izmit bay. Ambraseys, 2002a, 2006; revises the location of the event and places it southwest of the Çınarcık basin. Since Iznik was heavily damaged, one can interpret that the shock was on the southern fault segment of the Çınarcık basin.

**824 May 5: (VIII); Tekirdağ (1)**

Two accounts cite this event. It caused damage in Panion (Tekirdağ).

The city walls were collapsed due the large shock, so that the Emperor Micheal could easily conquer the city.

**926: (≥ VIII ≤ X); Thrace (1)**

This is a large earthquake which affected the villages in Thrace. "At that time there was a terrible earthquake in the Theme of the Thracians. It made a huge chasm, which swallowed up many villages and churches" (Theophanes Continuatus). The earthquake is said to have swallowed up buildings which presumably indicates surface faulting.

**989 Oct 26: (VIII), Ms = 7.2; Istanbul, Kocaeli (1)**

A destructive earthquake caused damage at St. Sophia and in Nicomedia. Many houses were ruined in Nicomedia and villages near the city were almost completely destroyed. Third of St. Sophia collapsed and was repaired afterwards. This event is not mentioned in Ambraseys and Finkel, (1991), but in Ambraseys, 2002a, 2006, where the epicentral area was placed on the western edge of the Çınarcık basin.

**1010 Jan and March 9: (VII); Istanbul, Gelibolu**

Two shocks occurred within a 40 day of period, which the second caused destruction in Istanbul (Constantinople). The event is described by several non-contemporary accounts. 11th-12th century historians describe damage in Istanbul (Scylitzes, Cedrenus, Glycas, Atteliates). Galanopoulos (1955 p.101) maintains that the earthquake occurred in Gallipoli (Gelibolu). Ambraseys and Finkel (1991) date the event as 1011 based on Cedrenus.

Damage distribution: Scylitzes mentions that the churches of Forty Martyrs and All Saints collapsed during the shock on 9 March. All damage records are limited to Constantinople.

Loss of live: No information available in Guideboni (2005). In contrast Ambraseys and Finkel, 1991 report a great loss of live in Bithynia.

Seismotectonic interpretation: The aftershocks lasted for two years (Attaliates), which indicates a very large shock. Since the damage is limited to Istanbul the

earthquake occurred presumably on the central segments of the North Anatolian Fault within the Sea of Marmara.

**1026 Dec 4: (; Istanbul**

This earthquake is not well known. Information is based only on the Arab historian al-Antaki. Byzantine sources do not mention this event. Al-Antaki notes:

*"In the second year of the reign of Constantine, there was a tremendous earthquake at Constantinople on the 4th day of the month of Canun I in the year 417 [4 December 1026]. Many buildings collapsed"*

The limited amount of information of the earthquake hinders us to do any interpretation on its existence and location.

**1032 Aug. 13: X ; Istanbul**

Byzantien historians report that a strong earthquake hit Constantinople (Scylitzes, Zonaras). Damage on some major buildings are given in these sources.

Damage distribution: where the hospital of St.Zoticus (Galata), the aqueduct of Valens, and the eastern arcade of St.Sophia was collapsed.

Although some major buildings were collapsed during this event the information is poor to constrain the dimensions of the shock. This is probably an intermediate size earthquake located close to Istanbul.

**1063 Sep 23: (VIII-IX), Ms = 7.4; Tekirdağ, Barbaros, Mürefte, Erdek, Istanbul**

A strong earthquake struck the western coasts of the Sea of Marmara. The main source for this event is Attaliates, following several other accounts. The date of the event is well obtained.

Damage distribution: There are no certain buildings mentioned to have experienced damage in Constantinople or in its surrounding. Many houses and some churches are written to been demolished almost entirely. The desctruction in Rhaedestus (Tekirdağ), Panium (Barbaros) and Myriophytus (Mütrefte) is described in general. Almost all houses are written to be ruined to the ground. Cyzicus (near Erdek) suffered as well from the shock. Many houses were turned to ruins and the Greek temple collapsed almost entirely. Hellespont is also reported to have suffered from the event.

Loss of live: There is no clear number given, however a large number of people have died (Attaliates).

Seismotectonic interpretation: The main shock was followed immediately by three other shocks, which were strong but not like the former. Ten to twelve aftershocks occurred during the following night of the event. The aftershocks continued for 2 years (Guideboni p.48). The main damage is centered on the western part of the Sea of Marmara. Istanbul as a capital suffered as well of the event however Rhaedestus, Panium, Myriophytus and Cyzicus were more affected. Therefore the events seems to have occurred along some part of the fault within the Tekirdağ basin or the Ganos fault on land. This interpretation is in accord with Ambraseys, 2002a, 2006; and Ambraseys and Finkel, 1991.

**1090 Dec 6: (VIII-IX); Istanbul**

This is a shock which caused great destruction in Istanbul. The event is mentioned by Glycas and Zonaras. Other authors date this event to years between 1081-1088. This event is not taken into account in Ambraseys, 2002a, 2006; Ambraseys and Finkel, 1991.

Damage distribution and loss of live: Glycas and Zonaras report damage in Constantinople where many houses, arcades and churches were collapsed and many people were also killed.

Seismotectonic interpretation: The destruction is limited to Constantinople there the earthquake was presumably in the central part or in the Çınarcık basin of the Sea of Marmara.

**1296 June 1 and 13: (VII-VIII), Ms = 7.0 Istanbul**

Two shocks, the first on June 1 and the second on Jun 13 demolished many buildings in Constantinople. In general most accounts report damage related to the first shock. Ambraseys and Finkel (1991) dates this earthquake to 1st Jun.

Damage distribution: Pachymeres describes that the former shock ruined many ancient buildings and several new buildings. The city walls, the roof of church of All Saints collapsed, as well some other parts. A bronze statue of the Archangel Michael fell down, too. The first shock is described by other accounts to have affected many houses, the city walls and to caused the churches to be split open (Athos Vatopediou 290 and Paris Supplementum gr. 682. I.).

Loss of live: No indication.

Seismotectonic interpretation: The event caused damage only in Constantinople. Therefore the shock must have occurred on the fault near to Istanbul within the Sea of Marmara. On the contrary, the event on 1st Jun is placed by Ambraseys, 2002a, 2006 on the southern branch of the NAF, near Bolu-Kaynaşlı.

**1343 Oct 14,18 and Nov 20: (VIII), Ms = 7.0; Istanbul, Gelibolu, Ortaköy, Beylerbeyi**

A foreshock on the 14th Oct was followed by violent shocks on the 18th October 1343. It caused destruction mainly in Constantinople. The event was felt as far as Lysimachia and Gallipoli, but less. On the 20 November another shock caused fear among people.

Damage distribution: Information on damage is only available for Constantinople. The walls of Theodosian are reported to have collapsed, however the walls of Constantine remained undamaged. Many Towers, palaces and churches collapsed, the east side of the apse of St. Sophia was damaged, and houses as well as vineyard and garden walls were ruined. The damage towards the western regions of Constantinople is unnamed.

Tsunami: The shock on the 18th was followed by a tsunami. The sea is described to have penetrated 1.8 km inland. Locations for the flooding is not given, expect one account which writes that the sea rose up as far as Stauros (Beylerbey) (Schreiner 1975, no.s). In a manuscript the height of the waves a described to be one to three men size (~2-5 m) (Athenagoras 1935)

Seismotectonic interpretation: The aftershocks lasted for one year, which indicates a large shock. The earthquake presumably occurred on the central and western part of the NAF within the Sea of Marmara; along the faults in the central basin and towards the Tekirdağ basin.

**1344 Nov 6: (IX); Gaziköy, Hoşköy, Istanbul**

This is a destructive shock, which affected mostly the western region of Constantinople. The shock occurred following the earthquake sequence of 1343. This event is excluded in Ambraseys, 2002a, 2006; but not in Ambraseys and Finkel, 1991, where he describes damage in the Ganos region.

Damage distribution: The fortresses of Ganos (Gaziköy) and Chora (Hoşköy) were completely destroyed. A citadel at Chora collapsed; more than half of the houses in the village were ruined to the ground (Schreiner 1975).

The St. Sophia at Constantinople had already suffered from the previous event (1343). This shock increased the split on the apse of the east side and caused many bricks and mosaics to fell down. A few days after, the east apse and the third of the dome collapsed entirely.

The bronze statue of St. Micheal was damaged again. The damaged related to Istanbul is not mentioned in detail which indicates is suffered less than other regions to the west. A fortress is also reported to be totally collapsed on the Marmara island.

Loss of live: An account indicated that more than three hundred people were buried under the ruins of the buildings at Chora (Schreiner 1975).

Seismotectonic interpretation: This event is a shock following the earthquake sequence in 1343. The earthquake of 1343 triggered most probably the fault to its west. The 1344 shocks seems to have occurred in some extend of the Tekirdağ basin and the Ganos fault. Ambraseys and Finkel, (1991) consider this earthquake to have occurred on the western part of the Ganos fault.

**1354 Mar 1: (VII-X), Ms = 7.4; Gelibolu, Eceabat, Tekirdağ, Bozcaada, Istanbul**

A devastating earthquake caused damage all along the western coast of the Sea of Marmara. Tenedos (Bozcaada) was also struck by the event. Information is available by several contemporary accounts like, Nicephorus Gregoras, Emperor John VI Cantacuzenus and Matteo Villani. The date of the event is precisely defined. The earthquake caused to collapse many fortress, which allowed the Turks to occupy Gelibolu.

Damage distribution: The earthquake was strongly felt at Constantinople and caused damage to large buildings and part of the city walls. Cantacuzenus records that almost all costal towns of Thrace were demolished; houses were reduced to ruins and walls were destroyed to their foundations. The castle of Gallipoli (Gelibolu) ruined so the people could not resist against the attacks of the Achaemenids (Turks). Villages between Madytus (Eceabat) and Rhaedestus (Tekirdağ) are reported to be ruined to its foundation (Schreiner 1975). Tenedos was also struck by the earthquake and Turks occupied the island.

Loss of live: Several accounts mentioned that many people died under the ruins, in Gallipoli, Madytus and Rhaedestus. However they also report that some were killed by the Achaemenids or were frozen while trying to flee from Gallipoli.

Seismotectonic interpretation: The event has affected the western cities of the Sea of Marmara. The damage indicates that the size of the event was very large. Therefore it can be considered that the earthquake occurred along the Ganos fault or on its western extension towards the Saros bay. The event is located inland on the Ganos fault by Ambraseys, (2002a, 2006) and offshore in the Saroz bay by Ambraseys and Finkel (1991)

**1509 Sep 10: ()Ms = 7.2; Istanbul,**

This event is the best studied historical earthquake along the North Anatolian Fault. First studies described this event as the largest and most destructive earthquake in the last five centuries in the Eastern Mediterranean and allege it is felt in a wide area; from Bolu to Edirne (Ambraseys and Finkel, (1995)). The earthquake occurred on 10 September 1509 (Gregorian Calendar) at around 22:00. Information about the event is based on contemporary and modern Turkish and occidental sources. Although some sources express damage within the vicinities of Bolu, Edirne and Gelibolu, detailed and reliable descriptions of damage exist only for Istanbul.

Damage and distribution: Istanbul suffered intensively from this event. 1 contemporary records indicate a destruction of 1070 – 1500 houses, where the household of Istanbul is estimated to be 54,000 at that time.

Among the many churches in Istanbul only the St. John Theologos church near the hippodrome is known to have collapsed. Mosques suffered as well from the earthquake. The newly built Beyazid mosque (of Sultan Beyazid-II) was damaged. (woodcut Coecke, Koysan mi?). Ottoman sources report some damage and a repair on some part of the aqueducts. The earthquake caused considerable damage chiefly to the vulnerable segments of the outer land walls. However the robust parts, which constituted the majority, remained preserved. The Galata tower did not collapse however the cantilevering parts or the structure fell off.

There is no evidence that the earthquake caused any destruction in Tekirdağ, Gelibolu and Bolu; though it was mentioned to be effected in some sources.

Loss of Live: The loss of life is estimated to be between 1500 – 5000; among a population of 250,000 at that time in Istanbul. This corresponds to 0.4 – 2% of the city population.

Seismotectonic interpretation: Previous studies defined the 1509 earthquake as a Little Apocalypse (Ambraseys and Finkel, (1990)). Further studies of the earthquake yielded to a Ms : 7.25. It is most probably that the earthquake occurred in central part of NAF within the Sea of Marmara. (Ambraseys, (2001))

**1542 June 12: () ; Istanbul, Edirne, Gelibolu**

The event is described as a destructive earthquake in Thrace, which caused extensive damage and much loss of life. Information relies on a dispatch and letter. However the event appears more to be spurious.

Damage and distribution: Many nobles and important buildings and the half of the Palace of the Sultan are reported to be felled down. Beside 1700 houses (Schmidt, (1879)) no certain structures are named to be destructed . It is written that the shock effected Edirne and Gelibolu however with no further explanation of damage.

Loss of life: A loss of 120.000 people is reported within Istanbul, Edirne and Gelibolu and their vicinity (Anonymous, (1542), Bataillon, (1966)) . The loss in Istanbul is described as 4500 and (Schmidt, (1879)). However in Anonymous, (1542) a loss of 2000 people is given inside the Palace of Sultan which means that 44% of the dead are within the palace. Ottoman sources provide no record for such an event. Later writers report this earthquake with an earthquake which occurred on 13 June 1542 in Tuscia – Italy. Therefore this event is most possibly fabricated.

**1556 May 10: Ms = 7.1; Edincik, Bursa, Istanbul**

At the dawn of this day, a large shock in the Sea of Marmara ruined many places like Edincik (Bandırma), Bursa and Istanbul.

Damage and distribution: Eyewitness sources report damage at Istanbul. The St. Sophia, Edirne gate, city walls at the Golden Horn and some domes in the Topkapı Palace have suffered damage. Beside Istanbul damage is also reported in Bursa. The Minearet of the Ertuğrul Mosque was collapsed and the Sultan Mehmet II mosque was repaired.

Loss of life: No clear number of human losses is available; expect that thousand of men perished in Edincik and Hamid-ili (?).

Seismotectonic interpretation: Beside Istanbul, all of the damage heap together in the southern part of the Sea of Marmara in the vicinity of Bandırma. This indicates that this event most possibly occurred on the second strand of the NAF.

**1659 Feb. 17: Ms = 7.2; Gelibolu, Tekirdağ, Istanbul**

A damaging earthquake occured in the West of the Marmara region. The shock came in the early evening and caused damage in Istanbul, Gelibolu and Tekirdağ. The event was also felt in Izmir, Manisa and in Skiathos (island east of Greece).

Damage and distribution: Old buildings, dwellings and many chimneys collapsed in Istanbul. The mosque of Sultan Süleyman was damaged as were others in the city. Mosques and churches in Tekirdağ suffered from the event. The namazgah in Gelibolu was partly ruined. Some damage to the domes of mosques in Manisa is also reported.

Loss of Live: No information available

Seismotectonic interpretation: The damage clusters mainly on the West of the Marmara region. The damage in Istanbul is restricted with weak structures, which indicates that the location of the shock is far to the city. Gelibolu and Tekirdağ are the main cities which suffered from the event. This implies that the earthquake occurred most probably either on the western part of the Ganos fault or in the Saros bay. Ambraseys, 2002a considers that the event was located in the Saros bay.

**1730 Jun 10: ; Saros, Evreşe**

Information about this event is poor, however there is some information that a shock caused destruction in the southern parts of Thrace.

Damage and distribution: Some villages along the road from Istanbul to Thessalonica were damaged of an event which was felt in Athos and Istanbul.

A castle in the Golf of Saros (Muarız) needed repair. This castle was possible the castle of Evreşe (Kadıköy).

Loss of life: No information available.

Seismotectonic interpretation: This event was most probably located in the bay of Saros.

**1752 Jul 29: ;Edirne, Havsa, Hasköy, Ipsala, Enez, Ezine, Evreşe, Bozcaada**

An earthquake shock in Thrace, preceded by foreshock caused damage from Ezine to Edirne. There are two contemporary narrative accounts, which one is a eyewitness. They are written by the 19th century historian Ahmet Badi from Edirne. Other sources are the notes of the English ambassador of Istanbul, and several references of repairs. All in all they provide wide information about the effects of the event.

The earthquake occurred Saturday evening 29 July 1752 and was followed by aftershock all night long (İzzi,????).

Damage and distribution: Edirne suffered great damage. All minarets were demolished or leaned expect that of Sultan Selim, Defterdar (Mustafa Paşa) and İbrahim Paşa mosques, domes collapsed, houses, shops and walls. For instance, 7 domes and 4 minarets of the Üç Şerefli mosque were ruined. The Taşlık, Ayşe hatun, and Şeyh Şüca mosques were also badly damaged. Numerous other names are mentioned in Ottoman records. On a note about estimates of damage, the city walls and the gates of Edirne are described devastated. As well military installations did not escape from destruction. Havsa, a village 30 km southeast Edirne was totally ruined. There were many deaths and injuries at Hasköy. Further south the destruction was increasing. Some walls of the Sultan Murad I mosque in Ispala collapsed and its minaret leaned. At Enez the castle suffered much more than the 1730 earthquake. Many parts, like its gate, domes, mosque and mihrap collapsed totally.

The earthquake was felt in Istanbul strongly, however damage occurred only on a few old buildings. The English ambassador Porter reported vertical ground motions following 3-4 strong shocks from NW to SE. The shock was also felt in Izmir, but no damage occurred. Some repair at the castles at Evreşe (Kadıköy), Bozcada and Molivo were recorded however reason of damage is not available.

Loss of live: A number of few thousand people were killed is given by European sources; however this seems to be exaggerated. There is no clear account on the number of deaths, except that a “considerable number” of people were killed in the Havsa-Zerna region.

Seismotectonic interpretation: The earthquakes continued for 3 month in Edirne and 1 year for the region (Dizer and İzgi 1987). As well as the damage and the aftershock indicate a large scale for the event. The damage clusters on an N-S trending line, between Enez and Edirne. The destruction at Istanbul was limited with only one old house and there is description of demolition along the western coasts of the Sea of Marmara. Therefore it is most possible that the earthquake occurred on the western extension of the NAF in the Saros bay.

**1756 Nov 26: ;Evreşe, Istanbul, Edirne**

Facts about this event is very limited. The shock was heavily felt in Edirne and in Istanbul. However, clear evidence about damage is restricted. Repairs of the castle in Evreşe castle may be related to this event rather than the 1752 shocks.

**1762 Jun 13:** A strong shock was felt in Adrianople (Edirne). The damage was limited and only local. The shock was not reported in Istanbul. Some repair of the Üç Şerefli mosque and complex in Edirne is dating 1762/63.

**1766 May 22: Ms = 7.1; Istanbul, Kemerburgaz, Çatalca, Çekmece, Çorlu Edirne, Bursa,**

A damaging earthquake in the Sea of Marmara. The destruction extended to a wide area, from İzmit to Tekirdağ (E-W) and from Edirne to Bursa (N-S). Sources are plentiful; this event is one of the best recorded events. Ottoman records are by the contemporary official court historian Hakim and contemporary chroniclers Çeşmizade, Şemdanizade and Vasıf. Ottoman archives provide information for Istanbul and Izmit, whereas Greek sources provide for outer regions. There are as well European eyewitness accounts giving information about the destruction.

Timing: The date is well established. The earthquake occurred half an hour after sunrise, on Thursday; 12 Zilhice 1179 a. H., which corresponds to 22 May 1766.

Damage and distribution: The majority of damage records are related to the structures within Istanbul. A high number of mosques were destructed, where some of them escaped serious damage. Their minarets were mostly overturned and the domes collapsed of some of them. Damage was reported at Galata, Pera, Üsküdar and some localities north along the Bosphorus. The land walls were ruined along most of their length. The imperial kitchenette, towers, and some walls collapsed at the Topkapı Palace, causing the Sultan to live under tents for several days. Damage

occurred at a number of churches, which names are unidentified. Many hans and the Grand Bazaar suffered as well from the earthquake. The damage extended to Çatalca and Çekmece, where houses and walls were strongly demolished. The Effect expanded further into the Thrace causing loss at Kemerburgaz, Çorlu and Karışdıran. Edirne escaped only with slight damages.

The effects further west at Tekirdağ, Ganos, Gelibolu and Çanakkale are not firm. Though there are accounts on some damage, this may be the result of the earthquake in Agust 1766.

To the east the damage was much stronger. Izmit was badly effected, the mosques Fevziye (Mehmet Bey) and Çalık Ahmet? (yapım 1907) were partly demolished. A seismic sea-wave caused heavy damage at the dockyards.

South of the Marmara, there is damage near Karamürsel, where a mosque is reported to be collapsed seriously. At Bursa, the Emir Sultan mosque suffered much so that is was unusable for praying until repair.

Sea wave intrusions were reported near Galata, Bosphorus and at Mudanya causing flooding at villages.

Loss of life: In Istanbul 4-500 people died mostly under the ruins of their houses. A number for other region in Marmara is unavailable.

Seismoectonic Interpretation: A S-N running shock lasted for 2 minutes as reported from Istanbul, which was felt as well for 2 minutes from Izmit.

**1766 Aug 5: Ms = 7.4; Tekirdağ, Gaziköy, Gölcük, Mürefte, Gelibolu, Biga, Bozcaada**

Another major shock further west of the Sea of Marmara ruined all damaged structures caused by the shock of May 1766. The distribution of damage enlarged further west to Tekirdağ, Ganos, Gelibolu, Biga and Edirne.

Timing: The earthquake occurred on 5 Aug (NS) at 12:30 AM.

Damage distribution: The destruction was mostly between Tekirdağ and Mürefte. At Gaziköy only one of ten houses remained. Though there is no detail of damage, the following places sustained destruction; Avdin, Ganos, Gaziköy, Gölcük, Hoşköy, Inceköy, Eriklice, Kalamış, Kestambol, Loupida, Güzelköy, Mürefte, Yeniköy, Palamut, Şarköy, Çınarlı, Senduk, and Sternaköy. In Hoşköy 800 houses were ruined

and most of the population died under the wrecks. Şarköy was destroyed mostly. Some accounts report that all stone houses and bread ovens were demolished at Silivri, Tekirdağ and Gelibolu. Several mosque have been destroyed totally or partly at Gelibolu. Two-thirds of the castle at Evreşe (Muarız Gulf) was ruined. Damage is reported at Enez; the castle and mosque Mehmet II needed repair. The castles Seddülbahir and Kilidülbahir at Dardanelles collapsed extensively. Sultanhisar, south of Dardanelles suffered badly; all pottery kilns, houses, minarets and chimneys collapsed entirely. 28 windmills were ruined as well. The castle at Bozcaada needed extensive repair. Though affected many buildings the damage in Istanbul was less according to the May event. Some hans, Edirne kapusu, mosques and masonry buildings were ruined. There is also few information of destruction in Edirne, Izmit, Yalova, Karamürsel and Bursa.

Loss of life: Much loss in mentioned in several places, however non of them ends up with a clear number. Available numbers are 30 people in Istanbul, 4 people in Karamürsel.

Seismotectonic Interpretation: The shock lasted less than 1 minute as reported by the Ambassador Murray from Istanbul. Some cracks on the ground and liquefaction was reported around Tekirdağ and Gelibolu.

## APPENDIX A2 – CO-SEISMIC AND CUMULATIVE OFFSET MEASUREMENTS

**Table A2.1 :** Cumulative offset measurements. Coordinates are in UTM ED50.

| Id | Offset | Error | Location | Structure | X | Y |
|---|---|---|---|---|---|---|
| 1 | 7.0 | 0.3 | Güzelköy | Tree limit | 524504 | 4510059 |
| 2 | 8.0 | - | Güzelköy | Stream | 524476 | 4510052 |
| 3 | 8.0 | 2.0 | Sofuköy Lok 495 | Stream | 501564 | 4500978 |
| 4 | 9.0 | 1.0 | Kavak | Paleo-channel | 488530 | 4495658 |
| 5 | 10.6 | 0.5 | Sofuköy | Stream | 500605 | 4500590 |
| 6 | 11.0 | 0.5 | Güzelköy | Paleo-channel | 522761 | 4509216 |
| 7 | 11.0 | 0.3 | Güzelköy | Stream | 522709 | 4509189 |
| 8 | 11.0 | 1.0 | Yayaköy | Stream | 516833 | 4507080 |
| 9 | 12.1 | 0.3 | Güzelköy | Stream | 523316 | 4509465 |
| 10 | 12.6 | 0.2 | Güzelköy | Ridge | 524400 | 4510024 |
| 11 | 12.7 | 0.5 | Gaziköy | Road | 528042 | 4511147 |
| 12 | 12.9 | 2.0 | Yörgüç | Stream | 511982 | 4505469 |
| 13 | 15.0 | 0.5 | Yayaköy | Road | 516791 | 4507070 |
| 14 | 17.1 | 0.5 | Sofuköy | Stream | 500538 | 4500572 |
| 15 | 18.0 | 0.5 | Güzelköy | Stream | 525052 | 4510201 |
| 16 | 19.0 | 2.0 | Yörgüç | stream | 513609 | 4506152 |
| 17 | 20.0 | - | Mursalli | Stream | 519436 | 4508116 |
| 18 | 21.0 | 0.5 | Güzelköy | Paleo-channel | 522775 | 4509223 |
| 19 | 21.0 | 1.0 | Mursalli | Ridge | 519353 | 4508081 |
| 20 | 22.0 | 1.0 | Mursalli | Stream | 519311 | 4508063 |
| 21 | 25.0 | 2.0 | Yörgüç | stream | 513919 | 4506265 |
| 22 | 25.5 | 2.0 | Yörgüç west | Stream | 511002 | 4505126 |
| 23 | 26.0 | 2.0 | Güzelköy west | Stream | 523948 | 4509830 |
| 24 | 29.0 | 0.5 | Güzelköy | Stream | 522726 | 4509198 |
| 25 | 30.0 | 1.0 | Yeniköy | Stream | 499366 | 4500295 |
| 26 | 31.0 | 2.0 | Yörgüç | Stream | 511380 | 4505289 |
| 27 | 35.0 | 0.5 | Sofuköy | Stream | 500390 | 4500505 |
| 28 | 36.0 | 1.0 | Güzelköy | Stream | 523285 | 4509450 |
| 29 | 36.0 | 3.0 | Gölcük east | Ridge | 510859 | 4505082 |
| 30 | 38.0 | 4.0 | Gölcük east | Ridge | 511327 | 4505264 |
| 31 | 40.0 | 5.0 | Sofuköy east | Stream | 502039 | 4501391 |
| 32 | 43.0 | 2.0 | Yeniköy | ridge | 501653 | 4500790 |
| 33 | 45.0 | 5.0 | Mursalli west | Ridge | 518724 | 4507686 |
| 34 | 45.0 | 1.0 | Yeniköy | Ridge | 499333 | 4500288 |
| 35 | 46.0 | 5.0 | Yayaköy east | Stream | 518134 | 4507490 |
| 36 | 47.0 | 2.0 | Yeniköy | stream | 501681 | 4500804 |
| 37 | 48.0 | 5.0 | Sofuköy east | Ridge | 502018 | 4501379 |
| 38 | 58.0 | 2.0 | Yörgüç | Stream | 511383 | 4505313 |
| 39 | 59.0 | 5.0 | Gölcük east | Stream | 511052 | 4505141 |
| 40 | 61.0 | 5.0 | Sofuköy east | stream | 501784 | 4501083 |
| 41 | 61.0 | 5.0 | Sofuköy east | Ridge | 501743 | 4501060 |
| 42 | 67.0 | 5.0 | Yayaköy east | Stream | 517829 | 4507408 |
| 43 | 70.0 | 10.0 | Yayaköy | Stream | 516143 | 4506871 |
| 44 | 72.0 | 5.0 | Yörgüç | stream | 514651 | 4506436 |
| 45 | 78.0 | 10.0 | Mursalli east | Stream | 521357 | 4508847 |
| 46 | 84.0 | 10.0 | Güzelköy east | Stream | 517869 | 4507408 |
| 47 | 84.0 | 5.0 | Yayaköy east | Stream | 523551 | 4509621 |
| 48 | 87.0 | 5.0 | Yörgüç | Ridge | 514626 | 4506444 |
| 49 | 150.0 | 5.0 | Gölcük | Ridge | 507440 | 4503849 |
| 50 | 181.0 | 10.0 | Gölcük | Stream | 505908 | 4503120 |
| 51 | 185.0 | 10.0 | Yeniköy west | Stream | 498842 | 4500064 |
| 521 | 188.0 | 10.0 | Yeniköy West | Stream | 499148 | 4500253 |
| 53 | 200.0 | 10.0 | Yörgüç west | Stream | 513103 | 4505960 |
| 54 | 200.0 | 20.0 | Yörgüç west | stream | 512418 | 4505670 |
| 55 | 221.0 | - | Gaziköy | Terrace | 528146 | 4510851 |

**Table A2.1 :** (continued) Cumulative offset measurements. Coordinates are in UTM ED50.

| Id | Offset | Error | Location | Structure | X | Y |
|---|---|---|---|---|---|---|
| 56 | 250.0 | 15.0 | Alibey west | Stream | 502902 | 4501824 |
| 57 | 251.0 | 10.0 | Güzelköy west | Stream | 523550 | 4509631 |
| 58 | 259.0 | 15.0 | Güzelköy west | Stream | 523053 | 4509341 |
| 59 | 323.0 | 10.0 | Gölcük east | Stream | 510775 | 4505054 |
| 60 | 575.0 | 15.0 | Yeniköy West | Stream | 499148 | 4500253 |
| 61 | 575.0 | 15.0 | Yeniköy West | Ridge | 499148 | 4500253 |
| 62 | 583.0 | 10.0 | Yeniköy west | stream | 499760 | 4500678 |
| 63 | 725.0 | 15.0 | Güzelköy west | Stream | 521659 | 4508646 |
| 64 | 750.0 | 15.0 | Gölcük west | Stream | 504518 | 4502586 |
| 65 | 1570.0 | 20.0 | Güzelköy west | Stream | 521656 | 4508649 |
| 66 | 1766.0 | 10.0 | Gölcük | Stream | 507386 | 4503962 |
| 67 | 2270.0 | 50.0 | Gölcük | Stream | 508202 | 4504188 |
| 68 | 4500.0 | 50.0 | Güzelköy west | Stream | 519255 | 4507487 |
| 69 | 9000.0 | 100.0 | Gölcük | Stream | | |

**Table A2.2 :** 1912 Mürefte earthquake co-seismic slip measurements. Coordinates are in UTM ED50

| Name | 1912 | Error | Cumul. | Error | Lon | Lat | REFERENCE |
|---|---|---|---|---|---|---|---|
| Gaziköy – road 2 | 3.30 | 0.30 | 12.70 | 1.00 | 528038 | 4511141 | This study |
| Gaziköy – road 1 | 5.00 | 0.50 | | | 527199 | 4510836 | This study |
| Gaziköy - creek/field 1 | 2.50 | 0.30 | | | 526672 | 4510412 | This study |
| Gaziköy - field 2 | 2.20 | 0.30 | | | 526632 | 4510395 | This study |
| Güzel - Lstream East | 3.18 | 0.50 | 17.80 | 0.50 | 525065 | 4510172 | Altunel et al., (2004) |
| Güzel - pavement | 2.60 | 0.10 | | | 524784 | 4510128 | Altunel et al., (2004) |
| Güzel - Chanel | 1.40 | 0.12 | | | 524713 | 4510095 | Altunel et al., (2004) |
| Güzel - wall | 3.28 | 0.15 | | | 524659 | 4510074 | Altunel et al., (2004) |
| Güzel - Champ | 4.22 | 0.30 | | | 524613 | 4510084 | Altunel et al., (2004) |
| Güzel - tree limit | 4.05 | 0.20 | 7.04 | 0.30 | 524503 | 4510062 | Altunel et al., (2004) |
| Güzel - Stream West | 4.00 | | 8.00 | | 524476 | 4510050 | Altunel et al., (2004) |
| Güzel - Lstream West | 4.00 | | 12.60 | 0.20 | 524395 | 4510033 | Altunel et al., (2004) |
| Güzel - Stream bed1 | 2.00 | 0.30 | | | 524134 | 4509875 | Altunel et al., (2000) |
| Güzel -Stream bed2 | 2.40 | 0.30 | | | 524114 | 4509864 | Altunel et al., (2000) |
| Güzel - Stream bed3 | 5.20 | 0.30 | | | 523966 | 4509797 | Altunel et al., (2000) |
| Güzel - Stream 8 | 4.70 | 0.30 | 12.10 | 0.30 | 523319 | 4509464 | Altunel et al., (2004) |
| Güzel - paleostr - East | 5.51 | 0.50 | 20.00 | 0.50 | 522772 | 4509220 | Altunel et al., (2004) |
| Güzel - paleostr - West | 5.00 | 0.50 | 8.40 | 0.50 | 522762 | 4509215 | Altunel et al., (2004) |
| Mursalli - ridge | 4.00 | | 26.00 | 1.00 | 520699 | 4508468 | Altunel et al., (2000) |
| Mursalli - road | 3.80 | 0.20 | | | 520318 | 4508378 | Altunel et al., (2004) |
| Mursallı – stream | 4.60 | 0.40 | | | 519832 | 4508266 | This study |
| Mursallı – stream | 4.50 | 0.40 | | | 519818 | 4508262 | This study |
| Yayaköy – road East | 3.50 | 0.50 | | | 517831 | 4507364 | This study |
| Yayaköy - Lstream | 4.00 | | 12.50 | 0.50 | 516828 | 4507078 | Altunel et al., (2004) |
| Yayaköy - Stream | 3.90 | 0.30 | | | 516801 | 4507072 | Altunel et al., (2004) |
| Yayaköy - road | 5.00 | | 15.00 | 0.50 | 516793 | 4507071 | Altunel et al., (2004) |
| Yaya W field | 5.00 | 0.50 | | | 516354 | 4506938 | This study |
| Yayaköy stream | 4.50 | 0.50 | | | 516155 | 4506866 | This study |
| Yörgüç - ridge | 5.50 | | 11.00 | 0.50 | 515409 | 4506694 | Altunel et al., (2000) |

**Table A2.2 :** (continued) 1912 Mürefte earthquake co-seismic slip measurements. Coordinates are in UTM ED50.

| Name | 1912 | Error | Cumul. | Error | X | Y | REFERENCE |
|---|---|---|---|---|---|---|---|
| Yörgüç - road | 5.00 | 0.20 | | | 514864 | 4506627 | Altunel et al., (2000) |
| Sofuköy E sagpond | 2.50 | 0.30 | | | 502795 | 4501911 | This study |
| Yeniköy - Field house | 5.40 | 0.20 | | | 500630 | 4500600 | Altunel et al., (2004) |
| Yeniköy - Field East | 5.30 | | 10.60 | 0.50 | 500602 | 4500591 | Altunel et al., (2004) |
| Yeniköy - Stream East | 3.57 | 0.20 | 17.10 | 0.50 | 500537 | 4500568 | Altunel et al., (2004) |
| Yeniköy-Field StrEast | 4.08 | 0.20 | | | 500515 | 4500566 | Altunel et al., (2004) |
| Yeniköy – tree | 3.90 | 0.10 | | | 500454 | 4500547 | Altunel et al., (2004) |
| Yeniköy - Stream West | 4.28 | 0.10 | 35.00 | 0.50 | 500381 | 4500514 | Altunel et al., (2004) |
| Yeniköy – road | 5.20 | 0.30 | | | 499791 | 4500286 | Altunel et al., (2004) |
| Yeniköy NNW | 4.00 | 0.20 | 30.00 | 0.50 | 498881 | 4500104 | Altunel et al., (2004) |
| W-Yeniköy field | 1.50 | | | | 498203 | 4499882 | This study |
| W-Yeniköy road | 4.00 | 0.50 | 15.00 | 1.00 | 497592 | 4499540 | This study |
| W-Yeniköy | 4.50 | 0.20 | | | 497142 | 4499297 | Altunel et al., (2004) |
| Kavak lake east2 | 3.20 | | | | 495891 | 4498955 | This study |
| Kavak lake east1 | 1.50 | | | | 495620 | 4498922 | This study |
| Kavak - trench | 4.50 | 0.20 | 9.00 | 0.20 | 488564 | 4495659 | Rockwell_etal_2002 |

## APPENDIX A3 – SUPPLEMENTARY DOCUMENTS OF THE 1912 MÜREFTE EARTHQUAKE

### Photographs of the 1912 earthquake damage and ground deformation

### The Damage

**Figure A3.1 :** Damage city walls at İstanbul (Mihailovic, 1933)

**Figure A3.2 :** The palace of the Austro-Hungarian Empire consulate was partly damaged (Çanakkale; Mihailovic, 1933).

**Figure A3.3 :** A collapsed house at Tekirdağ, build of wood on top of bricks.

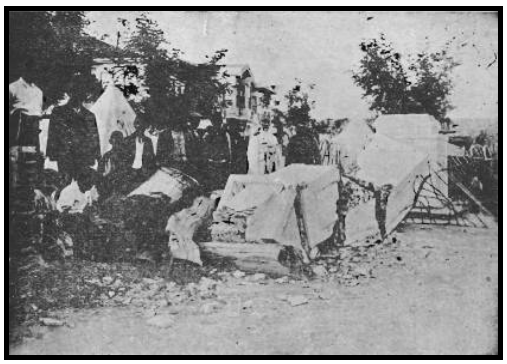

**Figure A3.4 :** The marble liberty statue at Tekirdağ collapsed towards South and broke into pieces.

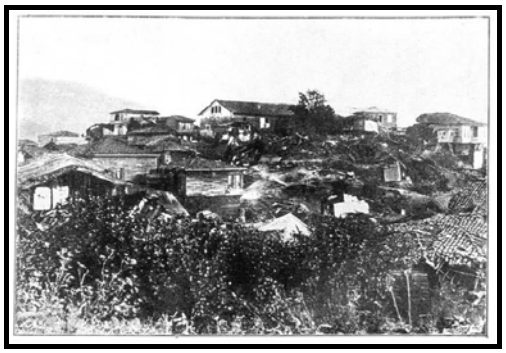

**Figure 5 :** Southern part of the Ganos village after earthquake (Macovei, 1912)

**Figure A3.6 :** A street at Hora (Hoşköy) after the earthquake (Macovei, 1912).

**Figure A3.7 :** Musala village after the earthquake. The single isolated houses are only which resisted after the earthquake (Macovei, 1912).

**Figure A3.8 :** Houses destroyed by tremor and fire at Mürefte (Sadi, 1912)

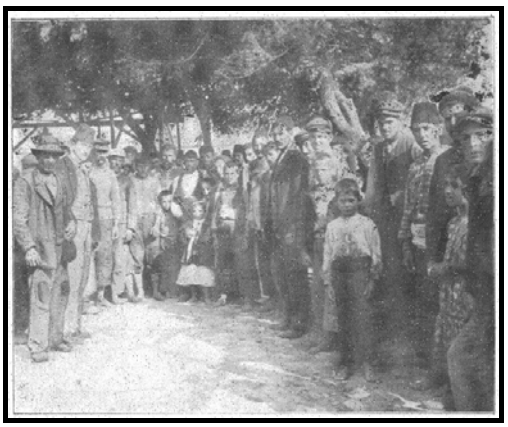

**Figure A3.9 :** Villagers who survived the earthquake (Sadi, 1912).

**Figure A3.10 :** Tumbled typical house of the region. Bottom of the construction is build by bricks, while the top is made of wood (Sadi, 1912).

**Figure A3.11 :** Collapsed buildings at Şarköy (Sadi, 1912).

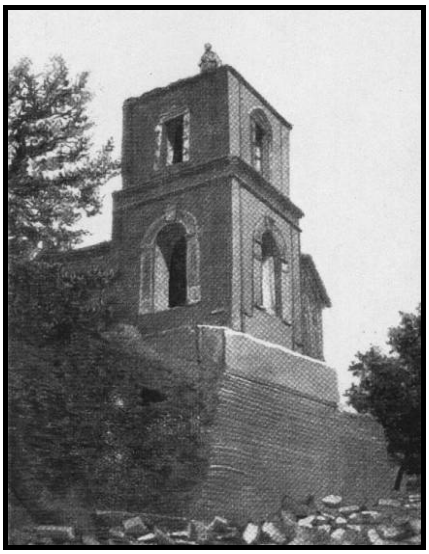

**Figure A3.12 :** Damaged clock tower at Gelibolu (Sadi, 1912).

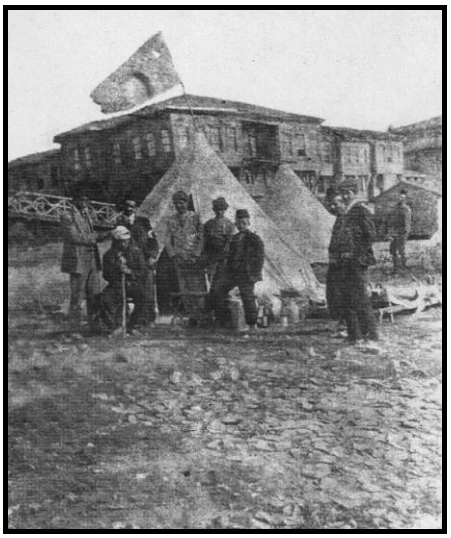

**Figure A3.13 :** Otoman red cross helping people (Sadi, 1912).

**Figure A3.14 :** The Gümrük mosque at Tekfurdağ experienced severe damage (Sadi, 1912).

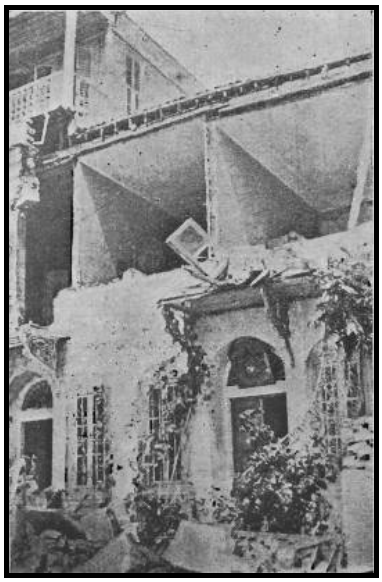

**Figure A3.15 :** Damaged building at Çanakkale (Sadi, 1912).

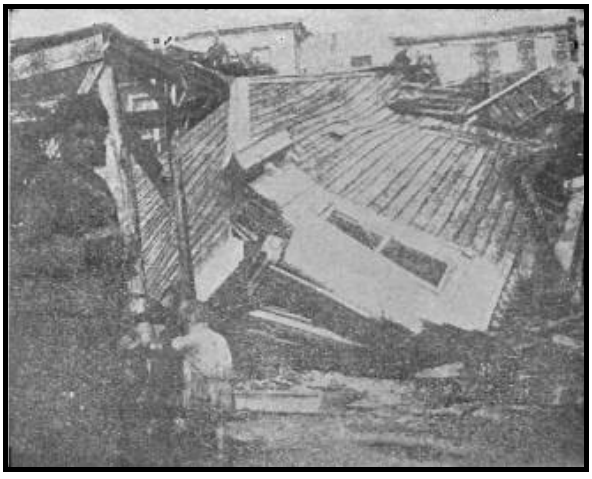

**Figure A3.16 :** Ruined street at Tekirdağ (Mihailovic, 1933).

**Figure A3.17** : Ruined main road at Ganos (Gaziköy; Mihailovic, 1933).

**Figure A3.18:** Three different type of buildings with damage at Ganos (Gaziköy). The left house was reduced to ruins, the middle was heavely damaged, the right house was slightly damaged (Mihailovic, 1933).

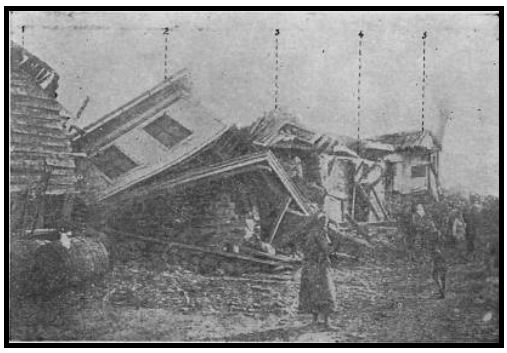

**Figure A3.19 :** Another ruined street at Ganos (Gaziköy).

**Figure A3.20** An isolated new building at Ganos experienced heavy damage by the strong tremor.

F**igure A3.21 :** At Hoşköy, the palace of the bishop and a fountain were ruined (left) (Mihailovic, 1933).

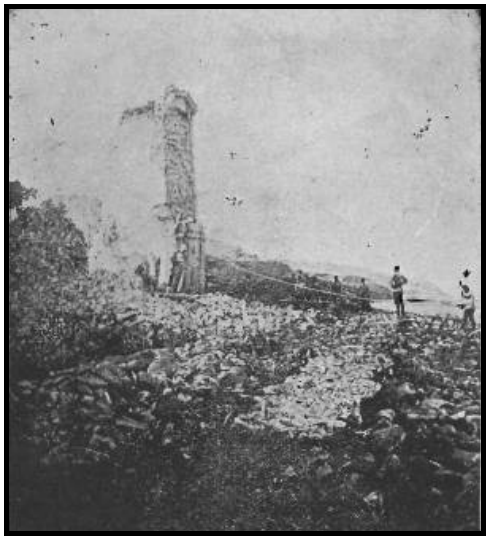

**Figure A3.22 :** The St. George church at Hoşköy was heavely damaged (Mihailovic, 1933).

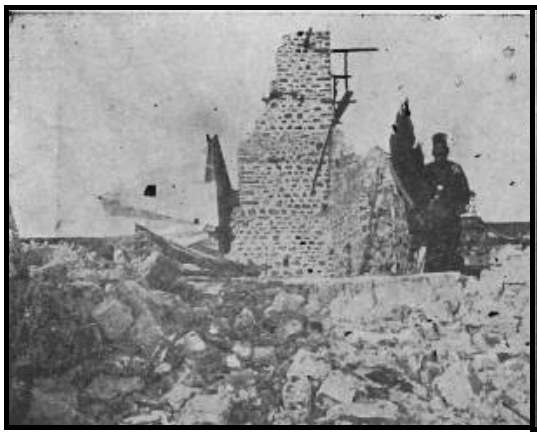

**Figure A3.23 :** The St. Jean monastry at Hoşköy was totally destroyed.

**Figure A3.26 :** A house, which wooden part tumbled to the side when the bricks underneath collapsed (Mürefte, Mihailovic, 1933).

**Figure A3.24 :** The main road of Mürefte after the earthquake.

**Figure A3.27 :** Destroyed Stone building at Şarköy (Mihailovic, 1933).

**Figure A3.25 :** Adjacent buldings of different type. The Stone building survived with slight damage, while the other was totally destroyed (Mürefte, Mihailovic, 1933).

## Ground Deformation

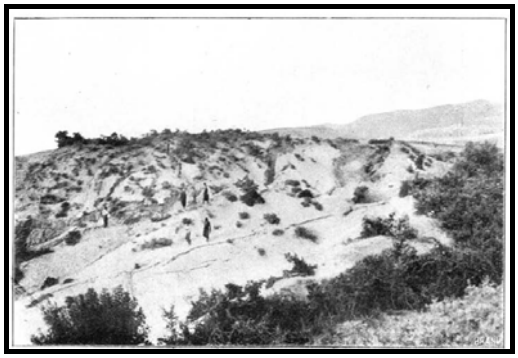

**Figure A3.28 :** Splay of ruptures at Kestanbol (Ormanlı; Macovei, 1912)

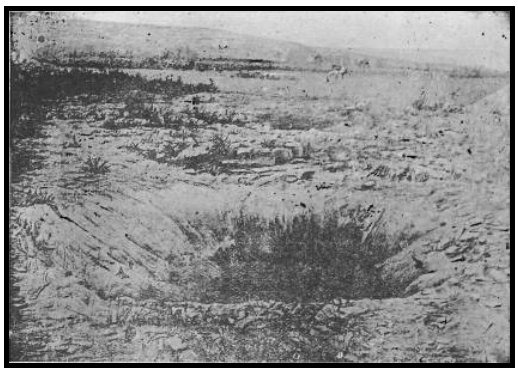

**Figure A3.29 :** A big hole opened during the earthquake at Eriklice. Most probably due to liquefaction (Mihailovic, 1933).

**Figure A3.30 :** Large cracks at Appolonia (Ulubat Lake; Mihailovic, 1933)

**Seismograms of the 1912 earthquakes**

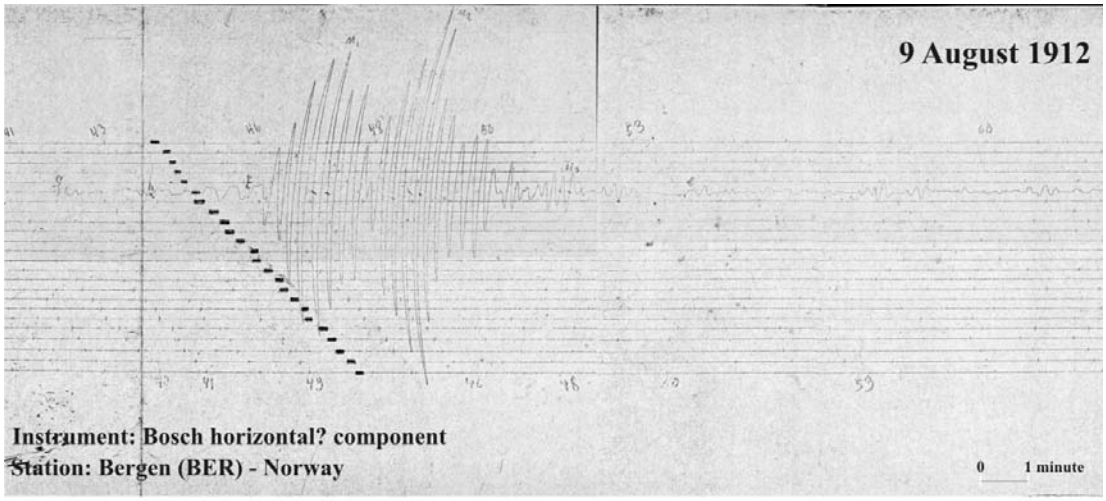


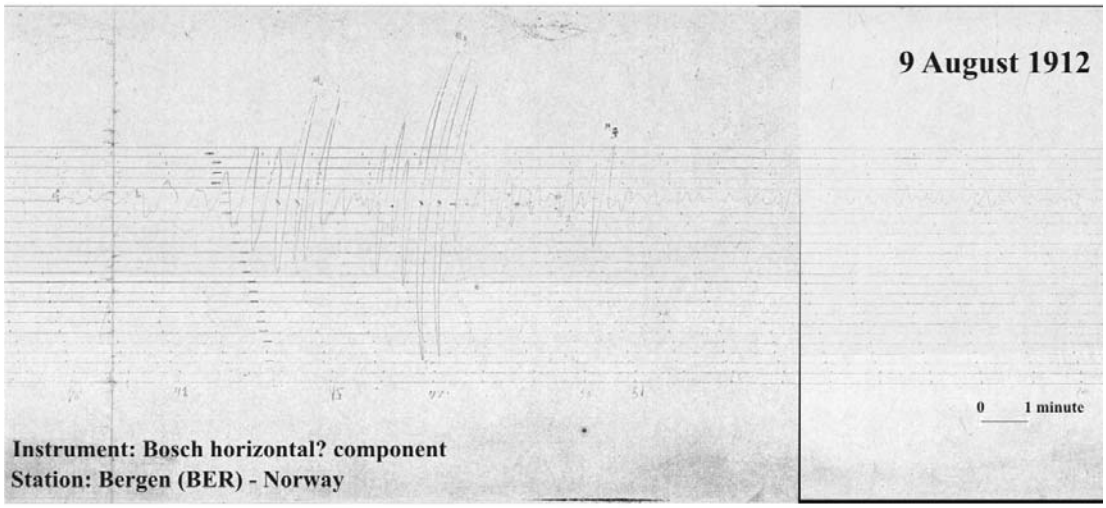


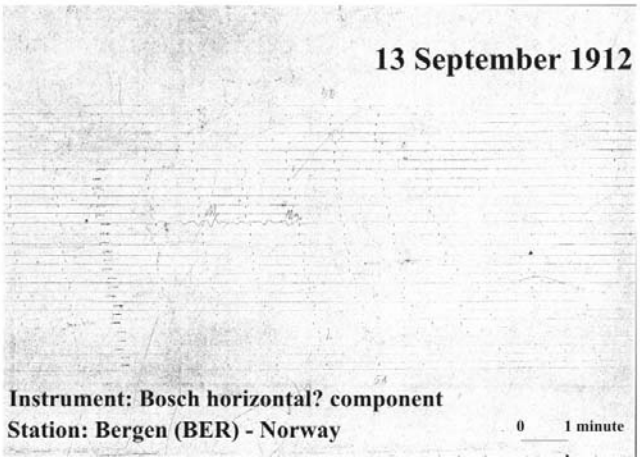


**Figure A3.31** : Seismograms of the 9 August and 13 September shock from Bergen station - Norway

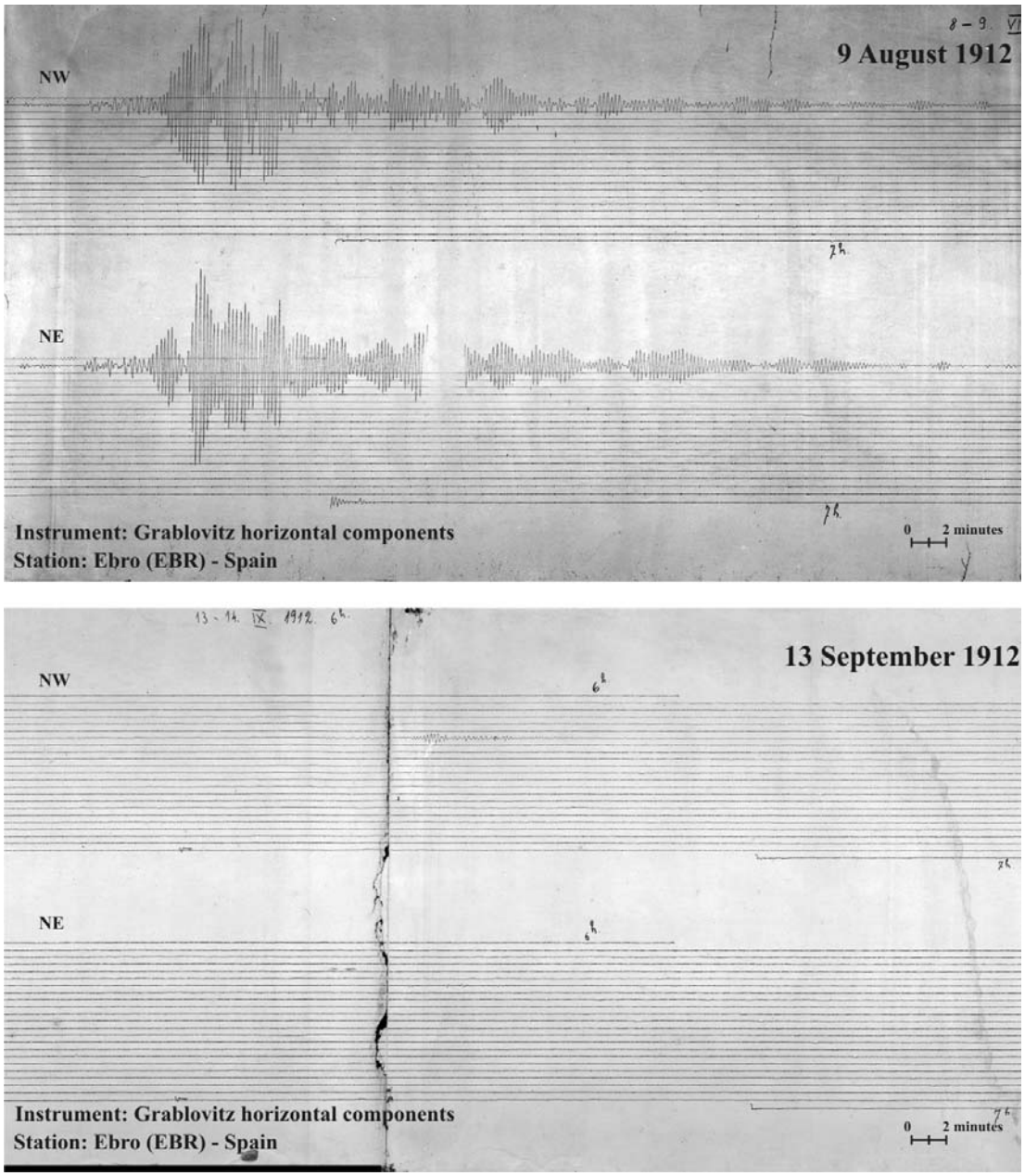


**Figure A3.32 :** Seismograms of the 9 August and 13 September shock from Ebro station – Spain

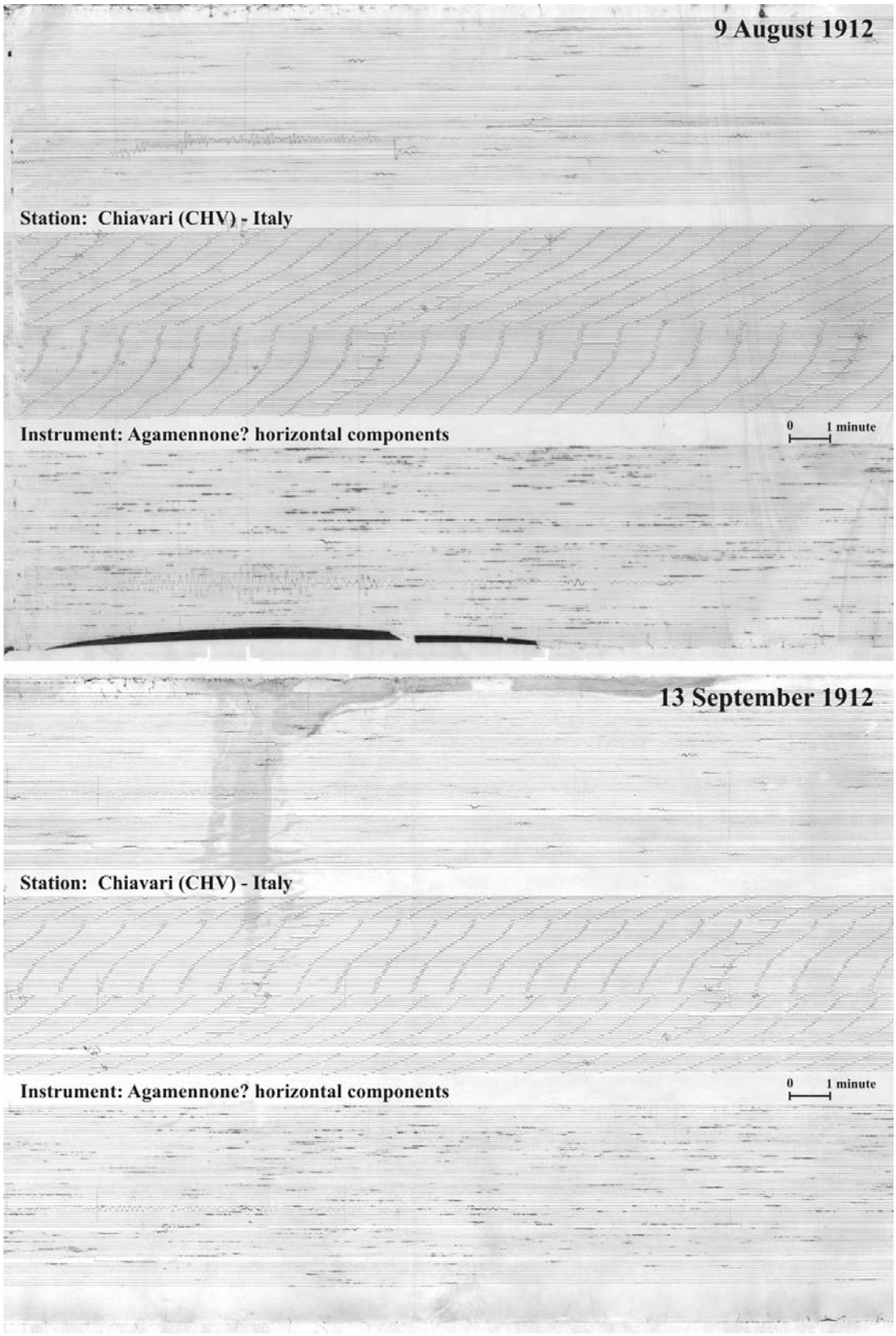


**Figure A3.33 :** Seismograms of the 9 August and 13 September shock from Chiavari station – Italy

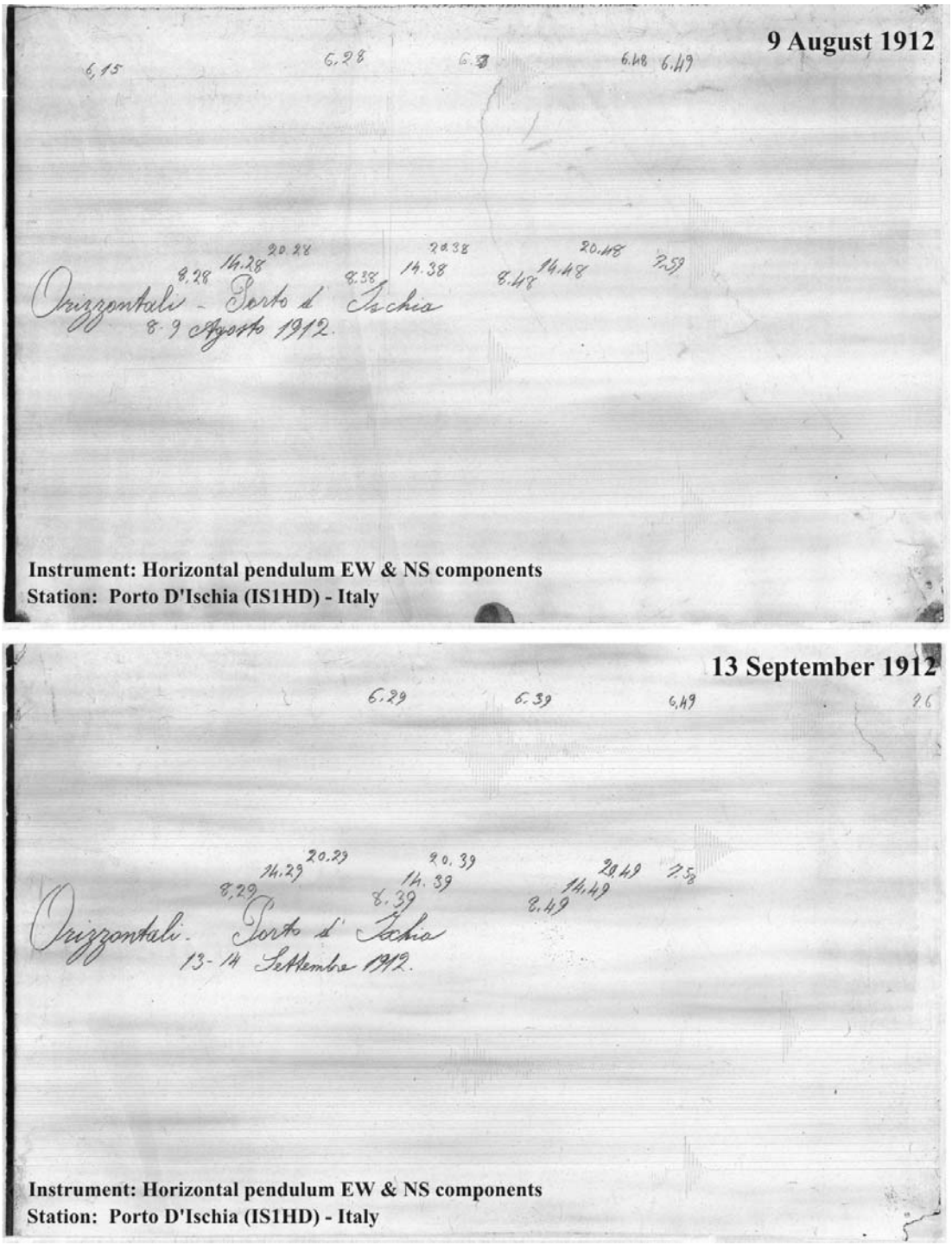


**Figure A3.34 :** Seismograms of the 9 August and 13 September shock from Porto d'Ischia station – Italy

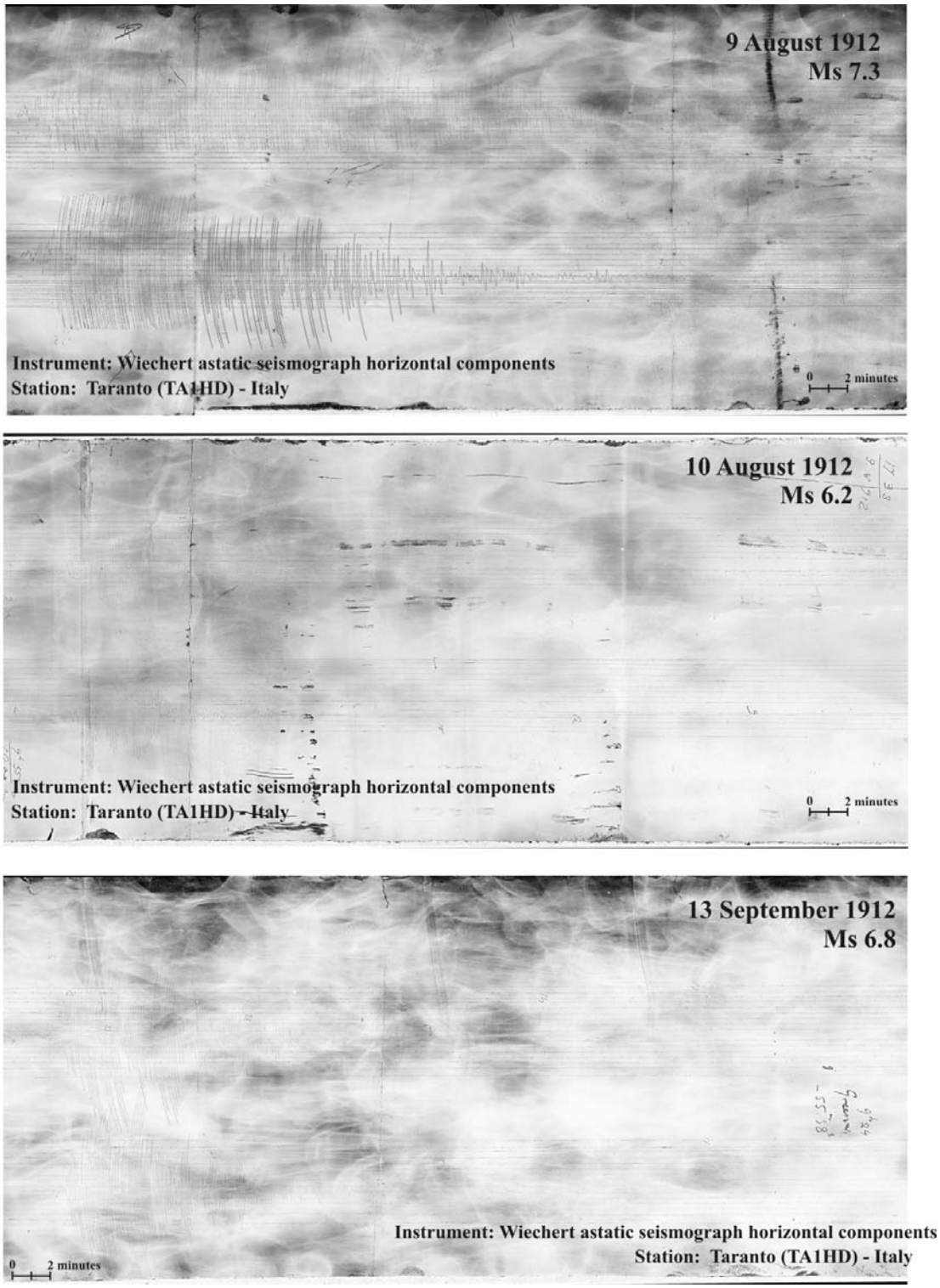


**Figure A3.35 :** Seismograms of the 9 & 10 August, and 13 September shock from Taranto station - Italy

**Table A3.1 :** List of world wide stations which recorded large earthquakes (M>5.5?) occurred in August and September 1912 (Mihailovic, 1927)

## Потрес № 26. — 9. августа 1912.

| Сеизмолошке опсерваторије (по даљини око епицентра) | Моменат фазе (ср. Грин. вр.) Претходне фазе P h m s | Претходне фазе S h m s | Главне фазе L h m s | Инструмент | Напомена и претходне одредбе |
|---|---|---|---|---|---|
| Buccarest | 1 31 02 | 1 31 18 | | Bosch-Omori | писаљка пенала |
| Athènes | 1 29 54 | | | Agamennone | △=510 km. |
| Beograd | 1 30 32 | 1 32 14 | 1 33 12 | Wiechert 200 | △=920 km. |
| Ungvár | 1 31 43 | | 1 32 52 | Bosch | △=620 km. |
| Sarajevo | 1 30 51 | 1 32 33 | 1 33 27 | Wiechert 200 | △=809 km. |
| Beyrouth | 1 30 30 | | 1 34 | Milne | |
| Budapest | 1 | | | Wiech. 1000 | нејасне индик. времена |
| Helwan Giza | 1 33 06 | 1 35 31 | 1 37 56 | Milne | |
| Ó-Gyalla | 1 31 | | | Vicent-Konk. | нејасне индик. времена |
| Zagreb | 1 31 10 | ? | 1 34 13 | Wiech. 1000 | △=1095 km. |
| Vale d. Pomp. | 1 31 22 | 1 32 08 | 1 33 24 | Omori-Alfani | Дарданели |
| Wien | 1 31 26 | 1 32 48 | 1 34 02 | Wiech. 1000 | △=1400 km. - Дарданели |
| Graz | 1 31 25 | ? | 1 34 40 | Wiech. 1000 | △=1300 km. - Дарданели |
| Pola | 1 31 27 | 1 34 09 | 1 34 51 | Wiechert 200 | △=1100 km. - Балк. п. о. |
| Triest | 1 31 25 | 1 34 03 | | Wiech. 1000 | △=1340 km. - Дарданели |
| Rocca di Papa | 1 32 11 | 1 34 26 | 1 34 51 | Agamennone | |
| Venezia | 1 30 46 | 1 31 44 | 1 32 44 | Vicentini | |
| Siena | 1 31 54 | 1 35 11 | 1 38 | Vicentini | |
| Sàlo | 1 32 33 | 1 35 | | Agamennone | |
| Tiflis | 1 32 25 | 1 34 58 | 1 52 57 | Galitzine | △=1460 km. - W₂ 4h 24m. Епиц. 41°,8 N; 27°,8 E. |
| Postdam | 1 32 39 | 1 36 | 1 38 | Wiech. 1000 | △=1800 km. SE. |
| Plauen | 1 | | 1 38 | Wiech. 1000 | Мраморно море. |
| Jena | 1 32 23 | 1 35 34 | 1 35 52 | Wiech. 1000 | △=1500 km. |
| Pulkowo | 1 33 24 | 1 36 57 | 1 37,8 | Galitzine | △=2100 km. — Мрам. м. Епиц. 41°,₈ N; 26°,₆ E. |
| Hohenheim | 1 32 24 | 1 35 20 | 1 37 26 | Omori-Bosch | △=1700 km. |
| Domodosola | 1 29 55 | 1 31 40 | 1 32 30 | Omori Alfani | △ = 200 kom. Зап. об. Мале Азије. |
| Moncalieri | 1 32 22 | 1 35 25 | 1 36 02 | Stiattesi | △ = 1655 km. |
| Göttingen | 1 31 45 | | | | △ = 1800 km. |
| Jugenheim | 1 32 40 | 1 35 46 | 1 37,7 | Wiech. 1000 | △ = 1765. kom. — Епиц. 42°,2 H; 26° E. |
| Strasbourg | 1 32 29 | 1 36 00 | | Wiech. 1000 | △ = 1780 kom. — Епиц. 40°40' H; 27°24' E |
| Hamburg | 1 32 59 | 1 36 10 | 1 37,8 | Wiech. 1000 | △=1900 km. - Дарданели |
| Besançon | 1 32 39 | 1 36 10 | 1 37 22 | Mainka | |
| Aachen | 1 33 02 | 1 36 25 | 1 38 38 | Wiechert | |
| De Bilt | 1 33 27 | 1 37 03 | 1 38 09 | Bosch | |
| Bruxelles | 1 33 20 | 1 35 48 | 1 36 58 | Wiechert | |
| Alger | 1 33 13 | 1 36 57 | 1 40 | Wiechert | Дарданели. |
| Tortosa | 1 33 32 | 1 37 14 | 1 42 26 | Vicentini | Епиц. између Галипоља и Родоста |
| Paris | 1 33 16 | 1 36 46 | 1 38 | Wiechert | осцилације до 5 h 30' |
| Pic du Midi | 1 46 | | | | осцилације 1 h 46'—4h37' |
| Paisley | 1 33 | 1 42,₉ | | Milne | |
| Edinbourg | 1 34,5 | | 1 48,5 | Milne | |
| Bergen | 1 33 46 | 1 38 04 | 1 42 30 | Bosch | △=2400 km.-Дарданели |
| Shide | 1 35,5 | 1 39 0 | 1 43,5 | Milne | |
| S. Fernando | 1 34 41 | 1 37 47 | 1 39 24 | Milne | |
| Cap of Good Hope | 1 50,4 | | 2 11,5 | Milne | |

**Table A3.1 :** (continued) List of world wide stations which recorded large earthquakes (M>5.5?) occurred in August and September 1912 (Mihailovic, 1927).

| Сеизмолошке оцсерваторије (по даљини око ецицентра) | Моменат фазе (ср. Грин. вр.) Претходне фазе P h m s | Претходне фазе S h m s | Главне фазе L h m s | Инструменат | Напомена и претходне одр |
|---|---|---|---|---|---|
| Irkoutzk | 1 38 37 | 1 46 04 | 1 53 | Galitzine | Δ = 5840 km. — W Епиц. 41°,5 H; 28 |
| Zi-ka-wei | 1 40 43 | 1 50 13 | 2 03 17 | Wiechert | Δ = 8200 km |
| Batavia | 1 42 0 | 1 52 26 | 1 58 47 | Wiechert | Епиц. у Турс |
| Tchemulpo | 1 41 14 | 1 59 21 | 1 06 14 | Omori | |
| Ottawa | 1 40 20 | 1 49 29 | 1 58,0 | Wiechert | Δ = 7780; епиц. бл. J |
| Berkeley | 1 52 14 | | (2 18 57) | Omori-Bosch | епиц. у Турс |
| Meridá(Youc) | 1 52 57 | 2 05 55 | 2 16 47 | Wiechert | Δ = 13000 km; у Ту |
| Hono lulu | 1 53,3 | 2 05,9 | 2 18,2 | Milne | Δ = 12400 k |
| Tacubaya | 1 55 29 | 2 10 43 | 2 23 29 | Wiechert | Δ = 12833 km; у Ту |
| Mazatlán | 1 56 05 | 2 07 29 | 2 24 12 | Wiechert | Δ = 11166 km; у Ту |
| **Потрес № 29. — 9. августа 1912.** | | | | | |
| Beograd | 5 27 06 | 5 28 40 | 5 30 21 | Wiechert | |
| Sarajevo | 5 27 21 | | 5 29 | Wiechert | Δ = 800 km. - Дар |
| Beyrouth | 5 28 | | 5 42 | Milne | |
| Zagreb | 5 27 22 | ? | 5 30 38 | Wiechert | |
| Triest | 5 30 40 | | 5 30 59 | Wiechert | |
| Pulkowo | 5 30 35 | | 5 35 | Galitzine | |
| Simla | 5 53 02 | 5 59 05 | 6 07 14 | Omori | |
| **Потрес № 61 — 10. августа 1912.** | | | | | |
| Buccarest | 9 26 12 | — | — | Bosch-Omori | на Мраморном |
| Athènes | 9 24 52 | 9 25 26 | 9 26 11 | Agamennone | Δ = 720 km. — Тр |
| Temisvàr | 9 26 46 | — | 9 29 | Vicent-Konk. | |
| Beograd | 9 25 30 | 9 27 42 | 9 29 08 | Wiechert | |
| Ungvár | 9 27 12 | — | 9 29 18 | Bosch | |
| Sarajevo | 9 25 39 | 9 27 15 | 9 27 45 | Wiechert | Δ = 800 km. - Дар |
| Lavovo | 9 26 19 | — | 9 27 39 | Boch | Δ = 1500 k |
| Beyrouth | 9 26,5 | — | 9 29,5 | Milne | |
| Budapest | 9 26 | — | — | Wiechert | нејасне индик. вр |
| Helwan (Giza) | 9 26 42 | 9 29 0 | 9 33 28 | Milne | |
| Mileto | 9 25 54 | 9 27 43 | 9 29 19 | Omori | Дарданели |
| Zagreb | 9 26 13 | 9 28 16 | 9 29 13 | Wiechert | |
| Krakovo | 9 29 34 | — | 9 31 13 | Boch | Δ = 550 km. Балк |
| Catania | 9 28 42 | 9 30 28 | 9 33 19 | Cancani | |
| Wien | 9 26 25 | 9 28 23 | 9 29 15 | Wiechert | Дарданели |
| Graz | 9 26 24 | 9 28 45 | 9 30 08 | Wiechert | Δ = 1300. km - Дар |
| Ljubljana | 9 26 25 | 9 28 31 | 9 29 41 | Belar | |
| Pola | 9 26 27 | 9 28 27 | 9 29 42 | Wiechert | |
| Triest | 9 27 39 | 9 29 43 | 9 31 10 | Wiechert | |
| Krietern (Bresl). | 9 26 52 | 9 29,3 | 9 33 | Wiechert | Δ = 1390. — Ту |
| Königsberg i Pr. | 9 27 19 | 9 30 07 | 9 31,3 | Wiechert | Δ = 1620 km. - Дар |

**Table A3.1 :** (continued) List of world wide stations which recorded large earthquakes (M>5.5?) occurred in August and September 1912 (Mihailovic, 1927)

| Сеизмолошке опсерваторије (по даљини око епицентра) | Моменат фазе (ср, Грин. вр.) Претходне фазе P h m s | Претходне фазе S h m s | Главне фазе L h m s | Инструмснат | Напомена и претходне одредбе |
|---|---|---|---|---|---|
| Venezia | 9 27 18 | 4 29 34 | 9 30 28 | Vicentini | |
| Siena | 9 28 30 | — | 9 33 | Vicentini | |
| München | 9 27 56 | 9 31 16 | 9 34 0 | Wiechert | |
| Tiflis | 9 26 57 | 9 29 34 | 9 37 38 | Galitzine | △ = 1400 km, |
| Potsdam | 9 27 | — | — | Wiechert | |
| Jena | 9 27 24 | 9 30 05 | 9 30 47 | Wiechert | |
| Pulkowo | 9 28 11 | 9 31 54 | 9 33 | Galitzine | Епиц. 40°,4 N; 24°,4 E |
| Hohenheim | 5 27 18 | 9 31 40 | 9 32 08 | Omori-Bosch | |
| Moncalieri | 9 27 24 | 9 30 02 | 9 32 32 | Stiattesi | |
| Königsstuhl | 9 27 | — | 9 33 | Wiechert | |
| Jugenheim | 9 27 26 | 9 30 41 | 9 34 48 | Wiechert | Δ = 1800 km - Дарданели |
| Strasburg | 9 27 41 | 9 30 45 | 9 33 | Wiechert | Мраморно море |
| Hamburg | 9 27 57 | 9 31 18 | 9 32,4 | Wiechert | △ = 1980 km |
| Besançon | 9 27 39 | 9 30 59 | 9 33 06 | Mainka | |
| Aachen | 9 28 03 | 9 31 28 | 9 33,3 | Wiechert | Δ = 1950 km - Дарданели |
| Marseille | 9 28 44 | 9 31 01 | 9 32 46 | Wiechert | |
| De Bilt | 9 28 19 | 9 31 52 | 9 33 20 | Bosch | |
| Bruxelles | 9 27 14 | 9 31 47 | 9 33 26 | Wiechert | |
| Alger | 9 28 16 | 9 31 52 | 9 35 16 | Wiechert | Дарданели |
| Tortosa | 9 33 48 | 9 31 12 | 9 35 30 | Grablowitz | |
| Paris | 9 29 19 | 9 31 53 | 9 34 | Wiechert | |
| Edinbourg | 9 33,7 | — | 9 40,0 | Milne | |
| Cartuja | 9 29 12 | 9 33 43 | 9 37,2 | Bifilar-Cart. | △ = 2750 km |
| San Fernando | 9 33 40 | 9 36 05 | 9 38 11 | Milne | |
| Cap of Good Hopen | 9 4,3 ? | — | 9 5,9 ? | Milne | |
| Irkoutzk | 9 33 11 | 9 44 11 | 9 50 | Galitzine | |
| Zi-ka-wei | 9 02 ? | — | — | Wiechert | |
| **Потрес № 62. — 10 августа 1912.** | | | | | |
| Buccarest | 18 32 55 | — | — | Bosch-Omori | |
| Athènes | 18 31 22 | — | 18 32 18 | Agamennone | △ = 510 km.— Тракија |
| Temisvar | 18 33 30 | — | — | Vicent-Konk. | |
| Beograd | 18 32 28 | 18 34 06 | 18 36 30 | Wiechert | |
| Sarajevo | 18 32 33 | 18 33 36 | 18 34 03 | Wiechert | △ = 800 — Дарданели |
| Helwan(Giza) | 18 40 36 | — | 18 41 41 | Milne | |
| Mileto | 18 32 36 | 18 34 16 | 18 36 08 | Omori | Дарданели |
| Zagreb | 18 32,5 | 18 35 30 | 18 36 41 | Wiechert | |
| Wien | 18 32 45 | — | 18 35,3 | Wiechert | △ = 1400 km. |
| Graz | 18 32 45 | 18 35,1 | 18 37 14 | Wiechert | △ = 1300 km. |
| Ljubljana | 18 34 14 | 18 36 56 | 18 37 26 | Belar | |
| Pola | 18 34 27 | — | 18 36 05 | Wiechert | |
| Triest | 18 34 | — | — | Wiechert | мин. контакт није радио |
| Krietern (Bresl) | 18 33 3 | — | 18 39 | Wiechert | |
| Königsberg i. Pr. | 18 36 32 | — | 18 38,7 | Wiechert | |
| Siena | 18 38 | — | — | Vicentini | врло споре осцилације |
| Potsdam | 18 07 | — | — | Wiechert | |

13*

**Table A3.1 :** (continued) List of world wide stations which recorded large earthquakes (M>5.5?) occurred in August and September 1912 (Mihailovic, 1927).

| Сеизмолошке опсерваторије (по даљини око епицентра) | Моменат фазе (ср. Грин. вр.) Претходне фазе P h m s | S h m s | Главне фазе L h m s | Инструменат | Напомена и претходне одре |
|---|---|---|---|---|---|
| Pulkowo | — | — | 18 40 | Galitzine | фазе за време пром. |
| Moncalieri | — | 18 36 58 | 18 39 04 | Stiattesi | |
| Strasbourg | 18 34 0 | — | 18 37 12 | Wiechert | Мраморно мо |
| Hamburg | 18 34 | 18 37,8 | 18 42,7 | Wiechert | |
| Aachen | 18 34 32 | 18 37 53 | 18 40,2 | Wiechert | Δ = 1980 km. - Дард |
| De Bilt | 18 35 30 | 18 38 30 | 18 40 26 | Bosch | |
| Paris | 18 34 44 | 18 37 19 | 18 41 | Wiechert | |
| Edinbourg | 18 40,2 | — | 18 47 8 | Milvne | |
| Irkoutzk | 18 46 55 | — | 19 00 | Galitzine | |
| **Потрес № 80. — 11. августа 1912.** | | | | | |
| Athènes | 7 20 43 | — | 7 21 39 | Agamenn. | △ = 510 km. Тра |
| Temisvar | 7 23 19 | — | 7 24 | Vicent-Konk. | |
| Beograd | 7 21 40 | — | 7 23 07 | Wiechert | |
| Sarajevo | 7 21 54 | — | 7 23 21 | Wiechert | Δ = 800 km - Дарда |
| Lavovo | 7 24,9 | — | 7 26,1 | Bosch | |
| Zagreb | 7 21,8 | — | 7 24 57 | Wiechert | |
| Ljubljana | 7 32 | — | 7 36 | Belar | |
| Triest | 7 25 | — | — | Wiechert | минут конт. није р |
| Königsberg i Pr. | 7 24 03 | — | 7 27,7 | Wiechert | |
| Potsdam | 7 58 ? | — | — | Wiechert | |
| Pulkowo | 7 24 13 | 7 28 03 | 7 30,4 | Galitzine | △ = 2320 km |
| Moncalieri | 7 25 51 | — | 7 28 50 | Stiatesi | |
| Hamburg | 7 28 | — | 7 31 | Wiechert | |
| Besançon | 7 28,3 | — | — | Mainka | |
| Paris | 7 29 | — | — | Wiechert | |
| **Потрес № 219. — 13. септембра 1912.** | | | | | |
| Athènes | 23 32 23 | — | 23 33 31 | Mainka | △=620 km. — Тра |
| Beograd | 23 33 02 | 23 33 35 | 23 35 50 | Wiechert | |
| Sarajevo | 23 33 10 | 23 33 40 | 23 35 04 | Wiechert | △ = 800. — Дарда |
| Lavovo | 23 33 43 | — | 23 36 07 | Omori-Bosdi | △ = 1200 km |
| Budapest | 23 33 12 | 23 34 24 | 23 36 05 | Wiechert | |
| Zagreb | 23 33 19 | ? | 23 36 21 | Wiechert | |
| Krakovo | 23 34 03 | 23 36 52 | 32 37 48 | Omori-Bosch | Δ = 930 km. - Дард |
| Vale di Pompeji | 23 33 28 | — | 23 40 0 | Omori-Alfani | Дарданели |
| Catania | 23 34 40 | 23 36 04 | 23 37 40 | Cancani | |
| Wien | 23 33 57 | 23 36 23 | 23 36,7 | Wiechert | Δ = 1220—1400 k Дарданели |
| Graz | 23 33 56 | 23 36 08 | 23 37 13 | Wiechert | Δ = 1330 km. - Дард |
| Ljubljana | 23 33 45 | 23 36 36 | 23 37 15 | Belar | |
| Pola | 23 33 57 | 23 35 51 | 23 37 12 | Wiechert | △ = 1000 km. — Бо |
| Triest | 23 30 ? | — | — | Wiechert | △ = 1200 km |

**Table A3.1 :** (continued) List of world wide stations which recorded large earthquakes (M>5.5?) occurred in August and September 1912 (Mihailovic, 1927).

| Сеизмолошке опсерваторије (по дальини око епицентра) | Моменат фазе (ср. Грин. вр.) Претходне фазе P h m s | Претходне фазе S h m s | Главне фазе L h m s | Инструменат | Напомена и претходне одредбе |
|---|---|---|---|---|---|
| Kríetern Bresl.) | 23 34 26 | 23 37,0 | 23 40 | Wiechert | |
| Königsberg i. Pr. | 23 34 48 | 23 37 30 | 23 39.7 | Wiechert | △=1600km.Дарданела |
| Venezia | 23 33 35 | 23 34 12 | 23 35 20 | Vicentini | |
| München | 23 35 22 | 23 38 28 | 23 40 36 | Wiechert | |
| Tiflis | 23 34 30 | 23 36 59 | 23 38 43 | Galitzine | Епиц. 42°,0 N; 27°,4 E. $W_2$ |
| Pulkowo | 23 35 42 | 23 39 13 | 23 40,5 | Galitzine | Епиц. између 41°.1 N; 26°,4 E 40°,1 N; 26°.3 E; △=2090-2220 км. |
| Moncalieri | 23 34 53 | 23 37 48 | 23 40 12 | Stiattesi | |
| Strasbourg | 23 35 05 | 23 38 21 | 23 40 30 | Wiechert | |
| Hamburg | 23 35 24 | 23 38 34 | 23 41 | Wiechert | Δ=1900kmSE-Дардавели |
| Besançon | 23 35 15 | 23 38 27 | 23 40 0 | Mainka | |
| Aachen | 23 35 31 | 23 39 0 | 23 40,5 | Wiechert | △=1970 km. - Турска |
| De Bilt | 23 35 47 | 23 39 16 | 23 39 57 | Bosch | |
| Bruxelles | 23 35 42 | 23 39 14 | 23 40 52 | Wiechert | |
| Alger | 23 35 51 | 23 39 57 | 23 43 | Wiechert | |
| Tortosa | 23 36 06 | 23 39 50 | 23 44 57 | Grabloutz | Балканско п. о. |
| Paris | 23 35 50 | 23 39 24 | 23 41 07 | Wiechert | Турска |
| Bergen | 23 40 01 | — | 23 45 01 | Bosch | Дарданели |
| Cartuja | 23 36 50 | 23 41 07 | 23 43 15 | Bifil.-Cart. | на обал. Мраморног море. |
| Cap of Good Hopen | 23 7,5 ? | — | — | — | |
| Irkoutzk | 23 40 31 | 23 47 51 | 23 55 | Galitzine | Епиц.39°,3 N; 28°.1 E.— Мраморног мора |
| Zi-ka-wei | 23 07 24 | — | 23 23 16 | Wiechert | |
| Ottawa | 23 51 51 | — | 24 01,4 | Wiechert | |

## Потрес № 230. — 16. септембра 1912.

| | | | | | |
|---|---|---|---|---|---|
| Athènes | 21 05 17 | — | 21 06 13 | Mainka | △=510k m. — Тракија |
| Beograd | 21 05 37 | 21 06 40 | 21 06 57 | Wiechert | |
| Lavovo | 21 07 48 | 21 09 06 | 21 09 40 | Omori-Bosch | △ = 1000 km. |
| Budapest | 21 06 07 | — | 21 08 10 | Wiechert | |
| Zagreb | 21 05 | — | — | Wiechert | регистр. до 2 h 25 m |
| Vale di Pompeji | 21 07 02 | — | 21 09 10 | Omori-Alfani | |
| Graz | 21 06 08 | 21 08 04 | 21 8,8 | Wiechert | Δ = 1100 km. - Јонска острва ? |
| Ljubljana | 21 05 07 | 21 06 45 | 21 07 08 | Belar | |
| Königsberg i Pr. | — | — | 21 11,6 | Wiechert | |
| Pulkowo | 21 08 34 | 21 11 49 | 21 12,6 | Galitzin | △ = 1910 km. |
| Strasbourg | 21 9,8 | 21 11 15 | — | Wiechert | |
| Hamburg | 21 9,6 | — | 21 14,3 | Wiechert | |

# APPENDIX - A4

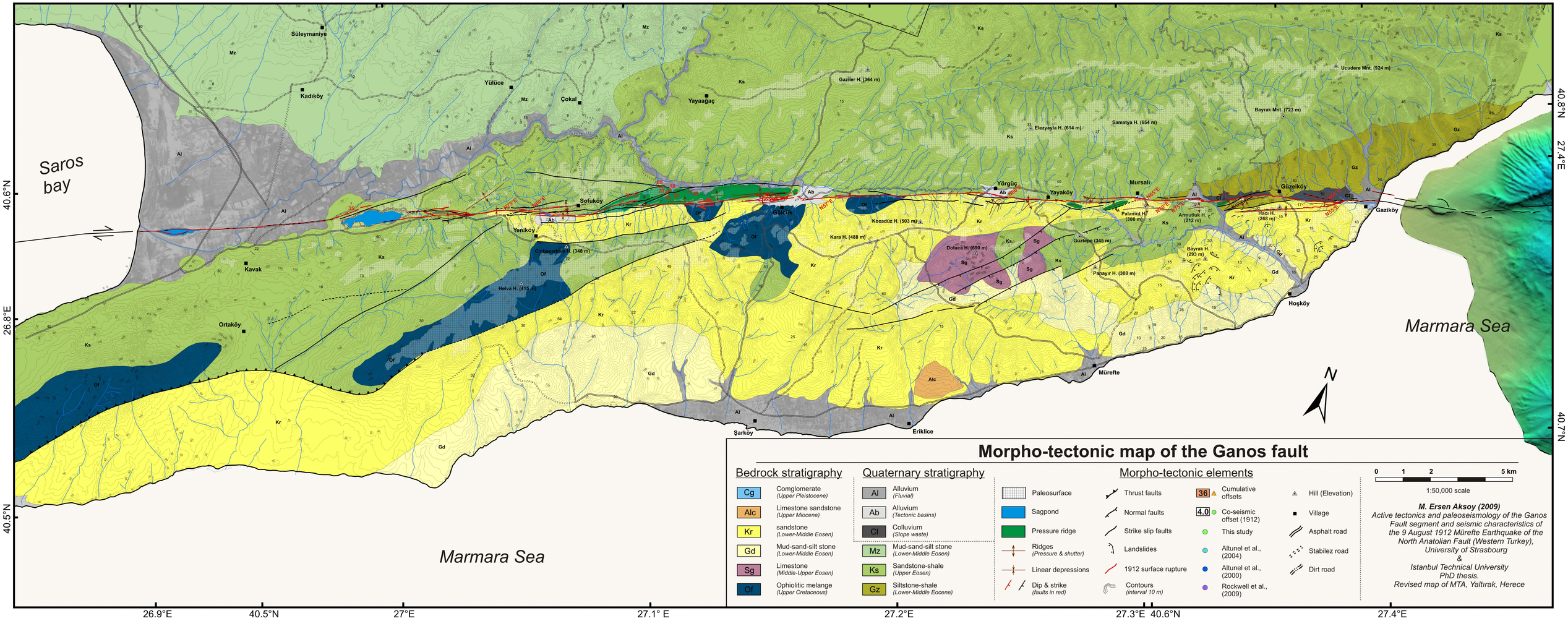


## Morpho-tectonic map of the Ganos fault

### Bedrock stratigraphy

- Cg — Comglomerate *(Upper Pleistocene)*
- Alc — Limestone sandstone *(Upper Miocene)*
- Kr — sandstone *(Lower-Middle Eosen)*
- Gd — Mud-sand-silt stone *(Lower-Middle Eosen)*
- Sg — Limestone *(Middle-Upper Eosen)*
- Of — Ophiolitic melange *(Upper Cretaceous)*

### Quaternary stratigraphy

- Al — Alluvium *(Fluvial)*
- Ab — Alluvium *(Tectonic basins)*
- Cl — Colluvium *(Slope waste)*
- Mz — Mud-sand-silt stone *(Lower-Middle Eosen)*
- Ks — Sandstone-shale *(Upper Eosen)*
- Gz — Siltstone-shale *(Lower-Middle Eocene)*

### Morpho-tectonic elements

- Paleosurface
- Sagpond
- Pressure ridge
- Ridges *(Pressure & shutter)*
- Linear depressions
- Dip & strike *(faults in red)*
- Thrust faults
- Normal faults
- Strike slip faults
- Landslides
- 1912 surface rupture
- Contours *(interval 10 m)*
- 36 — Cumulative offsets
- 4.0 — Co-seismic offset (1912)
- This study
- Altunel et al., (2004)
- Altunel et al., (2000)
- Rockwell et al., (2009)
- Hill (Elevation)
- Village
- Asphalt road
- Stabilez road
- Dirt road

0 1 2 5 km

1:50,000 scale


***M. Ersen Aksoy (2009)***


*Active tectonics and paleoseismology of the Ganos Fault segment and seismic characteristics of the 9 August 1912 Mürefte Earthquake of the North Anatolian Fault (Western Turkey), University of Strasbourg*
*&*
*Istanbul Technical University*
*PhD thesis.*
*Revised map of MTA, Yaltirak, Herece*

## Cumulative & 9 August 1912 EQ co-seismic slip distribution

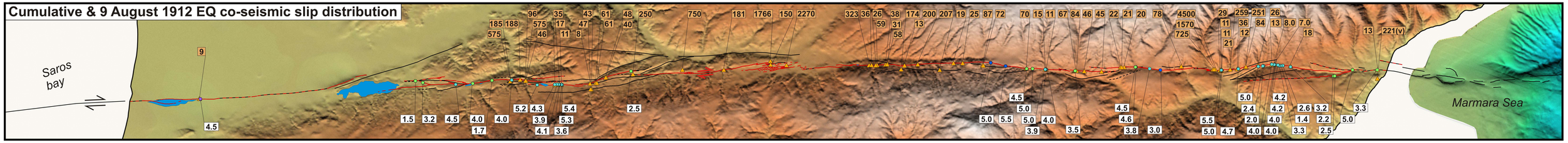

## CIRRICULUM VITAE

**Candidate's Full Name:** Murat Ersen AKSOY

**Place and date of birth:** Istanbul – 24.06.1973

Permenant address: Selamet sok. No 36/5 Üsküdar – Istanbul
e-mail: ersenma@hotmail.com

### Universities and Colleges attended:

- Eurasia Institute of Earth Sciences – M.Sc.
Solid Earth Sciences Department / Program of Geodynamic (1999 – 2002)
Thesis: The Neotectonic and Paleoseismology between Izmit and Sapanca, Kocaeli – Turkey
Advisors: Prof. Aykut BARKA & Asst. Prof. Serdar AKYÜZ

- Istanbul Technical University – B.Sc.
Geology Engineering Department, (1994 – 1999)
Thesis: The Geology of Kaleköy – Kuzulimanı - Güneytepe, Gökçeada, Çanakkale – Turkey
Advisor: Asst. Prof. Mehmet SAKINÇ

### Publications

- **Aksoy, M.E,** Meghraoui, M., Vallee, M., Çakır, Z, 2009, Rupture Characteristics of the 1912 Mürefte (Ganos) Earthquake Segment of the North Anatolian Fault (Western Turkey) submitted to Geology

- Meghraoui, M., **Aksoy, M.E,** Akyüz, S., Ferry M., Dikbaş, A., Altunel E., Paleoseismology of the North Anatolian Fault at Guzelkoy (Ganos segment, Turkey): Size and recurrence time of earthquake ruptures in the West Marmara Sea (in preparation)

- **Aksoy, M.E,** Meghraoui, M., Ferry M., Dikbaş, A., Akyüz, S., Ucarkus, G, Çakır, Z, Altın U., Sancar, T., Saki-Yaltırak, K., Kaplan, A., 2009, Paleoseismic history of the 1912 Mürefte earthquake segment of the North Anatolian Fault (Western Turkey) (in preparation for TJES)

- **Aksoy, M.E,** Meghraoui, M., Çakır, Z, Ferry M., Uçarkuş, G, 2009, A 20 kyr slip rate history deduced from stream offset along the Ganos fault segment of the North Anatolian Fault (Western Turkey) (in preparation for EPSL)

▪ Rockwell, T., Ragona, D., Seitz, G., Langridge, R., **Aksoy, M.E**., Ucarkus, G., Ferry, M., Meltzner, A.J., Klinger, Y., Meghraoui, M., Satir, D., Barka, A., and Akbalik, B., 2009, Palaeoseismology of the North Anatolian Fault near the Marmara Sea: implications for fault segmentation and seismic hazard: Geological Society, London, Special Publications, v. 316, 1, p. 31-54.

▪ **Aksoy, M.E,** Meghraoui M., Vallée, M., Çakır, Z, Rupture Characteristics of the 1912 Mürefte (Ganos) Earthquake Segment of the North Anatolian Fault (Western Turkey), T13C-1884 *AGU, 2009,* Fall Meet. San Francisco - Abstract

▪ **Aksoy, M.E,** Meghraoui M., Ferry M., Çakır, Z, Akyüz, S., Altunel E., Slip distribution and rupture characteristics of the 9 August 1912 earthquake, *ATAG-13, 18 March University., Çanakkale, 08-11 Sept 2009 (in Turkish),* Çanakkale – Oral - Abstract

▪ **Aksoy, M.E,** Meghraoui M., Vallée, M., Çakir, Z, Slip distribution and rupture characteristics of the 1912 earthquake sequence (Mw 7.4 and Mw 6.8) along the Ganos segment of the North Anatolian Fault (Turkey), *International Symposium on Historical Earthquakes and Conservation of Monuments and Sites in the Eastern Mediterranean Region - 500th Anniversary Year of the 1509 September 10, Marmara Earthquake*, 10 – 12 September 2009, Istanbul – Oral - Abstract

▪ **Aksoy, M.E,** Meghraoui M., Ferry M., Çakir, Z, Akyüz, S., Altunel E., Akyüz, S., Dikbaş, A., Altın, M.U. Paleoseismic investigation along the 1912 Ganos fault segment at Güzelköy, Yörgüç and Yeniköy – North Anatolian Fault / Turkey *International Symposium on Historical Earthquakes and Conservation of Monuments and Sites in the Eastern Mediterranean Region - 500th Anniversary Year of the 1509 September 10, Marmara Earthquake*, 10 – 12 September 2009, Istanbul – Poster - Abstract

▪ **Aksoy, M.E,** Meghraoui M., Ferry M., Çakır, Z, Vallée, M., Akyüz, S., Altunel E., Slip distribution and rupture characteristics of the 9 August 1912 Mürefte earthquake (Ms=7.3) along the Ganos segment of the North Anatolian Fault (Turkey), *SSA ,2009,* Anual Meet. Monterey - Abstract

▪ **Aksoy, M.E,** Meghraoui M., Ferry M., Çakir, Z, Akyüz, S., Altunel E., Altın, M.U. Paleoseimic investigations along the Ganos fault and characteristics of the 9 August 1912 Ganos earthquake (Ms=7.3) - North Anatolian Fault / Turkey, *Eos Trans. AGU, 89*(53), Fall Meet. Sn Francisco - Abstract

▪ **Aksoy M.E,** Meghraoui M., Altunel E., Ferry M., Karabacak V. And Çakir, Z, Fault characteristics, segmentation and paleoseismology along the 9 August 1912 Ganos earthquake-rupture (North Anatolian Fault, Turkey), Abstract in International Workshop on Comparative Studies of the North Anatolian Fault (Northwest Turkey) and the San Andreas fault (Southern California), p.40, Istanbul Technical University, 14-18 August 2006, - Abstract

▪ Rockwell, T.K., Okumura, K., Duman, T., Ragona, D., Seitz, G., Awata, Y., Ucarkus, G., **Aksoy, E.**, Ferry, M., And Meghraoui, M. Paleoseismology of the 1912, 1944 and 1999 ruptures on the North Anatolian fault:Implications for late Holocene patterns of strain release, Abstract in International Workshop on Comparative Studies of the North Anatolian Fault (Northwest Turkey) and the San Andreas fault (Southern California), p.11, Istanbul Technical University, 14-18 August 2006, - Abstract

▪ **Aksoy M.E**, Meghraoui M., Altunel E., Ferry M., Karabacak V. And Çakir, Z, Fault characteristics, segmentation and paleoseismology along the 9 August 1912 Ganos earthquake-rupture (North Anatolian Fault, Turkey), Abstract in special session on the North Anatolian Fault at the EGU meeting, EGU-A-10002 Vienna 2-8 April 2006, - Abstract

▪ Meghraoui, M**., E. Aksoy**, S. Akyuz, M. Ferry, And Z. Çakir, The seismic gap of the Marmara Sea: Paleoseismological and seismotectonic constraints from multi-segment ruptures along the North Anatolian Fault, Abstract in special session on the North Anatolian Fault at the EGU meeting, EGU-A-10008 Vienna 2-8 April 2006, - Abstract

▪ **Aksoy, M. E,** Meghraoui, M., Akyüz, H.S., Ferry, M., Dikbaş, A., Uçarkuş, G., Çakir, Z., Altunel, E., Zabci, C., Şatir-Erdağ, D. The morphology and paleoseismicity of the eastern section of the 9 August 1912 Mürefte earthquake rupture. ATAG-9 Abstract, p:13. Cumhuriyet University, Sivas. 22-24 Sept 2005 (in Turkish), - Abstract

▪ Dikbaş, A., Akyüz, H.S., Zabci, C., Sunal, G., Karabacak, V., Yalçiner,Ç., Ferry, M., Meghraoui, M., **Aksoy, E.** 2005. Paleoseismic studies on the 17 August 1999 earthquake rupture.. ATAG-9, Abstracts Cumhuriyet University., Sivas, 22-24 Sept 2005 (in Turkish), - Abstract

▪ Meghraoui, M., **Aksoy, E.**, Akyüz, H.S., Ferry, M., Dikbaş, A.E., Uçarkus, G., Çakir, Z. And Altunel, E., 2005. Paleoseismic investigations along the 1912 Ganos fault (North Anatolian Fault, Turkey): Insights for the expected large earthquake in the Marmara sea. Hokudan 2005, International Symposium on Active Faulting, Japan, - Abstract

▪ Rockwell, T.K., Okumura, K., Duman, T., Seitz, G., Ragona, D., Awata, Y., Ucarkus, G., **Aksoy, E**., Ferry, M., And Meghraoui, M. Paleoseismology of the 1912, 1944 and 1999 ruptures on the North Anatolian fault: implications for long-term patterns of strain release, Denver Annual Meeting, Paper No. 19-5, November 7–10, 2004, - Abstract

▪ Rockwell, T.K., Okumura, K., Duman, T., Seitz, G., Ragona, D., Awata, Y., Ucarkus, G., **Aksoy, E**., Ferry, M., And Meghraoui, M., 2004, Paleoseismology of the 1912, 1944 and 1999 ruptures on the North Anatolian Fault: implications for long-term patterns of strain release: Geological Society of America, Abstracts with Programs, 36 (5), 51. - Abstract

▪ Meghraoui, M., Akyüz S., Ferry, M., Altunel, E., Dikbaş, A., **Aksoy, M.E**., Uçarkuş, G., Çakir, Z., Sorensen, M., Pantosti, D., Pucci, S., Yalçiner, C., Zabci, C., Faulting Behaviour Along The 1912 Ganos Fault Segment West Of The Marmara Sea: Results From Paleoseismic Investigations, EGU04-A-06211, Poster, Nice-France, 2004 - Abstract

▪ Erturaç, M. K., Rizaoğlu G., Altun, B., Erçetin, T., **Aksoy, M.E**., The Geological Heritage of Turkey: Interactions Between the Mankind and Geology. 32th International Geological Congress, Florence, Italy, 20-28 August 2004, - Abstract

▪ Rockwell, T.K., **Aksoy, E**., Ferry, M., Klinger, Y., Langridge, R., Meghraoui, M., Meltzner, A., Ragona, D., Seitz, G., Ucarkus, G., Paleoseismic record of surface ruptures of the western third of the North Anatolian fault: Implications for fault segmentation models, EGS-AGU-EUG Joint Assembly, PO264, p:57, Nice, 6-11 April, 2003, - Abstract

▪ Ülgen, U.B., **Aksoy, M.E.**, Toraman, E., Sakinç, M., Yaltirak, C., Distribution and correlation of the Gökçeada (Imroz) and Gelibolu (Gallipoli) Peninsula paleo-enviroments (North Aegean, Turkey), EGS-AGU-EUG Joint Assembly, EAE03-A-11460, Nice-France, 6-11 April, 2003, - Abstract

▪ Rockwell Tom K., G. Seitz, R. Langridge, **Aksoy E.,** A. Barka, M. Ferry, Y. Klinger, M. Meghraoui, A. Meltzner, D. Ragona And G. Ucarkus, Paleoseismology of the Western North Anatolian Fault Near the Marmara Sea: The Past 400 Years of the Surface Ruptures East and West of Istanbul, 1st International Symposium of The Faculty of Mines (ITU) on Earth Sciences and Engineering, p:58, Istanbul, 16-18 May, 2002 - Abstract

▪ Ferry, M. Girard J.F., **Aksoy, M.E.,** Uçarkuş, G. et al., Ground-Penetrating radar prospecting across the 1999 Gölcük - Düzce surface ruptures of the North Anatolian Fault ,1st International Symposium of Istanbul Technical University, Faculty of Mines, Earth Sciences and Engineering, Istanbul - Turkey, 2002, - Abstract

▪ Rockwell, T. K ., Barka, A., Seitz, G., Ragona, D., **Aksoy, E.,** Klinger, Y., Meltzner, A., Meghraoui, M., Dier, D., Langridge, R., Ukarcus, G., Akoglu, A., Ferry, M., Akbalik, A., And Satir, D., Paleoseismology Of The North Anatolian Fault East And West Of The Marmara Sea: Implications For Seismic Hazard To Istanbul, 97th Annual Meeting and Pacific Section, American Association of Petroleum Geologists, Session No. 48, California, April 9-11, 2001, - Abstract

▪ Rockwell, T.K., **Aksoy, E.**, Ucarkus, G., Barka, A., Ragona, D., Dier, D., Ferry, M., Klinger, Y., Langridge, R., Meghraoui, M., Meltzner, A., Seitz, G., Results of Paleoseismic studies after the 1999 Izmit Earthquake: Implications for Seismic Hazard to Istanbul, EUG Meeting Abstracts, Strasbourg, L S01, p: 292, 2001, - Abstract

▪ **Aksoy, M.E.,** Rockwell, T.K., Meghraoui, M., Barka, A., Neotectonics of Izmit-Sapanca region and preliminary results of paleoseismic trenching studies, ATAG-4, Osmangazi University Eskişehir, 2000 - Abstract

**Projects:**

- Participant: Mapping and modelling coseismic and interseismic surface deformation in Turkey using Synthetic Aperture Radar Interferometry (InSAR) [Tübitak Project no: 107Y281: 2006-2009] Project Coordinator: Çakır, Z.

- Participant: RELIEF project (Reliable Information on Earthquake Faulting, EC Contract EVG1-CT-2002-00069), European Union Project. Project Coordinator: Meghraoui, M.

**Books:**

- **Aksoy M.E.** (Editor), 2003, Introduction to Information Technology, Istanbul Bilgi University Publishing.

- **Aksoy M.E.** (Author), 2003, Word Processing and Desktop Publishing, Introduction to Information Technology, s. 78-91 Istanbul Bilgi University Publishing.

**Honors and Awards:**

- Seismological Society of America Meetings, Monterey; Top Student Presenter, 2009

- Active Tectonic Research Group Meetings, Turkey – Çanakkale, Top 2. Student Presenter, 2009